Institut für Chemie
Arbeitskreis Angewandte Polymerchemie bei Prof. Dr. André Laschewsky

New Thermoresponsive Amphiphilic Block Copolymers with Unconventional Chemical Structure and Architecture

Dissertation zur Erlangung des akademischen Grades

"doctor rerum naturalium" (Dr. rer. nat.)

in der Wissenschaftsdisziplin "Kolloid- und Polymerchemie"

eingereicht an der

Mathematisch-Naturwissenschaftlichen Fakultät

der Universität Potsdam

von

M.Sc. Michelle Hechenbichler

Datum der Disputation: 08.02.2022

Das Leben ist bunt.
(Unbekannt)

Betreuer: Prof. Dr. André Laschewsky
Gutachter: Prof. Dr. Helmut Schlaad, Prof. Dr. Bernhard Schmidt

Published online on the
Publication Server of the University of Potsdam:
https://doi.org/10.25932/publishup-54182
https://nbn-resolving.org/urn:nbn:de:kobv:517-opus4-541822

ACKNOWLEDGEMENTS

Während meiner gesamten Promotion erhielt ich Unterstützung von zahlreichen Menschen, denen ich hier gerne danke möchte.

An erster Stelle möchte ich ein riesiges Dankeschön an Herrn Prof. Dr. André Laschewsky geben. Danke, dass Sie mich in Ihren Arbeitskreis so herzlich aufgenommen haben, dass Sie mir ein tolles und spannendes Promotionsthema gegeben haben, dass Sie immer ein offenes Ohr für alle möglichen und unmöglichen Probleme hatten, dass Sie mir so viele Möglichkeiten gegeben hatten, meine wissenschaftlichen Erfolge zu präsentieren und mich gleichzeitig viel selbst einbringen ließen. Danke einfach dafür, dass Sie mich auf dem Weg zur Wissenschaftlerin so hervorragend unterstützten.

Ohne meine lieben Kolleg:innen Cristiane Henschel und Alejandro Martinez, sowie zeitweise auch Seçkin Altuncu und fast zur Arbeitsgruppe gehörend Johannes Martin wäre die ganze Promotionszeit nur halb so schön gewesen. Egal ob im Büro, im Labor, auf Konferenzen oder einfach in der Mittagspause: Ich hatte mit euch eine tolle Zeit voller hilfreicher Diskussionen, lustigen Situationen und leckerem Kuchen.

Die hier hergestellten Polymere entfalten ihr volles Potential erst durch die Mühen meiner Kooperationspartner. Daher möchte ich mich an dieser Stelle ganz herzlich bei Herrn Prof. Dr. Michael Gradzielski, Benjamin von Lospichl und Albert Prause bedanken, die zahlreiche Streuversuche und rheologische Experimente durchgeführt haben. Danke auch dafür, dass ihr eure Ergebnisse immer so erklärt habt, dass diese auch für mich als Synthesechemikerin gut verständlich waren.

Des Weiteren gilt mein Dank Prof. Dr. Helmut Schlaad, Prof. Dr. Joachim Koetz und Dr. Matthias Hartlieb, die mir immer wieder geholfen haben meine Vorgehensweisen zu hinterfragen und mich mit ihren wissenschaftlichen Diskussionen unterstützt haben.

Ein Polymer bekommt erst wahren Wert, wenn man es charakterisieren kann. Ein großer Dank gilt an dieser Stelle daher den Menschen, die mir bei diesen Charakterisierungen geholfen haben. Namentlich möchte ich mich hier bei Dr. Dirk Schanzenbach (TGA, DSC, Brechungsindex), Angela Krtitschka (NMR), Sascha Prentzel (GPC), Dr. André Gessner (Fluoreszenz, UVvis), Dr. Oksana Sakhno (Fluoreszenz), Prof. Dr. Michael Kumke (Fluoreszenz), Katrin Brennenstuhl (Fluoreszenz) sowie Johannes Martin (MS) bedanken.

Ein ganz lieber Dank geht auch an Christoph Herfurth, meinem Vorgänger, der geduldig meine Fragen zu seinen ehemaligen Ergebnissen beantwortete.

Danke auch an alle Kolleg:innen am IAP und UP für die produktive Zusammenarbeit und angenehme Arbeitsatmosphäre, die den Wissenschaftscampus Golm so attraktiv macht.

SCIENTIFIC PUBLICATIONS

Parts of the results were already published, submitted or are still in preparation:

Scientific journals

- **M. Hechenbichler**, A. Laschewsky, M. Gradzielski: Poly(N,N-bis(2-methoxyethyl)acrylamide), a thermoresponsive non-ionic polymer combining the amide and the ethyleneglycolether motifs, *Colloid and Polymer Science* **2021**, 299, 205-219. (doi: 10.1007/s00396-020-04701-9)
- **M. Hechenbichler**, A. Prause, A. Laschewsky, M. Gradzielski: Thermo-responsive Self-assembly of Two-fold Fluorescently Labelled Block Copolymers in Aqueous Solution and Microemulsions, *Langmuir* **2021**, published. (doi: 10.1021/acs.langmuir.1c02318)
- A. Prause, **M. Hechenbichler**, B. von Lospichl, A. Laschewsky, M. Gradzielski: Aggregation behavior of non-symmetrically end-capped thermo-responsive block polymers in aqueous solution: between polymer coil and micellar state, in preparation.

Talks

- *European Detergents Conference,*: Poly(N,N-bis(2-methoxyethyl)acrylamide), a thermoresponsive non-ionic polymer combining the amide and the ethyleneglycolether motifs, **Berlin 2020**

Poster presentations

- *Macromolecular Colloquium:* Self-Assembly of Thermo-responsive Amphiphilic Block Copolymers by Variation of Chemical Structure and Architecture, **Freiburg 26-28 February 2020**.
- *15th European Detergents Conference:* Effect of Chemical Structure and Architecture on Self-Assembly of Thermo-responsive Amphiphilic Block Copolymers, **Berlin 23-25 October 2019**.
- *PolyDays:* Controlling the Self-Assembly of Thermo-responsive Amphiphilic Block Copolymers with Varying Chemical Structure and Architecture, **Berlin 11-13 September 2019**.

- *49th Conference of the German Colloid Society:* Influence of Chemical Structure and Architecture on Self-Assembly of Thermo-responsive Amphiphilic Block Copolymers, **Stuttgart, 23-25 September 2019**. (**Poster Award**)
- *14th European Detergents Conference:* Thermoresponsive Block Copolymers from One Pot Sequential RAFT Polymerizations and their Self-Assembly in Aqueous Solution, **Berlin, 10-12 October 2018**. (**Poster Award**)

ABSTRACT

Zusammenfassung

Das Aggregationsverhalten von amphiphilen Blockcpoolymeren ist wichtig für zahlreiche Anwendungen, beispielsweise in der Waschmittelindustrie als Verdicker oder in der Pharmazie zur kontrollierten Freisetzung von Wirkstoffen. Wenn einer der Blöcke thermoresponsiv ist, kann das Aggregationsverhalten zusätzlich über die Temperatur gesteuert werden. Während sich die bisherigen Untersuchungen solcher „intelligenten" Systeme zumeist auf einfache Diblockcopolymere beschränkt haben, wurde in der vorliegenden Arbeit die Komplexität der Polymere und damit die Vielseitigkeit dieser Systeme erhöht. Dazu wurden spezifische Monomere, verschiedene Blocklängen, unterschiedliche Architekturen und zusätzliche funktionelle Gruppen eingeführt. Durch systematische Änderungen wurde das Struktur-Wirkungsverhalten solcher thermoresponsiver amphiphiler Blockcopolymere untersucht. Dabei sind die Blockcopolymere typischerweise aus einem permanent hydrophoben „Sticker", einem permanent hydrophilen Block sowie einem thermoresponsiven Block, der ein Lower Critical Solution Temperature (LCST) Verhalten zeigt, aufgebaut. Während der permanent hydrophile Block aus *N*,*N*-Dimethylacrylamid (DMAm) bestand, wurden für den thermoresponsiven Block unterschiedliche Monomere, nämlich *N*-*n*-Propylacrylamid (NPAm), *N*-*iso*-Propylacrylamid (NiPAm), *N*,*N*-Diethylacrylamid (DEAm), *N*,*N*-Bis(2-methoxyethyl)acrylamid (bMOEAm), oder *N*-Acryloylpyrrolidin (NAP) mit entsprechend unterschiedlichen LCSTs von 25, 32, 33, 42 und 56 °C verwendet. Die Blockcopolymere wurden mittels aufeinanderfolgender reversibler Additions-Fragmentierungs-Kettenübertragungspolymerisation (RAFT Polymerisation) hergestellt, um Polymere mit linearer, doppelt hydrophober sowie symmetrischer Quasi-Miktoarm Architektur zu erhalten. Dabei wurden wohldefinierte Blockgrößen, Endgruppen und enge Molmassenverteilungen ($Đ \leq 1.3$) erzielt. Für komplexere Architekturen, wie die doppelt thermoresponsive und die nicht-symmetrische Quasi-Miktoarm Architekturen, wurde RAFT mit Atomtransfer-Radikalpolymerisation (ATRP) oder Single Unit Monomer Insertion (SUMI), kombiniert. Die dabei erhaltenen Blockcopolymere hatten ebenfalls wohldefinierte Blocklängen, allerdings war die Molmassenverteilung generell breiter ($Đ \leq 1.8$) und Endgruppen gingen zum Teil verloren, da komplexere Syntheseschritte nötig waren.

Das thermoresponsive Verhalten in wässriger Lösung wurde mittels Trübungspunktmessung und Dynamischer Lichtstreuung (DLS) untersucht. Unterhalb der Phasenüberganstemperatur waren die Polymere löslich in Wasser und mizellare Strukturen waren in der DLS sichtbar. Oberhalb der

Phasenübergangstemperatur war das Aggregationsverhalten dann stark abhängig von der Architektur und der chemischen Struktur des thermoresponsiven Blocks. Thermoresponsive Blöcke aus PNAP und PbMOEAm mit einer Blocklänge von $DP_n = 40$ zeigten keinen Trübungspunkt (CP) bis hin zu 80 °C, da durch den angebrachten hydrophilen PDMAm Block die bereits hohe LCST der entsprechenden Homopolymere bei den Blockcopolymeren weiter erhöht wurde. Blockcopolymere mit PNiPAm, PDEAm und PNPAm hinggeen zeigten abhängig von der Architektur und Blockgröße unterschiedliche CP's. Oberhalb der CP's waren größere Aggregate vor allem für die Blockcopolymere mit PNiPAm und PDEAm sichtbar, wohingegen der Phasenübergang für Blockcopolymere mit PNPAm stark abhängig von der jeweiligen Architektur war und entsprechend kleinere oder größere Aggregate zeigte.

Um das Aggregationsverhalten besser zu verstehen, wurden Fluoreszenzstudien an PDMAm und PNiPAm Homo- und Blockcopolymeren mit linearer Architektur durchgeführt, welche mit komplementären Fluoreszenzfarbstoffen an den entgegengesetzten Kettenenden funktionalisiert wurden. Das thermoresponsive Verhalten wurde dabei sowohl in Wasser als auch in Öl-in-Wasser Mikroemulsion untersucht. Die Ergebnisse zeigten, dass das Blockcopolymer sich, ähnlich wie die anderen hergestellten Architekturen, bei niedrigen Temperaturen wie ein Polymertensid verhält. Dabei bilden die hydrophoben Stickergruppen den Kern und die hydrophilen Arme die Corona der Mizelle. Oberhalb des Phasenübergangs des PNiPAm Blocks verhielten sich die Blockcopolymere allerdings wie assoziative Telechele mit zwei nicht-symmetrischen hydrophoben Endgruppen, die sich untereinander nicht mischten. Daher bildeten die Blockcopolymere anstatt aggregierter „Blumen"-Mizellen größere, dynamische Aggregate. Diese sind einerseits über die ursprünglichen Mizellkerne bestehend aus den hydrophoben Sticker als auch über Cluster der kollabierten thermoresponsiven Blöcke miteinander verknüpft. In Mikroemulsion ist diese Art der Netzwerkbildung noch stärker ausgeprägt.

Abstract

The self-assembly of amphiphilic polymers in aqueous systems is important for a plethora of applications, in particular in the field of cosmetics and detergents. When introducing thermoresponsive blocks, the aggregation behavior of these polymers can be controlled by changing the temperature. While confined to simple diblock copolymer systems for long, the complexity - and thus the versatility - of such smart systems can be strongly enlarged, once designed monomers, specific block sizes, different architectures, or additional functional groups such as hydrophobic stickers are implemented. In this work, the structure-property relationship of

such thermoresponsive amphiphilic block copolymers was investigated by varying their structure systematically. The block copolymers were generally composed of a permanently hydrophobic sticker group, a permanently hydrophilic block, and a thermoresponsive block exhibiting a Lower Critical Solution Temperature (LCST) behavior. While the hydrophilic block consisted of *N*,*N*-dimethylacrylamide (DMAm), different monomers were used for the thermoresponsive block, such as *N*-*n*-propylacrylamide (NPAm), *N*-*iso*-propylacrylamide (NiPAm), *N*,*N*-diethylacrylamide (DEAm), *N*,*N*-bis(2-methoxyethyl)acrylamide (bMOEAm), or *N*-acryloylpyrrolidine (NAP) with different reported LCSTs of 25, 32, 33, 42 and 56 °C, respectively. The block copolymers were synthesized by successive reversible addition fragmentation chain transfer (RAFT) polymerization. For the polymers with the basic linear, the twinned hydrophobic and the symmetrical quasi-miktoarm architectures, the results were well-defined block sizes and end groups as well as narrow molar mass distributions ($Đ \leq 1.3$). More complex architectures, such as the twinned thermoresponsive and the non-symmetrical quasi-miktoarm one, were achieved by combining RAFT polymerization with a second technique, namely atom transfer radical polymerization (ATRP) or single unit monomer insertion (SUMI), respectively. The obtained block copolymers showed well-defined block sizes, but due to the complexity of these reaction paths, the dispersities were generally higher ($Đ \leq 1.8$) and some end groups were lost.

The thermoresponsive behavior of the block copolymers was investigated by turbidimetry and dynamic light scattering (DLS). Below the phase transition temperature, the polymers were soluble in water and small micellar structures were visible. However, above the phase transition temperature, the aggregation behavior was strongly dependent on the architecture and the chemical structure of the thermoresponsive block. Thermoresponsive blocks comprising PNAP and PbMOEAm with $DP_n = 40$ showed no cloud point (CP), since their already high LCSTs were further increased by the attached hydrophilic block. Depending on the architecture as well as on the block size, block copolymers with PNiPAm, PDEAm and PNPAm showed different CP's. Large aggregates were visible for block copolymers with PNiPAm and PDEAm above their CP. For PNPAm containing block copolymers, the phase transition was very sensitive towards the architecture resulting in either small or large aggregates.

In addition, fluorescence studies were performed using PDMAm and PNiPAm homo- and block copolymers with linear architecture, functionalized with complementary fluorescence dyes introduced at the opposite chain ends. The thermoresponsive behavior was studied in pure aqueous solution as well as in an oil-in-water (o/w) microemulsion. The findings indicate that the block copolymer behaves as polymeric surfactant at low temperatures, with one relatively small

hydrophobic end group and an extended hydrophilic chain forming ‘hairy micelles’ similar as the other synthesized architectures. Above the phase transition temperature of the PNiPAm block, however, the copolymer behaves as associative telechelic polymer with two non-symmetrical hydrophobic end groups, which do not mix. Thus, instead of a network of bridged ‘flower micelles’, large dynamic aggregates are formed. These are connected alternatingly by the original micellar cores as well as by clusters of the collapsed PNiPAm blocks. This type of bridged micelles is even more favored in the o/w microemulsion than in pure aqueous solution.

CONTENTS

LIST OF ABBREVIATIONS AND SYMBOLS

Codes of the homo- and block copolymers

Homopolymers: [Code of architecture see Figure 0.1a][Code of the monomer repeat unit see Figure 0.1b][if applicable: batch number indicating different molar masses a,b,c,…]

Block copolymers: [Code of architecture see Figure 0.1a][Code of the monomer repeat unit see Figure 0.1b][if applicable: batch number a,b,c,…]-[Code of the monomer repeat unit of the second block see Figure 0.1b][if applicable: batch number indicating different molar masses a,b,c,…] etc.

For example:

- L1a-2b
  - L: linear architecture
  - 1a: PDMAm batch a
  - -2b: PNiPAm as second block, batch b

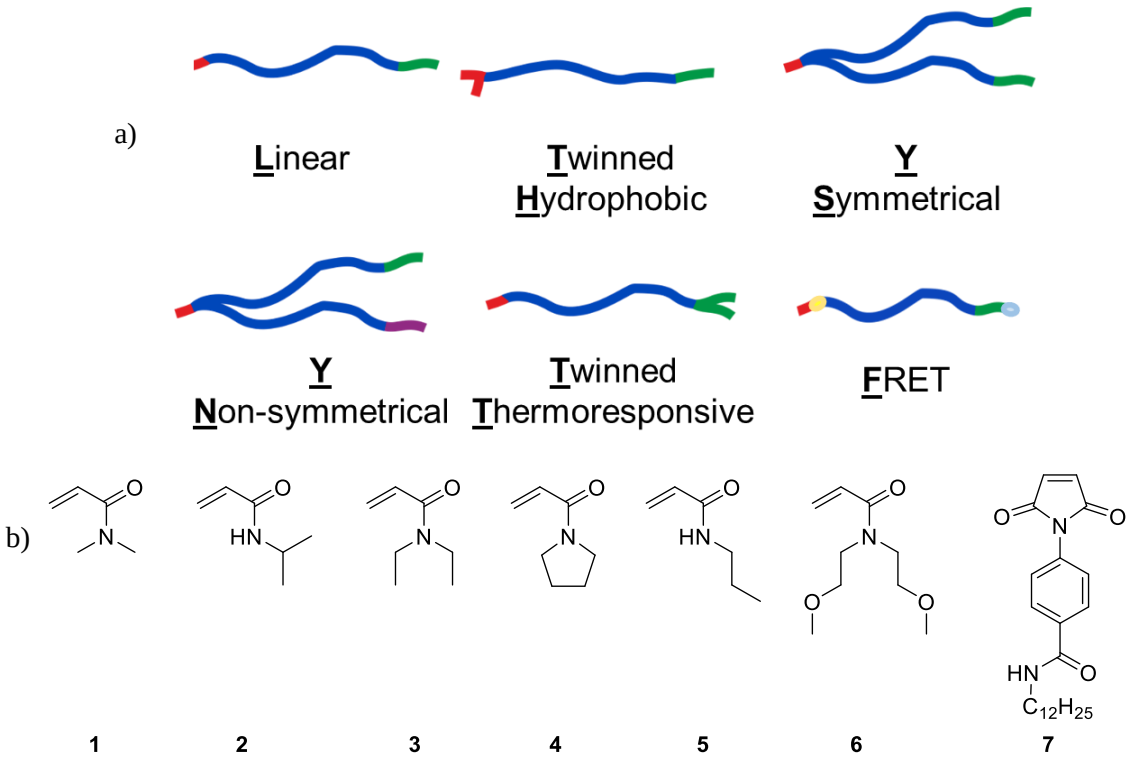

Figure 0.1: Code of the architecture (a) and the monomer repeat units (b) used for naming of the homo- and block copolymers synthesized in this thesis.

A	absorbance
AIBN	2,2′-azobis(2-methylpropionitrile)
AM	acrylamide
APT	Attached Proton Test
ATRP	Atom Transfer Radical Polymerization
bMOEAm	*N*,*N*-bis(2-methoxyethyl)acrylamide) (monomer **6**)
BPT	*S*-benzyl-*S*'-propyl trithiocarbonate
BTPT	*S*-benzyl-*S*'- (3-(trimethylsilyl)propyl)carbonotrithioate
c	concentration
c_{mass}	mass concentration
cmc	critical micelle concentration
c_{molar}	molar concentration
COSY	Correlated Spectroscopy
CP	Cloud Point
C-PEO-C	poly(ethylene oxide) end-capped on both chain ends with alkyl groups
CRP	Controlled Radical Polymerization
CRU	Constitutional Repeat Units
CTA	Chain Transfer Agent
d	path length
D	translational diffusion coefficient
DBMI	*N*,*N*-4-(2,5-dioxo-2,5-dihydro-1H-pyrrol-1-yl)-*N*-dodecylbenzamide (monomer **7**)
DCM	dichloromethane
d_h	hydrodynamic diameter
DLS	Dynamic Light Scattering
DMI	*N*-dodecyl maleimide

DMSO	dimethylsulfoxide
DP_n	number average Degree of Polymerization
DSC	Differential Scanning Calorimetry
Đ	dispersity
ESI	ElectroSpray Ionization
EtOH	ethanol
F	FRET “architecture”
FRET	Fluorescence (or Förster) Resonance Energy Transfer
FTIR	Fourier Transform Infrared Spectroscopy
HMQC	Heteronuclear Multiple-Quantum Correlation
HPMA	*N*-(2-hydroxypropyl)methacrylamide
ICP-OES	Inductively Coupled Plasma Optical Emission Spectrometry
iniferter	chemical compound that simultaneously acts as initiator, transfer agent, and terminator
i-PrOH	*iso*-propanol
k	Boltzmann’s constant
L	linear architecture
LAM	Less Activated Monomer
LCST	Lower Critical Solution Temperature
M	molar mass
MAM	More Activated Monomer
MBP	methyl 2-bromopropionate
MCP	methyl 2-chloropropionate
Me_6TREN	tris(2-dimethylaminoethyl) amine
MEHQ	4-methoxyphenol
MeOH	methanol
MMA	methyl methacrylate

M_n^{NMR}	number average molar mass calculated from ^{1}H-NMR measurements
M_n^{SEC}	number average molar mass determined by SEC
M_n^{theo}	theoretical number average molar mass calculated by monomer conversion
M_n^{UV}	number average molar mass calculated from UV-vis measurements
MS	Mass Spectrometry
Mt^z/L	metal in oxidation state z with ligands L
NMP	Nitroxide Mediated Polymerization
NMR	Nuclear Magnetic Resonance
o/w	oil-in-water microemulsion
OSET	Outer Sphere Electron Transfer
P (as prefix)	poly
PB	poly(1,2-butadiene)
PBO	poly(butylene oxide)
PDEAm	poly(*N*,*N*-diethylacrylamide)
PDMAm	poly(*N*,*N*-dimethylacrylamide)
PEG	poly(ethylene glycol)
PEMAm	poly(*N*-ethyl-*N*-methylacrylamide)
PEO	poly(ethylene oxide)
PEOEOVE	poly(2-(2-ethoxy)ethoxyethyl vinyl ether)
PEOVE	poly(2-ethoxyethyl vinyl ether)
PFO	poly(perfluoropropylene oxide)
PMOVE	poly(2-methoxyethyl vinylether)
PNAP	poly(*N*-acryloylpyrrolidine)
PNEAm	poly(*N*-ethylacrylamide)
PNiPAm	poly(*N*-isopropylacrylamide)
PNPAm	poly(*N*-*n*-propylacrylamide)

PPO	poly(propylene oxide)
PS	polystyrene
PVAc	poly(vinyl acetate)
PVME	poly(vinyl methylether)
RAFT	Reversible Addition Fragmentation chain Transfer
RDRP	Reversible-Deactivation Radical Polymerization
S_0	electronic ground state
S_1	first electronic excited state
SET-LRP	Single Electron Transfer – Living Radical Polymerization
SUMI	Single Unit Monomer Insertion
T	temperature
TDMAO	*N*-tetradecyl-*N*,*N*-dimethylammoniumoxide
T_g	glass transition temperature
TGA	ThermoGravimetric Analysis
TH	twinned hydrophobic architecture
THF	tetrahydrofuran
TLC	Thin Layer Chromatography
TMS	trimethylsilyl
TT	twinned thermoresponsive architecture
UCST	Upper Critical Solution Temperature
V	volume
V-40	1,1'-azobis(cyclohexan-1-carbonitril)
w/o	water-in-oil microemulsion
YN	non-symmetrical quasi-miktoarm architecture
YS	symmetrical quasi-miktoarm architecture
ΔG	change of Gibbs free energy

ΔH	change in enthalpy
ΔS	change in entropy
ε	extinction coefficient
η	viscosity of the solvent
Θ	scattering angle
$\lambda(A)_{em}$	emission wavelength of acceptor
$\lambda(A)_{ex}$	excitation wavelength of acceptor
$\lambda(D)_{em}$	emission wavelength of donor
$\lambda(D)_{ex}$	excitation wavelength of donor
λ_{max}	maximum absorbance wavelength

1. INTRODUCTION

1.1 AMPHIPHILIC HOMO- AND BLOCK COPOLYMERS

1.1.1 STIMULI-RESPONSIVE POLYMERS

Polymers capable of responding to a small external or internal stimulus by varying their conformation, structure and/or physical properties strongly, are of great scientific interest.[1,2] This property change should be reversible when suppressing the stimulus or applying a second "reverse" stimulus. Possible stimuli and their responses are listed in Figure 1.1.

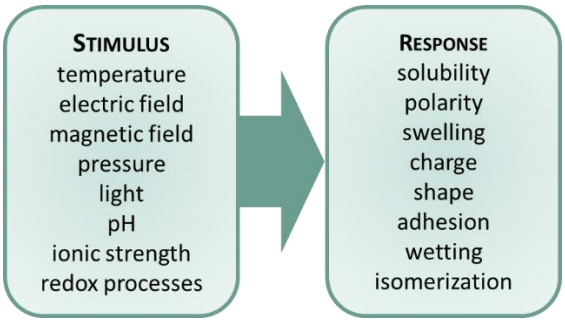

Figure 1.1. Potential responses of polymers on different stimuli.

Typical physical stimuli are temperature, electric and magnetic fields, pressure, light, pH and ionic strength, whereas redox processes belong to chemical stimuli. The responses can for instance result in a change of solubility,[1] polarity,[2] swelling,[3] charge,[4] shape,[5] adhesion,[6] wetting[7] and isomerization.[8] This great variability leads to manifold applications,[9] for example as smart coatings,[10] actuators,[11] sensors,[2] in drug delivery[12] or as smart emulsifiers.[13]

The temperature stimulus remains the most extensively studied stimulus in the field of responsive polymers in solutions.[14] Such thermoresponsive polymers are either dissolved upon heating showing therefore an Upper Critical Solution Temperature (UCST) behavior or they precipitate upon heating exhibiting a Lower Critical Solution Temperature behavior, which is frequently observed in aqueous solutions. As in this work, all of the thermoresponsive polymers employed show LCST behavior in water, the introduction will focus on this type of thermoresponsive behavior. In fact, most of the non-ionic water-soluble polymers exhibit LCST phase separation upon heating. This phenomenon is based on the balance between hydrophilic and hydrophobic groups and can be explained by the thermodynamics of the polymer-water-system. A polymer dissolves in water when the free energy of dissolution $\Delta G = \Delta H - T\Delta S$, i.e., the difference between the enthalpy and the entropy term is negative. Due to the hydrogen bonding between water and the

hydrophilic groups of the constitutional repeat units (CRU), the dissolution enthalpy ΔH is negative and therefore favors dissolution. However, the required organization of the water molecules is entropically unfavorable and counteracts the always effective ideal mixing entropy. Consequently, the entropy term TΔS outweighs the enthalpy gain by hydrogen bonding with increasing temperature and water molecules bound to the polymer chain are released into bulk water. Additionally, water molecules become more mobile, thus weakening the favorable interactions between polymer and water. This dehydration of the polymer segments leads to a stronger polymer-polymer interaction. Finally, the polymer chains collapse causing phase separation of the solution into two phases.[15] The transition points of the binodal curve are called phase transition temperatures. They are often referred by the cloud points (CP's) due to the turbidity of the biphasic solutions observed. For monodisperse solutes the minimum temperature of the binodal curve in the phase diagram is the LCST (Figure 1.2).

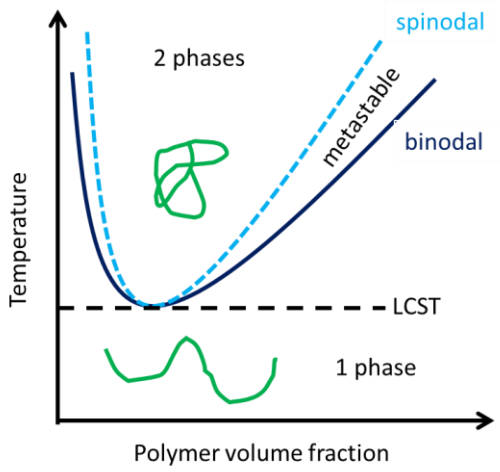

Figure 1.2: General illustration of isobaric phase diagrams for polymer solutions exhibiting a lower consolute boundary and an LCST.

Also, a phenomenological classification was developed to distinguish three different LCST types which were observed for different polymers:[16–18]

Type I represents the "classical" Flory-Huggins miscibility behavior. With increasing chain length, the CP's are shifted towards lower polymer concentration, i.e., the polymer becomes less soluble the higher the molar mass. A typical example is poly(*N*,*N*-diethylacrylamide) (PDEAm).[19]

Type II demonstrates a single off-zero limiting concentration and the CP's are almost independent on the polymer chain length. Poly(*N*-isopropylacrylamide) (PNiPAm) is the prime example for this behavior.[20]

Type III shows a behavior between type I and type III. At low polymer concentrations, the polymer behaves corresponding to the classical Flory-Huggins theory, whereas at high concentrations, the CP's are almost unaffected by the chain length. A well-known polymer showing this type of behavior is polyvinyl methylether (PVME).[21]

The phase transition behavior is not only influenced by polymer concentration and molar mass, but also by various other factors such as dispersity Đ, tacticity, end group, polymer architecture, pressure, and additives such as salts.[22–24] Besides the thermodynamic factors, also kinetic factors can influence the phase transition behavior. Consequently, experimental parameters such as the heating rate affect the apparent CP. Obviously, these factors make it difficult to compare the results from literature. Nevertheless, numerous investigations were executed to understand how the factors affect the phase transition. The more important ones for this thesis are discussed below.

When performing the measurements, the influence of the heating rate on the phase transition temperature has to be considered. For turbidimetry measurements on PNiPAm, Boutris et al. [25] observed that the CP was strongly shifted towards higher temperatures with increasing heating rates from 0.02 $K \cdot min^{-1}$ to 5 $K \cdot min^{-1}$. During the synthesis of thermoresponsive polymers, end groups are usually introduced in the polymer chain by initiators or chain transfer agents (CTA). In this context, hydrophobic end groups generally lower the LCST of thermoresponsive polymers, whereas hydrophilic end groups favor higher LCSTs because of the enhanced solubility in water.[26] The effect becomes less significant when polymers with high molar masses are used.[27,28]

Furthermore, the architecture of polymers can affect their thermoresponsive behavior. In theory, branched polymers are more soluble than their linear analogues,[29] however, different tendencies exist for water-soluble polymers. Miasnikova et al.[30] found a decrease of the LCST as well as of the rate of deswelling for acrylate based triblock and 3-arm star copolymers compared to the diblock analog. This behavior resulting in a hysteresis was explained by steric constraints caused by entanglement, which might hinder a quick reswelling. Similar results were found for methacrylate-based 4-arm star block copolymers[31] and acrylamide-based star block copolymers[32] compared to their single arms. Nonetheless, a lower CP was observed for oxazoline-based 4-arm star compared to the 8-arm star polymer, which was explained by the difference in the intramolecular density providing intensive interaction between hydrophobic cores and thus supporting aggregation behavior. Picos-Corrales et al.[33] compared different reports about the effect of polymer architecture of PNiPAm and simplified that a change of the phase transition is observed only when the molar content of PNiPAm is below 50 %. Since PNiPAm belongs to the

LCST type II, it might be less sensitive to the effects of the architecture than other LCST type I polymers.

The effect of the tacticity on the phase transition seems to depend on the specific polymer. For PNiPAm, isotactic rich[34] as well as syndiotactic rich[35] samples are poorly soluble in water whereas atactic PNiPAm is soluble. This was explained by the higher solubility in water of racemo-rich samples due to the balance between the hydration free energy and the conformational entropy.[36] In contrast, atactic PDEAm was found to be more hydrophobic than an isotactic rich sample,[37] however, syndiotactic PDEAm was found to be insoluble in water.[38] Additionally, mainly isotactic PDEAm showed not only a higher phase transition temperature but also a broad hysteresis of 10 °C between heating and cooling cycles compared to mainly heterotactic PDEAm samples.[39] Mori et al.[40] found for syndiotactic poly(*N*-*n*-propylacrylamide) (PNPAm) a highly cooperative phase transition due to local formation of an ordered structure in the dehydrated state, which also resulted in large hysteresis between heating and cooling cycles. This phenomenon was also observed for syndiotactic PNiPAm-*co*-PNPAm copolymers with increasing PNPAm content.[41] Recently, Hirano et al.[42] investigated the phase transition behavior of isotactic and syndiotactic copolymers of *N*-ethylacrylamide (NEAm) and NiPAm. While the syndiotactic copolymers showed a sharp transition with small hysteresis regardless of the chemical composition, the isotactic copolymers had a large hysteresis when the NiPAm content was higher than 9 %. This behavior was explained by the formation of insoluble domains due to the intramolecular hydrogen bonding between the amide groups. These domains of isotactic NiPAm stereosequences were explained to behave like cross-linking domains inducing such a large hysteresis.

When thermoresponsive polymers are tested in potential applications, they are usually dissolved in saline solutions, and the interaction between polymer and salts becomes important. The effect of ions on the LCST follows the so-called Hofmeister series, which originally describes the ability of salts to precipitate proteins from aqueous solution.[43] This phenomenon is more pronounced for anions than cations following a typical order:

$$SO_4^{2-} > F^- > Cl^- > NO^{3-} > Br^- > I^- > ClO^{4-} > SCN^-$$

Several ionic properties such as size, polarizability, hydration energetics and the partition coefficient influence the precipitation. The anions on the left of the series are referred to as kosmotropes, originally thought to “make” bulk water structure due to their strong hydration layer, resulting in a competition with polymer for hydration water and therefore decreasing the LCST. On the right side of the series starting with Cl^- are the so-called chaotropes thought to “break” bulk

water structure as those anions are weakly hydrated and highly polarizable, leading to favored interactions with the polymer surface and thus increasing the LCST.[44–46]

Probably the largest group of thermoresponsive polymers in aqueous media are polymers with amide groups.[15] Since in this thesis most of the polymers were synthesized by using acrylamides, the following chapter is going to describe their properties and thermoresponsive behavior.

1.1.2 POLYACRYLAMIDES

Among thermoresponsive polyacrylamides, PNiPAm became the most widely and successfully studied polymer,[20] since its first publication by Heskins and Guillet.[47] Due to the acidic hydrogen of the secondary amide group, the synthesis of *N*-monosubstituted polyacrylamides such as PNiPAm is limited to radical polymerization techniques, starting from simple free radical[48] to Reversible-Deactivation Radical Polymerization (RDRP) techniques like Reversible Addition Fragmentation Chain Transfer (RAFT) polymerization,[49] or Atom Transfer Radical Polymerization (ATRP).[28] On the other side, *N*,*N*-disubstituted polyacrylamides can be synthesized not only by radical polymerization, but also by anionic as well as group transfer polymerization.[39] Chapter 1.3 explains the details about controlled polymerization of acrylamides.

Depending on the type of substitution, a wide range of phase transition temperatures is available, which is depicted by the different acrylamide structures in Figure 1.3.

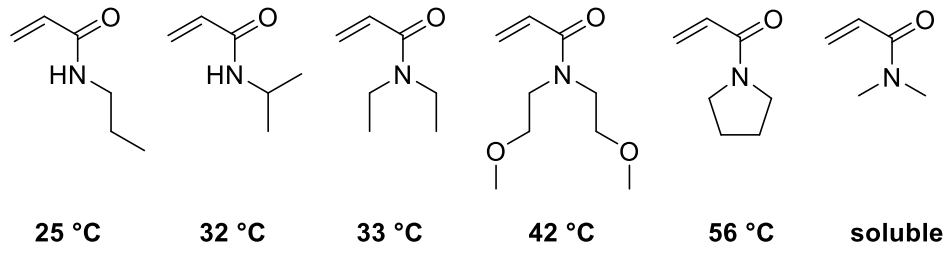

Figure 1.3: Structures of different acrylamides chosen for this work and their reported cloud points of their high molar mass polymers at ambient pressure in aqueous solution.

The block copolymers synthesized in this work always contain poly(*N*,*N*-dimethylacrylamide) (PDMAm) as permanently hydrophilic block. Attached to it is a thermoresponsive block consisting of one of the above-mentioned thermoresponsive polyacrylamides. Their transition is based on the balance of the hydrophilic amide group, which enables hydrogen bonding either between water molecules and the polymer, or between the polymer's repeat units themselves, and the hydrophobic polymer backbone as well as on the substituents. Regarding the *N*-monosubstituted polyacrylamides, PNPAm has a much lower LCST of 22-25 °C[50–52] depending on the preparation

compared to its structural isomer PNiPAm with a LCST of 32 °C.[50,47] Pang et al.[53] explained the enhanced solubility of PNiPAm with the different hydration characteristics exhibited mainly at the N-H side. The branched *i*-propyl group seems to allow a higher orientation of the water molecules compared to the straight chain of the *N*-propyl group. While PDEAm has a similar phase transition temperature as PNiPAm, it belongs to type I thermoresponsive polymers, and its thermoresponsive behavior depends sensitively on the molar mass, varying from 25 to 36 °C. [54,19,55] Another *N*,*N*-disubstituted polyacrylamide, which was used for this work, is poly-*N*,*N*-bis(2-methoxyethyl)acrylamide PbMOEAm. It was first described by Ito[56] as a LCST polymer with a transition temperature around 42 °C. Its chemical structure combines the two main motifs of non-ionic thermoresponsive polymers within the same molecule, which are the amide and ethyleneglycolether moieties.[18] Despite its particular structure, the homopolymer PbMOEAm has been hardly studied and the few available data on its thermoresponsive behavior in water have been conflicting.[57,58] Therefore, well-defined homo- and block copolymers containg PbMOEAm were prepared by RAFT polymerization, and its thermoresponsive behavior in aqueous solutions was investigated. The results were already published[59] and are summarized in this thesis in chapter 5. An even higher transition temperature of 56 °C[60] shows poly(*N*-acryloylpyrrolidine) (PNAP) indicating a better solubility of the cyclic alkyl group compared to the linear groups in PDEAm. Homo- and block copolymers containing PNAP were already described widely in literature.[13,18,61] In conclusion, depending sensitively on the substitution pattern of the polyacrylamides, the range of the transition temperature can be carefully chosen by the right selection of the monomer.

1.1.3 Amphiphilic Block Copolymers and Their Self-assembly

Amphiphilic block copolymers consist of covalently connected blocks with different chemical nature resulting in different molecular interactions. These differences might lead to microphase separation in bulk or, in the focus of this thesis, to a selective affinity towards two solvents, which are incompatible with each other, usually towards water and towards oil.[62,63] Typically, the more polar or hydrophilic block A is neutral or ionic,[64] while the less polar or hydrophobic block B is a hydrocarbon,[65] a fluorocarbon,[66] a hydrophobic polymer such as polybutylene oxide (PBO), polypropylene oxide (PPO), polystyrene (PS), or polymethylmethacrylate.[67] Such polymers offer a great variability in self-assembly behavior due to their adjustable length, morphology and domain functionality, which can be manipulated by the selection of monomer, composition and molar mass.[68] This variability enables the use in a plethora of applications in the fields of medical, cosmetic or agricultural formulations as controlled delivery and release media,[69] emulsifiers,[70] dispersants,[71] or thickeners.[72] This chapter is focused on linear nonionic amphiphilic block

copolymers and their self-assembly in aqueous systems. The self-assembly of amphiphilic block copolymers depends on the molecular structure, both the relative and absolute block lengths as well as on the architecture. The block sequence for linear architectures ranges from well-studied and relatively simple topologies such as AB diblock copolymers to ABA[73–75] and more complex ABC[68] triblock copolymers or even more versatile structures such as ABCD or ABAC multiblock copolymers. The diblock copolymer AB represents the simplest amphiphilic block copolymer structure. Below the so-called critical micelle concentration (cmc), only single dissolved copolymer chains, unimers, are present in the solution.[67] In this case, two coil formations for AB diblock copolymers are possible:[76]

1. If the blocks A and B are immiscible and the solvent is a good solvent for A but a poor solvent or nonsolvent for B, block A is solvated to an expanded coil, while block B is contracted or collapsed and thus, much smaller in size.
2. If the solvent is a good solvent for both blocks and the two blocks are immiscible, two blobs of comparable size occur while being covalently linked together. However, when both blocks are miscible, a permeated coil is visible.

The variations for BAB triblock copolymer below the cmc are based on similar considerations:

1. For immiscible blocks, if the solvent is only a good solvent for A and blocks B can come together, a loop is formed. But if blocks B are sufficiently small, block A can bring them into solution and dumbbell-type unimers can exist.
2. If the solvent is a good solvent for both blocks and the two blocks are immiscible, two blobs occur, but the sizes for the blocks B might be larger. When both blocks are miscible, a penetrating coil is visible similar as for AB diblock copolymers.

Above the cmc, however, micellization occurs in analogy to classical low molar mass surfactants (Figure 1.4a). The different morphologies of the obtained micellar aggregates, such as spherical, or cylindrical micelles, or polymersomes, are a result of the block ratios A and B influencing the packing of the polymer chains.[67,77] Block copolymers containing more than one associating block as in BAB or ABC, may form loops or flower-like micelles, or they can bridge between the micelles (Figure 1.4b and c).[77]

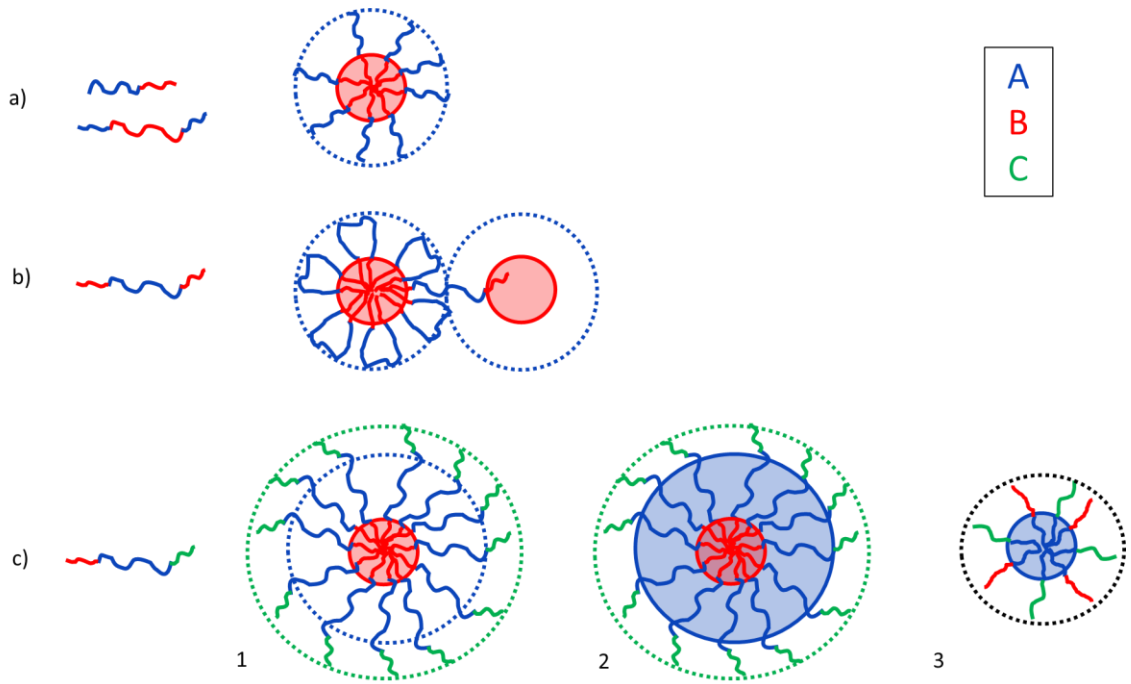

Figure 1.4: Schematic drawing of possible spherical micellar structures from linear amphiphilic block copolymers a) AB & ABA in a solvent selective for A showing a "hairy micelle", b) BAB showing flower-like micelles and bridging in a solvent selective for A and c) terpolymer BAC showing 1. core-inner corona-outer corona micelles in a solvent selective for blocks A and C, 2. core-shell-corona micelles in a solvent selective for block C and 3. mixed corona micelles in a solvent selective for blocks B and C. For comparison with the amphiphilic block copolymers synthesized in this work, the BAC structure is shown.

Well-known examples for BAB are commercially available poly(oxyalkylenes),[74,78] such as polyethylene oxide (PEO) end-capped on both chain ends with alkyl groups (C-PEO-C)[65] or PBO-PEO-PBO block copolymers. Renou et al. observed for hexadecyl end-capped C-PEO-C transient networks of bridged micelles, while single end-capped C-PEO formed loose micelles that are not crosslinked.[77] Castelletto et al.[79] also found crosslinked micelles for PBO-PEO-PBO block copolymers with short PBO blocks of around 12 repeating units. Due to the thermoresponsive behavior of such PBO blocks, the number of bridges increased with higher temperatures, while it remained relatively constant for C-PEO-C.[77] Bivigou-Koumba et al.[80] synthesized BAB block copolymers with PNiPAm as a long hydrophilic A block and with either 2-ethyl hexyl acrylate, octadecyl acrylate, 3,5-dibromobenzyl acrylate, or (4-tert-butyl) styrene as relatively short hydrophobic blocks B. Different from the above described BAB triblock copolymers, they found only small aggregates even for high concentrations up to 20 wt%. They explained this behavior with the strongly hydrophobic B blocks that are well-shielded from water, so that the tendency for

bridging is very low. Note that, due to the shielding as well as the high molar mass of PNiPAm, the phase transition temperature was not influenced by the hydrophobic end groups.

The introduction of a third block C in triblock terpolymers allows additional interactions with solvents and the other blocks, leading to diverse micellar architectures.[81,68] Generally, the basic micellar structures formed by such linear ABC, ACB or BAC terpolymers are

1. core-inner corona-outer corona micelles, if the solvent is selective for the middle and one of the end blocks (Figure 1.4c1)
2. core-shell-corona micelles, if the solvent is selective for only one of the end blocks (Figure 1.4c2)
3. mixed corona micelles if the solvent is selective for the outer blocks (Figure 1.4c3).[68]

If the end blocks are compatible with each other, they can also form flower-like micelles or bridges between the micelles similar to BAB block copolymers (Figure 1.4b). However, with incompatible blocks, the polymer may form multicompartment micelles.[82] Taribagil et al.[83] found that poly(1,2-butadiene)-b-PEO-b-poly(perfluoropropyleneoxide) (PB-b-PEO-b-PFPO) self-assembles into a compartmentalized network with PFPO disks distributed within thin PB sheets covered by PEO brushes. Since the end blocks are strongly hydrophobic but incompatible with each other, they try to avoid contact with water, but segregate into different domains. The hydrophilic PEO center block shields the hydrophobic blocks by surrounding them.

More subtle changes and more control are possible with stimuli-responsive block copolymers. In particular, thermoresponsive block copolymers are of high interest, since the thermally induced changes are reversible, and no reagents must be added or removed to induce the change. A full review of the aggregation behavior can be found by Strandman and Zhu.[84] The block copolymer poly(2-ethoxyethyl vinyl ether)-b-poly(2-methoxyethyl vinylether)-b-poly(2-(2-ethoxy)ethoxy-ethyl vinyl ether), PEOVE-b-PMOVE-b-PEOEOVE, for example, shows multistep self-assembly.[85] When the temperature is increased above the CP of the PEOVE block, the then surfactant-like block copolymer formed micelles. Above the CP of the second end block PEOEOVE, the micelles further associate to form a gel. When finally all blocks are hydrophobic, above the CP of PMOVE, the polymer is insoluble in water and precipitates. However, such a straight-forward aggregation behavior is not always the case. In fact, Skrabania et al.[13] synthesized ternary triblock copolymers based on the blocks PNiPAm, PNAP and PDMAm and found only for the combination PDMAm-b-PNiPAm-b-PNAP a distinct two-step transition indicating a complex associative behavior. Furthermore, Jia and Zhu[86] observed complex thermoresponsive behaviors for their amphiphilic block copolymers. They investigated the self-assembly of thermoresponsive

diblock copolymers with PNPAm and poly(*N*-ethyl-*N*-methylacrylamide) (PEMAm) with relative PNPAm to PEMAm block lengths of 1:2, 1:1 and 2:1. As PNPAm has a CP around 22 °C and PEMAm around 56 °C,[18] the block copolymers underwent multiple transitions in water, but they showed different transition and aggregation behaviors despite their structural similarity. During the first CP, the block copolymers underwent a transition from unimers to loose clusters. With increasing temperatures, these clusters separated into micelles, after which they formed compact aggregates. When the block sizes were similar, the block copolymer showed only one CP around 25 °C, after which the solution became clear again.[86] The authors explained this behavior by the formation of mesoglobules. With increasing relative block length of the more hydrophilic PEMAm block, the switched PNPAm block was better stabilized leading to a less abrupt CP.[86] Weiss and Laschewsky[87] went one step towards even more complex aggregation behaviors and synthesized a series of triple-thermoresponsive triblock copolymers from PNPAm, poly(methoxydiethylene glycol acrylate) (PMDEGA) and PNEAm. With PNPAm being the most hydrophobic block in the series, block copolymers with PNPAm as the center block formed unimolecular micelles after the thermal collapse of PNPAm. All other polymers showed a high tendency for cluster formation due to the successive collapses of the thermoresponsive blocks.

To summarize this chapter, the self-aggregation of thermoresponsive amphiphilic polymers has much evolved in recent years, but it remains a complex matter, since it depends sensitively on the chemical structure of the blocks, the block sequence, and on the phase transition temperature.

1.2 Microemulsions and Their Rheological Properties

By IUPAC definition, microemulsions are optically transparent, "isotropic, thermodynamically stable dispersions of water, oil and surfactant(s) with dispersed domain diameter varying from around 1 to 100 nm, usually 10 to 50 nm".[88] They form spontaneously by mixing two fluids and surface-active agents, namely a surfactant and a co-surfactant,[89] and are usually of low viscosity.[90,91] They are either oil-in-water (o/w) or water-in-oil (w/o) microemulsions. It is important to note that in contrast to emulsions, microemulsions are thermodynamically stable, since the surface tension is very low.[89] While Hoar and Schulmann[92] used ionic surfactants in their initial studies of microemulsions, starting in the 1960s, especially nonionic surfactants have been employed, such as alkylethoxylates or alkylphenolethoxylates. These surfactants had the major advantage that co-surfactants were not necessary leading to only ternary systems, which were easier to study.[90] Alternatives are semipolar nonionic surfactants such as tetradecyldimethylammoniumoxide (TDMAO), which exhibit properties that are intermediate

between those of a typical nonionic and those of typical cationic surfactants of equal chain length.[93] Co-surfactants are surface-active compounds, which do not form micelles by themselves like surfactants but become easily incorporated into the water-oil interface due to their amphiphilicity.[90] Typical compounds are medium alkyl chain alcohols such as pentanol, hexanol up to decanol.[90,94] With the presence of a co-surfactant, the interfacial tension is further decreased, since these compounds penetrate the surfactant film at the amphiphilic oil-water interface.[89]

Generally, dilute microemulsions exhibit low viscosities , which range from the viscosities of either their continuous component or the average of both in the case of bicontinuous systems.[90] However, well-controlled rheological properties are necessary for many applications of microemulsions, such as pharmaceutical applications,[95] consumer products and in enhanced oil revocery processes.[96] Three major possibilities of controlling rheology in microemulsions exist:[90]

1. For more rigid microemulsions, increasing micelle concentration leads to so-called cubic phases with densely packed microemulsion droplets, which have marked gel-like properties (Figure 1.5a). However, this option requires high surfactant concentrations.
2. Alternatively, the viscosity can be increased by adding nonadsorbing homopolymers that are soluble in the continuous phase (Figure 1.5b). Even though this option worked in some cases, [97] it has some limitations. For example, such mixtures tend to phase separate due to depletion forces.[98] This entropic force results, when so-called depletants, such as non-adsorbing polymers, are added to colloidal particles. Due to the constant thermal motion, the depletants collide randomly with the larger colloidal particles in the solution, pushing the latter together and leading to phase separation of the mixture.[99,100] An additional disadvantage is that the added polymer might affect the microemulsion phase behavior.[101]
3. The third option comprises the physical crosslinking of the microemulsion droplets by adding end group functionalized polymers (Figure 1.5c). Such telechelic polymers have two or more chain ends, so-called stickers, that are soluble in the microemulsion droplet.[102] For o/w microemulsions, this is achieved by hydrophobically modified polymers such as hydrophobically modified PEO (see chapter 1.1.3). For w/o microemulsions, oil soluble telechelics are needed, such as PEO-b-poly(isoprene)-b-PEO.[103] The larger the sticker group, the longer it resides in the microemulsion droplet due to increased interactions. As a result, the viscosity increases, because the physical crosslinking is stronger.[72] If the droplets are farther apart than the polymer chain length, the polymer forms flower-like micelles comprising loops with the chain ends in the same droplet. Otherwise, it forms a

network via bridging (see Figure 1.5c).[90] When architectures with more than 2 sticker groups are applied, the telechelic polymers are able to interconnect more than two droplets, thus increasing the viscosity markedly.[104] Structural characterization with scattering methods showed that the addition of such telechelic polymers does not influence the droplet shape and size, but only the interactions between the droplets.[32,104]

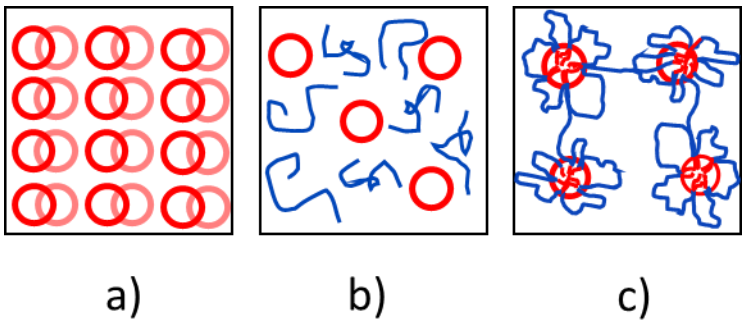

Figure 1.5: Schematic representation of the different possibilities of rheological control of microemulsions, namely a) cubic phases, b) nonadsorbing homopolymers and c) associative telechelics.

Therefore, the third method is a very attractive way of controlling the rheology of microemulsions. Replacing one hydrophobic sticker group with a thermoresponsive block offers additional control of the viscosity via temperature.[32] This is the reason, why this work is focused on new thermoresponsive amphiphilic block copolymers as potential rheological modifiers for microemulsions.

1.3 Reversible-Deactivation Radical Polymerization

RDRP combines the convenience of free radical polymerization with the controlled concepts of living polymerization. The resulting procedure allows controlled molar masses, relatively low dispersities, defined end groups, precise molecular architectures in terms of topology and composition, and diverse functionality. Mechanistically, this requires a fast dynamic equilibrium between propagating radicals and a dormant species. One approach includes a reversible deactivation of propagating radicals to form a dormant species, which can be reactivated either catalytically as in ATRP, or spontaneously as in stable radical mediated polymerization with aminoxyl radicals or organometallic species. The second approach uses a degenerative transfer process, as in RAFT polymerization or iodine transfer radical polymerization.[105,106]

In this work, the emphasis is on RAFT polymerization, since it is a robust, versatile and easy process for acrylic monomers. For some architectures, it was useful to combine two subsequent polymerization techniques. Therefore, I chose ATRP and combined it with RAFT polymerization. The following two chapters explain the mechanisms, advantages, and disadvantages of these polymerization techniques.

1.3.1 Reversible Addition Fragmentation Chain Transfer Polymerization

RAFT polymerization works similar to conventional free radical polymerization with initiation, propagation and termination reactions being the same. The main difference is an additional activation/deactivation process by degenerate chain transfer (Scheme 1.1).[107]

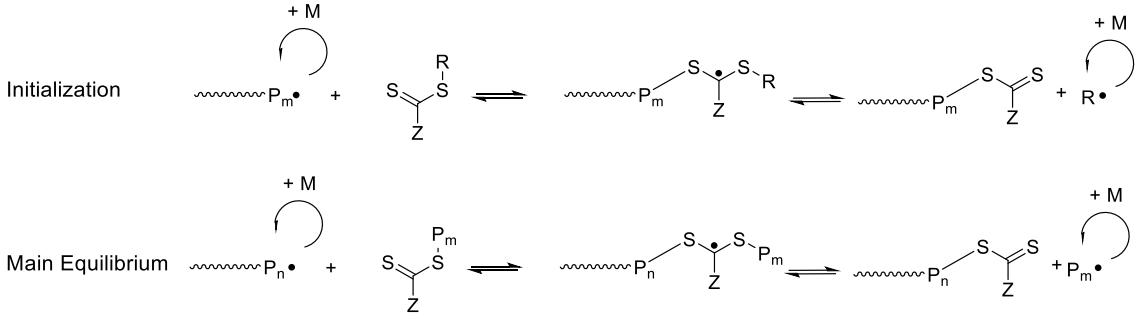

Scheme 1.1: Mechanism for RAFT polymerization with reversible deactivation by degenerate chain transfer.

To ensure this extra step, a chain transfer agent (CTA) is added to the reaction, usually in form of a thiocarbonylthio compound. The C=S double bond in the CTA is the reactive site, which is attacked during the RAFT polymerization process. Furthermore, the CTA holds two type of end groups, the so-called Z- and R-group. While the Z-group modifies the addition and fragmentation rate, the R-group should be a good homolytic leaving group and an reinitiating species.[108] In the beginning of the RAFT polymerization process, the initiator decomposes to produce radicals, which further attack monomers resulting in oligomeric radicals. These oligomeric radicals add to the CTA to form an intermediate radical in the initialization step (Scheme 1.1). This radical species can fragment into an oligomeric thiocarbonylthio compound, bearing the dormant oligomeric chain, and the radical R-group. The latter starts a new chain generating a propagating radical chain P_n·. During the main equilibrium, after all of the initial CTA is consumed, this radical attaches to a dormant species releasing another radical chain P_m·. This equilibrium allows the polymer chains to grow in parallel. The term “degenerate” describes the ability of the chain transfer

process to exchange the functionality between the chains P_n and P_m. These chains have different degrees of polymerization (n and m) but are similar in an effective process. The so controlled polymerization process leads to rather narrow molar mass distributions and polymers with well-defined end groups. Dormant polymers can also be reactivated to produce block copolymers.

Depending on the monomer and the end groups of the resulting polymer, the design of the CTA must be chosen carefully. The Z-group plays a crucial role during the addition of propagating radicals onto the CTA and during the fragmentation of the intermediate radicals. For more activated monomers such as methyl methacrylates, styrenes, methyl acrylates, acrylamides (AM) and acrylonitrile, more reactive RAFT agents such as dithioesters or trithiocarbonates are chosen to control the polymerization. On the other side, less activated monomers such as *N*-vinylpyrrolidone, vinyl acetate, and *N*-vinylcarbozole need RAFT agents with lower reactivity bearing a lone pair on nitrogen or oxygen adjacent to the thiocarbonyl, e.g. *O*-alkyl xanthates, *N*,*N*-dialkyldithiocarbamtes, and *N*-alkyl-*N*-aryldithiocarbamates.[107,109,110] Maintaining the Z-group is also important for the living character of the RAFT polymerization. A high end group fidelity can be achieved by minimizing the initiator concentration, choosing the right reaction conditions, and stopping the reaction before complete monomer conversion. [107,111] For optimal control of the polymerization, the R-group must be a good homolytic leaving group and the resulting radical R· must be able to reinitiate polymerization efficiently. The leaving group ability of R depends on steric factors, radical stability, and polar factors. Therefore, it is not enough for R to be a monomeric analog since penultimate unit effects may affect the leaving group ability. Monomers such as methacrylates or methacrylamides resulting in tertiary radicals P_n· need tertiary or secondary alkyl R groups.[112,109] However, monomers with fast propagation rates as acrylates, acrylamides, vinyl ester, and vinyl amides require secondary or primary R groups.[109]

The advantages of RAFT polymerization compared to other RDRP techniques are the very large range of suitable monomers and the minimal perturbations to radical polymerization kinetics. By using R- or Z-group approaches, various complex architectures are achieved, and well-designed end groups are applied. These approaches are especially used to obtain star architectures.[113] In the R-group approach, the R-group is found in the core of the CTA. During initialization and equilibrium steps, the thiocarbonylthio moiety leaves the core to allow chain growth at the R-groups.[32] With this approach, the polymerization takes place at the corona until a thiocarbonylthio compound deactivates the process again. This method allows relatively large polymer chains. However, bimolecular termination reactions such as recombinations are more likely to happen. In the Z-group approach the thiocarbonythio moiety remains in the core of a

growing polymer.[114] This approach leads to polymer chains growing in the reaction medium. However, to perform the equilibrium reaction (Scheme 1.1), the polymer chains must diffuse to that core, which can be difficult for large polymer chains due to steric effects. Therefore, the Z-group approach is limited to a maximum chain size. Other advantages of RAFT polymerization are that purely organic reagents are mostly used, and undesired metal traces in the resulting polymer are avoided. However, only few RAFT agents are commercially available as the thiocarbonyl group is relatively unstable, so that these compounds must be stored carefully. [106,107,115]

1.3.2 Atom Transfer Radical Polymerization

In contrast to RAFT polymerization, ATRP uses a catalytical activation and deactivation of chain ends to produce radicals. For that purpose, an alkyl halide P_m-X reacts with a transition metal complex Mt^z/L in a low oxidation state to form intermittently a growing radical P_m· and the resulting metal complex in a higher oxidation state coordinated with the halide X. The activated radical species P_m· reacts with monomers M, until it forms the deactivated species again (Scheme 1.2).[105]

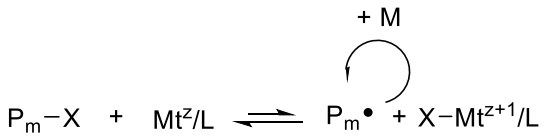

Scheme 1.2: ATRP equilibrium.

The mostly used catalysts are based on Cu^I, but other redox-active transition metal complexes based on Va, Co, Ni, Ru, Fe or Mo etc. are also known.[116,117] Polar solvents increase the ATRP equilibrium constants, since the solvent may stabilize the more polar Cu^{II} species better than the less polar Cu^I species.[105] Higher temperatures increase the propagation constant much more than the termination constant due to the lower activation energy of termination. However, this is limited by side reactions.[105] The structure of ligands strongly influences the Cu complex activity, which decreases in the following order: alkylamine ≈ pyridine > alkylimine >> arylimine > arylamine. Generally, chelating ligands bearing several nitrogen atoms stabilize the Cu^{II} complex. Its rearrangement from Cu^I to Cu^{II} state should lead to only small entropy changes. Therefore, branched tetradentate ligands as tris(2-dimethylaminoethyl)-amine (Me_6TREN) form the most active ligands, whereas the bidentate ligand 2,2′-bipyridine is among the least active.[105,118,119] As initiators, usually halides such as alkyl bromides or chlorides are used. Although an activation of an alkyl iodide works as well as an alkyl bromide, the stability of the Cu^{II}-I bond is very low. Within

the same halide species, the activation constant of α-substituted ester based initiators follows the order from tertiary over secondary to primary carbons 3° > 2° > 1°. In addition, substituents providing mesomeric effects directly attached to the carbon of the C-X bond stabilize the resulting radical in the order nitrile > phenyl > ester.[119]

Noteworthy, ATRP of acrylamides in solution is only partially controlled or confined to low molar masses. This may be due to the competitive complexation of the catalytic species by the multiple amide groups of the resulting polymer, which are weak ligands. Another problem is the loss of the halide, in particular the bromine end group, possibly due to a cyclization reaction usually followed by hydrolysis (Scheme 1.3).[120–122]

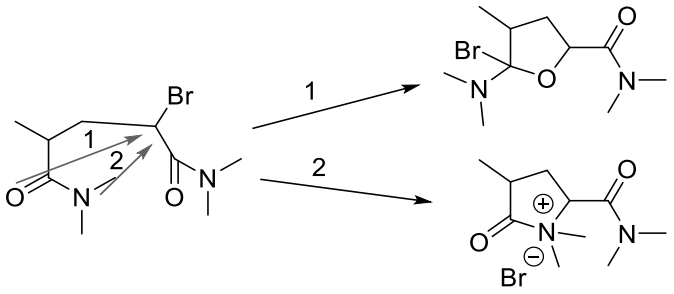

Scheme 1.3 Hypothetical cyclization side reaction during ATRP of acrylamides with a bromide initiator.[120–122]

Teodorescu and Matyjaszewski[121] explored the polymerization of DMAm, *tert*-butylacrylamide and *N*-(2-hydroxypropyl)methacrylamide (HPMA) either in bulk or solution with various ligands and methyl 2-chloropropionate (MCP), the bromine equivalent methyl 2-bromopropionate (MBP), or *N*,*N*-dimethyl-2-chloropropanamide as initiators. The results were either low monomer conversions or, in the case of the very active ligand 1,4,8,11-tetramethyl-1,4,8,11-tetraazacyclotetradecane, poor control of the polymerization. One year later, the group reported controlled polymerization of the above-mentioned monomers by using an initiating system of MCP/CuCl/Me_6TREN in different solvents.[120] Nevertheless, the conversion for DMAm, *tert*-butyl acrylamide and HPMA was limited to 56, 38 and 19 %, respectively, which was explained by the deactivation of the catalyst. When replacing CuCl by CuBr, and MCP by MBP, the value of the achieved conversion of DMAm by ATRP dropped from 56 % to 23 %, indicating a faster deactivation of the catalyst. Still, ATRP of acrylamides in pure water or water mixtures seems to lead to well-defined homo- and block copolymers as well as high conversions while having rapid polymerization rates. [123–127] For the polymerization of water-soluble monomers in pure water using Cu based catalyst components, as well as in some other polar solvents,[128] a different mechanism

than ATRP is proposed, namely single electron transfer – living radical polymerization (SET-LRP).[129,130] Upon addition of CuX and the N-containing ligand L to the solvent, the formed complex Cu(L)X disproportionates, resulting in highly active Cu^0 and deactivating $Cu(L)X_2$ species. An outer sphere electron transfer (OSET) of the nascent Cu^0 species has been proposed to mediate the activation process of alkyl halides via a radical anion intermediate.[128,131] To obtain high chain-end functionality, the polymerizations were performed in an ice bath rather than at room temperature. Various monomers are polymerizable by SET-LRP, particularly acrylamides, which is a convenient method to obtain block copolymers. Another benefit is that ATRP as well as SET-LRP require normally very mild conditions such as working at room temperature compared to RAFT polymerization.[127] On the other hand, Cu-mediated RDRP is still challenging for acidic monomers, since these molecules can protonate the amine-containing ligands and destroy the catalyst complexes by forming carboxylic copper salts. In addition, traces of copper remain in the polymer, which might be problematic for certain applications.[105]

1.4 Analytical Techniques Used for Characterization of Aqueous Solutions

When a thermoresponsive polymer undergoes a phase transition, various physical or physico-chemical properties of the aqueous polymer solution such as optical properties, polymer chain mobility, polymer chain conformation, and hydrogen bonding change significantly. Different analytical techniques such as turbidimetry, light scattering, nuclear magnetic resonance (NMR) spectroscopy, calorimetry, fluorescence spectroscopy or Fourier Transform Infrared spectroscopy (FTIR) are used to track the changes. The following chapters discuss the basics of the techniques used in this work.

1.4.1 Turbidimetry

Turbidimetry is the most commonly used method for determination of CP since it can be conveniently performed on a simple UV-vis spectrometer with temperature control. The phase transition is observed by measuring the transmittance vs. the temperature. Upon heating above CP, the thermoresponsive polymer chains switch from soluble to insoluble and start contracting strongly. The originally homogeneous solution turns into a heterogeneous turbid phase, if the resulting polymer agglomerates are large enough and sufficiently dehydrated to scatter the incident light. Due to this scattering of particles, the intensity of transmitted light decreases.[132] It is important to realize that the CP curve does not exactly coincide with the binodal curve. The reason

is related to kinetic aspects of determining CP and to the above-mentioned necessary large agglomerates.[20,133] In the literature, several definitions and protocols exist for the determination of CP, such as the temperature of the onset of the drop in transmittance, at 80 % or 50 % transmittance or the inflection point of the turbidity curve. Zhang et al.[133] suggest to use the temperature at 50 % of transmittance to facilitate comparison of data for "steep" clouding transitions, but 80 % when the transition is broad. Other authors define the transition point as the temperature of 2 % reduction in the transmittance.[134,135] However, the phase transition of the solution is reflected by the onset of the apparition of droplets of the second phase. Hence, the here reported CP's are determined via the onset of the drop in transmittance.

1.4.2 Dynamic Light Scattering

Another technique to measure the coil-to-globule transition of thermoresponsive polymers is dynamic light scattering (DLS). In DLS, macromolecules scatter the incident laser light in all directions and the scattering intensity is recorded. The observed signal depends on the phase addition or destruction of the scattered light reaching the detector. Due to Brownian motion, the resulting light intensity is fluctuating.[136] Brownian motion is the random movement of particles suspended in a medium, in this case water, and is strongly related to the particle size. Small particles are easily moved around by the surrounding water molecules, but the larger the particle the slower the Brownian motion will be. The resulting velocity is defined as the translational diffusion coefficient D and the correlated particle size is given by the Stokes-Einstein equation 1.1:[137]

$$d_h = \frac{kT}{3\pi\eta D} \qquad 1.1$$

d_h = hydrodynamic diameter, D = translational diffusion coefficient, η = viscosity of the solvent, k = Boltzmann's constant, T = absolute temperature

The obtained hydrodynamic diameter is the diameter of a hypothetical sphere having the same translational diffusion coefficient as the actual particle. [138] To determine the velocity and thus the diffusion and the related particle size, a digital autocorrelator correlates the intensity fluctuations with respect to time (ns-µs). Consequently, the earlier the correlogram decays, the smaller the particle, whereas for larger particles, the correlogram takes more time to decay (see Figure 1.6).

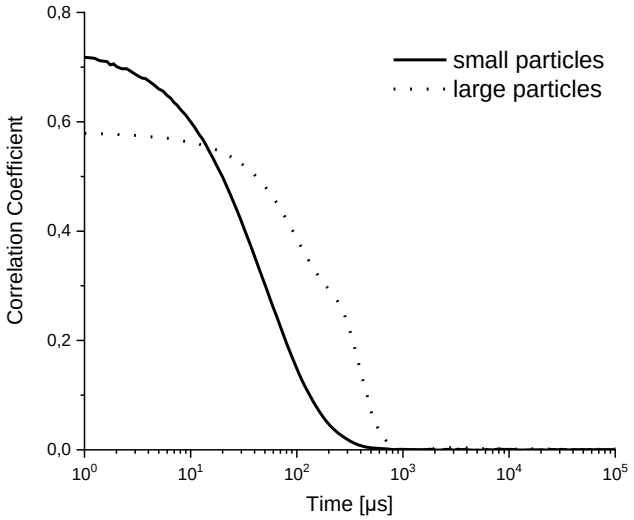

Figure 1.6: Typical correlogram for small particles (solid line) and large particles (dotted line).

Also, the steeper the line, the less disperse is the sample i.e., a broader decay shows a higher polydispersity of the sample.[136] The diffusion rate depends not only on the size of the particle, but also on the ionic strength of the medium and the surface structure.[139] When analyzing non-spherical particles, their shape and conformation changes can influence the diffusion speed making DLS a useful method to detect the phase transition of thermoresponsive polymers. The detector is placed either at 90 °, or at 173 ° close to the incident light, known as backscatter detection. Backscatter detection has the advantage that the light does not need to pass through the whole sample, therefore reducing multiple scattering events, by which light scattered by one particle is itself scattered by other particles. With using such a short path length, higher concentrations of the analytes can be used. Additionally, scattering contribution of large particles such as dust can be avoided in a backscatter detecting system.[136]

When the hydrodynamic diameter from DLS and the transmission from turbidimetry are plotted together against the temperature, a better picture of the evolving particle size and the macroscopic changes is obtained.[140,59] Thus, the combined techniques are very useful to get a good understanding of the phase transition of thermoresponsive polymers.

1.4.3 FÖRSTER RESONANCE ENERGY TRANSFER

Fluorescence or Förster Resonance Energy Transfer (FRET) is a highly sensitive tool to detect distance changes. The principle behind FRET, first established in 1948,[141] is a non-radiative energy transfer from a donor chromophore to an acceptor chromophore via dipolar coupling. The Jablonski diagram (Scheme 1.4) schematically shows the FRET process.

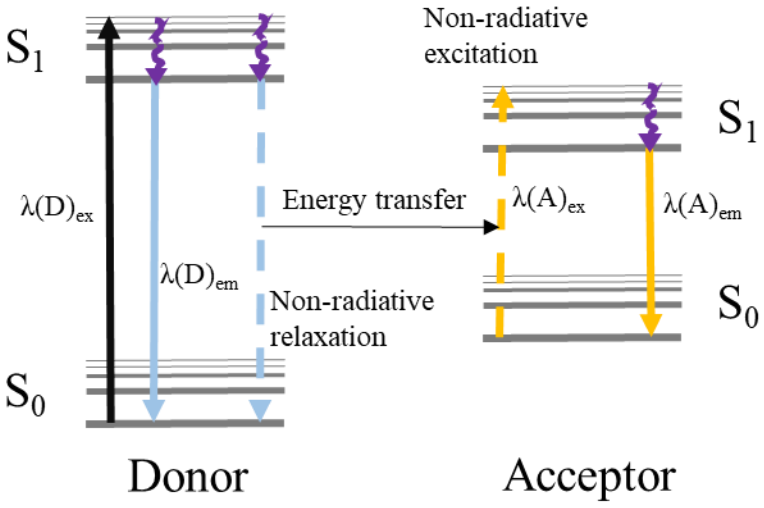

Scheme 1.4: Jablonski diagram for FRET from donor D to acceptor A.

Mechanistically, the process starts with the excitation of the donor D from the electronic ground state S_0 to the excited state S_1 following its radiative emission (solid line) or non-radiative relaxation (dotted line). When a resonance of the emission and the acceptor excitation dipoles exists, the energy from the relaxation process will be transferred to the acceptor. The so excited photon returns to the ground state via photon emission and, in case the acceptor is a fluorophore, the detection via fluorescence spectroscopy is possible. For a high efficiency of FRET, one must respect

1. a high spectral overlap between donor emission and acceptor excitation
2. the absorption of the donor which should be at a minimum or out of the range of the absorption of the acceptor, to get a maximum excitation of the donor without exciting the acceptor
3. a sufficient quantum yield of the donor
4. a short distance between donor and acceptor, typically between 1 – 10 nm
5. the relative orientation of the donor emission and the acceptor excitation dipoles, which should be parallel.[142,143]

Typical dyes used for FRET measurements are shown in Figure 1.7. Many fluorescence studies use in particular hydrocarbon based dyes such as pyrene, naphthalene or anthracene.[144–148] These molecules have the advantage of being chemically mostly inert, which is useful e.g. for ionic polymerization techniques. However, pyrene and similar dyes generally have a low emission yield and a low solubility in organic solvents.[149] Also, the chromophores tend to undergo some interchain interaction via hydrophobic interactions in water.[145,150] Another problem might be that they can easily undergo excimer and exciplex formation. More hydrophilic dyes are fluorescein and rhodamine, which are, however, rather bulky and pH-sensitive. Smaller but still more hydrophilic than the purely hydrocarbon based chromophores are coumarin, naphthalimide and carbazole.

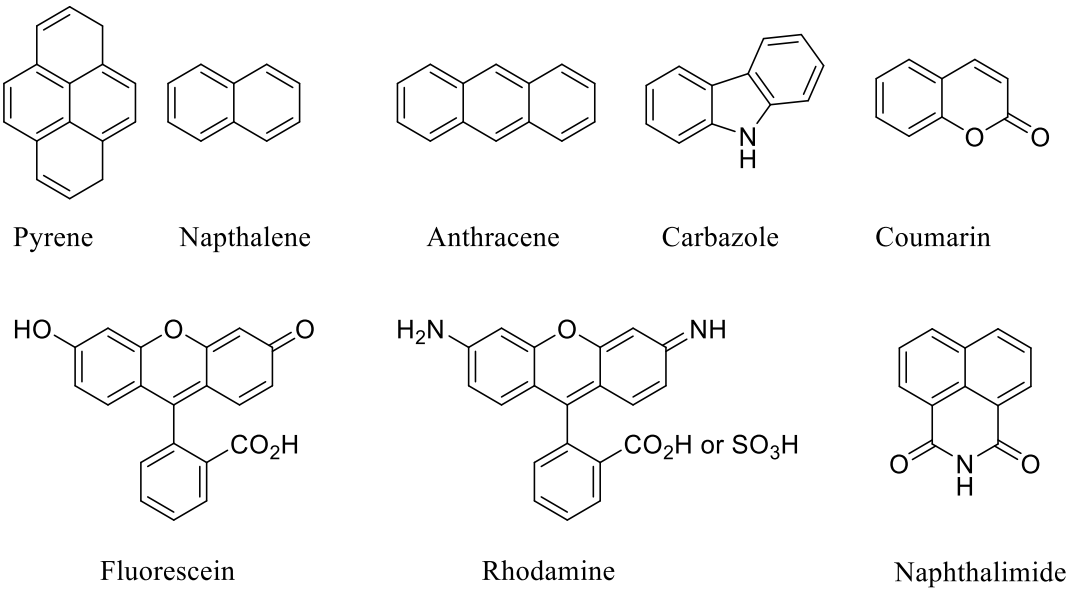

Figure 1.7: Structures of common dyes used for FRET.

FRET of heterochelic α,ω-dye functionalized polymers provides information on the distance of the chain ends, and is therefore used to characterize the conformations of polymer chains, intra- or intermolecular association and polymer chain dynamics: Sha et al.[151,152] introduced an anthryl moiety as the donor and a carbazoyl moiety as an acceptor to a CTA to produce PS and polymethacrylates via RAFT polymerization. They used the FRET pair to characterize the variation of chain dimensions in organic medium. Recently, Merckx et al. [153] synthesized thermoresponsive polyoxazolines bearing pyrene and coumarin structures on the opposite chain ends. Those polymers showed an increased FRET intensity above their phase transition in aqueous solution between 40 to 60 °C. Rager et al.[144] used FRET to study the influence of chain length and salt concentration

on the micellization of poly(acrylic acid)-b-poly(methyl methacrylate). Their FRET pair consisted of naphthalene as donor and pyrene as acceptor.

In this work, coumarin as the donor and naphthalimide as the acceptor were chosen because of their high extinction coefficients, large quantum yields, and good photostability. In addition, compared to pyrene, which is very sensitive to quenching by oxygen[154] or halides,[155,156] naphthalimides[157] need special designs such as protonable moieties to become sensitive to quenching. Importantly, the emission spectrum of specific coumarins overlaps very well with the naphthalimide absorption.[158–160] The detailed approach is described in chapter 6.

2 OBJECTIVES AND MOTIVATION

As described in the previous chapters, amphiphilic block copolymers are especially useful as rheological modifiers or "thickeners" for microemulsions. The classical structure of such polymers bears two hydrophobic blocks on opposite chain ends, which can stick to the oil phase, and a long hydrophilic center block that solubilizes the polymer in water.[77,161] However, it would be interesting to control the rheology of microemulsions by an external stimulus. In this thesis, I introduce a thermoresponsive block instead of the second permanently hydrophobic block to control the aggregation behavior via temperature (Figure 2.1).

Figure 2.1: Classical vs. new structure of amphiphilic block copolymer; red = permanently hydrophobic block, blue = hydrophilic block, green = thermoresponsive block.

Such thermoresponsive amphiphilic block copolymers can already form micellar aggregates at low temperatures due to their surfactant-like architecture. With increasing temperature, the thermoresponsive blocks switch from hydrophilic to hydrophobic and the interaction among thermoresponsive blocks is preferred. Therefore, the small aggregates can further connect and form a network via bridging of the thermoresponsive blocks (Scheme 2.1).

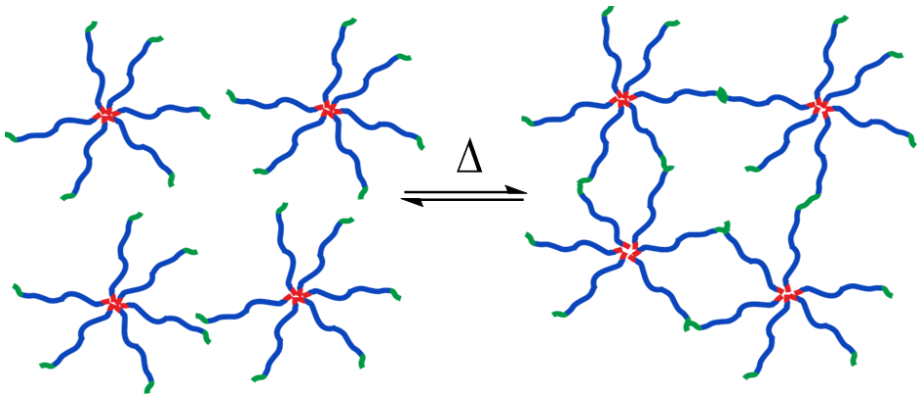

Scheme 2.1: Expected self-assembly of a linear thermoresponsive amphiphilic block copolymer in water; red = permanently hydrophobic block, blue = hydrophilic block, green = thermoresponsive block.

Alternatively, as the thermoresponsive blocks become hydrophobic, they might also undergo backfolding or they change position with the hydrophobic end group and remain in the hydrophobic core. Only few investigations on such hydrophobically modified thermoresponsive block

copolymers exist.[162,163] Therefore, the structure-property relationships of such diverse systems shall be explored. Starting from the basic architecture, increasingly complex architectures (Figure 2.2) shall be synthesized and parameters such as end groups, block length, and chemical structure (see Figure 1.3) of the thermoresponsive blocks be varied.

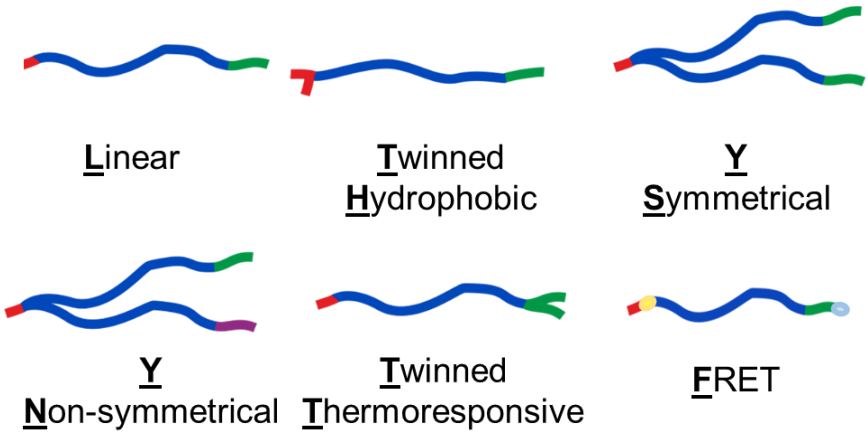

Figure 2.2: Targeted thermoresponsive amphiphilic block copolymers with linear L, twinned hydrophobic TH, symmetrical quasi-miktoarm YS, non-symmetrical quasi-miktoarm YN, twinned thermoresponsive and linear with fluorophores for FRET F architectures; 1-6: red = permanently hydrophobic block, blue = hydrophilic block, green = thermoresponsive block 1, violet = thermoresponsive block 2, yellow and light blue = fluorophores.

Controlled radical polymerization (CRP) techniques are used to obtain well-defined block copolymers with narrow dispersities. RAFT polymerization was chosen as the method of choice due to its applicability to a large range of monomers, tolerance towards many solvents, including water, and due to the effective introduction of functional end groups, such as the hydrophobic block or fluorophores (architecture **F**). For architecture **TT**, a second CRP technique was used, namely ATRP, to introduce the twinned thermoresponsive blocks. An even more complex compound is the non-symmetrical architecture **YN** bearing two different thermoresponsive blocks, which might also lead to a two-step transition. The influence of the varying parameters on the phase transition behavior in water is investigated by DLS and turbidimetry. Furthermore, complementary fluorophores are introduced to the opposite chain ends (architecture **F**) to analyze if network formation via bridging or flower-like micelles via back-folding occurs above the phase transition.

3 Chain Transfer Agents and Homopolymers

3.1 Synthesis and Characterization of Chain Transfer Agents

The chain transfer agents (CTAs) were designed to polymerize the acrylamides effectively, to enable characterization methods for the obtained polymers and to introduce the hydrophobic sticker group. The CTAs were therefore synthesized by alkylation of trithiocarbonate salts with alkyl halides following general literature procedures.[164] For the architectures **L**, **TT** and **YS**, the CTAs should introduce dodecyl chains as hydrophobic sticker groups via the R-group (Figure 3.1). This is a distinct advantage compared to most reported hydrophobically modified RAFT agents, where the hydrophobic group is placed at the hydrolysis sensitive Z-group.[165,166] Also for this reason, the dodecyl group is attached via an amide group instead of an easily hydrolyzable ester group. This approach also ensures that the hydrophobic sticker group is not lost when applied in aqueous systems such as microemulsions. On top of that, the used sticker group has the dodecyl group attached at the end of the benzamide group, which is the favoured structure for polymeric surfactants.[167] While for the basic linear **C12-CTA**, dodecylamine was used, the synthesis of the twinned hydrophobic **2C12-CTA** could be adapted easily by applying didodecylamine. For the alkylation of **C12Y-CTA**, a symmetrical benzamide analogue was employed to allow parallel chain growth of each arm. Additionally, the design should facilitate the molar mass characterization via NMR. Hence, a trimethylsilyl (TMS) group was implemented via the Z-group. These signals appear close to 0 ppm in the ^{1}H-NMR spectra, a region free of signals for most polymers and solvents, while the aromatic protons from the R-group appear around 8 ppm. The TMS group with its 9 protons appearing as a singlet facilitates not only the determination of the number average molar mass, but it also enables the estimation of the end group fidelity by comparing the integrals of R- and Z-groups.[168,169]

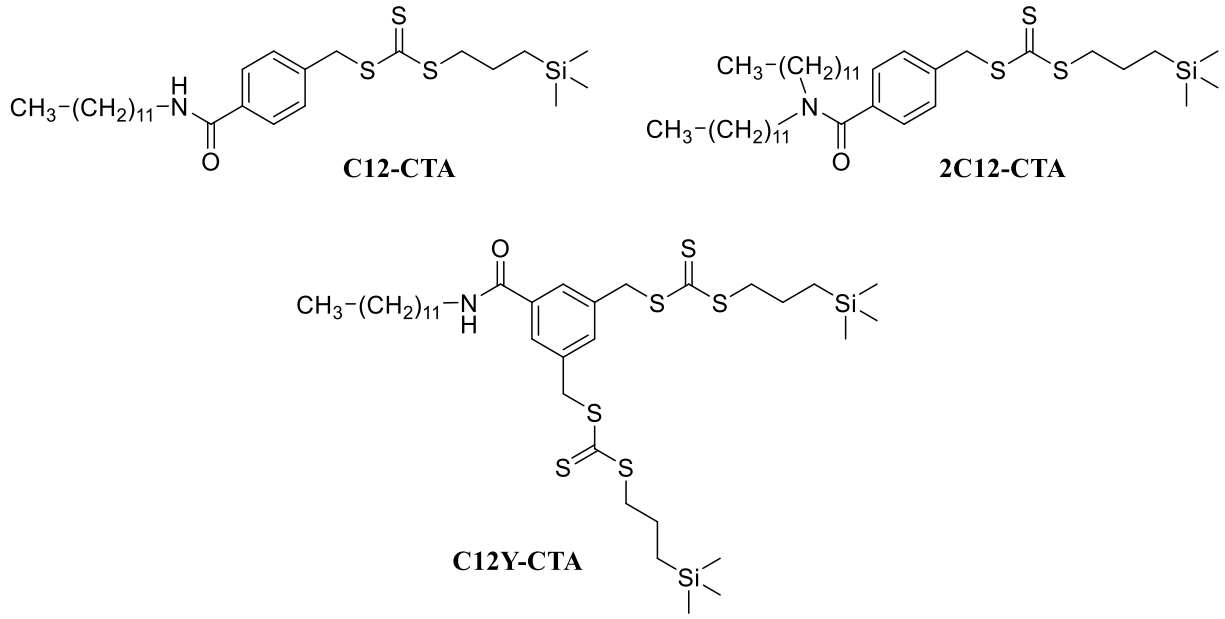

Figure 3.1: Chain transfer agents (CTAs) for linear (C12-CTA), twinned hydrophobic (2C12-CTA) and quasi-miktoarm (C12Y-CTA) architectures.

The synthesis of **C12-CTA** and **2C12-CTA** gave 39 % and 59 % yields, respectively. For **C12Y-CTA**, the yield was relatively low with 12 %, since monosubstituted side-products were produced due to statistics. However, these monosubstituted side-products could be reused in another synthesis leading to 51 % yield in total. The ^{1}H-NMR as well as ^{13}C-NMR the spectra of the CTAs are shown in Figure 3.2, Figure 3.3 and Figure 3.4. All ^{1}H-NMR spectra clearly show the characteristic singlet signal at around 4.6 ppm of the newly formed methylene-group between trithiocarbonate and phenyl group. The ^{13}C-NMR spectra also show the characteristic signal of the carbon of the trithiocarbonate group at around 220 ppm. Depending on the chemical structure, the aromatic protons appear as different signal patterns in the ^{1}H-NMR spectra. While the linear **C12-CTA** shows two well-separated signals of the aromatic protons, the same protons appear very close to each other for the twinned hydrophobic **2C12-CTA**. The **YC12-CTA** has a different pattern, since the aromatic ring is substituted in the 1,3,5-positions.

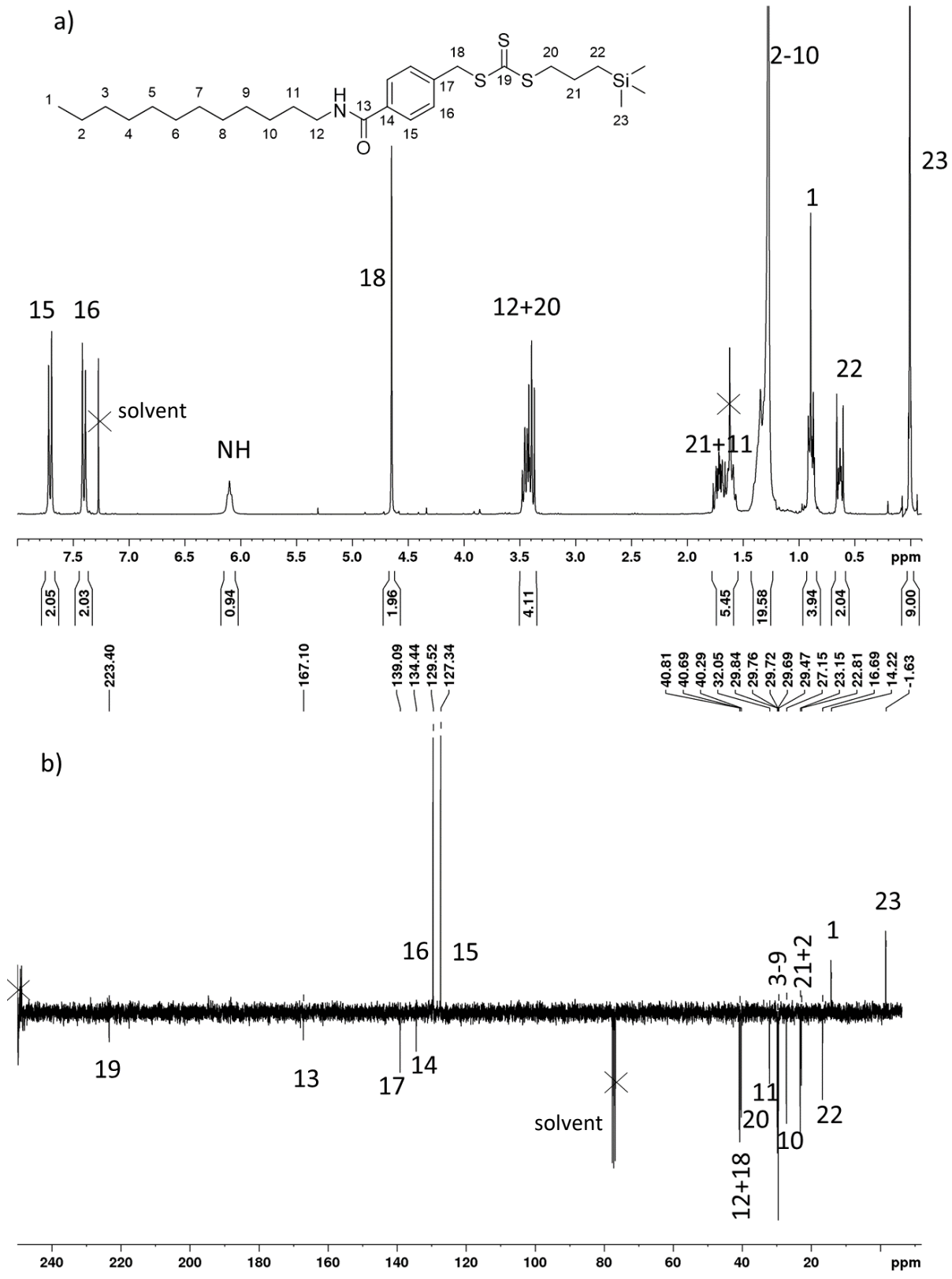

Figure 3.2: ^{1}H-NMR (a) and ^{13}C-NMR (APT mode) (b) spectra of **C12-CTA** in $CDCl_3$.

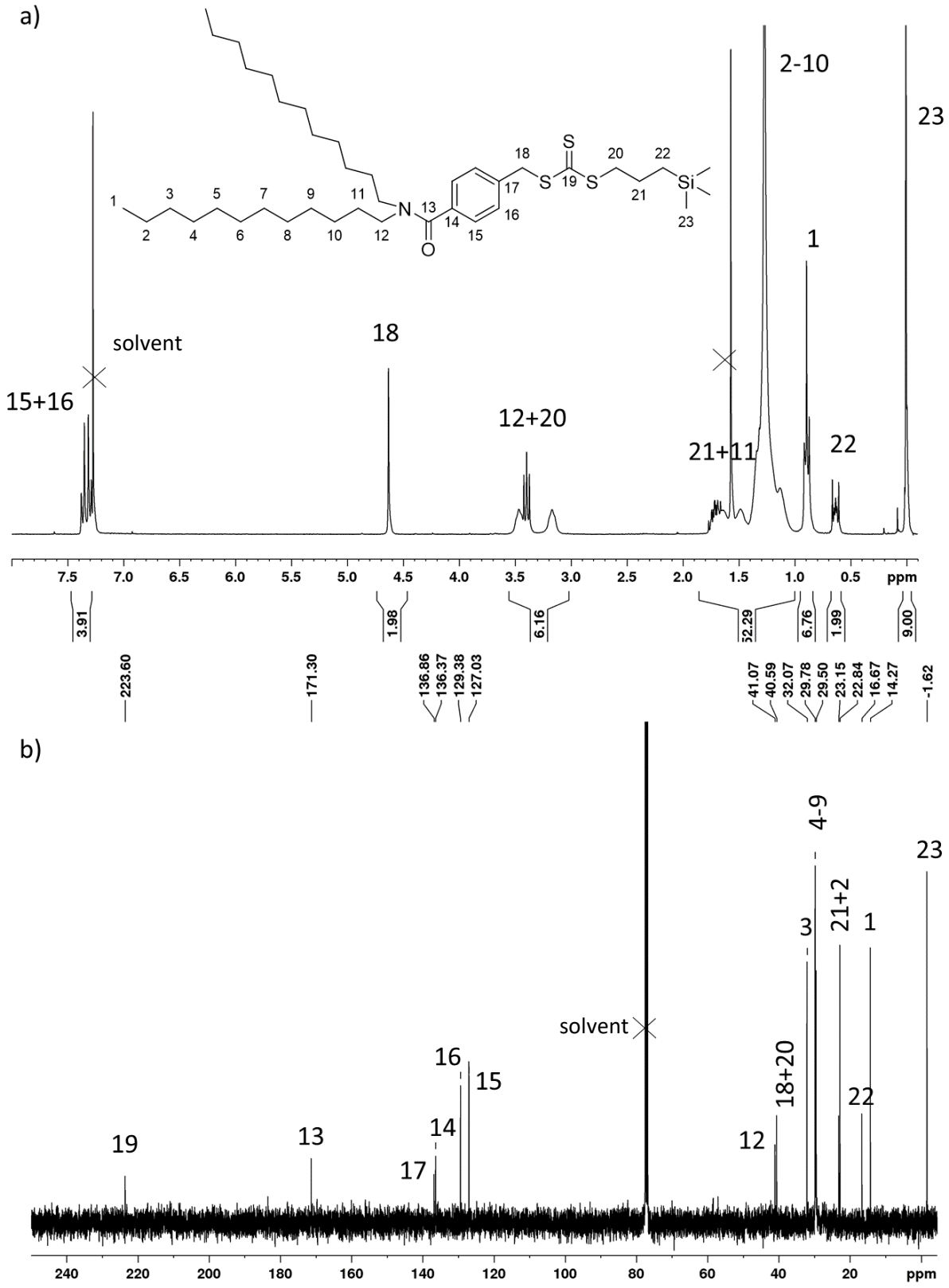

Figure 3.3: ^{1}H-NMR (a) and ^{13}C-NMR (b) spectra of **2C12-CTA** in $CDCl_3$.

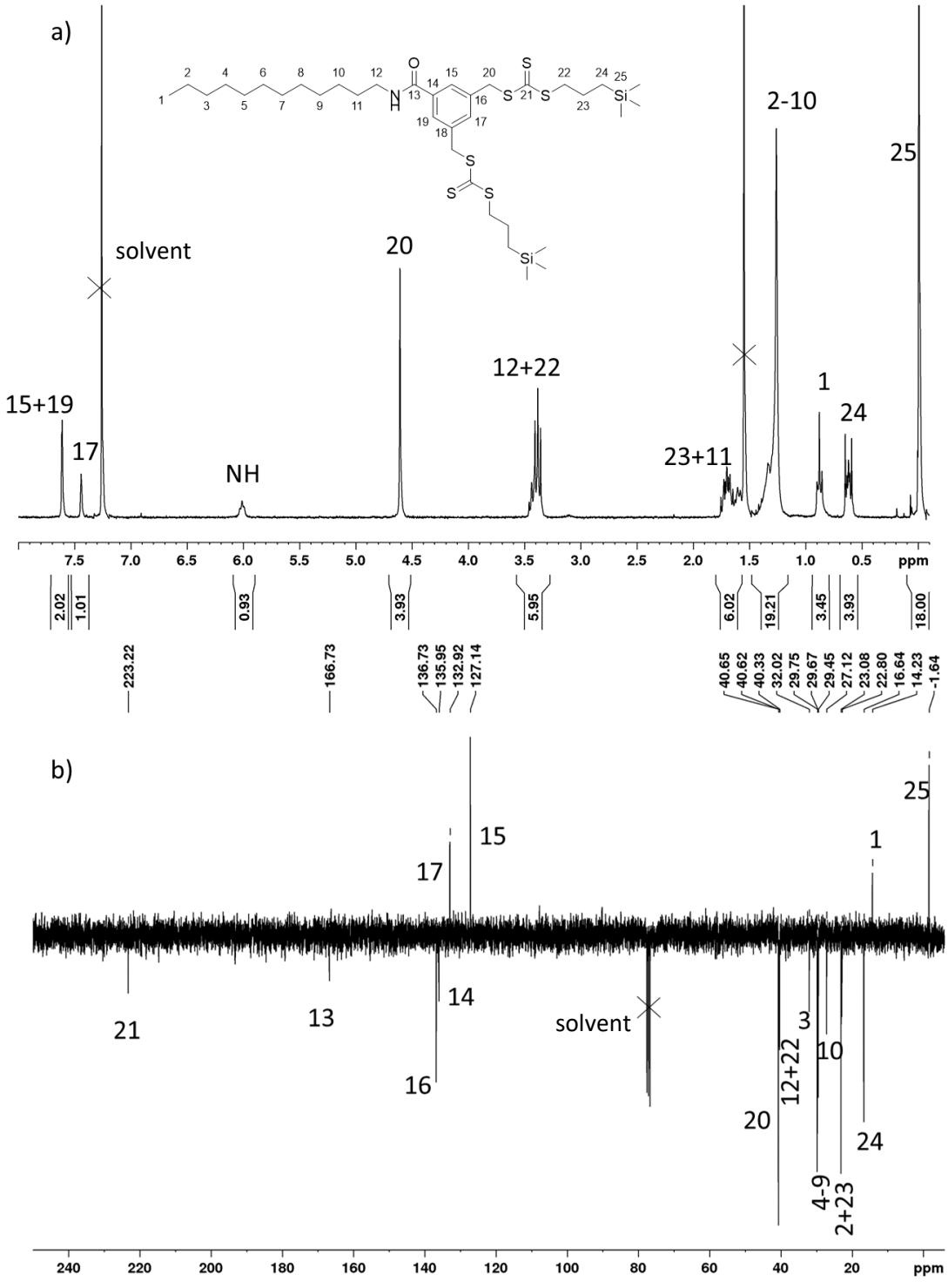

Figure 3.4: ^{1}H-NMR (a) and ^{13}C-NMR (APT) (b) spectra of **C12Y-CTA** in $CDCl_3$.

Another benefit of applying a trithiocarbonate-based CTA is the possibility of molar mass determination via UV/Vis spectroscopy. Since RAFT-generated polymers bear ideally one trithiocarbonate group per chain absorbing in the visible range due to an n- π* transition or near UV range due to a π-π* transition, this provides access to a convenient and sensitive end group analysis.[170] The UV-vis spectrometer measures the intensity of the transmitted light and gives the ratio between irradiated and transmitted light as the absorbance *A*. According to Lambert-Beer's law (equation 3.1), *A* is direct proportional to the molar concentration c_{mol} of an absorbing substance in a diluted solution with extinction coefficient ε and the path length *d* of the light:

$$A = \varepsilon * c_{mol} * d \qquad 3.1$$

For polymers, the molar concentration can be replaced by the mass concentration c_{mass} and the number average molar mass $M_n^{UV\text{-}Z}$ (equation 3.2):

$$c_{mol} = \frac{c_{mass}}{M_n^{UV}} \qquad 3.2$$

Combining and rearranging equation 3.1 and equation 3.2 gives equation 3.3:

$$M_n^{UV} = \frac{\varepsilon * c_{mass} * d}{A} \qquad 3.3$$

With this final equation, the number average molar mass $M_n^{UV\text{-}Z}$ can be calculated by UV-vis spectroscopy assuming full end group functionality and no change of λ_{max} and ε.

3.2 Synthesis and Characterization of Homopolymers

The polymerization of DMAm was carried out in benzene with 1,1'-azobis(cyclohexane-1-carbonitrile) (V-40) as the initiator. V-40 has a half life-time of 10 h at 88 °C, thus enabling to conduct the polymerization at elevated temperatures of 90 °C and favoring fast propagation. The [trithiocarbonate group]:[V-40] ratio was kept at 10:1 to ensure high end group fidelity and thus high livingness for the second polymerization step. Benzene was the solvent of choice because it dissolved well monomer, CTA, and final polymer, and because of its virtual inertness to radicals.[32] The polymerization worked well for concentrations of monomer plus (macro)CTA of 20 or 33 wt%. Nevertheless, with concentrations of 33 wt%, higher conversions were reached after the same time. More details about the reaction parameters can be found in Table 10.2 of the Experimental Part. Table 3.1 summarizes the analytical data of the synthesized homopolymers.

Table 3.1: Results of PDMAm from RAFT polymerization with C12, 2C12 and C12Y-CTA (see Figure 0.1a in case for linear, twinned hydrophobic, and Y-symmetrical architectures).

Code	Polymer	CTA	Yield %	Theo		NMR-Z[d]			SEC		UV-Z
				M_n kg/mol	DP_n	M_n kg/mol	DP_n	Z/R[e]	M_n kg/mol	Đ	M_n kg/mol
L1a	C12-PDMAm$_{213}$	C12	83	17 [a]	168	22	213	1.0	18	1.25	19
L1b	C12-PDMAm$_{157}$	C12	63	13 [a]	127	16	157	1.0	14	1.18	14
TH1a	2C12-PDMAm$_{193}$	2C12	57	16 [b]	158	20	193	1.0	18	1.14	18
TH1b	2C12-PDMAm$_{178}$	2C12	57	16 [b]	158	18	178	1.0	17	1.22	21
YS1	C12Y-PDMAm$_{181}$	C12Y	75	35 [b]	172 [c]	37	181 [c]	1.0	30	1.14	34

[a] determined by yield, [b] determined by conversion of monomer peaks in ^{1}H-NMR by comparing the signals at 0 h and after the final reaction time, [c] per arm, [d] calculated using integrals of TMS group, [e] calculated by comparison of the integrals of the aromatic protons and the TMS-group. Precision of all molar mass values is ± 20 %.

The ^{1}H-NMR spectra of the PDMAm samples **L1a**, **H1a** and **YS1** are shown in Figure 3.5 to Figure 3.7.

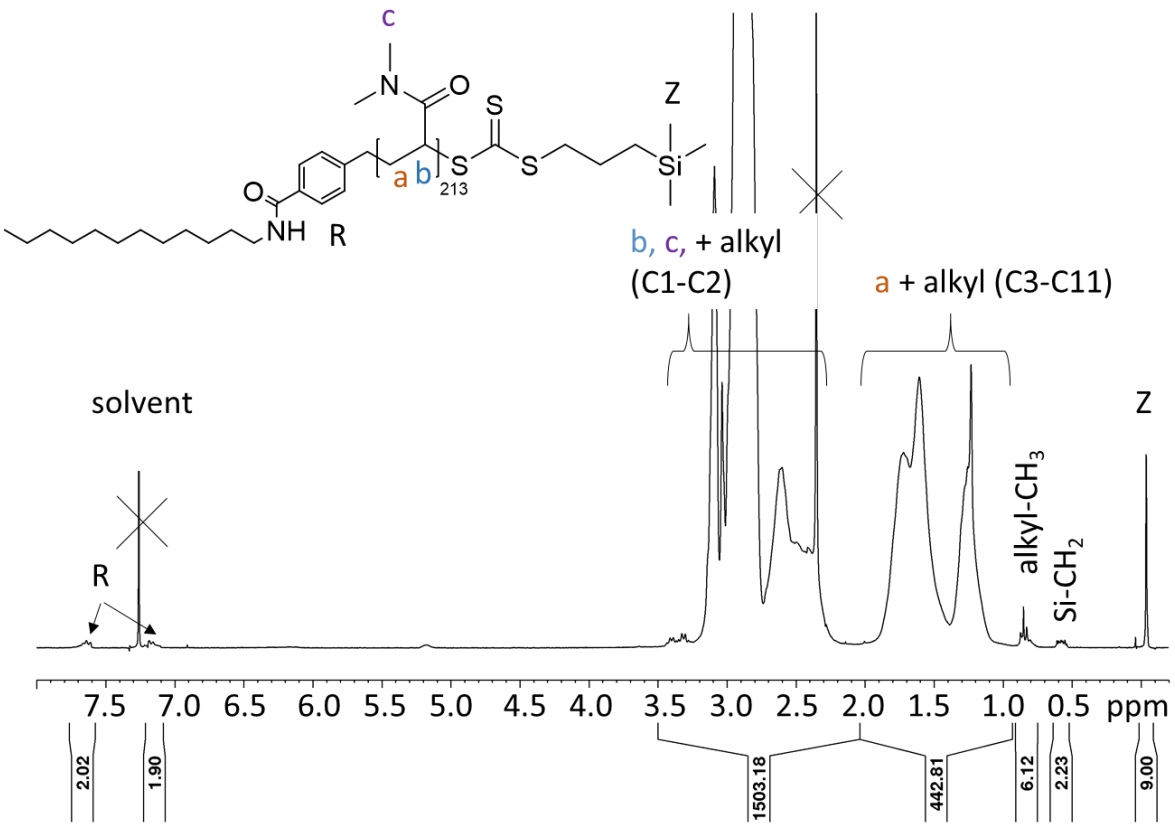

Figure 3.5: ^{1}H-NMR spectrum of PDMAm **L1a** in $CDCl_3$.

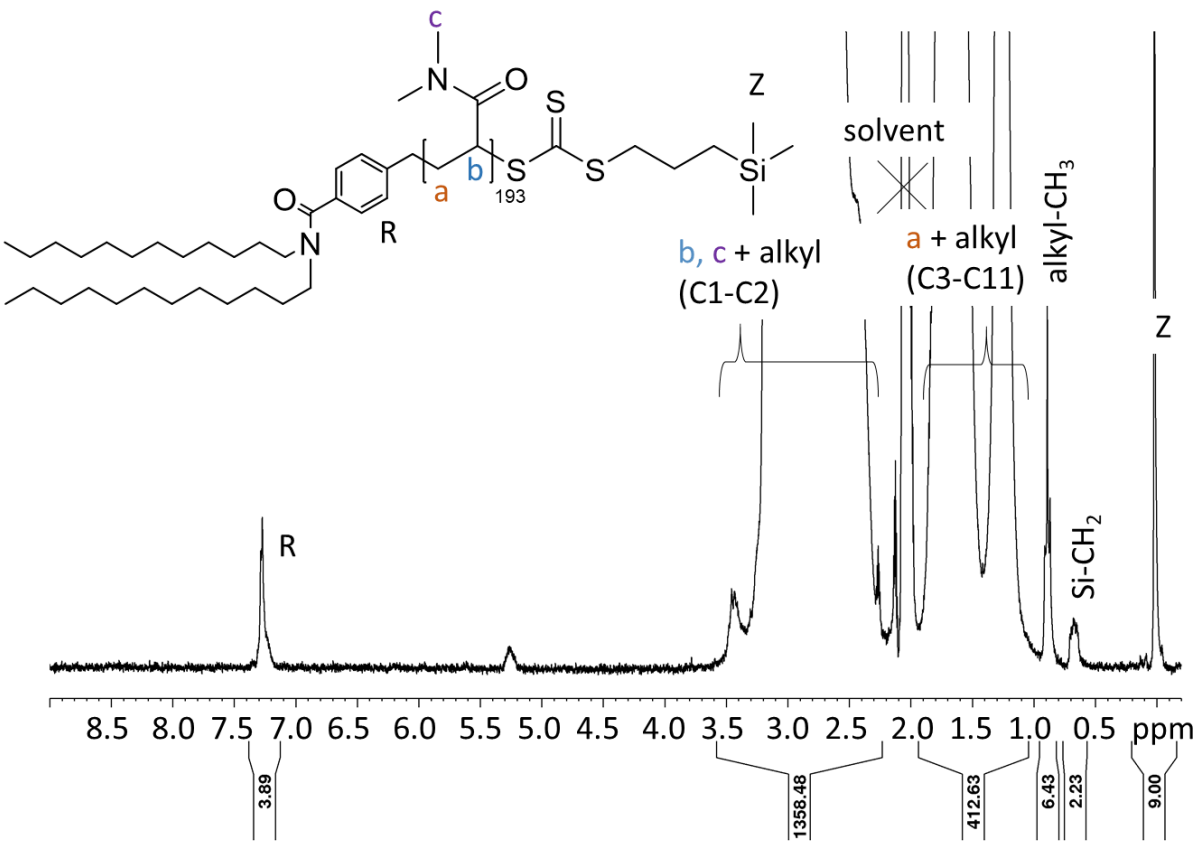

Figure 3.6: ^{1}H-NMR spectrum of PDMAm **H1a** in acetone-d_6.

The intense singlet of the TMS-group is well visible for all PDMAm samples. Also the aromatic protons from the R-group appear well separated from the other signals and can be used to determine the end group fidelity. The aromatic protons in the different polymer samples show the characteristic patterns from the different CTAs applied.

The polymers were characterized by various methods showing similar results of the molar mass and relatively low dispersities Đ of < 1.3. This is already a good indication for a controlled polymerization procedure. Assuming ideal conditions for the RAFT polymerization process, the theoretically expected number average molar mass M_n^{theo} can be calculated from the molar ratio of the monomer to the RAFT agent employed that is corrected by the monomer conversion (equation 3.4).

$$M_n^{theo} = conversion * \frac{[monomer]_0}{[CTA]_0} * M_{monomer} + M_{CTA} \qquad 3.4$$

The intense singulet signal of the TMS-group was a useful tool to estimate the end group fidelity by comparing the integrals of the Z and R group signals (see Figure 3.7). The TMS-signal also allowed the determination of M_n^{NMR} as well as DP_n^{NMR} using the respective polymer integrals normalized to the TMS signal and divided by the number of protons of the respective repeat unit, such as 9 for DMAm (see equations 3.5 and 3.6).

$$DP_n^{NMR} = \left(\frac{\int a + \int (b + c)}{9}\right) \quad 3.5$$

$$M_n^{NMR} = DP_n^{NMR} * M_{monomer} + M_{CTA} \quad 3.6$$

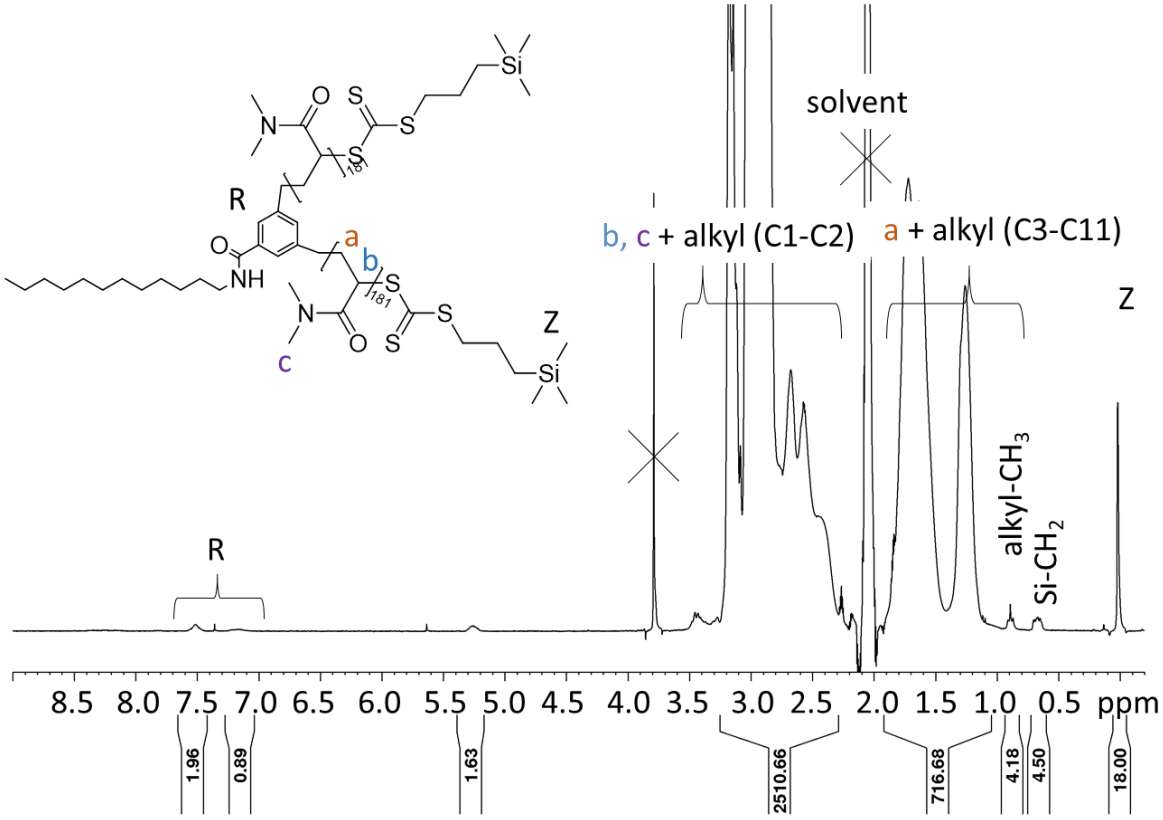

Figure 3.7: ^{1}H-NMR spectrum of PDMAm **YS1** in acetone-d_6.

The R/Z ratio was always 1.0, indicating indeed a high end group fidelity, which is important for the introduction of the second, thermoresponsive block. Furthermore, size exclusion chromatography (SEC) was used to determine M_n^{SEC} and dispersities Đ (calibrated to PS), leading to M_n^{SEC} values that agree very well with M_n^{theo}. The trithiocarbonate moiety in the Z-group allows the determination of the number average molar mass by UV-vis spectroscopy due to a prominent absorption band around 307 nm and an extinction coefficient ε in the order of 10^4 L mol^{-1} cm^{-1} using equation 3.3.[170] Notably, M_n^{NMR-Z} and M_n^{UV-Z} agree reasonably well with the other molar

mass values suggesting good preservation of the Z-group during the polymerization process. Still, both tend to be slightly higher than M_n^{theo} pointing to a certain amount of inevitable loss of the Z-group due to the inherent RAFT mechanism.[171] The values might also be higher than expected, since low molar mass polymer chains were lost during precipitation. Another reason for the slightly higher values of M_n^{UV-Z} might be the approximation that λ_{max} and ε do not change when the trithiocarbonate group is transferred from the CTA to the polymer. However, the absorptivity of the trithiocarbonate moiety is relatively sensitive towards changes in the micro-environment, so that λ_{max} and ε might be slightly shifted after the polymerization process.[170]

For the permanently hydrophilic DMAm block, the degree of polymerization DP_n was chosen to be between 150 and 200 to ensure a well soluble polymer even above phase transition of the thermoresponsive blocks. In any case, the hydrophilic chain must be long enough to be able to bridge aggregates for acting as effective associative thickener.

3.3 Behavior of Homopolymers in Water

The temperature-dependent behavior of the PDMAm homopolymers in water was investigated with DLS for concentrations of 5 $g \cdot L^{-1}$ (Figure 3.8). Since PDMAm is fully soluble in the temperature range of water,[172,173] the hydrodynamic diameter of the polymers remained virtually constant. Depending on the architecture, however, the sizes slightly differed from each other. The sample **L1b** with basic linear architecture shows the lowest hydrodynamic diameter of around 9 nm. The larger and more hydrophilic sample **YS1** has a slightly higher average diameter of 11 nm. The sizes of these structures are well comparable with the ones obtained by Herfurth et al.[174] who synthesized PDMAm homopolymers with varying number of arms and end-capped with dodecyl chains. The more hydrophobic PDMAm sample **TH1**, however, forms aggregates with an average diameter of 28 nm, which is more than twice the size than the other architectures. This suggests that the presence of two C12 groups allows the formation of larger aggregates than with only one C12 group. The sample **YS1** bearing also only one C12 group, but in the center of two hydrophilic PDMAm arms instead of at the chain end, might be more hindered in the formation of aggregates compared to the other two architectures.

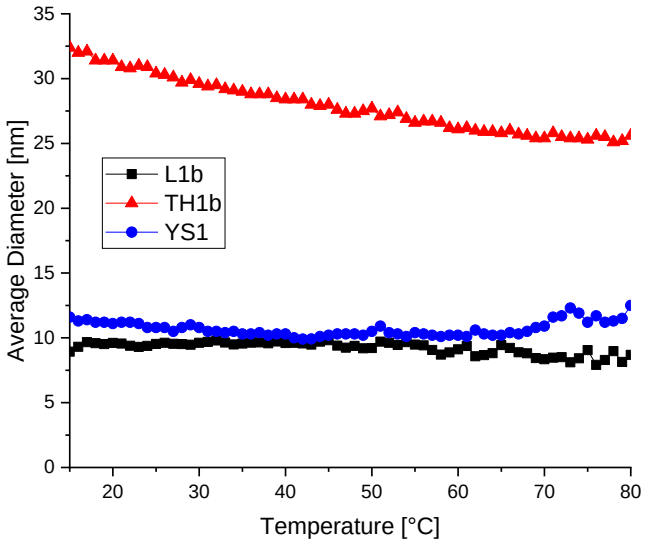

Figure 3.8: DLS measurements of aqueous 5 g·L^{-1} solutions of PDMAm homopolymers **L1b**, **TH1b** and **YS1**.

4 QUASI TRIBLOCK COPOLYMERS

4.1 SYNTHESIS AND CHARACTERIZATION OF BLOCK COPOLYMERS

The block copolymers with varying thermoresponsive blocks were synthesized via consecutive RAFT polymerizations according to the polymerization of PDMAm homopolymers with a [macroCTA]:[initiator] ratio of 10:1 in benzene. For a concentration of 33 wt%, high conversions up to 99 % could be achieved within 4 h. Still, the obtained yield is usually around 70 % due to the twofold precipitation during the workup process, in which some, in particular of the lower molar mass polymer chains were lost. More details about the reaction parameters can be found in Table 10.3. The results obtained from the molecular characterization are shown in Table 4.1.

Table 4.1: Molecular characteristics of the block copolymers derived from **L1** and **TH1** (see Figure 0.1a in case for linear and twinned hydrophobic architectures).

Code	Polymer	Yield %	Theo [a]		NMR-Z [b]			SEC		UV-Z
			M_n kg/mol	DP_n [c]	M_n kg/mol	DP_n [c]	Z/R [d]	M_n kg/mol	Đ	M_n kg/mol
L1a-2a	$C_{12}DMAm_{213}NiPAm_{11}$	74	19	15	23	11	0.9	21	1.25	25
L1a-2b	$C_{12}DMAm_{213}NiPAm_{34}$	82	21	33	25	34	0.9	22	1.26	25
L1b-2c	$C_{12}DMAm_{157}NiPAm_{66}$	77	19	50	24	66	-	23	1.21	26
L1a-3a	$C_{12}DMAm_{213}DEAm_{14}$	70	19	15	23	14	0.8	19	1.19	23
L1a-3b	$C_{12}DMAm_{213}DEAm_{45}$	67	20	27	27	45	0.9	22	1.25	25
L1b-3c	$C_{12}DMAm_{157}DEAm_{90}$	74	19	48	27	90	1.0	21	1.18	23
L1a-4a	$C_{12}DMAm_{213}NAP_{18}$	80	19	15	24	18	0.9	21	1.16	32
L1a-4b	$C_{12}DMAm_{213}NAP_{36}$	65	20	27	26	36	0.8	24	1.16	30
L1b-5a	$C_{12}DMAm_{157}NPAm_{45}$	72	17	31	21	45	0.8	20	1.25	28
TH1a-2	$2C_{12}DMAm_{193}NiPAm_{18}$	70	19	21	22	18	-	21	1.14	29
TH1a-3	$2C_{12}DMAm_{193}DEAm_{25}$	69	19	22	23	25	0.9	20	1.13	22
TH1a-5	$2C_{12}DMAm_{193}NPAm_{32}$	73	20	32	24	32	1.1	24	1.18	33

[a] determined by conversion of monomer peaks in ^{1}H-NMR by comparing the signals at 0 h and after the final reaction time, [b] calculated using integrals of TMS group, [c] values are related to the second block, [d] calculated by comparison of the integrals of the aromatic protons and the TMS-group. Precision of all molar mass values is ± 20 %.

A typical spectrum of a block copolymer with linear architecture is depicted in Figure 4.1 and with twinned hydrophobic architecture in Figure 4.2. The spectra exemplify the well-resolved signals of the aromatic protons from the R and the TMS signal of the Z-group. These signals allow the

determination of the molar mass and the end group fidelity by ^{1}H-NMR. All the other block copolymer spectra can be found in the Appendix.

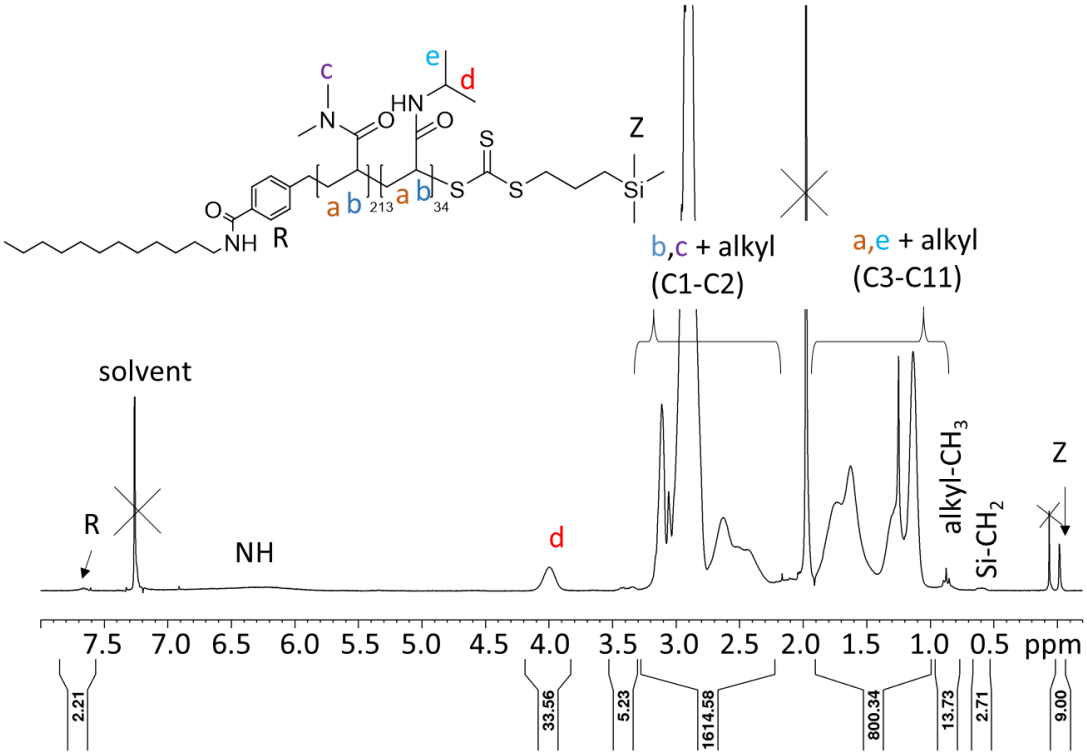

Figure 4.1: ^{1}H-NMR spectrum of **L1a-2b** in $CDCl_3$.

As for the homopolymers, molar masses of the block copolymers were determined by various methods to ensure a precise analysis of the samples. The obtained results match very well with each other, and the molar mass distributions are rather narrow with $Đ \leq 1.3$, indicating successfully controlled polymerizations. However, the dispersity Đ is probably slightly underestimated due to the twofold precipitation, in which low molar mass polymer fractions were mostly removed. Again, the R/Z ratio is high, being throughout > 0.8, and M_n^{NMR-Z} and M_n^{UV-Z} match reasonably well with the other molar mass values, indicating a high preservation of the Z-group during the polymerization process. However, the Z/R ratios are slightly decreased compared to the homopolymer precursors, and M_n^{NMR-Z} and M_n^{UV-Z} tend to be slightly higher than M_n^{theo} pointing to a certain amount of inevitable loss of the Z-group after the second RAFT polymerization step. Additionally, the twofold precipitation probably leads to an overestimation of the end group derived values. While the length of the permanently hydrophilic DMAm block was kept around 200 repeat units to be able to bridge the aggregates even in more dilute/semidilute conditions, much shorter block lengths for the thermoresponsive blocks ranging from 20 to 60 were implemented to study their influence on the phase transition behavior.

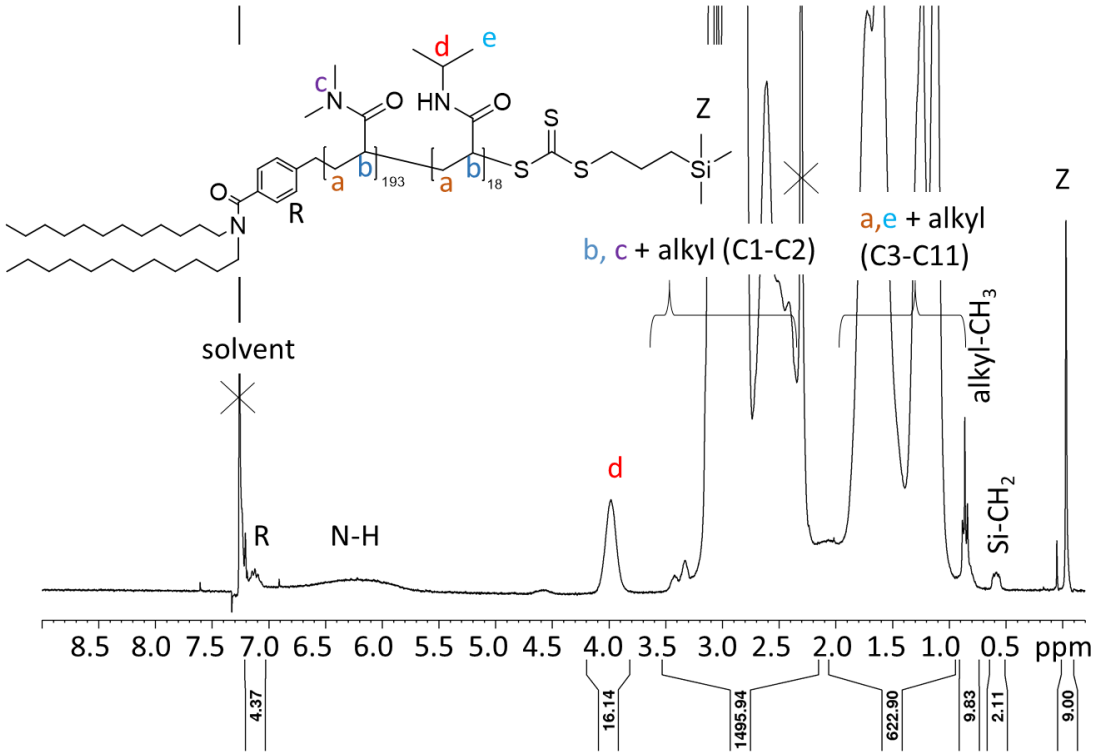

Figure 4.2: ^{1}H-NMR spectrum of **TH1a-2** in $CDCl_3$.

4.2 Phase Transition Behavior of Block Copolymers

The phase transition behavior of the thermoresponsive block copolymers was investigated by temperature dependent DLS (Figure 4.3 and Figure 4.4). While PDMAm is soluble in water from 0 to 100 °C, the homopolymers of NPAm, NiPAm, DEAm and NAP show typically LCST phase transitions around 25 °C,[175] 32 °C,[47] 33 °C,[50], and 56 °C.[176] Well below the phase transition temperature, the block copolymers are water soluble and form small aggregates with hydrodynamic diameters d_h around 20 – 30 nm. With increasing block size, the CP's of the block copolymers bearing PNiPAm and PDEAm as thermoresponsive blocks approach the ones of the respective polymers. For temperatures above the phase transition, the block copolymers bearing very short thermoresponsive blocks with $DP_n < 20$ showed no macroscopic phase separation, which is attributed to the very small block size and to the hydrophilic block increasing the phase transition temperature beyond the measurable range in water. This dependency on the block length was also observed by Convertine et al.[73] for PDMAm-b-PNiPAm diblock copolymers as well as PDMAm-b-PNiPAm-b-PDMAm diblock copolymers with carboxy and ethyl group on the opposite chain ends.[73]

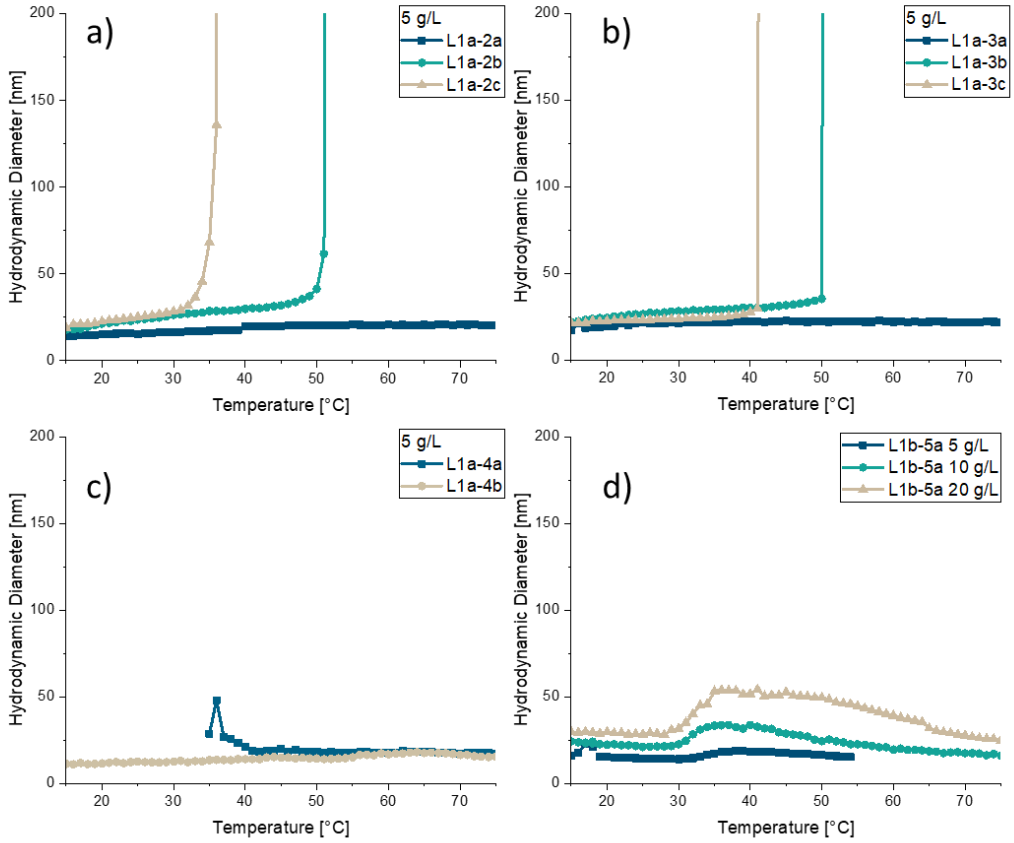

Figure 4.3: Temperature dependent DLS measurements of aqueous solutions of the linear block copolymers a) PDMAm-b-PNiPAm b) PDMAm-b-PDEAm c) PDMAm-b-PNAP and d) PDMAm-b-PNPAm series (cf. Table 4.1).

However, the size of the aggregates for these diblock and ABA triblock copolymers were much smaller even above the phase transition of the polymers compared to the here described block copolymers. This interesting effect might occur due to the different chain ends, since the dodecyl sticker group seems to enable the preorganization of aggregates, which can further form larger aggregates above the phase transition of the switchable blocks. In any case, the block copolymers described by Convertine et al.[73] can form micellar structures above the phase transition, when the PNiPAm blocks were turned hydrophobic. Although the LCSTs of homopolymers PNiPAm and PDEAm have virtually the same value of about 32 °C, for the block copolymer **L1b-2c** the CP is around 35 °C for a concentration of 5 g·L^{-1}, whereas the CP of **L1b-3c** is observed at more elevated temperatures of 41 °C (Figure 4.3a-b). The different LCST types of the thermoresponsive polymers, namely Flory-Huggins-like type I for PDEAm but type II for PNiPAm might explain this difference.[18] The block copolymers bearing PNAP as the thermoresponsive block did not show a

phase transition up to a temperature of 80 °C at concentrations of up to 5 g·L^{-1} (Figure 4.3c). Since the CP of the homopolymer PNAP, which also displays LCST behavior type I, is already quite high with about 55 °C, it seems likely that the additional hydrophilic PDMAm block increases the CP further, so that it is no longer in the interesting temperature range for water. Similar observations were also made for PNiPAm-b-PDMAm-b-PNAP block copolymers by Skrabania et al.[13] While a CP at around 45 °C was found accompanied by a maximum hydrodynamic diameter of 500 nm for the phase transition of the PNiPAm block, no second phase transition was seen for the PNAP block. It appears that the attached DMAm block increased the phase transition temperatures of the thermoresponsive blocks, so that for the PNAP block it is not visible in the temperature range of water anymore.

Importantly, the Z group bearing the hydrophobic TMS group, which is directly attached to the thermoresponsive block, decreases the phase transition temperature of the polymers in its turn, counteracting the effect of the hydrophilic block partially. When the Z group was intentionally removed by aminolysis and the thiol group quenched by subsequent thiol-ene chemistry with propargyl acrylate (see Experimental Part), the CP for **L1a-3b** increased from 50 °C to 59 °C for a concentration of 5 g·L^{-1}. This shows the strong effect of the small hydrophobic end group on the CP (see Appendix, Figure 11.5). Note that, however, for larger hydrophobic groups capable of forming separate domains in water, such as the sticker group, their effect of on the phase transition temperature tends to vanish.[164,177]

The block copolymer **L1b-5a** with PNPAm as the thermoresponsive block showed a very different behavior compared to the block copolymers bearing PDEAm and PNiPAm instead (Figure 4.3d). Upon a phase transition around 30 °C, the size of the aggregates increased gradually until reaching a maximum size, after which it slowly decreased again. This behavior is intensified with higher concentrations. However, the aggregate sizes always remain below an average diameter of 100 nm. This thermoresponsive behavior of the block copolymers was also visible in turbidimetry measurements (see Appendix Figure 11.6 & Figure 11.8). While for the PDMAm-b-NiPAm and PDMAm-b-PDEAm block copolymers, the transmission decreased from 100 down to 40 – 0 % depending on the concentration, the transmission of PDMAm-b-PNPAm block copolymer **L1b-5a** remains almost unchanged at 100 % up to a concentration of 10 g L^{-1}. However, when the relatively high concentration of 20 g·L^{-1} is reached, the aqueous system of **L1b-5a** showed only a weak drop of the transmission from 100 to 90 % in an apparent two-step transition. In the first step, the transmission starts to decrease slightly at around 30 °C, which is slightly higher than the phase transition temperature of 25 °C known for PNPAm.[175] Probably, the deviation is caused again by

the hydrophilic PDMAm block attached to the thermoresponsive block, elevating the phase transition temperature. In a second step, the transmission decreases more sharply, but after reaching a minimum at around 65 °C, it increases again. This two-step transition process also appeared in the cooling cycle indicating a reversible aggregation process. Nevertheless, the hysteresis between heating and cooling curves is large, which seems typical for thermoresponsive polyacrylamides bearing NH groups like PNiPAm. These groups allow intramolecular hydrogen bonding between the amide groups in the collapsed state acting as physical crosslinking points, which must be unmade during the re-dissolution process.[178] Upon phase transition of the block copolymers **L1a-2b** and **L1a-3b** with medium sized thermoresponsive blocks, the systems macroscopically separated into a polymer-rich and a polymer-poor phase, so that no correct cooling curve could be detected. However, when the systems were stirred, the clouding behavior was reversible due to phase separation process (see Appendix Figure 11.7). Interestingly, for larger thermoresponsive PNiPAm and PDEAm blocks as well as for **L1b-5a** having PNPAM as the thermoresponsive block, fully reversible phase transitions were observed without stirring (see Appendix Figure 11.8). This behavior agrees well with the formation of stable mesoglobules as described for PNiPAm homopolymer.[179,180] Stable aggregates were also observed for poly-*N*-ethylacrylamide-b-PNPAm (PNEAm-b-PNPAm) block copolymers for different block lengths, even above the phase transition of ~70 °C of PNEAm though the block copolymers consist then only of water-insoluble blocks.[140] However, when the block length of the hydrophilic PNEAm was lower than the collapsed PNPAm block, the formation of clusters was visible in transmission electron microscopy. The tendency towards cluster formation was explained by the relatively short hydrophilic PNEAm block, which might be insufficient to stabilize isolated micelles. Similar to **L1b-5a**, for block copolymers with shorter PNPAm blocks compared to hydrophilic PNEAm blocks, less turbid solutions were observed.[140] These findings suggest that not only the chemical structure of the thermoresponsive block, but also the ratio between hydrophilic and hydrophobic block plays an important role in the aggregation behavior of thermoresponsive block copolymers.

The block copolymers bearing a branched hydrophobic sticker group were synthesized to understand if the additional hydrophobic sticker group acts as a stronger anchor especially for the oil phase in microemulsions. Indeed, the additional hydrophobic end group in the sticker motif seems to allow larger aggregates compared to the linear block copolymers even below the phase transition in water (Figure 4.4). While the aggregates of the linear architectures **L1a-2a**, **L1a-3a** and **L1b-5a** had average diameters of around 20, 25 and 30 nm, the ones of the respective branched hydrophobic architectures **TH1a-2**, **TH1a-3** and **TH1a-5** had slightly higher average diameters of around 30, 30 and 45 nm.

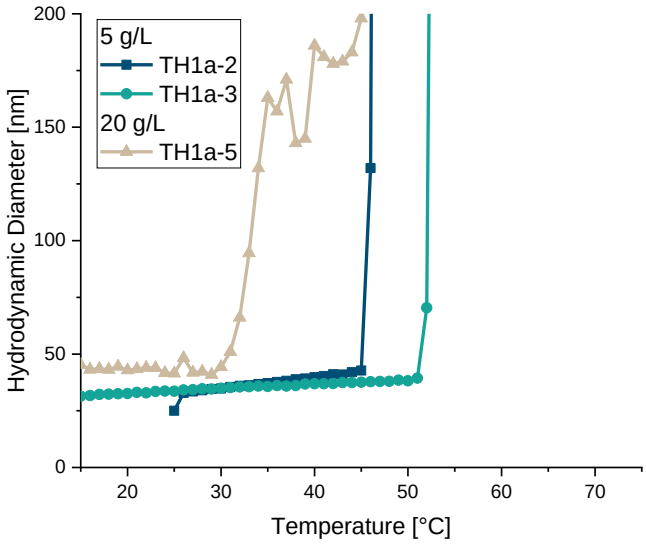

Figure 4.4: Temperature dependent DLS measurements of aqueous solutions of the branched hydrophobic block copolymers **TH1a-2**, **TH1a-3**, **H1a-5**.

Above the phase transition temperature, large aggregates with a hydrodynamic diameter d_h of > 300 nm were formed, even in the case of the PDMAm-b-PNPAm block copolymer **TH1a-5** for a concentration of 20 $g \cdot L^{-1}$. Similar to the linear architecture, the size increased suddenly in one step for PDMAm-b-PNiPAm **TH1a-2** at 45 °C, and for the PDMAm-b-PDEAm **TH1a-3** at 51 °C. For block copolymer **TH1a-5** however, the aggregates first increased at 30 °C from 45 to 150 nm, and only in a second step around 35 °C, the average diameter further increased to around 200 – 300 nm. Compared to the CP of the respective PNPAm homopolymer, these values are slightly increased, which is most probably caused by the attached hydrophilic PDMAm block. While the CP's of **TH1a-3** and of **TH1a-5** were virtually the same as of the reference with linear architecture, the CP of **TH1a-2** is relatively low compared to the linear equivalent **L1a-2b**. This behavior might be explained by some favored backfolding of the thermoresponsive PNiPAm block to the hydrophobic core of the aggregates, so that the hydrophobic environment reduces the CP of the PNiPAm block. Still, this does not explain why the other block copolymers with the twinned hydrophobic architecture bearing thermoresponsive PNPAm and PDEAm blocks do not show a reduced phase transition temperature. Additionally, the phase transition temperatures of block copolymers with these architectures are more sensitive to the concentration than the respective linear block copolymers (see Appendix Figure 11.6). On the one hand, while CP's of **L1a-2b** and **L1a-2c** differ by around 5 °C between the concentrations 1 to 5 $g \cdot L^{-1}$, the respective twinned

hydrophobic architectures **TH1a-2** and **TH1a-3** differ by up to 30 °C between 1 and 5 $g \cdot L^{-1}$. On the other hand, the CP's of **TH1a-5** for concentrations lower than 10 $g \cdot L^{-1}$ are less obvious to identify due to the smooth transition. Still, phase transition seems to occur around 30 °C for concentrations between 5 – 20 $g \cdot L^{-1}$. While for concentrations < 20 $g \cdot L^{-1}$, the transmission decreases only from 100 to 40 % up to a temperature of 80 °C, at 20 $g \cdot L^{-1}$, the solution becomes completely turbid and the two-step transition, which also appeared in the DLS measurement, is visible. Generally, the additional hydrophobic sticker group seems to have a rather high impact on the phase transition behavior, either by reducing the CP for **TH1a-2** and/or by allowing larger aggregates, visible as turbid solutions for **TH1a-5**.

5 HOMO- AND BLOCK COPOLYMERS OF BMOEAM

This chapter was already published in *Colloid and Polymer Science*[59] and thus, just changed slightly to fit into this thesis.

5.1 SYNTHESIS AND CHARACTERIZATION OF HOMO – AND BLOCK COPOLYMERS

Monomer bMOEAm was synthesized by the straightforward reaction of the amine with acryloylchloride, adapting previous procedures,[58,56] and the so far scarce molecular analytical data available were completed (see Experimental Part). Initially, bMOEAm monomer was homopolymerized by radical polymerization employing the RAFT method to control molar masses and minimize the polymers' dispersities Đ. For preparing a series of increasing molar masses of PbMOEAm **P6**, the established RAFT agent S-benzyl-S'-propyl trithiocarbonate **BPT** was employed as CTA.[181,182] More details about the reaction parameters can be found in the Appendix in Table 10.5. The key characteristics of the obtained polymers are compiled in Table 5.1. A typical ^{1}H-NMR spectrum is shown in Figure 5.1.

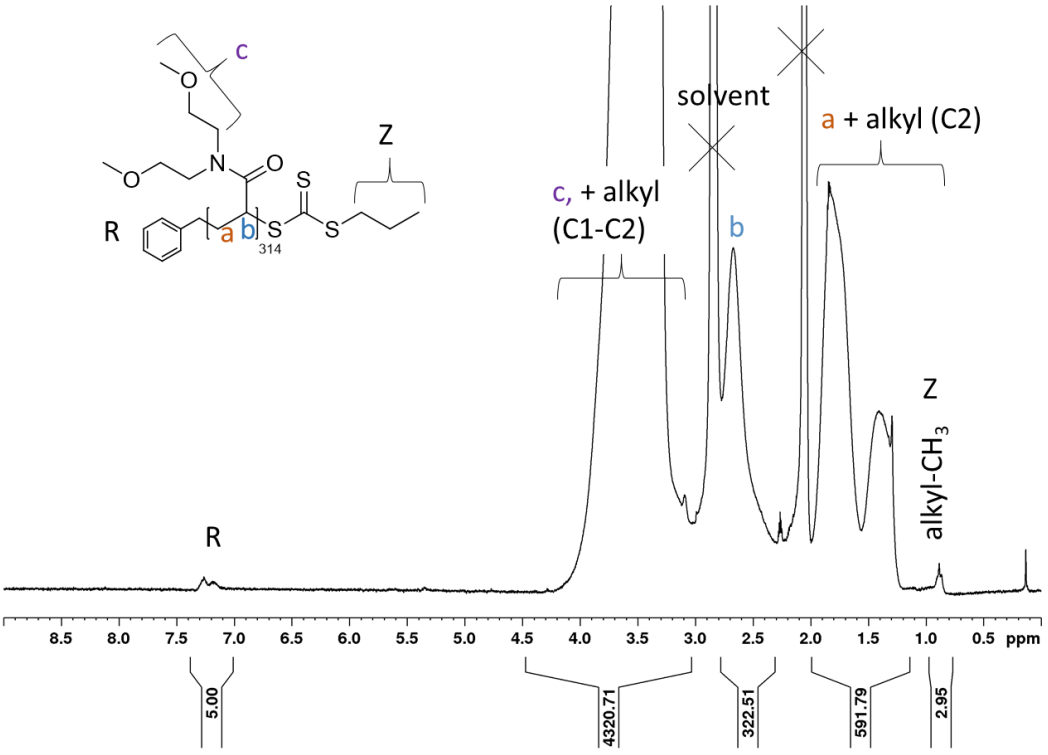

Figure 5.1: ^{1}H-NMR spectrum of bMOEAm homopolymer in acetone-d_6.

In analogy to statistical copolymers of 2-methoxyethylacrylate and DMAm,[183] all polymers **P6** were soluble in a large variety of solvents of strongly differing polarities, such as cold water, methanol, ethanol, trifluoroethanol, hexafluoropropanol, acetonitrile, *N*-methylpyrrolidone, dimethylsulfoxide (DMSO), ethyl acetate, acetone, α,α,α-trifluorotoluene, dioxane, tetrahydrofuran (THF), chloroform, dichloromethane, and benzene. Only diethylether and plain hydrocarbons such as pentane and hexane were found to be nonsolvents.

Table 5.1 Results of bMOEAm homo- and block copolymers from RAFT polymerization.

Code	Polymer	Yield %	Theo [a]		NMR-Z[b]			SEC		UV-Z
			M_n kg/mol	DP_n	M_n kg/mol	DP_n	Z/R[c]	M_n kg/mol	Đ	M_n kg/mol
P6a	C_3bMOEAm$_{10}$	68	1.9	9	2.1	10		1.4	1.20	2.1
P6b	C_3bMOEAm$_{29}$	78	4.9	25	5.7	29	0.9	3.2	1.26	4.9
P6c	C_3bMOEAm$_{54}$	68	10	53	9.8	54	-	6.3	1.21	15
P6d	C_3bMOEAm$_{141}$	61	32	168	27	141	0.8	18	1.19	44
P6e	C_3bMOEAm$_{314}$	91	51	269	59	314	0.9	27	1.25	180
P6f	C_3bMOEAm$_{524}$	91	99	528	98	524	1.0	51	1.18	93
L6a	C_{12}bMOEAm$_{185}$	59	29	152	35	185	0.9	13	1.46	37
L1b-6a	C_{12}DMAm$_{156}$bMOEAm$_{91}$	79	21	39	59	91	0.8	18	1.16	78
L1b-6b	C_{12}DMAm$_{156}$bMOEAm$_{99}$	71	39	99	-	-		26	1.17	-

[a] determined by conversion of monomer peaks in ^{1}H-NMR by comparing the signals at 0 h and after the final reaction time, [b] calculated using integrals of TMS group, [c] calculated by comparison of the integrals of the aromatic protons and the TMS-group. Precision of all molar mass values is ± 20 %.

Due to the low molar mass of the sample **P6b**, characteristic signals of both end groups can be easily distinguished in the spectrum, namely of the phenyl moiety originating from the R-group of **BPT** at 7.1 to 7.3 ppm, and of the methyl moiety of the *n*-propyl residue originating from the Z-group at about 0 ppm (Figure 5.1). The comparison of these signals enables calculation of the R/Z ratio and thus, the end group fidelity. Additionally, the Z-group corresponding to 3 protons was used to determine the number average molar mass M_n^{NMR-Z}. However, the accuracy inevitably decreases rapidly with increasing molar masses (see Appendix, Figure 11.32). Additionally, the thiocarbonyl moiety of the Z-group is a strong UV-chromophore with an absorbance maximum in the range of 305-310 nm and an extinction coefficient ε in the order of 10^4 L·mol^{-1}·cm^{-1}.[170] This allows for a rather sensitive determination of the polymer's Z-group content even for high molar masses when the value of ε is known, and thus to derive M_n^{UV-Z}. Furthermore, SEC was used to

analyze M_n^{SEC} and dispersities Đ (calibrated to PS). Altogether, the comparison of the various analytical molar mass data allows judging the controlled character of the polymerization, and in particular, to estimate the degree of Z-group fidelity. This is a crucial information for successful further chain extension in the synthesis of block copolymers. Analyzing the data for **P6a** – **P6f**, the dispersities Đ of 1.2 - 1.3 are relatively low, and M_n^{theo} and M_n^{NMR-Z} agree well with each other suggesting that the RAFT polymerization of bMOEAm is well controlled. Notably, M_n^{SEC} values systematically underestimate the molar masses of the **P1** samples. Further, the values for M_n^{NMR-Z} and M_n^{UV-Z} values agree reasonably well with the values of M_n^{theo}, indicating good preservation of the RAFT-active trithiocarbonate end group. Still, it appears that the M_n^{NMR-Z} and in particular the M_n^{UV-Z} values tend to become higher than the M_n^{theo} values with increasing molar masses, pointing to an increasing loss of active end groups. Such a loss is inevitable due to the inherent RAFT mechanism.[184] Moreover, the ether functions of bMOEAm are prone to radical side reactions via hydrogen abstraction and might contribute to the loss. In any case, if molar masses up to 20,000 $g \cdot mol^{-1}$ are aspired, the data demonstrates that RAFT polymerization of bMOEAm proceeds smoothly. Even for higher molar masses, the extent of polymerization control is still reasonably good.

Furthermore, the homo- and block copolymerization of bMOEAm was carried out using **C12-CTA** or **L1b** to obtain potential thermoresponsive polymeric surfactants **L6a**, **L1b-6a** and **L1b-6b**. Key molecular data are described in Table 5.1. For **L6a**, M_n^{theo}, M_n^{NMR-Z} and M_n^{UV-Z} agree well with each other. This finding suggests that the RAFT polymerization using **C12-CTA** and bMOEAm as the monomer is well controlled. Still, notwithstanding the good agreement of the mentioned values, **L6a** presents a relatively high dispersity of 1.46 in the SEC analysis. Moreover, the M_n^{SEC} value underestimates the true molar mass of linear PbMOEAm **L6a** even more than for the series of samples **P6a** – **P6f** prepared by using **BPT**. These apparently inconsistent findings might be due to some weak interaction of the end-functionalized polymer **L6a** with the column material, thus provoking a tailing of the elugram towards longer elution times, which consequently reduces M_n^{SEC} but increases Đ. In any case, the analytical data show that the trithiocarbonate group is largely preserved. Chain extension of **L1b** with bMOEAm was also successfull up to high conversions to produce the block copolymers **L1b-6a** and **L1b-6b**. Still, the analytical data indicate that the RAFT-active trithiocarbonate group was largely lost at the end of the chain extension step, despite the low values of about 1.2 for Đ. A reason might be again the ether functions of bMOEAm that are prone to radical side reactions.

Thermal analysis showed that the polymers were thermally stable up to at least 200 °C according to thermogravimetric analysis TGA (Figure 5.2a), when presumably the decomposition of the trithiocarbonate end groups sets in.[185,186] Notable mass loss took only place at temperatures beyond 300 °C. Differential scanning calorimetry (DSC) showed (compared to most reported polyacrylamides) a rather low glass transition for polymers **P6** (Figure 5.2b), which approaches about 10 °C for high molar masses (Figure 5.3), indicating an intramolecular plasticizer effect of the 2-methoxyethyl groups. This value compares surprisingly well with the reported glass transition of about 5 °C for the 1:2 statistical copolymer of DMAm and 2-methoxyethylacrylate.[183]

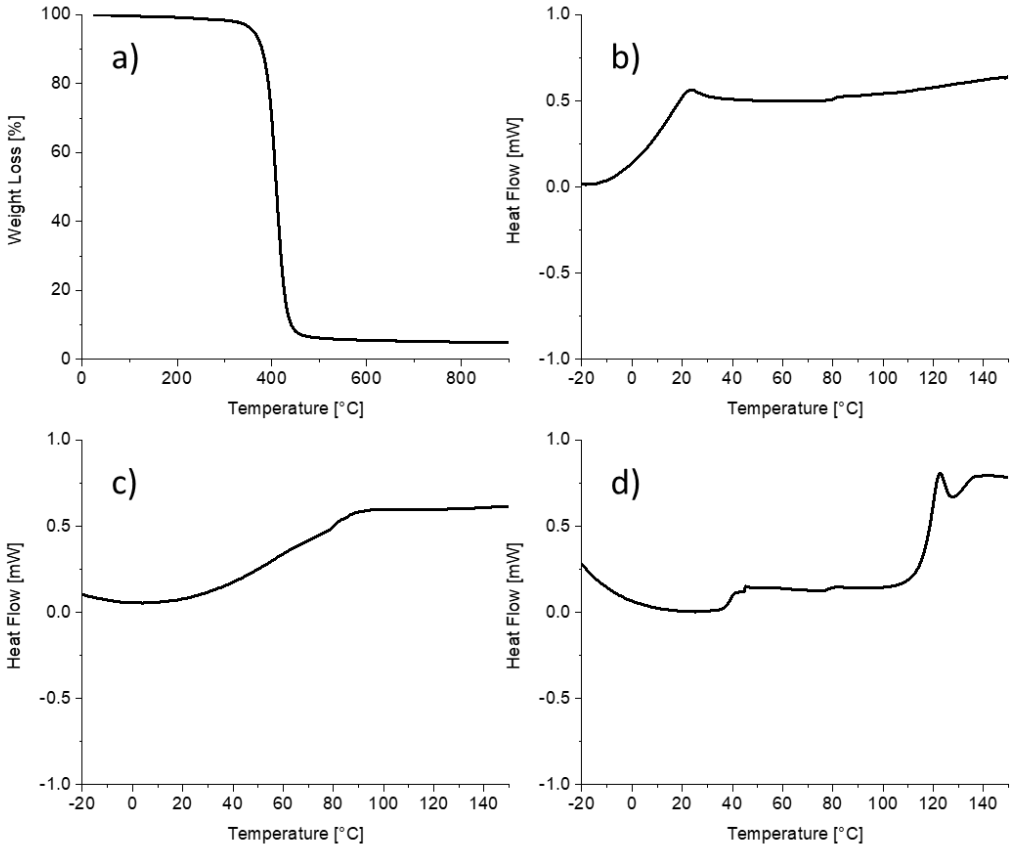

Figure 5.2: a) TGA and b) DSC of homopolymer **P6d** as well as DSC of c) macroCTA **L1b** and d) block copolymer **L1b-6b**.

In contrast, sample **L1b** displayed a glass transition at about 115-120 °C (Figure 5.2c), in agreement with the literature on PDMAm.[183,187,188] Noteworthy, polymers **L6a** and **L1b-6b** showed an additional small transition at about 40 °C, which is attributed to the alkyl chain terminus (Figure 5.2d). Interestingly, the block copolymers **L1b-6a** (T_g = 80 °C) and **L1b-6b** (T_g = 58 °C) (d) did only show one glass transition, which is located between those of the homopolymers and decreases

with an increasing share of PbMOEAm in the block copolymers. This suggests that the two different polyacrylamide blocks are compatible in the bulk phase.

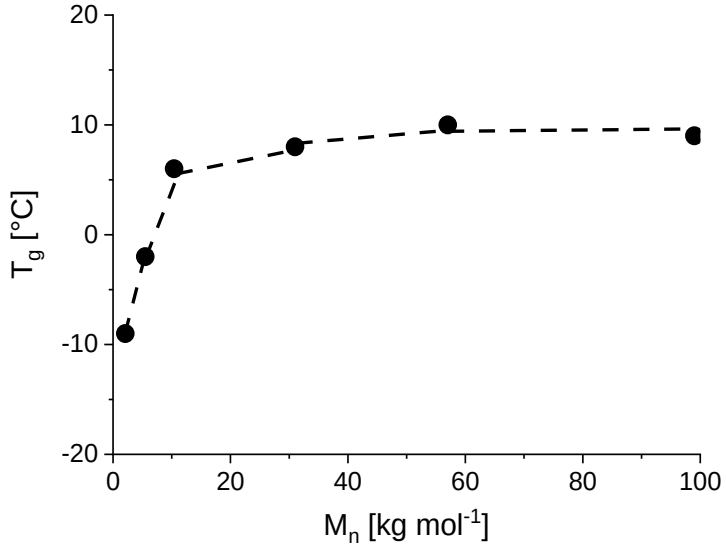

Figure 5.3: Molar mass dependence of the glass transition temperatures T_gs of homopolymers **P6a-f**.

5.2 THERMORESPONSIVE BEHAVIOR

The thermoresponsive behavior of the polymers **P6** in aqueous solution was investigated by temperature-dependent turbidimetry (see Figure 5.4). The transmission of the solutions showed a sharp transition from clear to opaque for the heating, and vice versa for the cooling runs (Figure 5.4a). These transitions were fully reversible. The hysteresis between cooling and heating runs was very small indicating a relatively quick rehydration and resolubilization of the collapsed polymer coils. This behavior is similar to the one of PDEAm,[189–191] but contrasts with the one of PNiPAm.[189,191,178] The different transition behaviors were attributed to the N-H group of the secondary amide moiety specific for PNiPAm, which is assumed to enable interchain hydrogen bonds that act as "cross-linking points" inside the swollen polymer chain and delay the diffusion of water into the dense aggregates,[189–191,178] but other kinetic effects seem also responsible.[192–194] Furthermore, the two methoxyethyl groups attached to the amide moiety of **P6** might facilitate the diffusion of water because they provide additional hydrophilicity in analogy to vinyl polymers that bear oligo(ethylene oxide) side chains.[30,195]

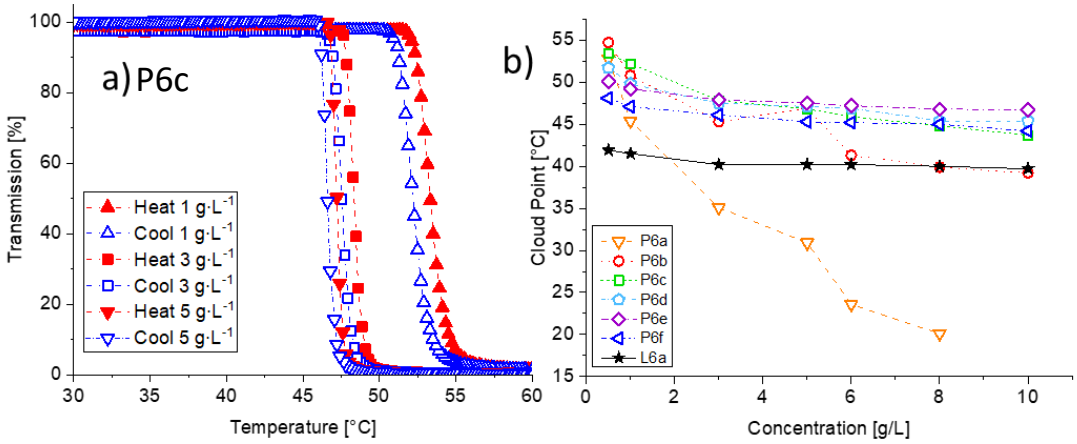

Figure 5.4: Temperature-dependent turbidimetry measurements of the thermoresponsive homopolymers of bMOEAm: a) transmission as a function of temperature for different concentrations of **P6c**, heating cycles are shown by full symbols, cooling cycles by open symbols; b) concentration dependence of the cloud points of homopolymers **P6** having various molar masses and/or end groups.

Up to 10 g·L^{-1}, the CP's shift towards lower temperatures with increasing concentration. Except for the oligomeric sample of **P6a** with a molar mass of 1.9 kg·mol^{-1}, the phase transitions of all samples slowly approached a temperature minimum with increasing concentration (Figure 5.4b). To investigate the influence of the molar mass, homopolymers **P6a-f** were synthesized with molar masses varying from about 2 to 100 kg·mol^{-1} using **BPT**. This CTA was chosen to introduce only rather small propyl and benzyl end groups into the polymers, in order to minimize end group effects on the LCST. Figure 5.4b illustrates that with increasing molar mass, the CP's are initially increasing. Only when the molar mass becomes sufficiently high at around 10 kg·mol^{-1} (**P6c**), the CP at 10 g·L^{-1} seems to approach a maximum temperature, reaching a plateau value of around 46 °C. This trend does not follow the classical Flory Huggins theory, according to which polymers become less soluble with growing molar mass as the combinatorial entropy term of mixing becomes less favorable.[196,197] This behavior might be explained by the sensitivity of the coil-to-globule transition of **P6** to the presence of even small hydrophobic end groups, as known for other thermoresponsive polyacrylamides as e.g. PNiPAm[27,197] or PNAP.[13] With increasing length of the polymer chain, the polymer's inherent hydrophilicity can increasingly outweigh the hydrophobic contribution of the end groups, so that the CP approaches an upper limiting value.

To gain a better understanding how such hydrophobic end groups influence the phase behavior of **P6**, the homopolymer **L6a** bearing a marked hydrophobic end group incorporating the hydrophobic dodecyl chain was studied as well. Having a molar mass of around 30 kg·mol^{-1}, **L6a** is well

comparable to **P6d**, their main difference being the hydrophobicity of the end groups. For **L6a** the CP's are notably lowered to a temperature of about 42 °C compared to the CP of **P6d** of around 46 °C. This indicates a higher solubility for the polymer with the less hydrophobic end groups. This marked influence of the hydrophobic end group is in agreement with the explanation proposed above for the observed increase of the CP's with increasing molar masses up to 10 kg mol^{-1}.

Noteworthy, the limiting CP values of these samples approached the range between 42 and 46 °C with increasing molar masses, which is above the originally reported value of 41.5 °C by Ito,[56] but lower than the values of 49.5 °C reported by Yamazaki et al.[58] and of 58.4 °C reported by Hidaka et al.[57] These differences might be due to both differing molar masses, dispersities and/or end groups of these samples, which were synthesized by classical free radical polymerization. Also, different tacticities might be responsible taking the reports for other polyacrylamides including PDEAm into account.[39,37,198,199] However, the scarce analytical data reported preclude from a more thorough discussion.

In most cases, thermoresponsive polymers are not employed in pure water but their possible applications include solution additives such as salts. The presence of such anions can also influence the phase transition behavior of thermoresponsive polymers as PNiPAm[39,45,200–202] or PDEAm.[39] Consequently, the effect of representative sodium salts on the CP of **P6** was explored using sample **P6f** via DLS, employing the fluoride F^- that is regarded to be highly kosmotropic, the thiocyanate SCN^- that is regarded to be highly chaotropic, and the chloride Cl^- designating the dividing line between those two types (Figure 5.5). At temperatures well below the phase transition, **P6f** has a hydrodynamic diameter of ~25 nm, which is comparable to values reported for PDEAm of similar molar mass.[55] Within the precision of the measurement, the hydrodynamic diameter seems to be unchanged upon the addition of the salts. In pure water, the CP of **P6f** is 45 °C. When NaCl is added, the CP shifts slightly towards lower temperatures. The observed rather weak salting-out effect of Cl^- was similar not only to other polyacrylamides such as PNiPAm[45] or PDEAm[39] but also to PEG-derived vinyl polymers.[195] The ability to lower the phase transition temperature becomes more pronounced when NaF is added. The strongly hydrated F^- induces a marked salting–out effect, decreasing the CP of **P6f** to 34 °C. Contrariwise, the addition of NaSCN raises the CP to 52 °C, clearly showing the salting-in effect of the weakly hydrated and highly polarizable SCN^- anion. The kosmotropic and chaotropic nature of F^- and SCN^-, respectively, was also demonstrated on low dispersity PNiPAm with a similar molar mass of ~500 kg·mol^{-1}.[44] However, the influence on the phase transition temperature of PNiPAm was less pronounced than for **P6f** revealing the higher ion specific response of polymers of bMOEAm to such salts.

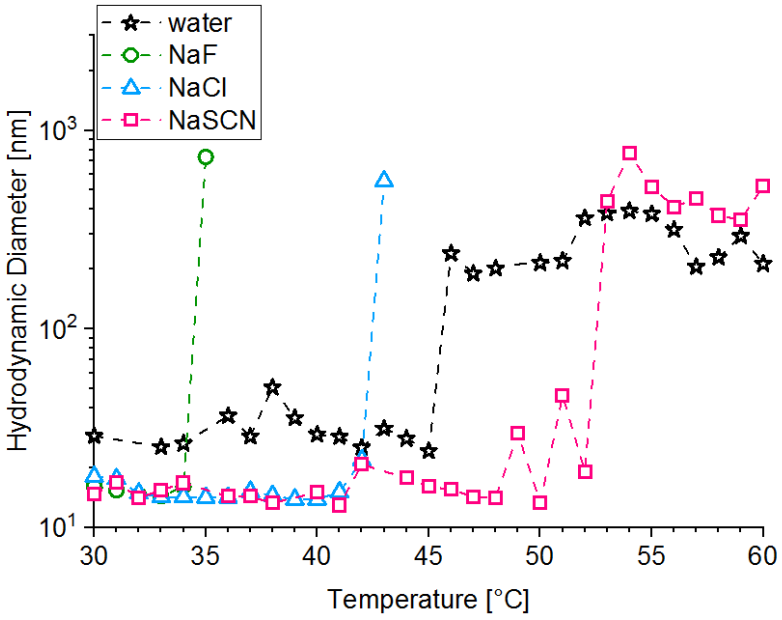

Figure 5.5: Temperature dependent hydrodynamic diameters of **P1f** in aqueous solution for different added salts from DLS (polymer concentration = 1 g·L^{-1}, salt concentration = 200 mM).

In addition to the homopolymers, the thermoresponsive behavior of the block copolymers **L1b-6a** and **L1b-6b** was explored by DLS and turbidimetry (Figure 5.6). Both block copolymers had a hydrodynamic diameter of ~10 nm at temperatures well below the phase transition. This is similar to homopolymer samples **P6c-d** with comparable chain lengths as the thermoresponsive block of the copolymers, but lower than the hydrodynamic diameter observed for the high molar mass polymers **P6e-f**. This points to a marked influence of the thermoresponsive block on the coil size in water (see Figure 5.6b), possibly due to the compatibility of the PDMAm and PbMOEAm blocks as indicated in the DSC thermograms. Noteworthy, for **L1b-6a** bearing a short PbMOEAm block of around 40 repeating units, no phase transition occurred up to a concentration of 5 g·L^{-1}, which is similar to **L1a-4** block copolymers bearing PNAP as thermoresponsive blocks. In contrast, when a longer thermoresponsive block of around 100 repeating units was incorporated as in **L1b-6b**, we observed a fully reversible phase transition with a very small hysteresis analogously to the behavior of the homopolymers. Still, the phase transition temperature increased markedly compared to the homopolymers. As demonstrated above, the water solubility of polymers **P6** is strongly affected by hydrophobic end groups. Obviously, this is also the case for hydrophilic groups attached to PbMOEAm, such as PDMAm. The enhanced solubility in water increases the CP and shifts the phase transition to around 60 °C, which is almost 15 °C higher than for the **P6** homopolymers.

Most likely, enhanced solubility accounts also for the lacking phase transition of **L1b-6a** in the studied temperature range, as the thermoresponsive PbMOEAm block is apparently too short to counterbalance the effect of the strongly hydrophilic PDMAm block attached. We note that structurally similar block copolymers PDMAm-b-PDEAm showed only slightly higher phase transition temperatures compared to PDEAm homopolymers.[32] Accordingly, the additional ethyleneglycol ether motifs in the analogous tertiary polyacrylamide PbMOEAm render the phase transition considerably more sensitive to attached hydrophilic blocks.

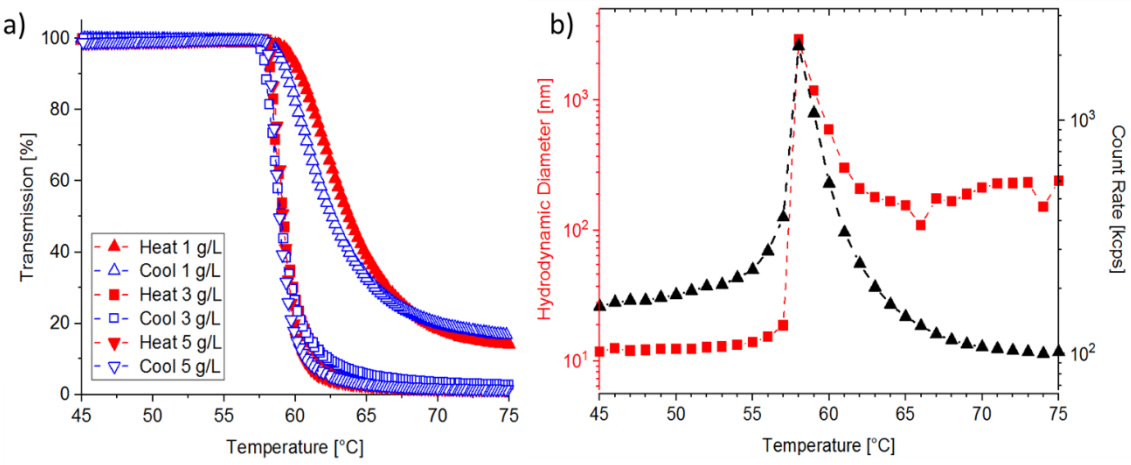

Figure 5.6: Thermoresponsive behavior of **L1b-6b** in aqueous solution. Temperature dependent a) transmission for different concentrations; and b) hydrodynamic diameter for c = 5 g·L^{-1}.

6 FRET-Analysis of Self-Assembly of Linear Homo- and Block Copolymers in Water

When the thermoresponsive blocks of the applied thermoresponsive amphiphilic block copolymers switch from hydrophilic to hydrophobic, they might form a network via bridging. Alternatively, they might also form a flower-like micelle via backfolding to the hydrophobic core. The latter would be disadvantageous for a rheological modifier, since the viscosity is mostly increasing as a result of the network formation. With complementary fluorescence dyes introduced at the opposite chain ends of the polymer, backfolding via FRET can be detected (Scheme 6.1).

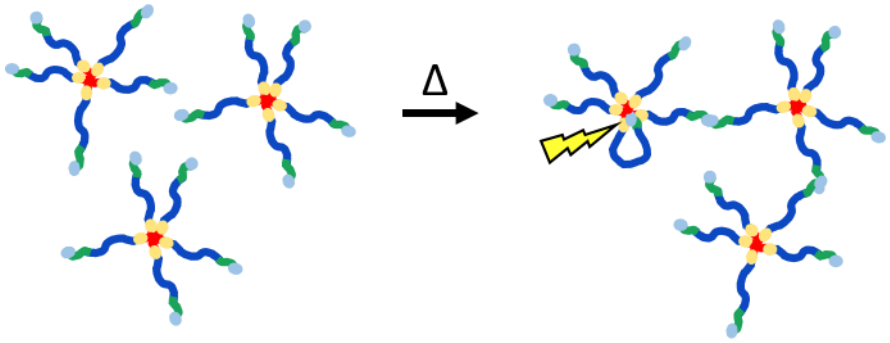

Scheme 6.1: Network formation via flower-like micelles.

Therefore, specific polymers were designed to enable the study of the aggregation behavior via FRET. The syntheses as well as the phase transition behavior and fluorescence studies are described in the following chapters.

6.1 Design and Synthesis of FRET-Chain Transfer Agent

The wanted FRET-chain transfer agent (**FRET-CTA**) must fulfill several requirements in order to achieve efficient FRET, but also to polymerize the monomers in a controlled manner and to introduce the hydrophobic sticker group. In addition, the introduced fluorophores should be rather small and not exceedingly hydrophobic. Moreover, they should be nonionic to be comparable to the basic polymer structure. Finally, they should be inert to different solvents and relatively insensitive to quenching in order to facilitate analytics. Therefore, a trithiocarbonate compound bearing a coumarin dye as the donor and a naphthalimide dye as the acceptor was synthesized as **FRET-CTA** (Figure 6.1).

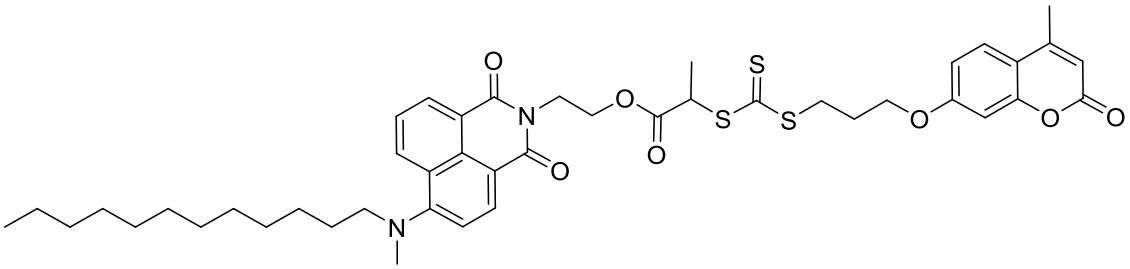

Figure 6.1: Structure of FRET-CTA.

Coumarin and naphthalimide dyes are rather small compared to established FRET pairs such as fluoresceine and rhodamine. Also, they are less hydrophobic than pyrene or anthracene and less sensitive to quenching (see chapter 1.4.3). Both dyes are also virtually inert against radical attack and thus, they do not intervene during the polymerization process. These features make them ideal candidates for the usage in a labeled CTA. Starting with 7-hydroxy-4-methylcoumarin, the hydroxy-group was alkylated by allyl bromide in a Finkelstein reaction giving 76 % yield. In the next step, 7-allyloxy-4-methylcoumarin underwent a thio-ene reaction with thioacetic acid reaching 75 % yield. The following hydrolysis with sodium hydroxide gave 97 % yield of the thiol, when it was performed in ethanol. However, when the thioester was hydrolyzed in tetrahydrofuran (THF), the disulfide was formed with 51 % yield, while the other half remained unchanged educt. In literature, if hydrolysis of thioesters is done in THF, usually HCl is used as well as methanol as an additional solvent.[203] This suggests that an alcoholic solvent is needed to obtain the thiol. This coumarin functionalized thiol was one of the educts needed for the FRET-CTA, the other compound being the naphthalimide. The synthesis was adapted to the one already described by our group,[204] using dodecylmethylamine instead of dimethylamine to introduce the hydrophobic sticker group. In a further step, the naphthalimide reacted with 2-bromopropionyl bromide to give

the alkylating reagent for the FRET-CTA synthesis resulting in 19 % yield. However, when the chloride analog was used, no **FRET-CTA** was obtained. Also in literature, the bromide equivalent seems to be the alkylating agent of choice for the formation of a trithiocarbonate group in α-position to a carboxy-group.[205,206] The ^{1}H-NMR of the obtained **FRET-CTA** is shown in Figure 6.2. Despite the complexicity of the structure, all peaks of the coumarin and the naphthalimide moiety are clearly visible and no impurities are apparent.

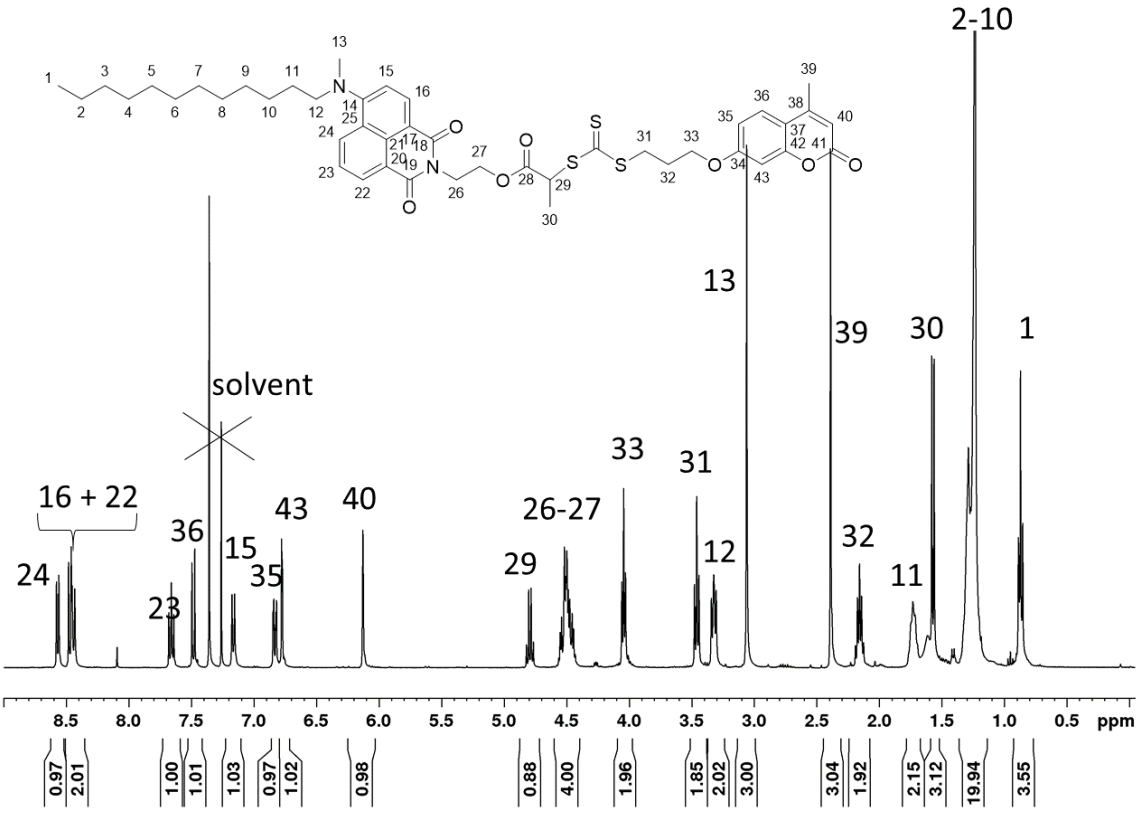

Figure 6.2: ^{1}H-NMR spectrum of **FRET-CTA** in $CDCl_3$.

In the ^{13}C-NMR-spectrum (Figure 6.3) the new formed C=S signal at around 220 ppm is well visible, clearly showing that the product was obtained. All other carbon signals are also well visible.

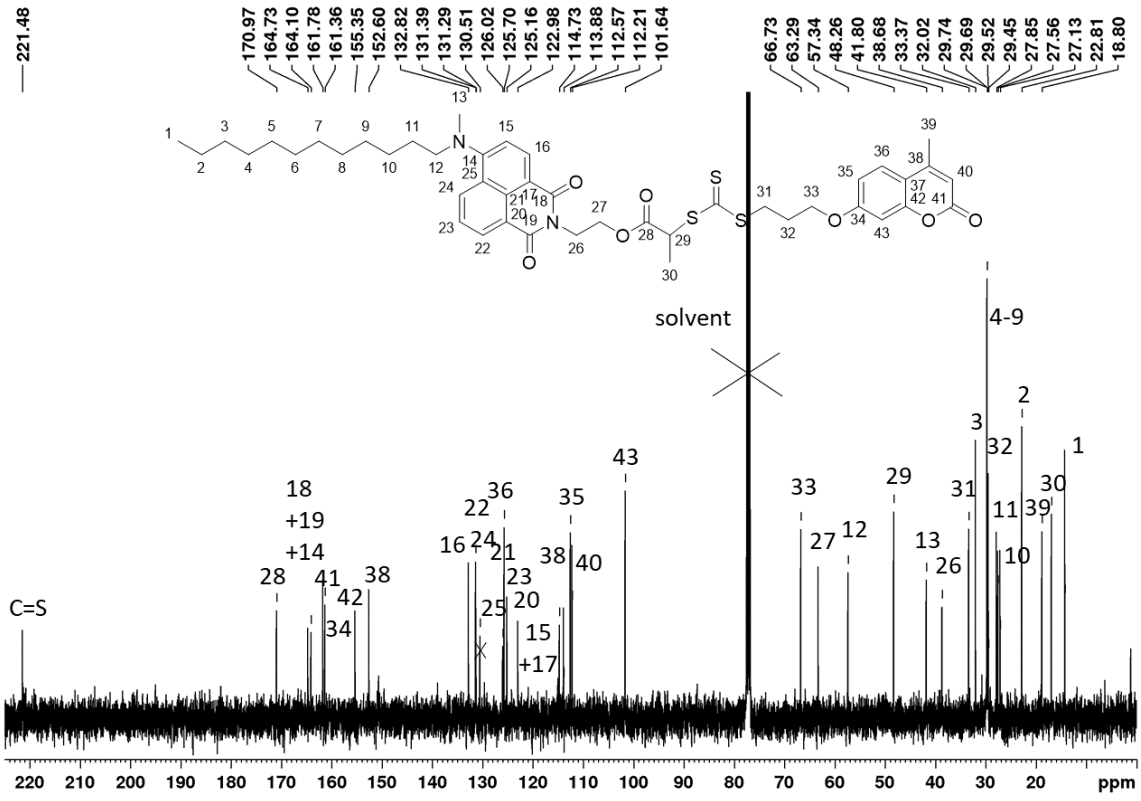

Figure 6.3 ^{13}C-NMR spectrum of **FRET-CTA** in $CDCl_3$.

For the FRET process, coumarin acts as the donor with an excitation maximum around 324 nm (Figure 6.4a), which is the excitation minimum of the naphthalimide acceptor (Figure 6.4). Hence, the acceptor is only weakly excited directly (Figure 6.4b), but its emission will be stimulated by the FRET-process.

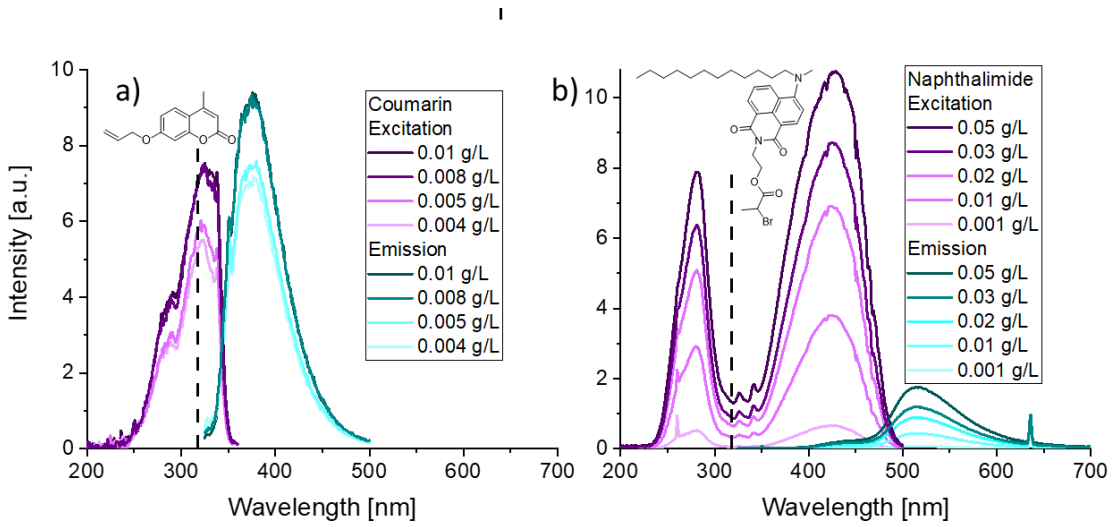

Figure 6.4: Fluorescence spectra of coumarin (excitation at 318 nm and emission at 376 nm) and naphthalimide (excitation at 318 nm and emission at 520 nm) derivative in THF for varying concentrations.

6.2 Synthesis and Characterization of Homo- and Block Copolymers

The polymerization procedure for the homo- and block copolymers synthesized with FRET-CTA is similar to the one described in chapter 3.2. However, when a 33 wt% monomer and CTA solution was used, the reaction took 15-20 h to achieve high conversions (60 – 88 %). A similar result was achieved for the polymerization of NiPAm in dimethylformamide (DMF) or dimethylsulfoxide (DMSO) with a CTA bearing a similar R-group.[205,207] That might suggest that this type of R-group is less efficient in the RAFT process than the benzyl group. Still, a 50 wt% monomer and CTA solution gave 82 % conversion after only 3 h of polymerization time. More details about the reaction parameters can be found in Table 10.4. Table 6.1 summarizes the results of the polymerization. The molar masses determined by different methods match well with each other within the precision of the methods, and the dispersities Đ are low, indicating a well-controlled polymerization process. Only the blockpolymer **F1a-2a** shows a slightly higher dispersity, most likely a result of the long polymerization time of 20 h. Compared to the other molar mass values, M_n^{NMR-R} tends to be higher, since the signal used for determination became very small compared to the polymer signals. ^{1}H-NMR also provided end group analysis for the Z/R ratio, which suggests that almost every polymer chain is carrying a Z- and an R-group. Although those signals were visible in the spectra, they are rather small compared to the polymer signals especially for the large block copolymers **F1a-2a** and **F1b-2b**, or the NH-band is overlapping with some of the end group signals as for **F2**. Still, the Z/R ratio close to 1 for the FRET-polymers is a good indication for the

high end group functionality. For the polymers containing N-H groups from the PNiPAm block, the Z/R ratio could not always be determined due to the overlapping N-H signal. When the ^{1}H-NMR spectrum was measured in D_2O to exchange the protons with deuterium, the end group signals were either not visible (see Appendix Figure 11.36) or very broad (see Appendix Figure 11.35). This points to a poor solvation of the end groups and possibly their aggregation into hydrophobic nanodomains. Additionally, the introduced naphthalimide group allowed molar mass determination with UV-vis spectroscopy applying the molar extinction coefficient $\varepsilon = 8500\ L \cdot mol^{-1} \cdot cm^{-1}$ at a maximum wavelength $\lambda_{max} = 424$ nm determined for the FRET-CTA in dichloromethane (DCM) (see Appendix Figure 11.10). The obtained values fit very well with the theoretical ones. The ^{1}H-NMR spectra of the homo- and block copolymers in $CDCl_3$ are shown in Figure 6.5. The integrals and the shifts of the polymer end groups match reasonably well with the respective signals of the **FRET-CTA**. Despite the relatively high molar mass of **F1a**, the signals of the end groups are well ressolved and can be assigned to the naphthalimide or the coumarin moiety.

Table 6.1: Results of PDMAm from RAFT polymerization with FRET-CTA (see Figure 0.1a in case for FRET architecture).

Code	Polymer	Yield %	Theo [a]		NMR-R[b]			SEC		UV-R
			M_n kg/mol	DP_n	M_n kg/mol	DP_n	Z/R[c]	M_n kg/mol	DP_n	M_n kg/mol
F1a	FRET-PDMAm$_{334}$	61	17	166	34	334	0.9	16	1.25	22
F1b	FRET-PDMAm$_{217}$	80	16	157	22	217	1.0	20	1.21	15
F2	FRET-NiPAm$_{311}$	69	25	212	36	311	-[d]	27	1.23	20
F1a-2a	FRET-PDMAm$_{334}$-b-PNiPAm$_{34}$	48	25	26	39	34	0.8	24	1.43	23
F1b-2b	FRET-PDMAm$_{217}$-b-PNiPAm$_{64}$	84	21	37	30	64	-[d]	28	1.26	20

[a] determined by conversion of monomer peaks in ^{1}H-NMR by comparing the signals at 0 h and after the final reaction time, [b] determined by using the integrals of the aromatic protons of napthalimide, [c] calculated by comparison of the integrals of the aromatic protons of naphthalimide and coumarine, [d] could not be determined due to overlapping N-H signal. Precision of all molar mass values is ± 20 %.

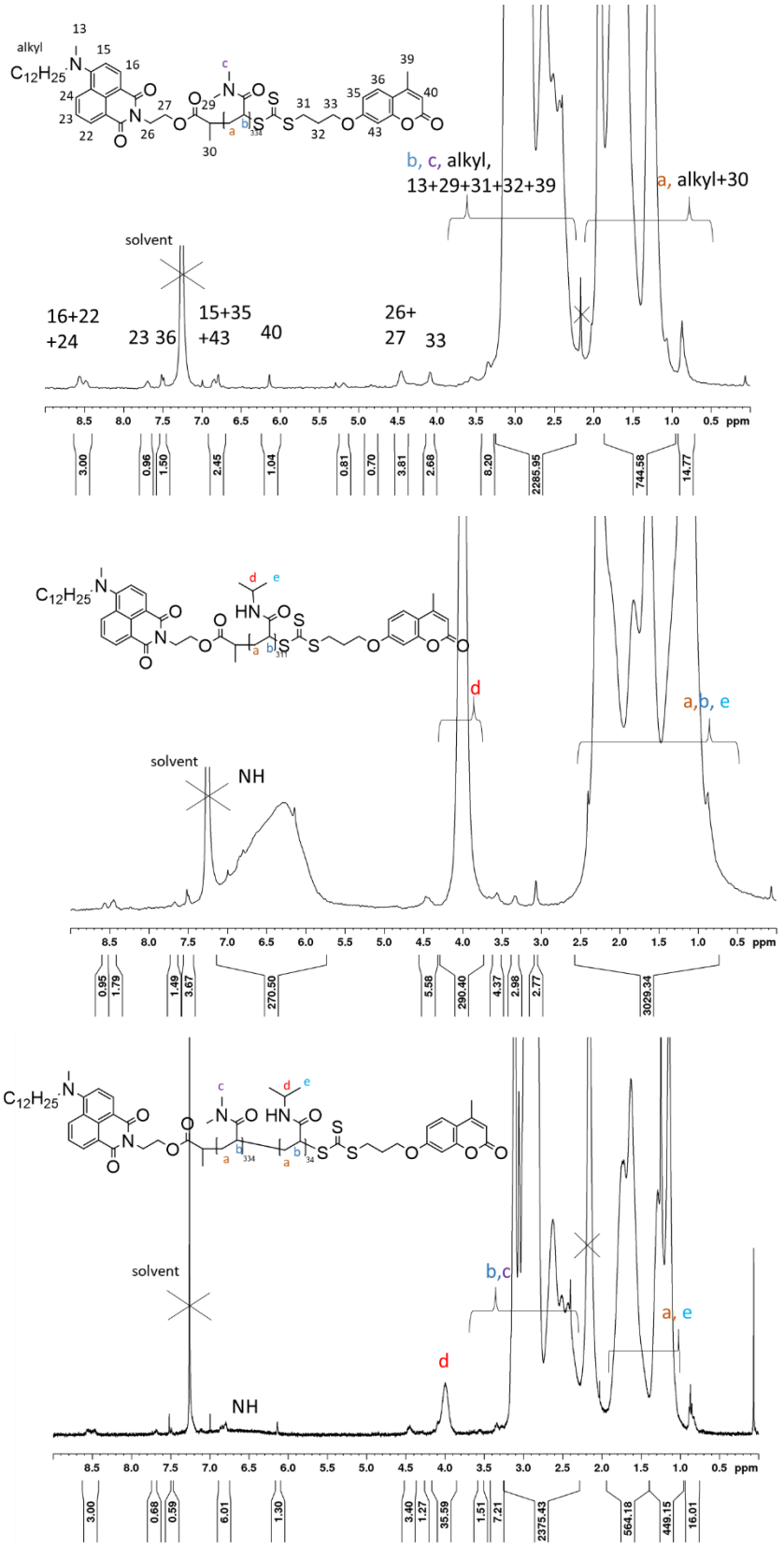

Figure 6.5: ^{1}H-NMR spectra of FRET homo- and block copolymers in $CDCl_3$.

According to TGA, all polymers were thermally stable up to at least 200 °C (see Appendix Figure 11.54a, c, e). Significant mass losses were observed only when the temperature exceeded 300 °C. DSC revealed a glass transition for homopolymers **F1a** at 118 °C and **F2** at 132 °C, in good agreement with the literature (see Appendix Figure 11.54b, d).[208,59] Block copolymer **F1b-2b** showed only one glass transition at 122 °C, i.e., a value between those of the respective homopolymers (see Appendix Figure 11.54f). This is an indication that the two polyacrylamide blocks are compatible in the bulk phase and do not (micro)phase separate.

6.3 Phase Transition Behavior of Polymers in Water

The phase transition behavior of the FRET-polymers in water was investigated by turbidimetry (Figure 6.6).

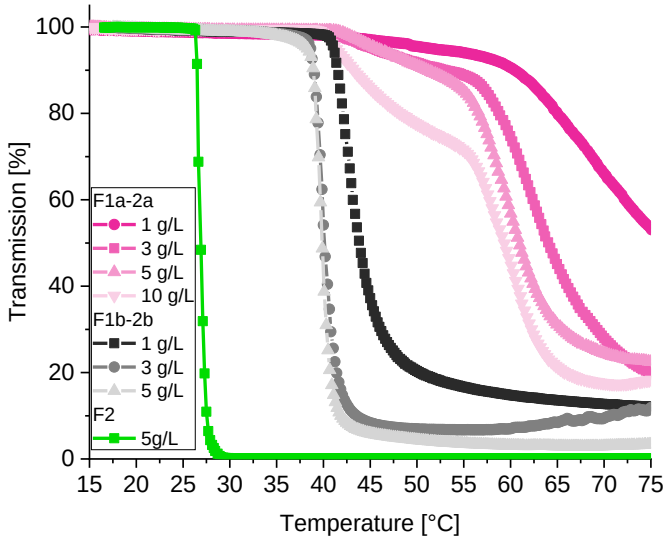

Figure 6.6: Turbidimetry measurements for aqueous solutions of **F2**, **F1a-2a** and **Fba-2b** for varying concentrations (only heating curves).

The permanently hydrophilic **F1a** homopolymer as well as the thermoresponsive homo- and block copolymers **F2**, **F1a-2a** and **Fba-2b** below their phase transitions were well soluble in water. The pure thermoresponsive **F2** switches at around 25 °C, which is lower than the value of 32 °C generally reported for PNiPAm.[50] This is most probably attributed to the effect of the hydrophobic coumarin end group directly attached to the PNiPAm block reducing the CP. The moderately

reduced CP in comparison with other end group effects reported suggests that its effective hydrophobicity is lower than the one of end groups bearing a naphthyl, azobenzene or dodecyl moiety.[209,210,26] The phase transition temperature of the block copolymers **F1a-2a** and **Fba-2b**, however, are strongly raised up to around 40 °C, due to the hydrophilic PDMAm block. With increasing concentrations, the CP's slightly shift to lower temperatures for both polymers, which is in agreement with the literature for such dilute solutions.[18] After the heating run, the polymers usually separated in a polymer-rich and polymer-poor phase, so that no cooling cycle was applied. However, with stirring, the phase transitions were completely reversible (data not shown). A closer inspection of the evolution of turbidity with increasing temperature reveals a striking difference between the two block copolymers. Whereas the clouding transition is sharp and pronounced for **F1a-2a** indicating the rapid formation of rather large aggregates once the phase transition temperature is crossed, the turbidity of the solutions of **F1b-2b** evolves in two stages. In a first step, the drop of transmittance is small, before in a second step, the solutions become opaque at about 15 °C higher than CP. Qualitatively, this suggests the formation of small aggregates initially, which transform only after further dehydration of the polymer coils at more elevated temperatures into much larger ones. An analogous behavior was observed in DLS measurements (Figure 6.7). Below their phase transitions, the polymers have an average hydrodynamic diameter of 25 nm pointing to the formation of small aggregates due to the surfactant-like structure of the α-terminal dodecyl chain.[211] Above the phase transition of the block copolymers, **F1a-2a** immediately forms large aggregates, while the block copolymer **F1b-2b** shows an apparent two-step transition with slowly increasing size, which rises markedly above 55 °C. This behavior is most probably a result of the higher dispersity Đ of 1.43 resulting in different sizes of the thermoresponsive block and thus, in slightly varying phase transition temperatures for the polymer chains. Also the shorter size of the thermoresponsive block compared to **F1b-2b** might lead to the slowly increasing aggregate sizes. This behavior matches the observations on the phase transitions (Figure 6.6) discussed above.

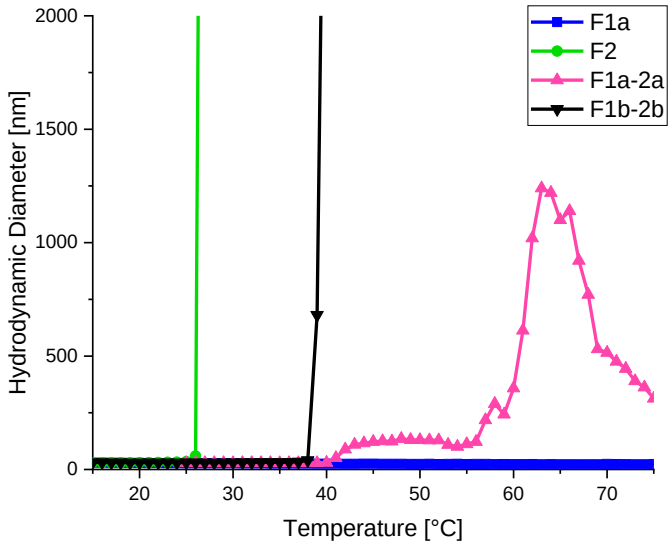

Figure 6.7: DLS measurements of 5 g·L^{-1} aqueous solutions of FRET-polymers **F1a**, **F2**, **F1a-2a** and **F1b-2b**.

6.4 Fluorescence Spectroscopy of Aqueous Polymer Solutions and Microemulsions

Temperature-dependent fluorescence measurements of the homo- and block copolymers were studied with the fixed excitation wavelength of 318 nm (Figure 6.8). At this wavelength, the excitation of the donor fluorophor is efficient but of the acceptor fluorophore at a minimum (see Figure 6.4). The systems were studied either in pure water or in a TDMAO/decane microemulsion. Figure 6.8 reveals on a first view that the spectra of all polymer–solvent systems are subject to changes with increasing temperature. Furthermore, these changes vary markedly not only between the different polymers studied, but also when pure water as solvent (Figure 6.8a, c, e) is replaced by a TDMAO/decane microemulsion (Figure 6.8b, d, f). Generally, the fluorescence intensity decreased with increasing temperature, due to the increased quenching by water.[212] Figure 6.9 shows the analysis of the spectra with respect to the relative emission intensities of the donor and acceptor chromophores revealing changes in the extent of FRET occurring.

In aqueous solution and in microemulsion, the permanently hydrophilic reference PDMAm **F1a** shows only little FRET independent of the temperature, while a strong increase of FRET for the thermoresponsive PNiPAm reference **F2** is visible just above the CP. The extent of FRET increases

also for the block copolymer **F1a-2a** when crossing the CP but the effect is much weaker (Figure 6.9b).

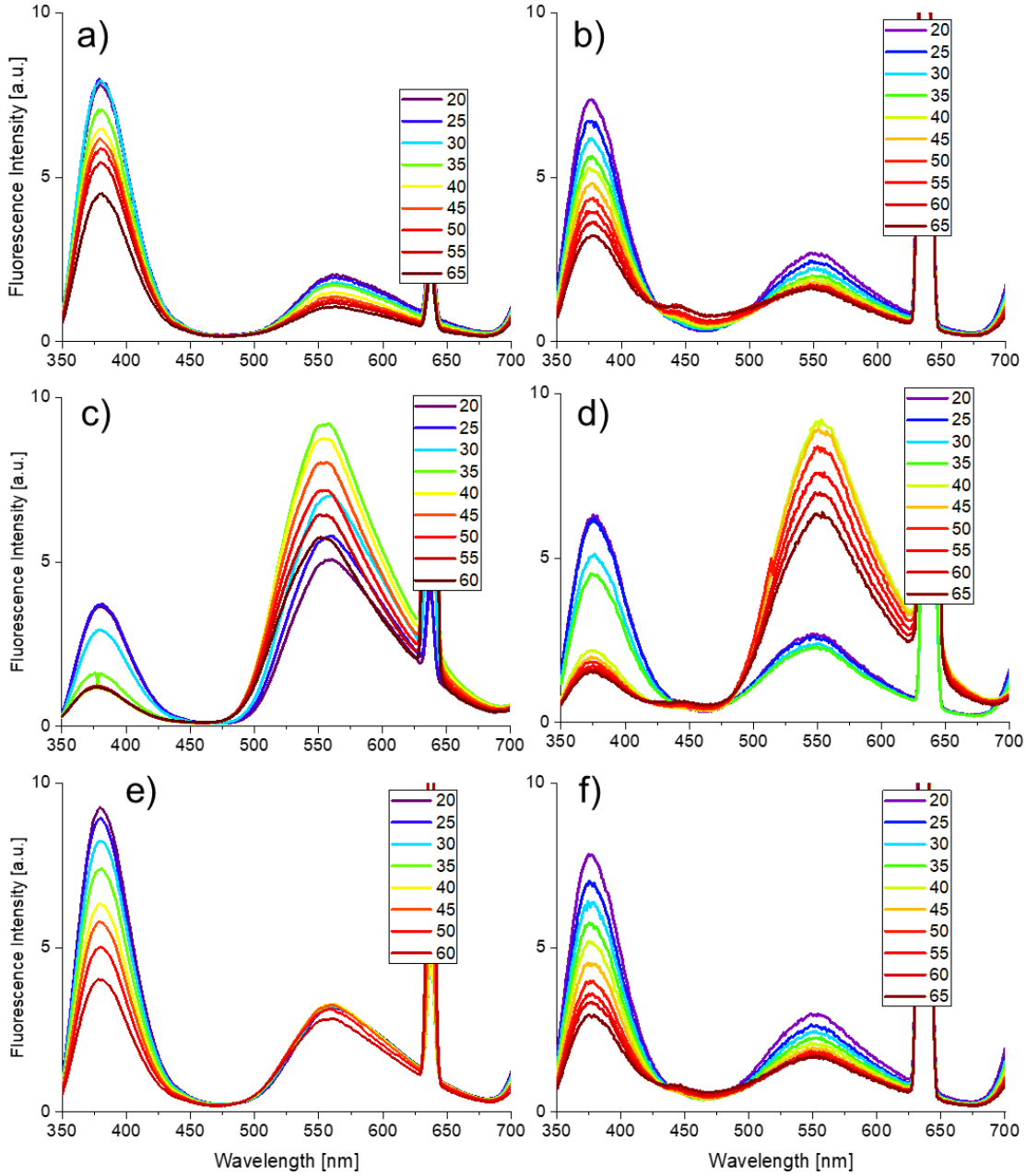

Figure 6.8: Temperature-dependent fluorescence measurements of 1 g·L^{-1} concentrations of **F1a** (a-b), **F2** (c-d) and **F1a-2a** (e-f) in pure water (left) and microemulsion (right) (190 mM TDMAO, *n*-decane).

When changing the medium from water to microemulsion, the general behavior is rather similar (Figure 6.9a). The FRET efficiency is strongly enhanced for the thermoresponsive PNiPAm **F2**

when crossing the cloud point, whereas temperature effects are small for the permanently hydrophilic reference **F1a** and the block copolymer. Overall, at room temperature, the extent of FRET is higher for all polymers in the microemulsion compared to the aqueous solution. Still, a closer look reveals important differences, in particular when comparing the samples **F1a** and **F1a-2a** (Figure 6.9b). On the one hand, the FRET effect increases continuously, but very slightly, for PDMAm **F1a** with increasing temperature, in contrast to its virtual independence in pure water. On the other hand, the increase of FRET for the block copolymer **F1a-2a** when passing the CP is markedly weaker in micromeulsion than in water and parallels the behavior of the reference sample **F1a** (Figure 6.9b).

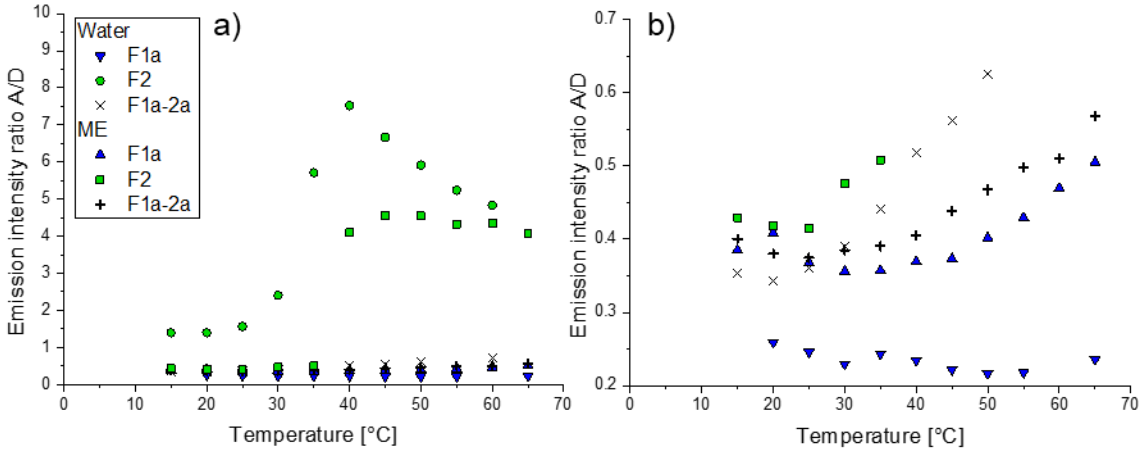

Figure 6.9: Temperature-dependent emission intensity ratio of acceptor A and donor D for the homo- and block copolymers in water and in microemulsion: a) overview, b) magnified section of a).

In addition, the solvatochromism of the naphthalimide[213] was used to analyze the position of the emission maximum of the acceptor fluorophore, which provides more information about the polymer's aggregation behavior.[214] In pure aqueous solution, the emission maximum of the acceptor chromophore is located at 561 nm below 25 °C for all polymers studied. This value corresponds to a surrounding of the chromophore close to pure water.[213] Whereas the peak position did not change between 15 and 65 °C for permanently hydrophilic homopolymer **F1a**, a hypsochromic shift of about 10 nm was observed for the thermoresponsive homopolymer **F2** in this temperature range with increasing temperature (Figure 6.8). The value indicates a less, though still highly polar surrounding of the chromophore at elevated temperatures, similar to a mixture of water and *N*-methylformamide, for example.[213] It is also evident that the solvatochromic shift does not occur linearly, but seems to follow an S-shape with the maximum slope between 25 and 35 °C, i.e., around the CP of **F2**. The combined findings suggest that the shift is a consequence of the

coil-to-globule collapse of the PNiPAm chains and their concomitant partial dehydration, changing the local environment of the fluorophore from 'nearly aqueous' to 'water-swollen NiPAm groups'. In the case of block copolymer **F1a-2a**, a similar behavior is seemingly observed, though being much less pronounced. The hypsochromic shift amounts to only about 2 nm, and the maximum slope of the S-shaped curve seems shifted to higher temperatures, between 30 and 45 °C (Figure 6.8). Again, this behavior can be correlated with the phase transition of the block copolymer. The weakness of the solvatochromism value compared to the homopolymer may be easily explained by the much shorter PNiPAm block in the copolymer, as well as by the separation of the collapsed PNiPAm block and the naphthalimide moiety by the long PDMAm block in between.[214] In microemulsion, the behavior changes characteristically. The position of the emission maximum of the acceptor fluorophore is located at 551 nm for samples **F1a** and **F1a-2a** at all temperatures, and for sample **F2** at temperatures above 30 °C. This indicates a less, though still highly polar surrounding of the chromophore in the presence of the microemulsion's oil droplets compared to the pure aqueous solution. Interestingly, below 30 °C, **F2** is further hypsochromically shifted to 548 nm, indicating an even less polar surronding at low temperatures.

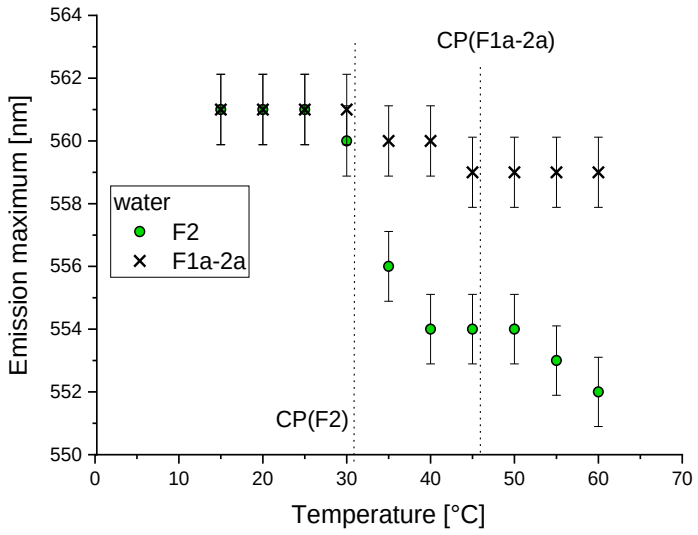

Figure 6.10: Temperature-dependent emission maximum of **F2** and **F1a-2a** in water at 1 $g \cdot L^{-1}$.

In conclusion, the findings of the fluorescence studies leads to the following picture: In water, at ambient temperatures, the acceptor dye itself is not located in the hydrophobic domain of micellar aggregates but rather at their interface. Moreover, the moderately hydrophobic ω–termini with the coumarin moiety show little tendency to approach the micelles surface, either by backfolding of

the polymer chains or by bridging different micelles. In microemulsion, the hydrophobic C12-chain prefers to insert into the oil droplets of the microemulsion as shown by the solvatochromic effects. The permanently hydrophilic reference PDMAm **F1a** is a well-dissolved polymer coil in water as well as in microemulsion. In contrast, the thermoresponsive **F2**, shows already stronger FRET in pure water. Since the phase transition temperature lies around 25 °C, **F2** seems to be already in a more contracted state even at 15 °C. With increasing temperature, FRET of the sample **F2** also increases with a clear step between 25 and 30 °C, pointing to a collapse of the polymer chains. In addition, the transition was macroscopically visible, as the solution turned turbid. When applied in microemulsion, below the phase transition, **F2** displays a similar behavior like PDMAm with only weak FRET. However, as soon as the temperature exceeds 35 °C, FRET increases in a large step pointing to a strong collapse of the polymer. This can be explained with the affinity of the C12-chains to insert into the oil droplets of the microemulsion, while the ω–termini are not sufficiently hydrophobic for this behavior. Therefore, the donor and acceptor are relatively well separated and do not undergo FRET easily. Nevertheless, when PNiPAm is sufficiently dehydrated, the coumarin chain end can also fold back leading to efficient FRET. In pure water, below the phase transition, the block copolymer **F1a-2a** shows only little FRET similar to **F1a**. Above the phase transition around 40 °C, however, the napthalimide emission slightly increases, indicating more backfolding. However, in the microemulsion, the block copolymer shows a very similar behavior like PDMAm for the full temperature range. These results suggest that in the microemulsion, even above the phase transition, the thermoresponsive PNiPAm block is still too hydrophilic to fold back to the oil droplet due to the attached PDMAm block pointing to the right scenario of Scheme 6.1. This means, that the polymer micelles are interconnected by clusters of collapsed PNiPAm chains, eventually forming a network with two different, alternating types of crosslinks formed by micellar cores (or oil droplets, respectively) and PNiPAm microdomains.

7 THERMORESPONSIVE AMPHIPHILIC BLOCK COPOLYMERS WITH QUASI-MIKTOARM ARCHITECTURE

Thermoresponsive amphiphilic block copolymers with quasi-miktoarm architecture were intended (see Figure 2.2, architecture **YS** and **YN**), since this architecture bears an additional arm allowing more network joints and might therefore enable a stronger network. The architecture is called quasi-miktoarm due to the relatively short "3rd arm" being the dodecyl chain, while the other two arms contain the PDMAm + *thermoresponsive block*. Still, this short permanently hydrophobic sticker has an important impact on the aggregation behavior of the polymers, as discussed in chapter 3.3. While the symmetrical quasi-miktoarm block copolymer (see Figure 2.2 **YS**) should immediately form a network upon phase transition, the non-symmetrical quasi-miktoarm block copolymer bearing two different thermoresponsive blocks (see Figure 2.2 **YN**) should enable a stepwise increase of the network formation (Scheme 7.1). With such a non-symmetrical quasi-miktoarm architecture a more sensitive control of the network formation would be possible.

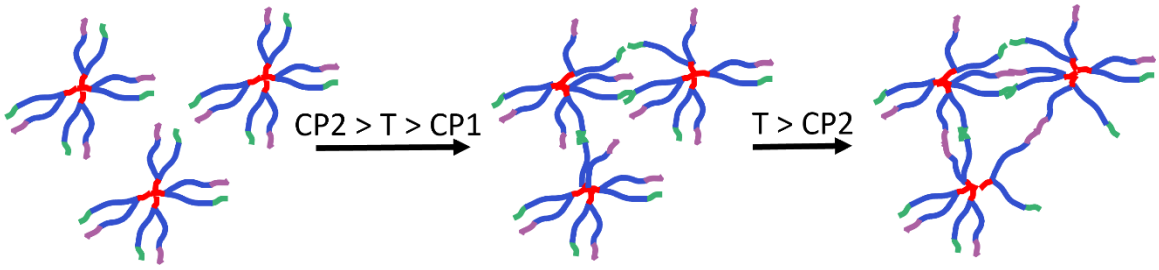

Scheme 7.1: Stepwise network formation of the non-symmetrical block copolymer with quasi-miktoarm architecture bearing two different thermoresponsive blocks with CP2 > CP1. (red = permanently hydrophobic block, blue = permanently hydrophilic block, green = thermoresponsive block 1 with CP1, violet = thermoresponsive block 2 with CP2).

7.1 SYNTHESIS AND CHARACTERIZATION OF SYMMETRICAL BLOCK COPOLYMERS

The synthesis of the symmetrical quasi miktoarm block copolymer is similar to the one already described for the homopolymer **YS1** C12Y-PDMAm$_{178}$. Again, V-40 was used as the initiator in a ratio of [initiator]:[macroCTA] 1:5, which means that the ratio of [initiator]:[trithiocarbonate group] was 1:10 as for the linear reference architecture. The polymerization took place in benzene with a 33 wt% monomer and macroCTA solution, and gave usually around 70 % conversion after 3 h for

the polymerization of NiPAm and DEAm. For NPAm, when applying a 50 wt% monomer and macroCTA solution, the polymerization was very fast, reaching quantitative conversion within 2.5 h. More details about the reaction parameters can be found in the Experimental Part in Table 10.3. The molecular characteristics of these block copolymers are summarized in Table 7.1.

Table 7.1: Molecular characteristics of symmetrical block copolymers with miktoarm architecture using **YS1** as bifunctional macroCTA (see Figure 0.1a in case for Y-symmetrical architecture).

Code	Polymer	Yield %	Theo[a)]		NMR-Z[c)]			SEC		UV-Z
			M_n kg/mol	DP_n[b)]	M_n kg/mol	DP_n[b)]	Z/R[d)]	M_n kg/mol	DP_n	M_n kg/mol
YS1-2	C12Y-[$PDMAm_{178}$-b-$PNiPAm_{32}$]$_2$	70	42	32	44	32	-[e)]	39	1.15	44
YS1-3	C12Y-[$PDMAm_{178}$-b-$PDEAm_{29}$]$_2$	73	42	29	44	29	1.1	36	1.14	49
YS1-5	C12Y-[$PDMAm_{178}$-b-$PNPAm_{51}$]$_2$	76	46	49	48	51	-[e)]	43	1.26	57

[a)] determined by conversion of monomer peaks in ^{1}H-NMR by comparing the signals at 0 h and after the final reaction time, [b)] per arm, [c)] calculated using integrals of TMS group, [d)] calculated by comparing the integrals of the aromatic protons and the TMS-group, [e)] could not be calculated due to overlapping NH-signal. Precision of all molar mass values is ± 20 %.

The molar mass values determined by the different methods match well with each other, and also the dispersity is low with Đ < 1.3 indicating a well-controlled RAFT polymerization process. The molar mass values M_n^{SEC} are somewhat lower than the other values, which is most probably due to the PS-standard used for calibration. Interestingly, the elugram of the sample with PDEAm as the thermoresponsive blocks **YS1-3** is shifted towards higher volumes and therefore lower molar masses than its precursor **YS1** (see Appendix Figure 11.50). Such a tendency was also observed for the linear reference architecture with the large PDEAm blocks **L1b-3c** (see Appendix Figure 11.48). This seems to indicate that a high amount of the PDEAm block leads to smaller hydrodynamic volumes in DMF or *N*-methyl-2-pyrrolidone. The result might be explained by the additional interactions of blockscopolymers with the different block types as well as dispersities of the block sizes themselves leading to smaller hydrodynamic volumes.[259] Molar masses determined by UV-vis measurement and ^{1}H-NMR are slightly higher than the theoretically expected values, which might be caused by the two-fold precipitation during workup. This purification method leads to the removal of low molar mass fractions, and thus, the M_n^{UV} and M_n^{NMR-Z} overestimate the true values, and the dispersity Đ is narrowed. Still, the molar mass values differ not much and the Z/R ratio close to 1 shows high end group fidelity. A typical ^{1}H-NMR spectrum of such a

quasi-miktoarm block copolymer is shown in Figure 7.1, in which the signal of the TMS-group is clearly visible and used to determine the block length of the PNiPAm block. The ^{1}H-NMR spectra of the other block copolymers of this type of architecture are shown in the Appendix.

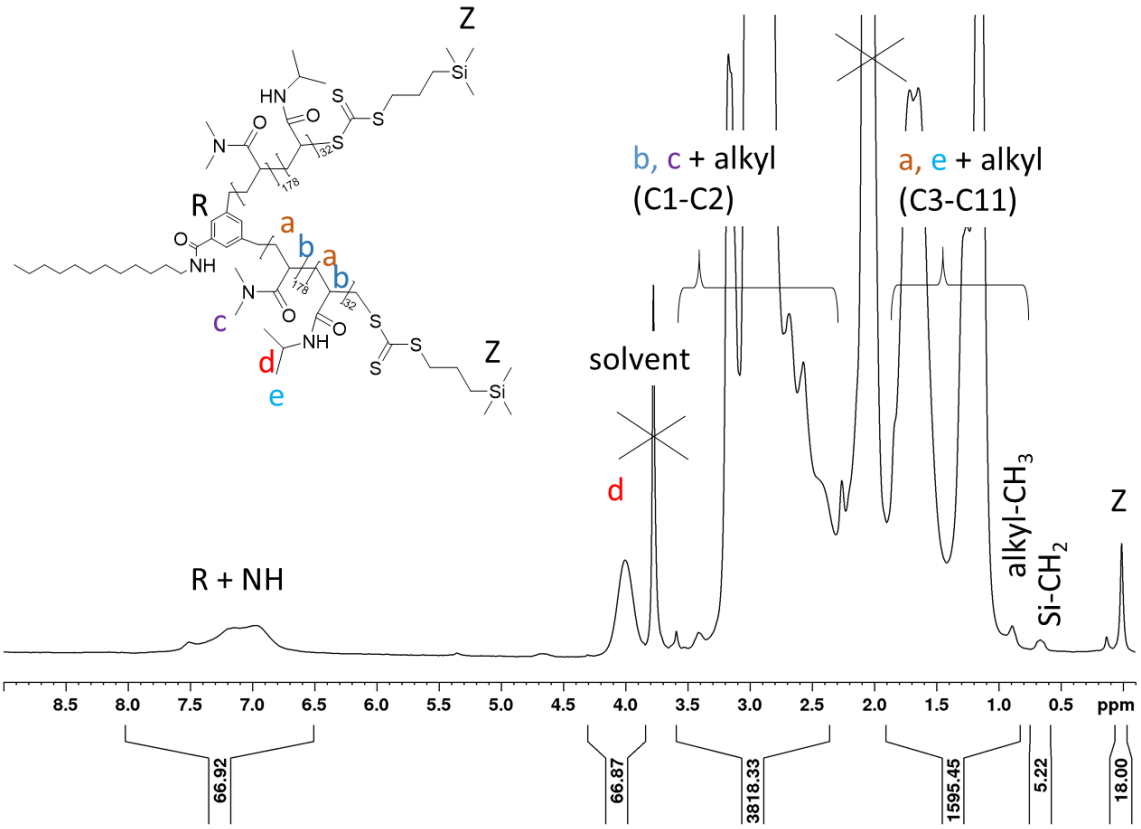

Figure 7.1: ^{1}H-NMR spectrum of **YS1-2** in acetone-d_6.

7.2 Synthesis and Characterization of Non-symmetrical Quasi-Miktoarm Block Copolymers

The design of the non-symmetrical miktoarm architecture demanded a more complex approach than the symmetrical one. Therefore, a combination of RAFT polymerization and Single Unit Monomer Insertion (SUMI) was explored to introduce the hydrophilic and the thermoresponsive blocks as well as a hydrophobic sticker group (Scheme 7.2). The SUMI technology allows the addition of one single vinyl monomer to the initiator without the continuous growth of polymer chains with a larger number of monomer units.[215–217] The synthesis starts with two consecutive RAFT polymerization steps using a relatively simple CTA, namely benzyl (3-(trimethylsilyl)propyl)carbonotrithioate (**BTPT**), during which the first thermoresponsive block and the hydrophilic block is introduced. Then, SUMI is used to insert only one monomer

bearing the hydrophobic chain. Afterwards, two consecutive RAFT polymerizations are again applied to introduce the other hydrophilic arm and the second thermoresponsive block.

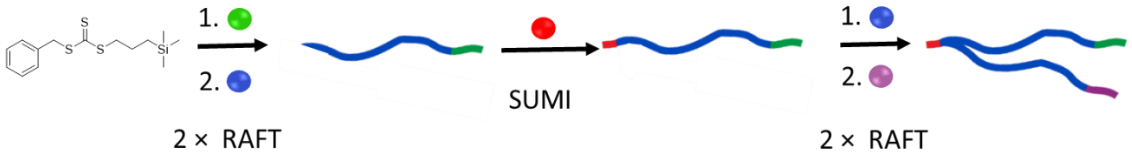

Scheme 7.2: Synthesis strategy of the non-symmetrical quasi-miktoarm block copolymer by combining RAFT polymerization and Single Unit Monomer Insertion (SUMI).

While the potential of SUMI was discussed widely,[218,219] in reality, the technology is limited to few non-homopolymerizable monomers or monomers with low propagation rate constants restricting multiple monomer insertions.[217] For example, the combination of RAFT polymerization with SUMI is a method known for discrete oligomer synthesis and macro-RAFT agents.[215,217,220] In some cases, SUMI was also used to introduce a specific end group into a polymer chain.[221,222] Some of the first SUMI reactions were therefore performed with maleimides,[223] which do not efficiently homopolymerize under typical RAFT conditions.[224,221] Therefore, a dodecyl-functionalized maleimide was used to insert the hydrophobic sticker group between the two hydrophilic blocks. Two dodecyl-functionalized maleimides, *N*-dodecyl maleimide (DMI)[195,196] and *N*,*N*-4-(2,5-dioxo-2,5-dihydro-1H-pyrrol-1-yl)-*N*-dodecylbenzamide (DBMI)[225,226] were synthesized by adapting literature procedures (Figure 7.2).

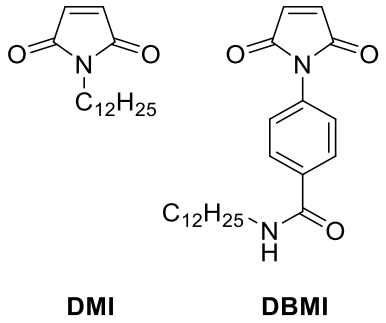

Figure 7.2: Chemical structures of two dodecyl-functionalized maleimides *N*-dodecyl maleimide (DMI) and *N*,*N*-4‐(2,5‐dioxo‐2,5‐dihydro‐1H‐pyrrol‐1‐yl)‐*N*-dodecylbenzamide (DBMI), used for SUMI.

Preliminary SUMI experiments using only the PDMAm blocks were performed, and the molecular characteristics of the employed and obtained polymers are summarized in Table 7.2. PDMAm homopolymers were obtained by RAFT polymerization using **BTPT** as the CTA and V-40 as the

initiator. More details about the polymerization procedures can be found in the Experimental Part in Table 10.6.

Table 7.2: Molecular characteristics of SUMI pre-experiments using the consecutive approach with macroCTA PDMAm derived from RAFT polymerization with **BTPT** (see Figure 0.1a in case for Y-non-symmetrical architecture).

Code	Polymer	CTA	Yield %	Theo [a]		NMR-Z [c]			SEC		UV-Z
				M_n kg/mol	DP_n	M_n kg/mol	DP_n	Z/R[d]	M_n kg/mol	Đ	M_n kg/mol
YN1a	$PDMAm_{202}$	BTPT	-[b]	17	166	20	202	1.0	16	1.25	25
YN1b	$PDMAm_{208}$	BTPT	73	19	187	21	208	0.9	19	1.18	20
YN1a-7	$PDMAm_{202}$-$DBMI_{0.29}$	YN1a	-[b]	17	1	20	0.29	1.2	-[b]	-[b]	-[b]
YN1b-7	$PDMAm_{208}$-$DBMI_{0.39}$	YN1b	59	19	1	21	0.39	0.9	-[b]	-[b]	22
YN1b-7-1a	$PDMAm_{208}$-$DBMI_{0.39}$-$PDMAm_{106}$	YN1b-7	24	26	72	32	106	1.0	23	1.21	30

[a] determined by conversion of monomer peaks in ^{1}H-NMR by comparing the signals at 0 h and after the final reaction time, [b] was not determined, [c] calculated using integrals of TMS group, [d] calculated by comparison of the integrals of the aromatic protons and the TMS-group. Precision of all molar mass values is ± 20 %.

First, a test SUMI reaction adapted to reported literature procedure[221] with DMI was tried using **YN1a** as a macroCTA and an excess of DMI monomer in benzene. After 19 h of polymerization time, the reaction mixture became brownish indicating some change of the usually yellowish trithiocarbonate compound. However, an introduction of the DMI monomer was not visible, neither in the ^{1}H-NMR, nor in the FTIR spectrum (see Figure 7.3) due to the overlap of characteristic DMI signals with the polymer signals.

Therefore, DMI was replaced by DBMI, which bears the dodecyl chain attached to a benzamide instead to the maleimide group making its chemical structure more similar to the CTA with the linear reference architecture **C12-CTA**. The details of the reaction conditions are depicted in the Experimental Part in Table 10.6. Still, when performing the polymerization using **YN1b** as the macroCTA with an excess of DBMI monomer in benzene and V-40 as the initiator at 90 °C, the reaction mixture became brownish, and either too much DBMI was introduced, or most of the Z-group was lost and only 24 % DBMI was introduced. To reduce side reactions, a lower polymerization temperature of 60 °C was tried using AIBN as the initiator and DMF similar to a reported procedure.[221] Even though DMF is a poor solvent for DBMI compared to benzene, it does

not evaporate as easily, which makes it more practicable for the deoxygenating process. The resulting sample **YN1b-7** incorporated 39 % of DBMI monomer after 17 h of polymerization time. Due to the additional aromatic group, the introduced DBMI unit was well visible in the ^{1}H-NMR (Figure 7.4) as well as in the FTIR spectrum (see Figure 7.3).

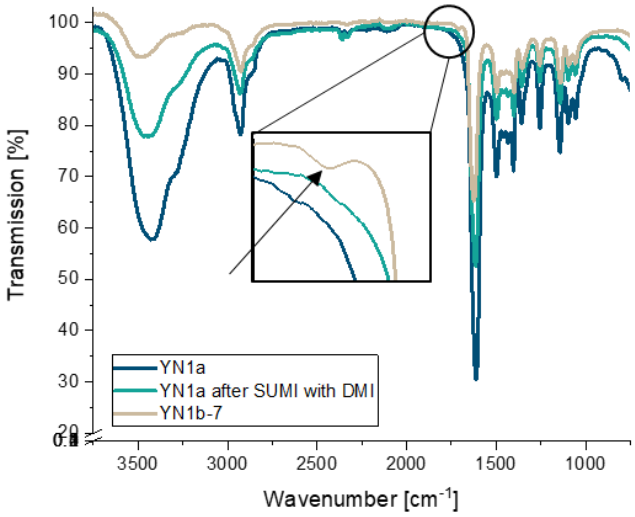

Figure 7.3 FTIR spectrum of PDMAm macroCTA **YN1a** before and after SUMI reaction with DMI or DBMI **YN1b-7**.

Next, chain extension of **YN1b-7** with DMAm was tried. The reactivation of the macroCTA was difficult and conversion was low with 36 %. Since higher than 50 % conversions of using SUMI could not be achieved, chain extension of the DBMI ends would always remain difficult, because more chain ends with the easier activating DMAm ends exist. Therefore, a different approach was applied to obtain a more efficient reactivation. In this approach, DBMI was added during the RAFT polymerization of the DMAm blocks, as soon as high conversions of the DMAm monomer were reached. This should result in a block copolymer with the DBMI unit at the very end of the polymer chain followed by some DMAm units facilitating the reactivation in the next polymerization step. For this procedure, DMAm conversion was traced by ^{1}H-NMR. This was followed by two successive RAFT polymerizations, during which the second PDMAm block and the second thermoresponsive block were attached. More details about the polymerization procedures of the different steps can be found in the Experimental Part in Table 10.7.

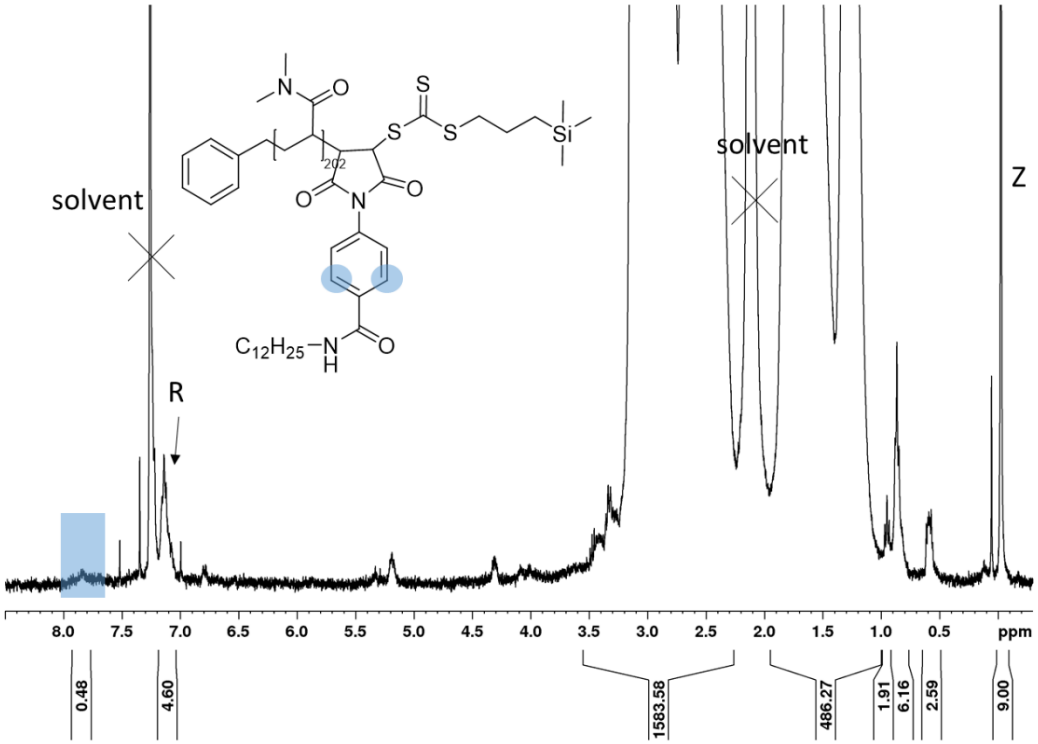

Figure 7.4: ^{1}H-NMR spectrum of PDMAm$_{202}$-DBMI$_{0.29}$ **YN1a-7** in $CDCl_3$.

The molecular characteristics of the homo-and block copolymers of this "one-pot" approach derived from **BTPT** as the starting CTA for the samples **YN2** and **YN5** are summarized in Table 7.3. In the first step, a thermoresponsive block was synthesized, which was either a PNiPAm block **YN2** or a PNPAm block **YN5**. Both samples were polymerized under typical RAFT polymerization conditions using **BTPT** as the CTA and V-40 as the initiator in benzene at 90 °C. The monomer and CTA concentration was 50 wt% and the ratio [CTA]:[initiator] 5:1. These homopolymers were obtained in good yields of > 70 %. The molar masses calculated using different methods matched very well with each other and the dispersities Đ were below 1.3 indicating good control over the polymerization process. Although the N-H signal is usually overlapping with aromatic protons of the R-group, for the samples **YN2** and **YN5**, the Z/R ratio could be calculated by subtracting the integral of the N-H proton leading to the integral of the aromatic protons (see Appendix, Figure 11.39 and Figure 11.42). This is probably possible due to the low molar mass of the polymers leading to more intense signals of the end group compared to the block copolymers with relatively large molar mass. In the next step, the thermoresponsive blocks were chain extended with DMAm under the same reaction conditions (except for sample **YN2-1a-7**, for which AIBN at 60 °C was used) and the conversion was monitored carefully by ^{1}H-NMR. Hourly visual control of the polymerization was very important, since the reaction mixture usually solidified after 3 h of

polymerization time, when a constant monomer and CTA concentration of 50 wt% was used. Therefore, more benzene was added, as soon as the reaction mixture became too viscous and the stirring bar stopped moving. After reaching high conversions of more than 90 %, a deoxygenated solution of DBMI in THF was added to the polymerization mixture via syringe. THF was used, since benzene did not dissolve the DBMI monomer.

Table 7.3: Molecular characteristics of homo- and block copolymers with non-symmetrical quasi-miktoarm architecture using the "one-pot" approach and derived from the starting CTA **BTPT** (see Figure 0.1a in case for Y-non-symmetrical architecture).

Block	Code	Polymer	Yield %	Theo [a]		NMR-Z [b]			SEC		UV-Z
				M_n kg/mol	DP_n	M_n kg/mol	DP_n	Z/R[d]	M_n kg/mol	Đ	M_n kg/mol
A	YN2	$PNiPAm_{44}$	77	4.8	40	5.3	44	1.1[e]	4.8	1.19	5.8
	YN5	$PNPAm_{47}$	71	5.2	43	5.6	47	0.8[e]	6.4	1.25	5.8
A-b-B-SUMI	YN2-1a-7	$PNiPAm_{44}$-b-$PDMAm_{240}$-$DBMI_2$	50	23	174+2	29	240+2	-[f]	24	1.37	35
	YN2-1b-7	$PNiPAm_{44}$-b-$PDMAm_{299}$-$DBMI_{0.4}$	51	25	200+1	48	299+0.4	0.7	30	1.26	80
	YN5-1c-7	$PNPAm_{47}$-b-$PDMAm_{272}$-$DBMI_1$	57	25	200+1	33	272+1	-[f]	33	1.25	77
A-b-B-SUMI-B'	YN2-1a-7-1d	$PNiPAm_{44}$-b-$PDMAm_{240}$-$DBMI_2$-b-$PDMAm_{297}$	73	41	182	59	297	0.6	45	1.43	235
	YN2-1b-7-1e	$PNiPAm_{44}$-$PDMAm_{299}$-$DBMI_{0.4}$-$PDMAm_{359}$	43	44	194	71	359	0.8	57	1.42	231
	YN5-1c-7-1f	$PNPAm_{47}$-$PDMAm_{272}$-$DBMI_1$-$PDMAm_{379}$	40	40	149	71	379	-[f]	54	1.51	248
A-b-B-SUMI-B'-A	YN2-1a-7-1d-5a	$PNiPAm_{44}$-$PDMAm_{299}$-$DBMI_2$-$PDMAm_{297}$-$PNPAm_{11}$	33	42	9	60[g]	11[g]	-[f]	48	1.36	-[g]
	YN5-1c-7-1f-2a	$PNPAm_{47}$-$PDMAm_{272}$-$DBMI_1$-$PDMAm_{379}$-$PNiPAm_{36}$	41	42	14	75	36	-[f]	57	1.50	362

[a] determined by conversion of monomer peaks in ^{1}H-NMR by comparing the signals at 0 h and after the final reaction time, [b] calculated using integrals of TMS group, [d] calculated by comparison of the integrals of the aromatic protons and the TMS-group, [e] could be calculated by substracting the N-H signal and by comparison of the integrals of the aromatic protons and the TMS-group, [f] could not be calculated due to overlapping NH-signal, [f] band not visible in the UV-vis spectrum for applied concentrations. [g] determined by comparison with PNiPAm block. Precision of all molar mass values is ± 20 %.

Even when THF was used, the mixture had to be heated to dissolve the DBMI completely. While an excess DBMI was necessary for the SUMI pre-experiments using the consecutive approach (Table 7.2), the "one-pot" approach worked well with 1-2 eq. DBMI.

Additionally, the FTIR-spectra of the polymers before and after SUMI confirm the introduction of the DBMI monomer indicated by the small C=O band of the DBMI (Figure 7.5).

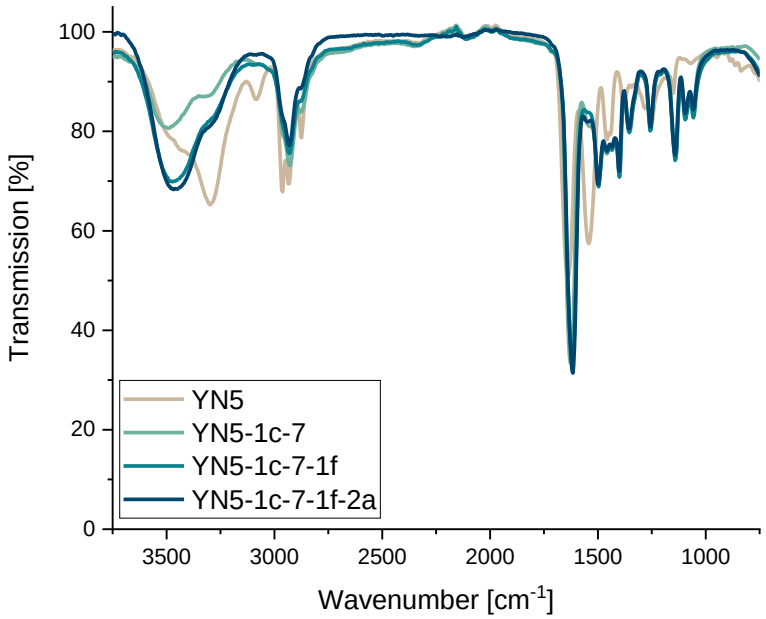

Figure 7.5: Evolution of the FTIR spectra of the homo- and block copolymers derived from macroCTA PNPAm **YN5**.

Still, the total polymerization time was relatively long with 6-18 h illustrating the difficult incorporation of the DBMI monomer. The block copolymer was obtained after two- to 4-fold precipitation in mixtures of pentane and diethylether to remove the residual DBMI completely. The resulting yield was around 50 %, clearly indicating the loss of some low molar mass material by the precipitation process. This is also visible in the molar mass values determined by ^{1}H-NMR and by UV-vis, which tend to be higher than the theoretical values. The precipitation process also narrowed the distributions and therefore, the dispersities Đ remain below 1.4. Nevertheless, the dispersities Đ are higher than in the first step. A reason for the broadened molar mass distributions might be the added THF, which can undergo chain transfer reactions by hydrogen abstraction at the α-methylene group next to the oxygen.[72] The molar masses determined by SEC match well with the values of the other methods. Overall, the polymerization process was relatively well

controlled, which is also indicated by the monomodal SEC elugrams (Figure 7.6). Still, the high M_n^{UV-Z} values and the Z/R ratio of 0.7 of the sample **YN2-1b-7** indicate a notable loss of Z-groups. This is most probably attributed to the long polymerization time, during which most of the initiator V-40 decomposed. Each starting initiator radical leads to the inevitable loss of one Z-group due to the inherent RAFT mechanism.[171] Nevertheless, the "one-pot" approach improved the insertion of DBMI, with less side reactions than the "consecutive" approach.

In the following step, the SUMI product was chain extended with DMAm. The polymerization took place in benzene using V-40 at 90 °C and 50 wt% of monomer and CTA. High conversions were obtained within 5 h. The quasi-tetrablock copolymers **YN2-1a-7-1d**, **YN2-1b-7-1e**, and **YN5-1c-7-1f** were purified by twofold precipitation in diethylether. The obtained molar mass values increased by at least a factor of 2 indicating the successful chain extension with DMAm. While the values M_n^{theo} and M_n^{SEC} match very well with each other for samples **YN2-1a-7-1d**, **YN2-1b-7-1e**, and **YN5-1c-7-1f**, the values obtained by ^{1}H-NMR and especially UV-vis are markedly higher. Also, a lower molar mass shoulder appears in the SEC elugrams. Thus, also the dispersities Đ are further increased to 1.4-1.5 compared to the precursors **YN2-1a-7**, **YN2-1b-7** and **YN5-1c-7**. Since the precursor polymers have lost part of their end groups, the chain extension only occured for the polymer chains with preserved Z-groups.

In the last step, the second thermoresponsive block was introduced into the block copolymers to obtain the final non-symmetrical quasi-miktoarm architecture. In the case of polymer **YN2-1a-7-1d**, PNPAm was chosen as the second thermoresponsive block and in the case of polymer **YN5-1c-7-1f**, PNiPAm was chosen as the second thermoresponsive block. This step led to the final quasi-pentablock copolymers **YN2-1a-7-1d-5a** and **YN5-1c-7-1f-2a**, respectively.

Within 3-4 h, 22 and 30 % conversion was reached for the samples **YN2-1a-7-1d-5a** and **YN5-1c-7-1f-2a**, respectively. The molar masses obtained by the different methods are very similar to the precursor polymer, since the newly attached block is relatively small compared to the rest of the polymer. Nevertheless, the SEC elugrams (Figure 7.6) showed a notable, although small, shift of the elugrams compared to the precursor polymers, demonstrating that quasi pentablock copolymers were obtained.

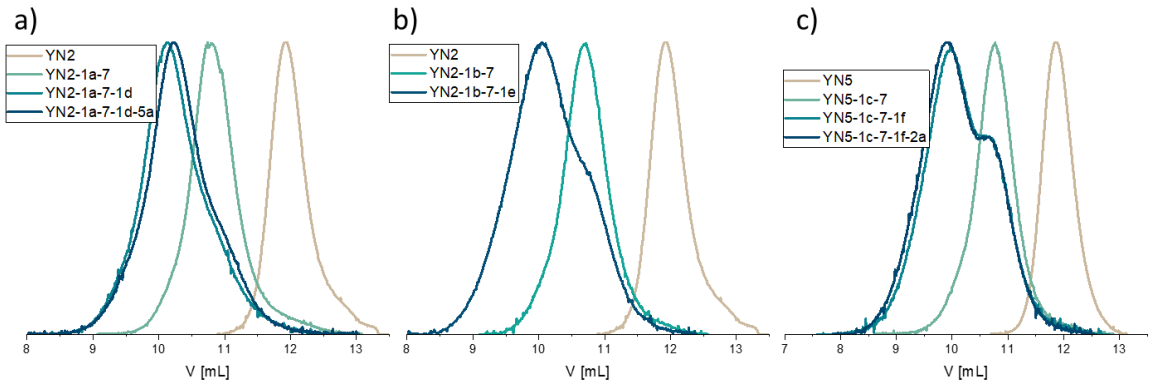

Figure 7.6: SEC elugrams of the homo- and block copolymers of the SUMI "one-pot" experiments derived from macroCTAs **YN2** or **YN5**.

The results show that the last chain extension is challenging. This is not only because of the loss of many Z-groups in the previous polymerization steps, but also because of the low monomer and end group concentration rendering the chain growth slow. The ^{1}H-NMR spectra of the final non-symmetrical quasi-miktoarm block copolymers are shown in Figure 7.7. Due to the high molar mass of the block copolymers, the intensity of the singlet signal of the Z-group is relatively low, especially for the sample **YN2-1a-7-1d-5a**, which was also subject to a higher end group loss than **YN5-1c-7-1f-2a**. Therefore, the PNPAm block length was calculated by comparison with the PNiPAm block. Still, the intensity of the TMS signal was sufficiently high for the sample **YN5-1c-7-1f-2a** and was therefore used to calculate the block length of the PNiPAm block.

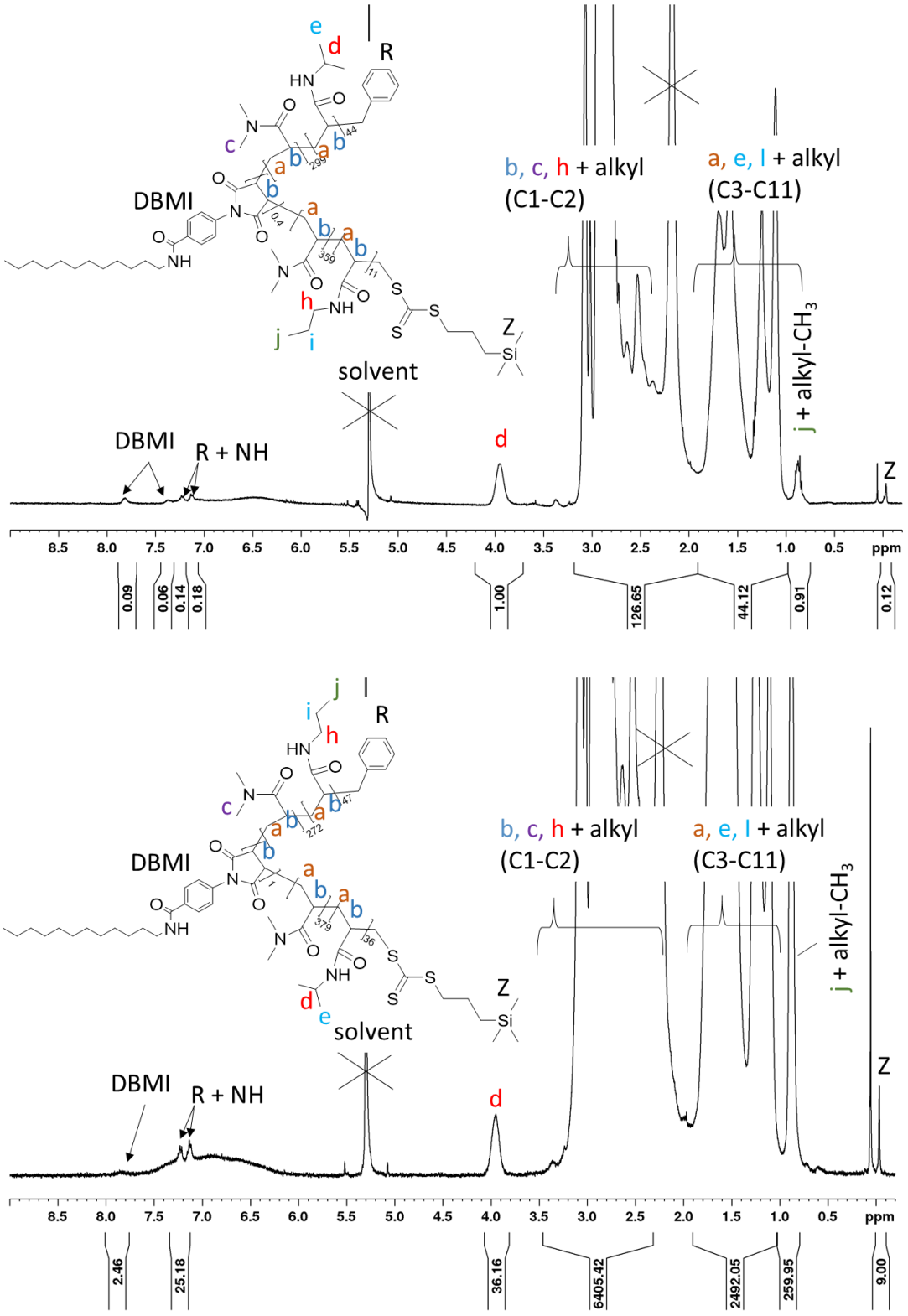

Figure 7.7: ^{1}H-NMR spectra of quasi-pentablock copolymers **YN2-1a-7-1d-5a** (top) and **YN5-1c-7-1f-2a** (bottom) in CD_2Cl_2.

In the aromatic region, the signals of the R-group as well as of the DBMI unit appear, however, they are mainly overlapping with the NH group. When the sample **YN2-1a-7-1d-5a** was measured in D_2O, the signals of the R-group were better visible, but the aromatic protons of the DBMI unit were still overlapping with the N-H group (see Appendix Figure 11.45).

Compared to the symmetrical quasi-miktoarm architecture of the **YS**-series, where the chain could grow in parallel on two sides, the non-symmetrical architecture bears only one end for chain growth, thus slowing chain extension down for the high molar mass polymers. Due to the decrease in chain-end fidelity and the necessary purification after each step, the synthesis of such multiblock copolymers with RAFT polymerization remains challenging. The relatively best results by RAFT polymerization were usually achieved, when one-pot procedures were applied for the synthesis of the complete macromolecules, and reaction times were kept short.[111,227,228] Regarding the non-symmetrical quasi-miktoarm polymers, such an approach would be problematic. First of all, the blocks have to be very precise in their chemical structure. However, a one-pot approach for the synthesis of the complete macromolecule can lead to the incorporation of some monomers from the first block to the second block, if the conversions are not close to complete. Furthermore, the dodecyl chain should be placed right in the center of the block copolymer, which is difficult to assure if a complete one-pot procedure is applied. Still, the undertaken chain extension experiments demonstrate the a priori feasibility of this approach. They worked to a large extent, and the incompletely chain-extended polymer chains should not interfere too much when the polymers are applied as rheological modifiers, but only act as diluent.

7.3 Phase Transition Behavior of Block Copolymers with Symmetrical Quasi-Miktoarm Architecture

The phase transition behavior of the symmetrical quasi-miktoarm block copolymers was investigated by DLS and turbidimetry in aqueous solutions for a concentration of 5 $g \cdot L^{-1}$ for the samples **YS1-2** and **YS1-3**, and of 20 $g \cdot L^{-1}$ for the sample **YS1-5** (Figure 7.8). Below their phase transitions, the block copolymers were soluble in water. With increasing temperature, the transmission of the block copolymers **YS1-2** and **YS1-3** started decreasing at around 50 °C and 73 °C, respectively, from 100 % to around 20 % turning the solution turbid (Figure 7.8a-b). A very different behavior showed the sample **YS1-5** bearing the PNPAm block (Figure 7.8c). For this block copolymer, the transmission first slightly increased from around 95 to 100 % reaching a maximum at 20 °C. After that, it slightly decreased again, even though a relatively high concentration of 20 $g \cdot L^{-1}$ was used. These behaviors were also found in the DLS measurements.

With increasing temperature, all the hydrodynamic diameters of the block copolymers slowly increased, until their size changed significantly at their phase transition temperature of 50 °C for **YS1-2**, 73 °C for **YS1-3**, and 22 °C **YS1-5**. While the samples **YS1-2** and **YS1-3** underwent phase separation turning the solution turbid, sample **YS1-5** showed only a slight increase of the hydrodynamic diameter from 25 to 55 nm, after which the size slowly decreased again towards a diameter of 32 nm with increasing temperature. Since the architectures are the same and the block sizes comparable, the differences in the thermoresponsive behavior should be attributed to the chemical structure of the thermoresponsive blocks. The sample **YS1-2** bearing a PNiPAm block has a similar CP as the linear reference architecture **L1a-2b**. However, the clouding transition of the quasi-miktoarm architecture is less steep than the linear one, pointing out the enhanced stability of the solitary micelles due to the additional arm. Such stable micellar structures were also observed by Aljuaid et al.[229] for similar quasi-miktoarm architectures with alkyl chains as central sticker group and PEO chains as hydrophilic arms. The alkyl chains formed a core group and the two PEO chains formed the corona layer.[229] The quasi-miktoarm architecture bears the hydrophobic sticker in the center, and not in the end of the polymer chain, which might hamper the formation of large aggregates. Interestingly, the sample **YS1-3** bearing PDEAm as the thermoresponsive block, has a CP of 73 °C that is much higher compared to the linear architecture with a CP of around 50 °C. This shows that the PDEAm block is affected more by an additional hydrophilic block than the PNiPAm block, which is presumably caused by the different LCST types of the polymers. As PDEAm is a LCST type I polymer, its phase transition behavior is relatively sensitive to molar mass and end groups.[19] A quite different behavior shows the sample **YS1-5**, which did not undergo a phase separation into a turbid solution. Instead, the aggregate sizes started increasing at a CP of around 20 °C reaching a maximum aggregate size of 55 nm at around 30 °C, after which the size slowly decreased again reaching a final diameter of 32 nm. The respective linear reference architecture **L1b-5a** also showed a similar behavior, with a CP around 30 °C and a maximum aggregate size of around 54 nm at 35 °C. The comparison shows that the miktoarm architectures have a very similar phase transition behavior as the linear reference architectures, especially for the samples **YS1-2** and **YS1-5** bearing PNiPAm and PNPAm as the thermoresponsive blocks, respectively. These results demonstrate that the additional arm as well as the changed position of the hydrophobic sticker group enhance the stability of loose micelles. With increasing temperature, these micelles can aggregate further to larger structures when the thermoresponsive blocks are sufficiently dehydrated.

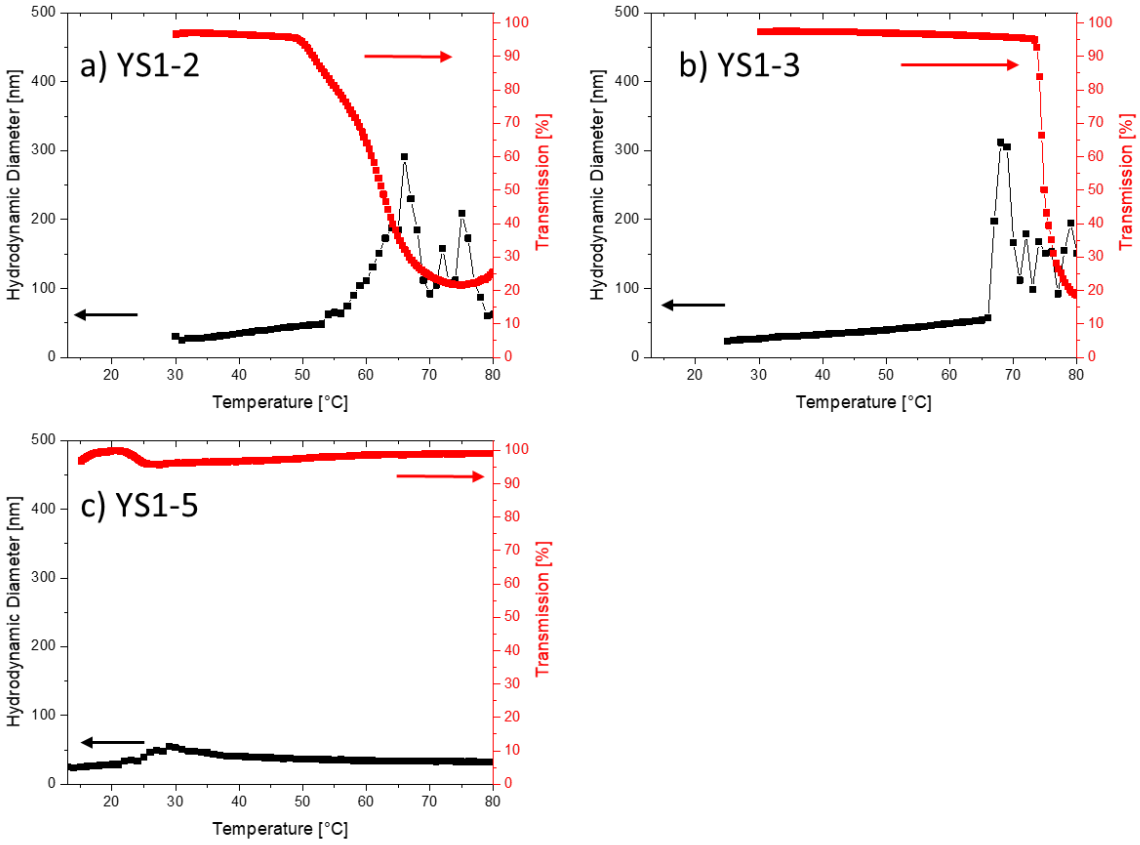

Figure 7.8: Temperature-dependent hydrodynamic diameter from DLS and transmission from turbidimetry for 5 g·L^{-1} aqueous solutions of a) PDMAm$_{178}$-b-PNiPAm$_{32}$ **YS1-2** and b) PDMAm$_{178}$-b-PDEAm$_{29}$ **YS1-3**; and for 20 g·L^{-1} aqueous solutions of c) PDMAm$_{178}$-b-PNPAm$_{51}$ **YS1-5**.

7.4 Phase Transition Behavior of Block Copolymers with Non-symmetrical Quasi-Miktoarm Architecture

The thermoresponsive behavior of aqueous solutions of quasi-pentablock copolymers **YN2-1a-7-1d-5a** and **YN5-1c-7-1f-2a** were investigated by turbidimetry measurements for concentrations of 5 g·L^{-1} and 20 g·L^{-1} (Figure 7.9). All phase transitions were fully reversible as indicated by the heating and cooling curves. For aqueous solutions of 5 g·L^{-1} of **YN2-1a-7-1d-5a** and **YN5-1c-7-1f-2a**, the transmission decreases to 1-2 %, after which it increases again. When increasing the concentration to 20 g·L^{-1} of **YN5-1c-7-1f-2a**, the phase transition step becomes more

markedly with a transmission decrease of around 6 %. After reaching a minimum, the transmission increases again reaching a plateau at around 95 %.

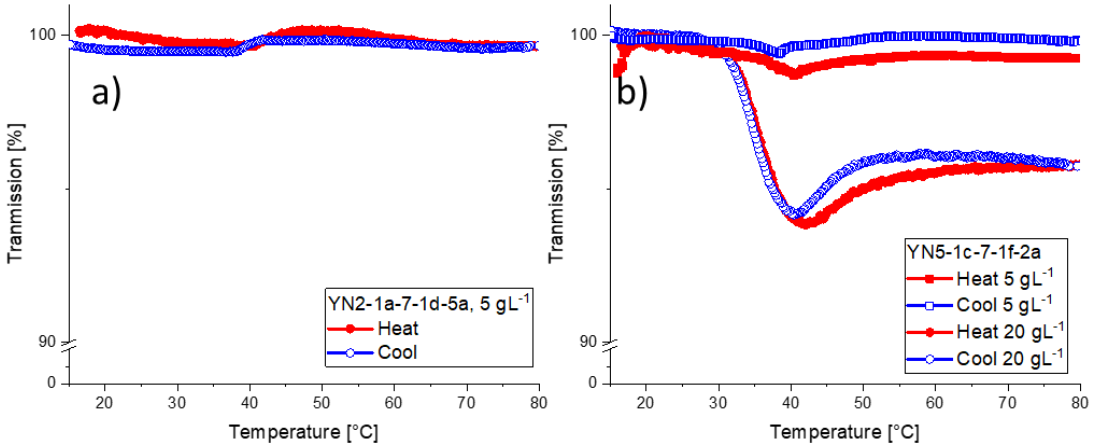

Figure 7.9: Turbidimetry measurements for aqueous solutions of $PNiPAm_{32}$-$PDMAm_{299}$-$DBMI_{0.4}$-$PDMAm_{359}$-$PNPAm_{11}$ **YN2-1a-7-1d-5a** (a) and $PNPAm_{32}$-$PDMAm_{272}$-$DBMI_{1}$-$PDMAm_{379}$-$PNiPAm_{36}$ **YN5-1c-7-1f-2a** (b) for varying concentrations.

These behaviors were also visible in the DLS measurements and were directly compared to the precursor polymers (Figure 7.10). Starting with the PNiPAm SUMI series (Figure 7.10a), the very first block, which is the thermoresponsive homopolymer PNiPAm **YN2** showed a CP at around 20 °C. This CP is much lower than the reported one for PNiPAm of 32 °C,[50] which can be explained by the strong influence of the hydrophobic end groups on the relatively short polymer chains. The therefrom-derived block copolymer **YN2-1a-7** however, was soluble at a larger range, with a CP of 50 °C. This CP-shift towards higher temperatures is presumably a result of the attached hydrophilic PDMAm block increasing the solubility range of the thermoresponsive block copolymer. During the phase transition, the hydrodynamic diameter of the PNiPAm containing sample **YN2-1a-7** strongly increased from around 40 nm to more than 100 nm. Such a behavior was also observed for the linear analog **L1a-2b** demonstrating how similar the architectures and chemical structures are, even though different synthesis routes were used. When the quasi-triblock copolymer **YN2-1a-7** is further chain extended with PDMAm, giving the quasi tetra-block copolymer **YN2-1a-7-1d**, the thermoresponsive behavior changes markedly. Above the phase transition at around 50 °C, the hydrodynamic diameter increases only slightly from around 30 nm to around 40 nm indicating small aggregates. The final quasi-pentablock copolymer **YN2-1a-7-1d-5a** had a very similar thermoresponsive behavior to its precursor with a blurred phase

transition at around 40 °C. Presumably, this is because the attached PNPAm block was also relatively short. Still, at temperatures below 25 °C, the sample **YN2-1a-7-1d-5a** showed an increase of the hydrodynamic diameter from 30 to 60 nm. This might indicate that despite its very small size, the attached PNPAm block still undergoes a phase transition thus effecting the aggregation behavior. With increasing temperature, these aggregates might become smaller due to the further dehydration of the short PNPAm block, which would explain the apparent maximum at around 20 °C.

The PNPAm SUMI series started with the PNPAm homopolymer **YN5**. The clouding of the sample **YN5** took place at very low temperatures, which could not be reached by the experimental setup. Similar to the PNiPAm homopolymer **YN2**, the phase transition temperature of **YN2** is well below the reported one for PNPAm of 20 °C,[50] which can again be explained by the strong influence of the hydrophobic end groups on the relatively short polymer chains. When the PDMAm block as well as the DBMI unit was attached as in **YN5-1c-7**, the CP increased to around 40 °C. Again, this CP shift is presumably caused by the attached hydrophilic PDMAm block. Instead of forming large aggregates like the PNiPAm analog **YN2-1a-7**, the size of the PNPAm containing sample **YN5-1c-7** increased only slightly from ~25 nm to 30 nm, i.e. by 5 nm. Such a behavior was also observed for the linear analog **L1b-5a** at the same concentration, which seems again to show that the incorporation of the DBMI unit via SUMI leads to a similar architecture as the **C12-CTA** based quasi-triblock copolymers. When another PDMAm block is attached, the phase transition for the sample **YN5-1c-7-1f** remains unchanged. This behavior indicates that a larger hydrophilic block as well as the position of the dodecyl group has almost no influence on the phase transition behavior for this block copolymer. In the final step, when the second thermoresponsive block PNiPAm is incorporated resulting in the quasi-pentablock copolymer **YN5-1c-7-1f-2a**, the thermoresponsive behavior changes markedly. The sample **YN5-1c-7-1f-2a** showed a pronounced phase transition around 32 °C accompanied by an increase of the average diameter from 30 to 60 nm. Since the newly attached thermoresponsive PNiPAm block had a sufficient high DP_n of around 40 to show a marked effect on the phase transition behavior. Compared to its precursor **YN5-1c-7-1f**, the CP of the sample **YN5-1c-7-1f-2a** decreased from around 50 °C to 32 °C, even though two separate "arms" such as the samples **YN5-1c-7** and **YN2-1a-7** had higher CP's of around 50 °C. This behavior indicates that the two different thermoresponsive blocks with medium size reduce the phase transition temperature due to favored interactions between each other.[13,230] Therefore, in contrast to the symmetrical analogues, the non-symmetrical quasi-miktoarm block copolymers are not showing a two-step transition but only one blurred phase transition step leading to small aggregates with hydrodynamic diameters of around 40 or 60 nm.

Since the hydrodynamic diameter remained well below 100 nm even above the phase transition, the non-symmetrical quasi-miktoarm block copolymers are apparently better stabilized in water than the symmetrical quasi-miktoarm architecture. Nevertheless, the broad molar mass distribution of the samples does not allow a direct comparison to the symmetrical quasi-miktoarm polymers. Still, it is obvious that the non-symmetrical quasi-miktoarm polymers have a very different behavior than the symmetrical ones, which makes them interesting in the use as rheological modifiers for microemulsions.

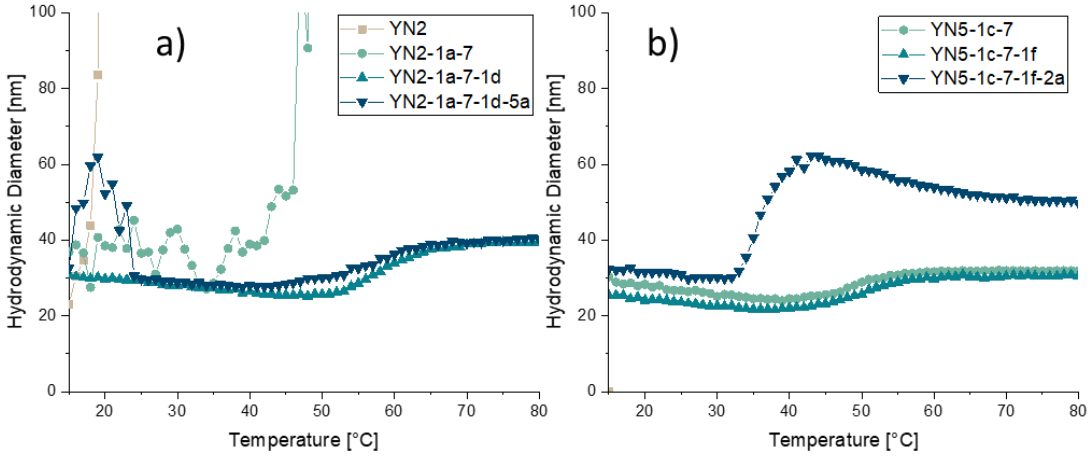

Figure 7.10 DLS measurement of aqueous solutions of 5 g·L^{-1} of **YN2** (a) and **YN5-1c-7** (b) and therefrom derived block copolymers.

8 Amphiphilic Block Copolymers with Miktorarm Architecture and Twinned Thermoresponsive Blocks

8.1 Challenges and Strategies for the Studied System

In comparison to the basic architecture **L** (linear quasi-triblock copolymer), the shape of the planned architecture **TT** (Figure 2.2) is comparable to the architecture **TH**, but, instead of the twinned hydrophobic sticker groups, branching is achieved by attaching two thermoresponsive blocks at the end of the permanently hydrophilic outer block. This thermoresponsive branch was hypothesized to enable a stronger network formation above the phase transition due to the additional interactions and thus, to increase the viscosity of a microemulsion more than the basic linear architecture **L** could achieve. Despite its apparent simplicity, the twinned thermoresponsive architecture **TT** poses some challenges in its synthesis, since it is not possible to use successive RAFT polymerization for the branching step. Hence, after polymerization of the hydrophilic block via the RAFT method, two basic strategies were considered to introduce the twinned thermoresponsive blocks, namely either by click chemistry (Scheme 8.1a) or by employing a second RDRP technique (Scheme 8.1b).

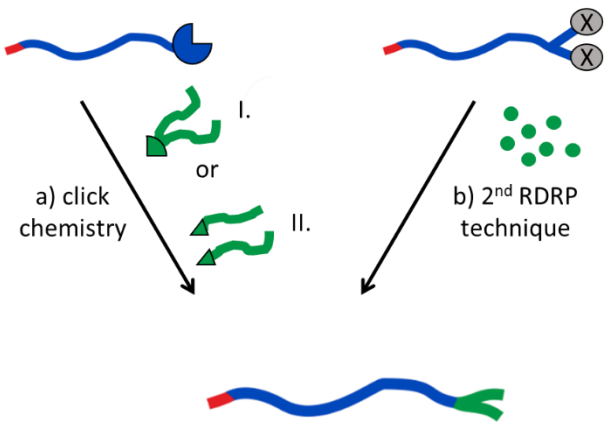

Scheme 8.1: Possible strategies for the synthesis of twinned thermoresponsive miktoarm block copolymer via a) click chemistry and b) via a second RDRP technique with reactive sites X.

In the former case, for example, copper catalyzed 1,3-dipolar azide-alkyne "Huisgen" click reaction could be used since it is an efficient method to obtain 1,4-disubstituted 1,2,3-triazole products under moderate reaction conditions.[231] However, when polymers are used, the coupling reagent is usually a low molecular weight compound employed in excess, otherwise complete reaction and

product purification remain difficult. Still, in literature some click reactions were tried to obtain block copolymers. As an example, Quémener et al.[232] synthesized block copolymers of PS and poly(vinyl acetate) (PVAc) by coupling chemistry with molar masses of the different blocks from 8 to 35 kg/mol. While the dispersity Đ of the coupled products was ≤ 1.3, some remaining homopolymer was detected due to the difficulty to work at a perfect stoichiometry of 1:1 with polymers. Liu et al.[233] achieved the coupling of PDMAm-b-PNiPAm with PDMAm, to obtain a triblock copolymer. While the diblock copolymer had a molar mass of around 20 kg/mol, which would be similar to the hydrophilic blocks used here, the coupling reagent PDMAm had a low molar mass of 3.7 kg/mol. Architecture **TT** , however, acquires either the coupling of the branched thermoresponsive polymer (Scheme 8.1a-I) or two thermoresponsive blocks (Scheme 8.1a-II) having molar masses > 4 kg/mol per block. This might lead to more complication in the coupling reaction. Since the molar masses are relatively high, the concentration of reacting end groups is low and the overall reactivity decreases.[234] In addition, both thermoresponsive blocks must couple successfully (Scheme 8.1a-II), otherwise a mixture of mono- and disubstitued block copolymers would be obtained. This would render the purification by precipitation very difficult due to the structural similitary of the polyacrylamides.

Therefore, it seemed more reasonable to combine two RDRP techniques to achieve the twinned thermoresponsive architecture (Scheme 8.1b). Thus, a well-designed CTA with initiating sites for a second RDRP technique was developed. ATRP was the method of choice, since nitroxide-mediated polymerization (NMP) for acrylamides is either limited to tertiary acrylamides,[235] or the molar masses and conversions remain low and the dispersities Đ high,[236–238] or complicated nitroxide compounds are needed.[239] Nevertheless, ATRP in solution is still challenging for acrylamides as discussed in chapter 1.3.2. Combining RAFT polymerization and ATRP is a priori possible, but requires careful experimental planning since the polymerization mechanism can be affected by the choice of monomer and catalyst.[240] The group of Matyjaszewski synthesized bromoxanthate[241] and bromotrithiocarbonate[242] iniferters,[243] which are chemical compounds that simultaneously act as initiator, transfer agent, and terminator, to selectively conduct RAFT polymerization or ATRP with acrylates, MMA, styrene or VAc. Regarding the bromoxanthate, RAFT polymerization was strongly limited to the VAc monomer, while ATRP worked well for styrene and methyl acrylate. Similar work was also done by Qiu et al.[244] for miktoarm star-block copolymers using VAc for RAFT polymerization and styrene for ATRP. For MMA, however, the bromide end group was exchanged with a chloride to improve the initiation efficiency.[241] Also, RAFT polymerization had to be performed first, otherwise ATRP could also

take place at the xanthate moiety.[241] With the bromoxanthate, only RAFT polymerization occurred for styrene and acrylates under typical conditions as heating of the reaction mixture and using AIBN as the initiator for acrylates. When CuBr, *N*,*N*,*N*,*N´´*,*N´´*-pentamethyldiethylenetriamine were used at 90 °C, however, RAFT and ATRP at the bromide as well as at the trithiocarbonate moiety took place as concurrent mechanisms.[242] The combination of RAFT and ATRP in the form of an iniferter especially for polyacrylamides is nearly unknown.[245] Therefore, a proper design for an iniferter, that allows the introduction of the hydrophobic sticker group and of the hydrophilic block via RAFT polymerization and of the twinned thermoresponsive blocks via ATRP, is required. First, the hydrophilic PDMAm block should be polymerized via RAFT, as in this way copper residues of the ATRP are avoided that can interfere with the RAFT process. Subsequently, the obtained PDMAm should be used as a macroinitiator for ATRP of the thermoresponsive blocks.

8.2 Synthesis and Molecular Characterization of the ATRP-CTAs

The combination of RAFT and ATRP requires an iniferter not only providing a thiocarbonylthio compound for the RAFT process, but also two alkyl halides suited as initiating sites. Additionally, the iniferter should introduce the hydrophobic sticker group, ideally via the R-group so that the basic chemical structure *hydrophobic sticker group – hydrophilic center block – thermoresponsive block* can be obtained. The accordingly aspired CTA designs are depicted in Figure 8.1.

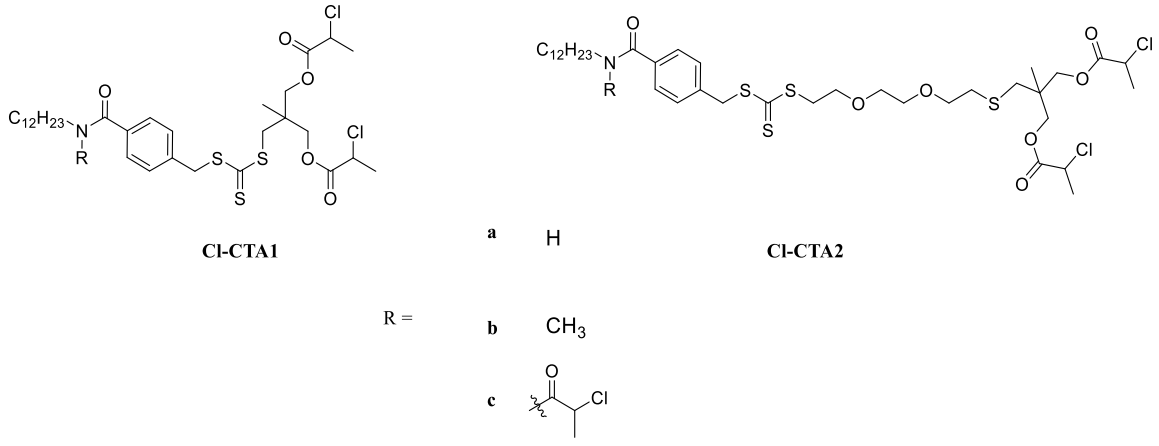

Figure 8.1: Chemical structures of the ATRP-CTA designs aimed (**Cl-CTA1a, Cl-CTA2a**, and **Cl-CTA2b**) and unintentionally obtained (**Cl-CTA1c, Cl-CTA2c**).

The structure of **Cl-CTA1** was designed to have a very short spacer between the trithiocarbonate group and ATRP initiating sites, since the obtained block copolymer should be as comparable as

possible to the other architectures to fully understand the impact of the twinned thermoresponsive blocks. Additionally, the initiating sites are symmetrical, so that chain growth can occur in parallel. **Cl-CTA1** was synthesized by forming the trithiocarbonate triethylammonium hydrosulfide salt of 2-(mercaptomethyl)-2-methylpropan-1,3-diol and subsequent alkylation with 4-chloromethyl-*N*-dodecylbenzamide. In a second step, which was adapted to a reported procedure,[246] the raw diol product was esterified with 2-chloropropionyl chloride. When this procedure was performed as one-pot reaction using pyridine as base in the esterification step instead of triethylamine, complete ester formation could be achieved using an excess of the 2-chloropropionyl chloride. However, it turned out that due to the excess of base and 2-chloropropionyl chloride, the imide **Cl-CTA1c** was formed with 30 % yield instead of the amide structure **Cl-CTA1a**. In the FTIR spectrum, the imide formation was clearly visible due to the lack of N-H peak (see Appendix Figure 11.4). Imides prepared from amides usually need an excess of an activated form of a carboxylic acid and strong basic or acidic conditions.[247,248] Noteworthy, the described reaction was performed at 0 °C using relatively weakly basic compounds to neutralize the released HCl, which means no harsh conditions were applied. However, pyridine was used for the reaction, which can act as a catalyst for the acylation of the amide,[249] possibly explaining this peculiar result of the imide formation. **Cl-CTA1c** was used to polymerize DMAm successfully via RAFT. The dispersity Đ was 1.2 and the molar masses obtained from different methods matched with each other very well (see Appendix Figure 11.51) indicating a controlled polymerization process. However, when the obtained PDMAm was used as a macroinitiator for ATRP of NiPAm with CuCl or CuBr, only side reactions leading to shoulders in the SEC elugram were observed. Different ligands and solvent systems were tested, such as 4,4′-dinonyl-2,2′-dipyridyl in butanone at 80 °C, Me_6TREN in toluene, in water or in water/ethanol mixture at room temperature, but no control of the reaction could be achieved. The reason for the lack of control could be either the imide structure of **Cl-CTA1c** giving another opportunity for the reaction with copper, or the proximity of the trithiocarbonate moiety to the initiating halide-site. To understand if the trithiocarbonate group is generally interfering with the ATRP of NiPAm, a test reaction was performed using methyl 2-chloropropionate as initiator, PDMAm as the potential interfering macroCTA and CuCl with Me_6TREN as the catalyst system in ethanol/water. The SEC elugram of the resulting polymers showed two distinct populations belonging to the PDMAm macroCTA and to the PNiPAm from ATRP (Figure 8.2a). This means that the ATRP proceeded mainly without interfering with the trithiocarbonate compound. In addition, the ^{1}H-NMR spectrum indicated that the polymerization proceeded via the methyl 2-chloropropionate initiator. However, the ^{1}H-NMR spectrum as well as the UV-vis

measurement showed some loss of end groups, which is probably a result of the radicals produced during the ATRP process interacting with the trithiocarbonate group. Interestingly, the band of the trithiocarbonate group in the UV-vis spectrum showed a shoulder (Figure 8.2b), which could be due to the influence of the copper species, which was not completely removed. The experiment suggested that a certain distance between RAFT and ATRP sites might help to reduce the interactions of the radicals with the trithiocarbonate group during the ATRP process.

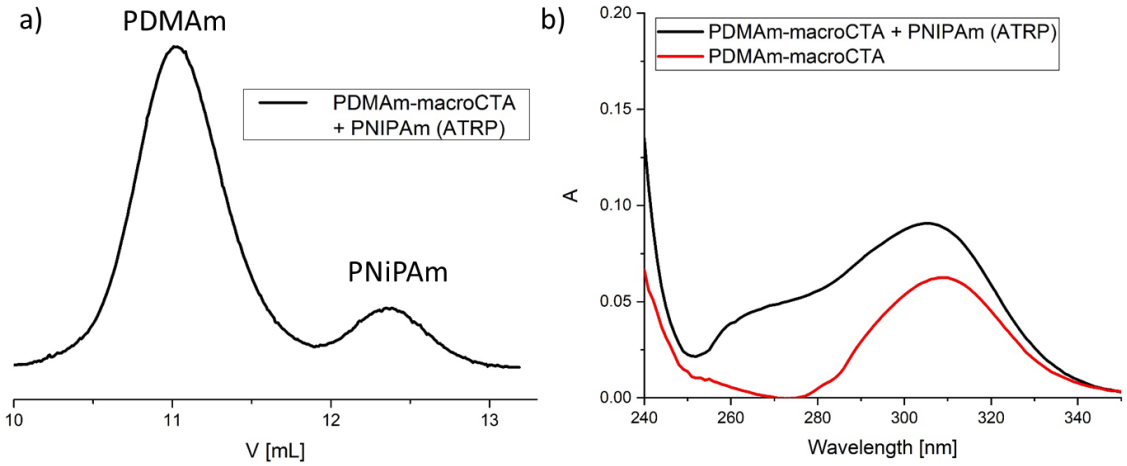

Figure 8.2: a) SEC elugram and b) UV-vis spectra in MeOH of the product of ATRP of NiPAm with PDMAm-macroCTA as potentially interfering trithiocarbonate species.

Therefore, **Cl-CTA2b** was designed, bearing an amide group, which is deactivated toward acylation by introducing a methyl group, and a spacer increasing the distance between the radical-sensitive functional groups. The spacer was based on a diethylene oxide structure, since a single alkyl structure was expected to be too hydrophobic and a direct comparison with the other synthesized architectures would be more difficult. The synthetic approach was similar as for the structure of **Cl-CTA2b**, and the product was obtained with 41 % yield in the final step. ^{1}H-NMR and ^{13}C-NMR spectra of **Cl-CTA2b** are shown in Figure 8.3. The ^{1}H-NMR clearly shows the introduced 2-chloropropionyl group, characterized by the large doublet of its methyl groups at about 1.7 ppm (Figure 8.3a). Due to the quick exchange of the cis-and trans-positions of the amide substituents, the methyl and methylene protons of the α- and β-position of the amide group appear as broad signals. All of the other peaks are clearly visible in the spectrum and no impurities from side reactions were found after purification by column chromatography. Additionally, all of the carbon peaks are well visible in the ^{13}C-NMR spectrum, especially the characteristic carbon of the trithiocarbonate group at around 220 ppm (Figure 8.3b). The signal assignment was also confirmed

by 2D-NMR-spectroscopy (see Appendix Figure 11.26). The polymerization procedure using **Cl-CTA2b** is described in the following chapter.

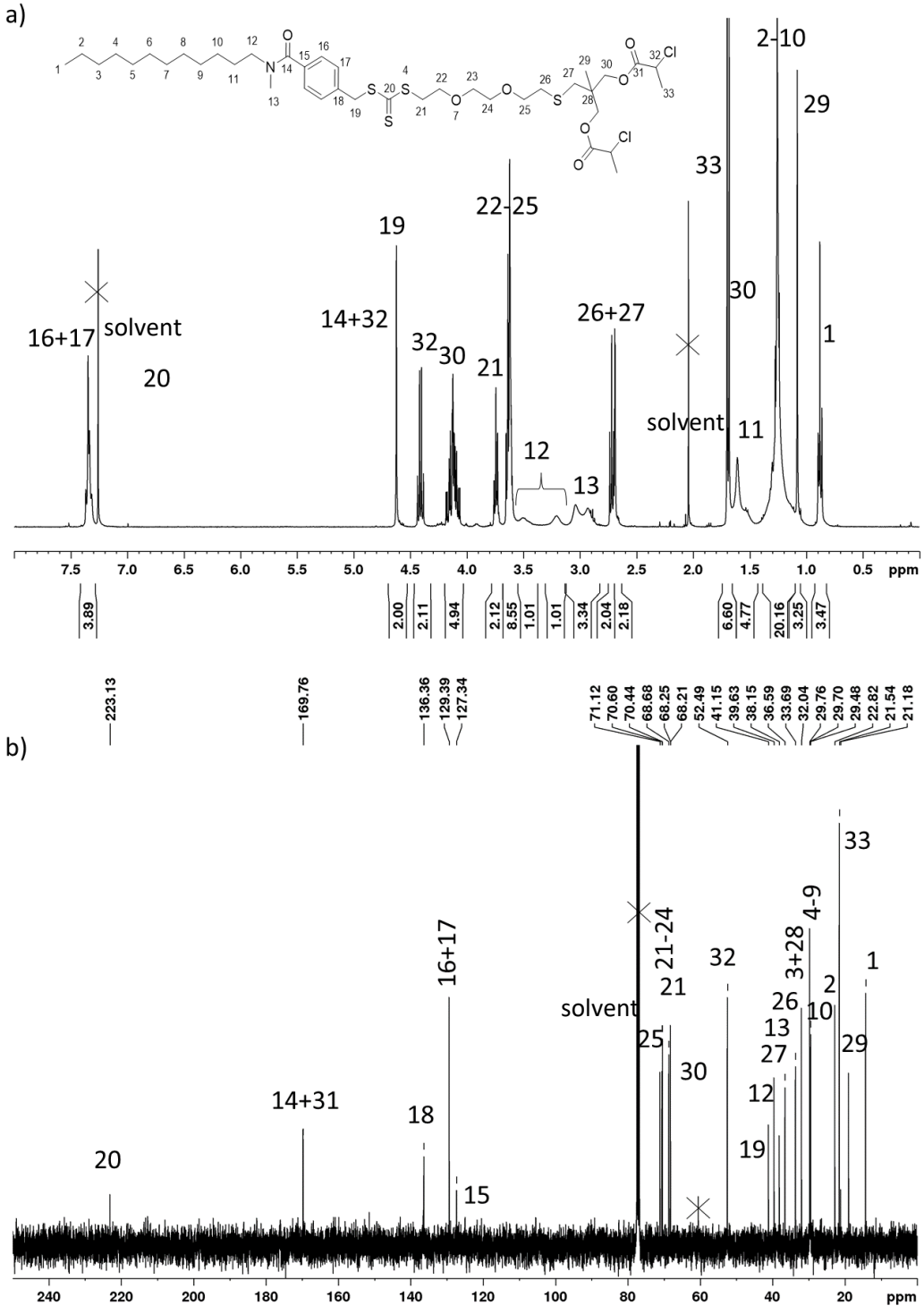

Figure 8.3: ^{1}H-NMR (a) and ^{13}C-NMR (b) spectra of **Cl-CTA2b** in $CDCl_3$.

8.3 SYNTHESIS AND CHARACTERIZATION OF HOMO- AND BLOCK COPOLYMERS BEARING RAFT- AND ATRP ACTIVE GROUPS

The key characteristics of the synthesized homo and block copolymers are summarized in Table 8.1. More details regarding the experimental procedure can be found in the Experimental Part in Table 10.8.

Table 8.1: Molecular characteristics of the homo- and block copolymers derived from **Cl-CTA2b** (RAFT polymerization: 50 wt% solution in benzene using V-40 as intiator; ATRP: using **TT1** as intiator, Cu(I)Cl as catalyst and Me_6TREN as ligand in DMF/H_2O (2/1, v/v)) (see Figure 0.1a in case for twinned thermoresponsive architecture).

Code	Polymer	CTA or initiator	Yield %	Theo [a]		NMR-Z [b]			SEC		UV-Z
				M_n kg/mol	DP_n	M_n kg/mol	DP_n	Z/R[d]	M_n kg/mol	Đ	M_n kg/mol
TT1	Cl-PDMAm$_{198}$	Cl-2b	49	21	198	26	250	1.0	22	1.23	27
TT1-2a	C1-PDMAm$_{198}$-NiPAm$_{128}$	TT1	64	28	126[g]	33	128[g]	0.8	26	1.33	49
TT1-2b	C1-PDMAm$_{198}$-NiPAm$_{118}$	TT1	60	28	126[g]	39	118[g]	-[e]	27	1.31	79
TT1-2c	C1-PDMAm$_{198}$-NiPAm$_{178}$	TT1	43	34	123[g]	46	178[g]	1.2	32	1.77	56
TT1-3a	C1-PDMAm$_{198}$-DEAm$_{168}$	TT1	52	29	130[g]	36	168[c] [g]	-[f]	21	1.51	97
TT1-3b	C1-PDMAm$_{198}$-DEAm$_{146}$	TT1	50	24	54[g]	35	146[g]	0.9	19	1.59	48
TT1-5	C1-PDMAm$_{198}$-NPAm$_{178}$	TT1	20	28	130[g]	34	142[g]	-[e]	24	1.28	168

[a] determined by conversion of monomer peaks in ^{1}H-NMR by comparing the signals at 0 h and after the final reaction time, [b] calculated using integrals of alkyl protons from diethylene oxide spacer, [c] calculated using integrals of aromatic protons from R-group, which were better visible than the Z-group signals, [d] calculated by comparison of the integrals of the aromatic protons and alkyl protons from diethylene oxide spacer. [e] could not be calculated due to overlap of N-H signal with aromatic protons, [f] could not be calculated due to partial overlapping of alkyl protons from diethylene oxide spacer with polymer signals. [g] related to 2nd block. Precision of all molar mass values is ± 20 %.

The ^{1}H-NMR spectra of **TT1** and **TT1-2a** in CD_2Cl_2 are shown exemplarily in Figure 8.4. In the precursor polymer **TT1**, all peaks are well visible and can be used to determine the end group fidelity as well as the molar mass via NMR. For the block copolymers containing PNiPAm or PNPAm blocks, the aromatic protons are usually overlapping with the N-H signal (see Appendix Figure 11.47).

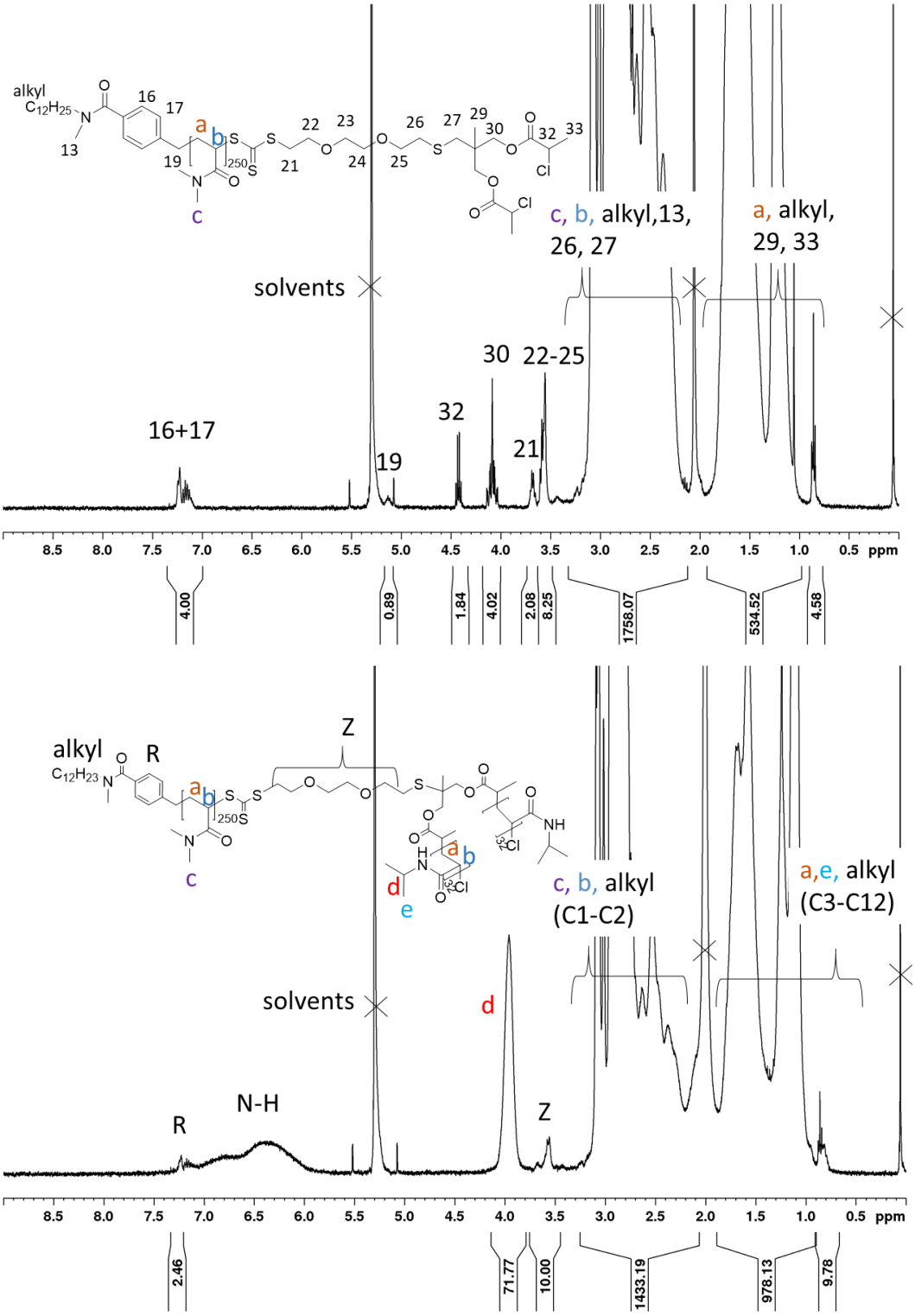

Figure 8.4: ^{1}H-NMR spectra of **TT1** (top) and **TT1-2a** (bottom) in CD_2Cl_2.

However, the protons of the spacer group are relatively well resolved in the ^{1}H-NMR spectra and were therefore used to determine the block lengths via NMR. For the samples with PDEAm blocks, the aromatic protons are well visible (see Appendix Figure 11.46), while the protons of the spacer group are partly overlapping with the polymer signals. Therefore, for the PDEAm samples, the aromatic protons were used to calculate the block lengths of the PDEAm blocks.

The polymerization of DMAm using the tailored RAFT agent **Cl-CTA2b** was carried out in the same way as described in chapter 3.2. The obtained macroCTA **TT1** carried around 200 DMAm repeat units to ensure enough hydrophilicity and thus solubility, even above the phase transition of the twinned thermoresponsive blocks. The molar mass values calculated from different methods match very well with each other and the dispersity Đ is below 1.3, confirming a well-controlled RAFT process. Still, the values M_n^{NMR-Z} and M_n^{UV-Z} are slightly higher, indicating some loss of end groups or of low molar mass fractions during precipitation. This purification process might also explain the relatively narrow dispersity Đ of 1.30-1.35. The obtained PDMAm was used in a second step as a macroinitiator for the ATRP of NiPAm, DEAm and NPAm. The ATRP conditions were adapted from reported procedures,[250,251] which used a structurally similar 2-chloropropionylated PEG macroinitiator. The catalyst system was based on CuCl and Me_6TREN in a DMF/water mixture. The conversions of the ATRP for all the block copolymers listed were always around 70 % after 3 h. Higher conversions could not be reached even after 24 h of polymerization, which is most probably due to the inactivation of the catalyst.[120] Molar masses M_n^{SEC} match very well with M_n^{theo} and the dispersities are relatively low with Đ ≤ 1.3 indicating good control over the polymerization. Only **TT1-2c** and the samples containing PDEAm as thermoresponsive blocks **TT1-3a** and **TT1-3b** show higher dispersities of Đ = 1.77, 1.51 and 1.59, respectively. Since the sample **TT1-2c** bears relatively large PNiPAm blocks with $DP_n \approx 90$ per arm, the ATRP procedure might be more difficult with increasing molar mass and thus, less accessible initiating sites, leading to the increased dispersity. Regarding the block copoplymers **TT1-3a** and **TT1-3b**, side reactions seemed to occur, as low molar mass shoulders were apparent in the SEC elugram (Figure 8.5). The molar masses M_n^{NMR-Z} and M_n^{UV-Z} determined by the use of the Z-group overestimate the molar masses, which is probably caused by some loss of end group during the polymerization or of low molar mass fractions during dialysis. Still, the values for M_n^{UV-Z} are quite large, which might be due to some loss of Z-groups during the polymerization process. Another possibility is some remaining copper, which could mislead the M_n^{UV-Z} calculation. However, Cu determination via "inductively coupled plasma optical emission spectrometry" (ICP-OES) showed that only around 0.024 wt% Cu remained. The purification method employed using a basic AlO_x filter column seems therefore

sufficient to remove the catalyst. Alternatively, homopolymerization could have occurred during ATRP, and indeed, the SEC results for **TT1-3a/b** showed a shoulder indicating some low molar mass chains (Figure 8.5). The resulting SEC elugrams of the samples with the PDEAm blocks **TT1-3a/b** differ markedly from each other, even though a similar polymerization procedure was applied. In contrast, the different samples **TT1-2a/b** containing similar PNiPAm blocks resulted in similar SEC elugrams. Additionally, the SEC elugrams for the PNiPAm block copolymer series **TT1-2** as well as for the sample **TT1-5** were all monomodal. Despite the relative high values for M_n^{UV-Z}, the ATRP of the different acrylamides seemed to work. Still, the results suggest that the ATRP of a tertiary acrylamide such as DEAm remains more difficult than of secondary acrylamides such as NiPAm and NPAm as reported previously in literature.[120,122,125]

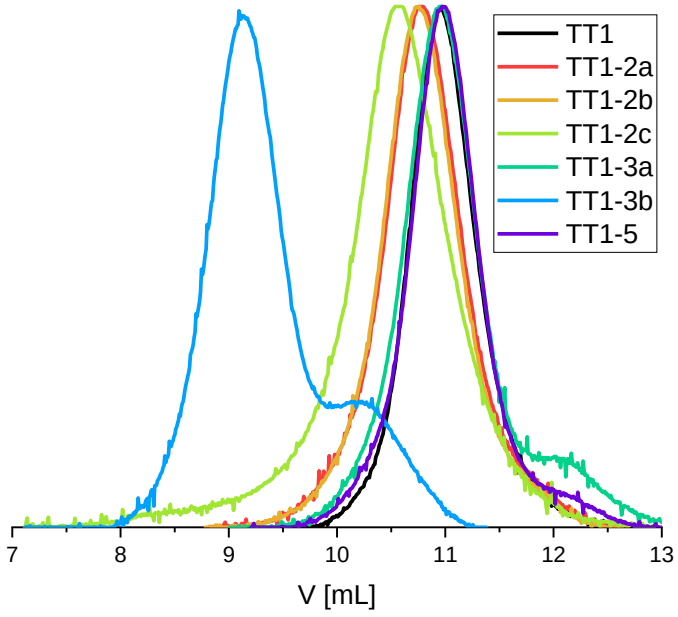

Figure 8.5: SEC elugrams of homo- and block copolymers (see Table 8.1) derived from **Cl-CTA2b**.

To understand, if the ATRP really took place via the chloride moiety, aminolysis of the trithiocarbonate group was performed on **TT1-2b** (Figure 8.6a). Mild aminolysis should break down the trithiocarbonate moiety, but keep the ester groups intact. The resulting mixtures of polymer blocks should show two distinct populations in the SEC, if ATRP had occurred at the chloride moieties. The SEC elugram of the aminolysis clearly shows a new low molar mass signal at high elution volumes, while the main peak is slightly shifted towards higher elution volumes,

i.e., towards lower molar mass. This is a good indication that the ATRP had occurred mainly at the chloride moieties, since the amines attacked the trithiocarbonate group breaking the covalent connection between PDMAm and PNiPAm apart. Additionally, hydrolysis using sodium hydroxide was performed on sample **TT1-2b** (Figure 8.6b). The hydroxide anions should degrade the trithiocarbonate group as well as the ester groups leading to smaller polymer fragments. Indeed, the elugram shows that after hydrolysis, the high molar mass signal is similar to the macroinitiator **TT1**, while the shoulder belongs to low molar mass polymers and has an even lower intensity compared to the product from aminolysis. Thus, both SEC results from aminolysis and hydrolysis prove that at least most, if not all of the chain extension by NiPAm happened via the ATRP chloride-initiator site, and not via the trithiocarbonate group.

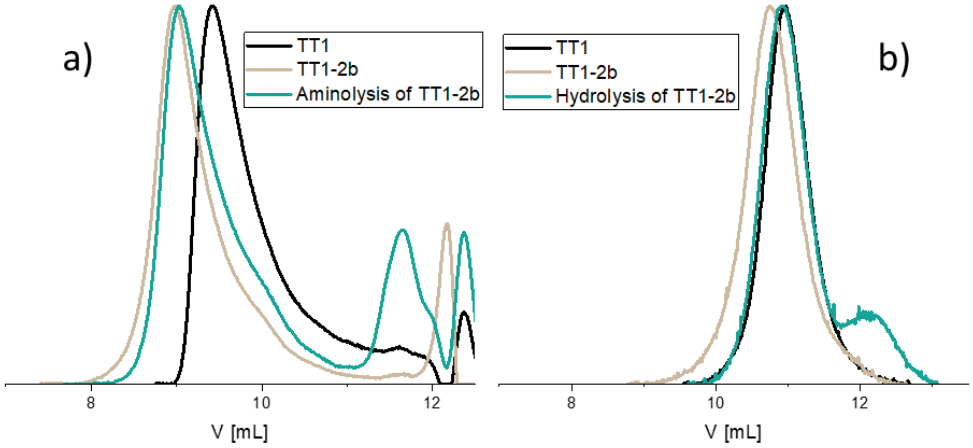

Figure 8.6: SEC elugrams of **TT1**, **TT1-2b** and its aminolysis products (a: SEC in THF) or hydrolysis products (b: SEC in *N*-methyl-2-pyrrolidone).

8.4 Phase Transition Behavior in Aqueous Solution

The temperature-dependent aggregation behavior of the twinned thermoresponsive block copolymers was investigated via DLS and turbidimetry for a concentration of 5 $g \cdot L^{-1}$ in water (Figure 8.7). The combination of both DLS and turbidimetry is advantageous to understand different temperature-induced changes such as aggregate formation and phase separation.[13] While the homopolymer PDMAm **TT1** is soluble in water in the full temperature range, the block copolymers with PNiPAm, PDEAm and PNPAm as the twinned thermoresponsive blocks show phase separation upon heating, visible as turbid solutions in the turbidimetry. Generally, all twinned thermoresponsive block copolymers have their CP's very close to the ones of the respective homopolymers. Specifically, the CP's of **TT1-2a** and **TT1-3a** are around 32 °C, and the CP of

TT1-5 is around 22 °C. When decreasing the concentration, the CP's shifted towards lower temperatures (see Appendix Figure 11.9), which is in agreement with the literature for such dilute solutions.[18] For a concentration of 5 g·L^{-1}, sample **TT1-5** containing PNPAm seems to start phase separation at even lower temperatures than 22 °C, which were below the accessible range for the measurement.

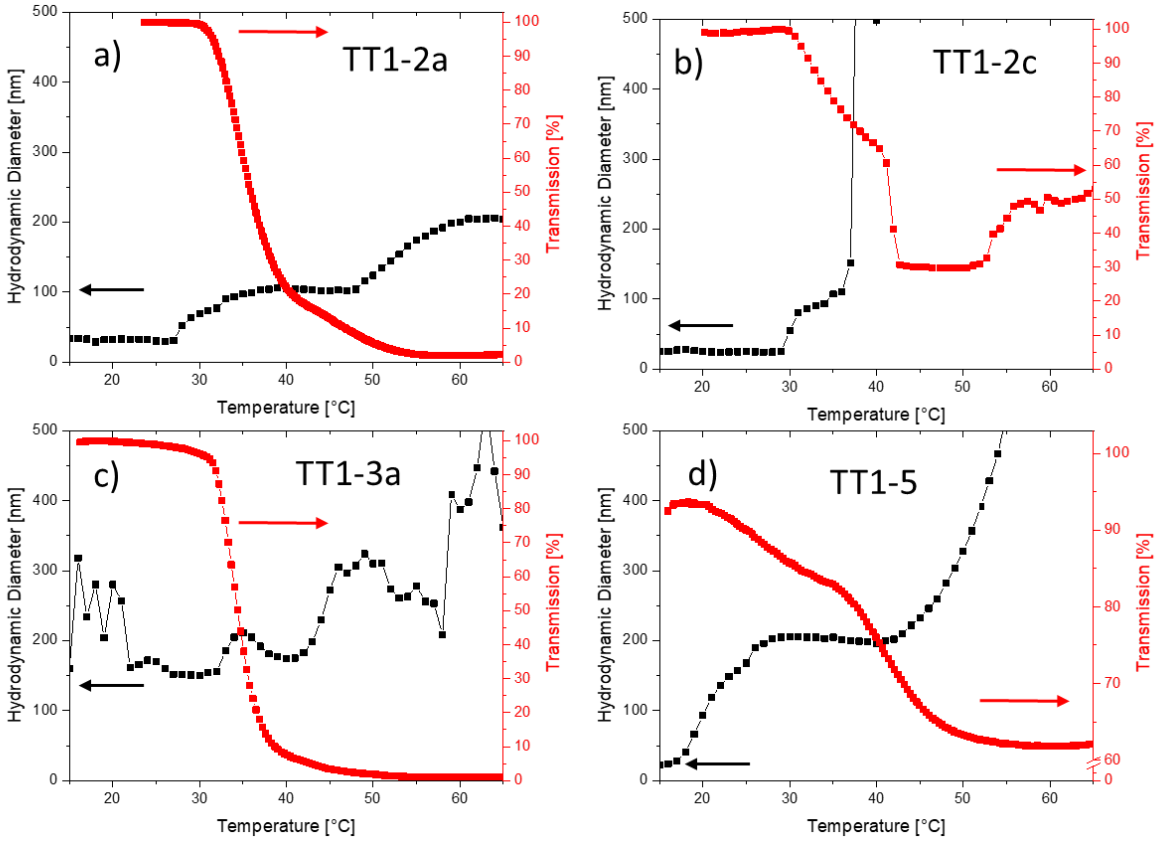

Figure 8.7: Temperature-dependent hydrodynamic diameter from DLS and transmission from turbidimetry for 5 g·L^{-1} aqueous solutions of block copolymers a) **TT1-2a**, b) **TT1-2c**, c) **TT1-3a** and d) **TT1-5**.

Compared to the basic linear, the twinned hydrophobic and the symmetrical quasi-miktoarm architectures (see Figure 2.2 **L**, **TH**, and **YS**), the CP's of the twinned thermoresponsive block copolymers are very low. This is probably caused by two factors. Firstly, in contrast to the symmetrical quasi-miktoarm architecture, the two thermoresponsive blocks are relatively close, resulting in an enhanced interaction between the two blocks, thus decreasing the CP's. Secondly, the thermoresponsive blocks are not directly attached to the hydrophilic PDMAm block but are separated by a somewhat hydrophobic spacer. This might reduce the solubility of the thermoresponsive blocks in water. Except for samples **TT1-2c** and **TT1-5**, the transmittance of all

block copolymer solutions decreases with increasing temperature from 100 % to 0 %, which was reached at around 55 °C. In fact, block copolymer **TT1-2c** most probably underwent strong phase separation before reaching 0 % transmission with sedimented polymer on the bottom of the cuvette and a polymer-poor solution on top. In consequence, turbidimetry was measured for the polymer-poor solution, (in which polymer even continued to precipitate) as visible in the increase of transmission at around 55 °C. For the PNPAm containing sample **TT1-5**, however, this was not observed. Due to the low CP of **TT1-5**, the measurement already started with a slightly decreased transmission of 95 % at 15 °C. Upon heating to 65 °C, the transmission decreased to only ~60 %, similar as for the respective linear and twinned hydrophobic architectures **L1b-5a** and **TH1a-5** (see Appendix Figure 11.8). Then again, in the latter case, the concentration was higher than 5 $g \cdot L^{-1}$ clearly showing the strong influence of the additional thermoresponsive PNPAm block of **TT1-5** on the phase transition. Another interesting new feature of the twinned thermoresponsive architecture is the apparent two-step transition, which is visible for samples **TT1-2a**, **TT1-2c** and **TT1-5**, but not for **TT1-3a**. The second transition takes place at elevated temperatures of around 43 °C, 40 °C and 37 °C for **TT1-2a**, **TT1-2c** and **TT1-5**, respectively. These behaviors could be also observed in the DLS measurements. Below the CP's, the block copolymers **TT1-2a**, **TT1-2c** and **TT1-5**, had hydrodynamic diameters of around 30 nm, while the block copolymer **TT1-3a** containing PDEAm had a much higher hydrodynamic diameter of > 150 nm. In the first transition step, the DLS experiment showed that aggregate formation already starts at slightly lower temperatures than the clouding itself observed by turbidimetry. At the second transition, the hydrodynamic diameter further increases up to diameters > 100 nm, which is well visible in the DLS measurement. With increasing temperature, the thermoresponsive blocks are becoming more hydrophobic favoring the intermolecular interaction with other thermoresponsive blocks, leading to larger aggregates. Exceptionally, sample **TT1-3a** shows only a one-step transition. This is probably caused by the fraction of low molar mass PDEAm homopolymer chains contained in the sample. These homopolymer chains might cover any two-step transition of the twinned thermoresponsive architecture. In conclusion, the additional thermoresponsive block seems to allow more interactions resulting in a two–step transition. In the first step, the polymer micelles probably start aggregating leading to some larger but stable aggregates. With increasing temperature, the thermoresponsive block becomes even more dehydrated leading to even larger aggregates in a second step.

9 SUMMARY AND CONCLUSION

Thermoresponsive amphiphilic block copolymers with unconventional architectures based on polyacrylamides were synthesized by Reversible Deactivation Radical Polymerization (RDRP) techniques. The block copolymers were generally composed of a permanently hydrophobic sticker group, a permanently hydrophilic block, and a thermoresponsive block exhibiting a Lower Critical Solution Temperature (LCST) behavior. Using well-designed Chain Transfer Agents (CTAs), block copolymers with linear, twinned hydrophobic and symmetrical quasi-miktoarm architecture L, TH and YS, respectively, were synthesized by successive Reversible Addition-Fragmentation chain Transfer (RAFT) polymerization. During the RAFT polymerization, the hydrophobic sticker group, an alkyl chain, was implemented by the R-group of the CTA. The permanently hydrophilic blocks consisted of *N*,*N*-dimethylacrylamide (DMAm) with block lengths of around 200 repeat units. For the thermoresponsive blocks, different monomers were used such as *N*-*n*-propylacrylamide (NPAm), *N*-*iso*-propylacrylamide (NiPAm), *N*,*N*-diethylacrylamide (DEAm), *N*,*N*-bis(2-methoxyethyl)acrylamide) (bMOEAm), or *N*-acryloylpyrrolidine (NAP) with different reported LCSTs of their homopolymers of 25, 32, 33, 42 and 56 °C, respectively. For the thermoresponsive blocks, much shorter block lengths of around 20 to 40 repeat units were aimed at. The resulting polymers had low dispersities, precise block lengths and well-defined end groups.

In addition, more complex architectures were synthesized such as the non-symmetrical quasi-miktoarm (YN) and the twinned thermoresponsive (TT) architectures using different techniques. For the YN architecture, a combination of Single Unit Monomer Insertion (SUMI) and RAFT polymerization was realized to obtain quasi-pentablock copolymers with quasi-miktoarm architecture bearing two non-symmetrical arms, each with the same permanently hydrophilic PDMAm block and different thermoresponsive blocks with unlike LCSTs such as PNiPAm and PNPAm. The central hydrophobic sticker group was incorporated by the SUMI technology. Due to the 4 polymerization steps necessary and the long polymerization time of SUMI, the molar mass distributions of the final block copolymers were relatively broad. Still, the performed chain extensions worked to a large extent, leading to the complex non-symmetrical quasi-miktoarm architecture. A very different approach was used for the TT architecture, for which two distinct RDRP techniques were combined, namely RAFT polymerization and Atom Transfer Radical Polymerization (ATRP). A carefully designed CTA was synthesized bearing a trithiocarbonate group for RAFT polymerization and chloride-initiating sites for ATRP. After the successive RAFT polymerization of DMAm and the ATRP of a thermoresponsive monomer NPAm, NiPAm or DEAm, a miktoarm blockcopolymer with twinned thermoresponsive blocks was obtained. These

block copolymers had low dispersities and well-defined block lengths. Still, the results from Size Exclusion Chromatography (SEC) suggested that ATRP of the tertiary acrylamide DEAm is more difficult than of the secondary acrylamides such as NiPAm and NPAm.

The thermoresponsive behavior of the block copolymers with the different architectures was investigated by turbidimetry and Dynamic Light Scattering (DLS) in water. Generally, the cloud points (CP) of the block copolymers increased compared to the ones of the respective thermoresponsive homopolymers due to the attached hydrophilic PDMAm block. As a result, the aqueous solutions of 5 $g \cdot L^{-1}$ of block copolymers with PbMOEAm or PNAP blocks with a block length of around 40 repeat units showed no CP in the studied temperature range of water, since their LCSTs are already at elevated temperatures. Thus, for these block copolymers, only architecture L was applied. However, aqueous solutions of 5 $g \cdot L^{-1}$ of block copolymers bearing PNiPAm and PDEAm blocks showed marked phase transitions turning the solution turbid. For aqueous solutions of 5 $g \cdot L^{-1}$ of block copolymers containing PNPAm as the thermoresponsive block, the phase transition is very sensitive towards the architecture. Compared to the reference architecture L, the TH architectures of PNiPAm, PDEAm and PNPAm have a rather high impact on the phase transition, either in form of reducing the CP and/or allowing larger aggregates. A similar effect was observed for the analogue TT architecture of these block copolymers. Due to the additional thermoresponsive block, which allows more intra- as well as intermolecular interactions after the phase transition, the CP's of the block copolymers are very close to the ones of the respective homopolymers. Moreover, a second phase transition step was observed, at least for PNiPAm and PNPAm block copolymers. Block copolymers with TT architecture bearing PDEAm showed only a one-step transition probably caused by the low molar mass PDEAm homopolymer chains that were in the sample covering a second transition step. In contrast, the DLS results of the block copolymers with YS architecture demonstrated that the additional arm as well as the changed position of the hydrophobic sticker group enhance the stability of loose micelles leading to higher CP's than the reference architectures L. Only block copolymer containing PNPAm showed no indication of larger aggregates above the phase transition. The block copolymers with analog but non-symmetrical architecture YN bearing PNPAm and PNiPAm as the thermoresponsive blocks showed a one-step transition as well, but with well-stabilized and relatively small aggregates below and above their CP's. These CP's are between the ones of the reference architectures L of PNPAm and PNiPAm indicating the additional interactions between the different thermoresponsive blocks.

Furthermore, the aggregation behavior of the amphiphilic block copolymers was investigated by fluorescence spectroscopy. Therefore, linear homo- and block copolymers of PDMAm and

PNiPAm with a hydrophobic sticker group and complementary fluorescence dyes introduced at the opposite chain ends of the polymers were synthesized to detect backfolding via Förster Resonance Energy Transfer (FRET) in aqueous solution and in microemulsion. Below the phase transition temperature, the block copolymers are well soluble in water. Due to their surfactant-like architecture, they form loose micellar aggregates, which was observed by DLS. With increasing temperature, the thermoresponsive blocks switch from hydrophilic to hydrophobic changing the aggregation behavior leading to either backfolding to the micellar core or to network formation via bridging of the thermoresponsive blocks. While indeed the PNiPAm homopolymer showed backfolding above its CP in pure water as well as in microemulsion, the PDMAm-b-PNiPAm block copolymer preferred network formation above its CP, especially in microemulsion.

The results show that the here synthesized block copolymers with their unconventional architectures and the different chemical structures of the thermoresponsive blocks have an interesting aggregation behavior, which can be employed to control the viscosity of aqueous systems. In conclusion, such block copolymers might be interesting candidates for the use as tailored rheological modifiers for microemulsions. Such smart systems could control the rheology of microemulsions by a simple temperature switch, thus potentially leading to intelligent applications especially in pharmaceutics or cosmetics.

10 EXPERIMENTAL PART

10.1 CHEMICALS

Table 10.1: Utilized materials.

Name	Purity	Additives	Supplier
1,1,1,3,3,3-hexamethyldisilazane	> 96.0 %		TCI
1,1′-azobis(cyclohexanecarbonitrile) (V--40)	98 %		Merck
1-bromododecane	≥ 95 %		Fluka
1-pentanol	≥ 99 %		Sigma Aldrich
2,2’-(ethylenedioxy)diethanethiol	95 %		Sigma Aldrich
2,2′-azobis(2-methylpropionitrile) (AIBN)	98 %		Merck
2,6-lutidine	98 %		Sigma Aldrich
2-bromopropionyl bromide	97 %		Sigma Aldrich
2-chloropropionyl chloride	> 95.0 %		TCI
2-chloropropionyl chloride	97 %		Sigma Aldrich
3,5-dimethylbenzoyl chloride	≥ 97.0 %		TCI
3,5-di-*tert*-butylcatechol	≥ 98.0%		Sigma Aldrich
3-methyl-3-oxetanemethanol	97 %		abcr
4-chloro-1,8-napthalic anhydride	95.0 %		Fluka
4-chloromethylbenzoyl chloride	> 98 %		TCI
4-dimethylaminopyridine	≥ 99.0 %		Fluka
7-hydroxy-4-methylcoumarin	97 %		Acros Organics
acetic anhydride	≥ 99.0 %		Fluka

acetic anhydride	≥ 99.0 %		Fluka
acetone	≥ 99 %		vwr
acetone-d6	≥ 99.5 atom% D		Armar Chemicals
acryloyl chloride	≥ 96.0 %	stabilized with phenothiazine	Merck
acryloyl chloride	≥ 96.0 %	stabilized with phenothiazine	TCI
acryloyl chloride	96 %	stabilized with phenothiazine	Alfa Aesar
allylbromide	99 %	stabilized with propylene oxide	Sigma Aldrich
allyltrimethylsilane	98 %		abcr
aluminum oxide	-	Al_2O_3 activated basic, Brockmann I	Sigma Adrich
aqueous hydrochloric acid	1 M		Th. Geyer
benzene	99.5 %		Roth
benzyl bromide	99 %		Alfa Aesar
bis(2-methoxyethyl)amine	> 98.0 %		TCI
butanone	> 99 %		Acros Organics
carbon disulfide	≥ 99.9 %		Merck
carbon disulfide	≥ 99.9 %		Honeywell
chloroform	≥ 99.5 %	stabilized with amylene	Th. Geyer
chloroform-d	99.8 atom% D		Armar Chemicals

copper (I) chloride	97 %		Sigma Aldrich
deuterium oxide	99.8 atom% D		Armar Chemicals
dichloromethane	≥ 99.8 %	stabilized with amylene	Th. Geyer
dichloromethane	≥ 99.5 %		Roth
didodecylamine	> 97 %		TCI
diethylether	≥ 99.5%		Th. Geyer
dimethylsulfoxide	> 99.0 %		TCI
ethanol	absolute		Merck
ethanol	Uvasol		Merck
ethanolamine	≥ 99.0 %		Sigma Aldrich
ethyl acetate	99.9 %		vwr
ethylenediamine	≥ 99.5 %		Roth
hydrochloric acid, concentrated			chemsolute
hydrogen bromide	48 %		Sigma Aldrich
iso-propanol	100 %		vwr chemicals
magnesium sulfate, anhydrous	-		Applichem
magnesium sulfate, anhydrous	≥ 99.5 %		Alfa Aesar
maleic anhydride			Alfa Aesar
maleic anhydride	≥ 99.0 %		Fluka
maleic anhydride	> 98 %		Alfa Aesar
methanol	technical		vwr
methyl 2-chloropropionate	97 %		Sigma Aldrich
methylamine-hydrochloride	≥ 98 %		Fluka

N,*N*-bis(2-methoxyethyl)amine	> 98.0 %		TCI
N,*N*-diethylacrylamide	≥ 98.0 %	stabilized with MEHQ	TCI
N,*N*-dimethylacrylamide	≥ 99.0 %	stabilized with MEHQ	TCI
N,*N*-dimethylformamide	Uvasol		Merck
N,*N*-dimethylformamide	> 99 %		Acros Organics
N,*N*-dimethylformamide	≥ 99.9 %		vwr
n-dodecyl-1-amine	97 %		Alfa Aesar
n-hexane	≥ 95.0 %		Chemsolute
N-isopropylacrylamide	97 %		Merck
n-propyl amine	> 99 %		Acros Organics
p-aminobenzoic acid			Ferak
pentane	> 95 %		Roth
petrol ether	ACS Reagent grade		Avantor
petrol ether 60-80 °C	analytical grade		Chemsolute
potassium carbonate, anhydrous	≥ 99 %		Roth
potassium carbonate, anhydrous	≥ 99.0 %		Sigma Aldrich
potassium iodide	≥ 99.99 %		Sigma Aldrich
propane-1-thiol	98 %		Alfa Aesar
propargyl acrylate	98 %		Sigma Aldrich
pyridine	≥ 99 %		Roth
pyrrolidine	99 %		Merck
silica gel 60			Merck

sodium acetate, anhydrous	≥ 99 %		Acros Organics
sodium acetate, anhydrous	> 99 %		Acros Organics
sodium chloride	≥ 99.0 %		THGeyer
sodium fluoride	≥ 99 %		Fluka
sodium hydrogensulfide	pure		Acros Organics
sodium hydroxide	≥ 98.8 %		Chemsolute
sodium thiocyanate	≥ 98 %		Roth
sulfuryl chloride	98.5 %		Acros
tetrahydrofurane	pure		Merck
tetrahydrofurane	≥ 99.9 %	stabilized with BHT	Chemsolute
tetrahydrofurane, extra dry	99.5 %	stabilized with BHT	Acros Organics
thioacetic acid	≥ 98 %		Merck
thionyl chloride	≥ 99.0 %		Fluka
toluene	≥ 99.5 %		Merck
tributylphosphine	97 %		Sigma Aldrich
triethylamine	99 %		Acros Organics
triethylamine	≥ 99.5 %		Roth
tris[2-(dimethylamino)ethyl]amine (Me_6TREN)	97 %		Sigma Aldrich
zinc (II) chloride	≥ 98 %		Merck

NiPAm was recrystallized from *n*-heptane prior to use. DEAm and DMAm were distilled to remove the inhibitors. Tetrahydrofuran for polymerization and for spectroscopic studies was distilled prior to use to remove inhibitors. AIBN and V-40 were recrystallized from *n*-hexane (AIBN) or

chloroform (V-40) prior to use. Acetic anhydride, DMF, ethanolamine, 1,1,1,3,3,3-hexamethyldisilazane were distillied prior to use. Solvents were usually dried over $MgSO_4$. Deionized water was used for synthesis. Deionized water was further purified by a Millipore Milli-Q Plus water purification system (resistivity 18 $M\Omega \cdot cm^{-1}$) for turbidimetry, DLS and fluorescence measurements.

10.2 METHODS AND INSTRUMENTATION

Elemental analysis

Elemental analysis was performed with a Vario ELIII microanalyzer (Elentar Analysensysteme, Hanau, Germany).

Refractive Indices

Refractive indexes were determined with a NAR-3T refractometer (ATAGO CO., LTD., Tokio, Japan) equipped with a DTM-3 thermostat.

NMR spectroscopy

NMR spectra were recorded using a Bruker Avance 300 NMR spectrometer operating at 300 MHz for ^{1}H measurements and 75 MHz for ^{13}C measurements or a Bruker Avance 400 NMR operating at 100 MHz for ^{13}C measurements. Chemical shifts δ are given in ppm referring to the respective solvent peaks at δ (^{1}H) 7.26 ppm and δ (^{13}C) 77.16 ppm for $CDCl_3$, δ (1H) 2.05 ppm for acetone-d_6, δ (1H) 4.79 ppm for DMSO-d_6, δ (1H) 3.31 ppm for CD_3OD and at δ (1H) 4.79 ppm for D_2O.

FTIR spectroscopy

Fourier-transform infrared spectroscopy (FTIR) spectra were recorded using a Nicolet Avatar 370 FT-IR spectrometer equipped with an ATR Smart Performer element and AMTIR crystal.

Fluorescence-Spectroscopy

Temperature-dependent static fluorescence experiments were performed with an FluoroLog-3 fluorometer (HORIBA Jobin Yvon, France). Optical silica cuvettes with an optical path length

d = 1 cm were utilized. The excitation wavelength was set to 318 nm and emission to 376 nm for the coumarin compound and the polymers, or 520 nm for the naphthalimide. Temperature was precise within 1 K. The samples were prepared in Millipore water or in a microemulsion. The microemulsion was gifted by Albert Prause and prepared by him using tetradecyldimethylamine oxide (TDMAO) (c = 190.0 mmol·L^{-1}), decane (c = 57.3 mmol·L^{-1}) in water.

Dynamic Light Scattering (DLS)

DLS was carried out with an instrument high performance particle Sizer (HPPS-5001, Malvern Instrument, Malvern, UK) using a He-Ne laser beam and a thermoelectric Peltier element to control the temperature of the sample cell. The backscattering mode was used at a scattering angle of Θ = 173 °. Samples were prepared by dilution with Millipore water to the desired concentration and filtered before measurement (0.45 μm).

Turbidimetry

Temperature dependent turbidimetry measurements were performed with a Cary 5000 (Varian) spectrometer at 600.00 nm with heating and cooling rates of 0.5 K·min^{-1}. Temperatures are precise within 0.5 K. The temperature at which the solution's transmittance starts to decrease (onset) is taken as cloud point (CP).

Size Exclusion Chromatography (SEC)

Polymers were also analyzed by size exclusion chromatography (SEC) in *N*-methyl-2-pyrrolidone + 0.5 % LiBr with simultaneous UV and RI detection at room temperature (flow rate 0.5 mL·min^{-1}). The stationary phase used was a 300 x 8 mm^2 PSS GRAM linear M column (7 μm particle size). Regarding the aminolysis experiment, samples were analyzed by SEC in THF with simultaneous UV and RI detection at room temperature (flow rate 0.5 mL·min^{-1}). The stationary phase used was a 300 x 8 mm^2 PSS SDV linear M column (3 μm particle size). Only polymers **L1a** and therefrom-derived block copolymers were measured by SEC in DMF + 0.1% LiBr with RI detection at 50 °C (flow rate 1.0 mL·min^{-1}). The stationary phase used was a 300 x 8 mm^2 PSS GRAM linear M column (7 μm particle size). All samples were filtered through 0.45 μm filters and the injected volume was always 100 μL. Narrowly distributed polystyrene standards (PSS, Mainz, Germany) were used for calibration.

Thermogravimetric analysis (TGA)

TGA was conducted under N_2 purged atmosphere using an apparatus SDTA851e (Mettler-Toledo, Gießen, Germany), in the temperature range from 25 °C to 900 °C with a heating rate of 10 K min^{-1}.

Differential scanning calorimetry (DSC)

DSC was performed with an apparatus DSC822e (Mettler-Toledo, Gießen, Germany), applying heating and cooling rates of 10 K min^{-1} for the first and second, and 30 K min^{-1} for the third and fourth heating and cooling cycles. Glass transition temperatures T_g were taken from the second heating cycle that used a heating rate of 10 K min^{-1} via the midpoint method.

UV-visible spectroscopy

UV-vis spectra were recorded on a Perkin Elmer Lambda 25 UVVis Spectrometer, using quartz sample cells with 1 cm path length. Number average molar masses M_n^{UV} were calculated by end group analysis, using the extinction E at 309 nm of the π-π* transition of the trithiocarbonate chromophore in methanol. In case of the FRET-CTA based polymers, the extinction coefficient was calculated to ε = 8500 $L \cdot mol^{-1} \cdot cm^{-1}$ at a maximum wavelength λ_{max} = 424 nm determined for the FRET-CTA in dichloromethane (DCM) (see Appendix, Figure 11.10). Values were calculated according to $M_n^{UV} = \varepsilon \cdot c \cdot d \cdot E^{-1}$ where ε [$L \cdot mol^{-1} \cdot cm^{-1}$] is the extinction coefficient, c [$g \cdot L^{-1}$] is the concentration of the polymer in solution and d [cm] is the optical path length. The molar extinction coefficient ε of the trithiocarbonate chromophore was assumed to be 15,800 $L \cdot mol^{-1} \cdot cm^{-1}$ at 309 nm in methanol, due to the structural similarity of the polymer bound trithiocarbonate end groups with the reference *N*,*N*-dimethyl-2-(((butylthio)carbonothioyl)thio)propionamide.[170] For the FRET-polymer series, the molar extinction coefficient ε of the trithiocarbonate chromophore was determined to be 8500 $L \cdot mol^{-1} \cdot cm^{-1}$ at 424 nm in DCM.

10.3 SYNTHESES OF MONOMERS

Synthesis of *N*-acryloylpyrrolidine[252]

A solution of acryloyl chloride (10.0 mL, 8.98 g, 124 mmol) in anhydrous DCM (50 mL) was added dropwise over 1 h to a solution of pyrrolidine (20.4 mL, 17.4 g, 248 mmol, 2.0 eq) in DCM (120 mL) at 0 °C under stirring and argon atmosphere. The solution was stirred for further 2 h at room temperature under repeated argon flushing to remove evolving undissolved HCl. Then, the solution was diluted with further DCM (80 mL) and washed with distilled water (100 mL), aqueous 1 M $KHSO_4$-solution (100 mL), distilled water (100 mL), saturated $NaHCO_3$ solution (100 mL) and again distilled water (100 mL). The solution was dried over $MgSO_4$ and the organic solvent was removed under reduced pressure. The amide was distilled under reduced pressure to obtain the product as a colorless oil. Yield 4.24 g, 33.9 mmol, 27 %, Lit.: 45 %

^{1}H-NMR (300 MHz in $CDCl_3$, δ in ppm): δ = 1.87-1.97 (m, 4H, N(-CH_2-CH_2)$_2$), 3.50-3.56 (m_c, 4H, N(-CH_2-CH_2)$_2$), 5.65 (dd, *J* = 9.7 Hz, *J* = 2.8 Hz, 1H, CH-CH^E), 6.35 (dd, *J* = 16.8 Hz, *J* = 2.8 Hz, 1H, CH-CH^E), 6.45 (dd, *J* = 16.8 Hz, *J* = 9.7 Hz, 1H, CO-C*H*).

Synthesis of *N*-propylacrylamide adapted from a previously reported procedure[50]

A solution of acryloyl chloride (9.7mL, 10.8 g, 119 mmol) in anhydrous DCM (50 mL) was added dropwise over 1.5 h to a solution of *N*-*n*-propylamine (9.8 mL, 7.1 g, 119 mmol, 1.0 eq) and trimethylamine (18.3 mL, 13.4 g, 132 mmol, 1.1 eq.) in DCM (20 mL) at 0 °C under stirring. The solution was stirred overnight. Then, triethylammoniumhydrochloride was filtered off, and the solvent was removed under reduced pressure. Benzene (50 mL) was given to the residue and the precipitate was again filtered off. After removing the solvent under reduced pressure, the residue was distilled under high vacuum. The monomer was further purified by column chromatography on silica gel using petrol ether:ethyl acetate with a fixed ratio of 1:1 (v/v) Yield: 4.33 g, 38.26 mmol, 32 %

^{1}H-NMR (300 MHz in $CDCl_3$, δ in ppm): δ = 0.94 (t, 3H, *J* = 7.4 Hz, CH_3), 1.56 (qt, *J* = 7.3 Hz, 2H, N-CH_2-CH_2), 3.29 (m_c, 2H, N-CH_2-CH_2), 5.62 (m, 2H, N*H* & CH-CH^E), 6.06 (m, 1H, CH-CH^E), 6.26 (m_c, 1H, CO-C*H*).

Synthesis of N,N-bis(2-methoxyethyl)acrylamide) (bMOEAm) adapted from previously reported procedures [56,58,59]

A solution of acryloyl chloride (11.3 mL, 12.6 g, 0.139 mol, 1.1 eq.) in DCM (40 mL) was dropped over 3 h into a stirred solution of bis(2-methoxyethyl)amine (18.7 mL, 16.8 g, 0.127 mol) and triethylamine (26.5 mL, 19.3 g, 0.191 mol, 1.51 eq.) in DCM (350 mL) at 0 °C. The reaction mixture was allowed to warm up to ambient temperature and continued to be stirred overnight. The precipitated triethylammonium hydrochloride was filtered off and washed with DCM (100 mL). The combined organic solutions were extracted subsequently with 1 M HCl (3 × 50 mL), water (50 mL) and brine (100 mL). The organic layer was dried over anhydrous $MgSO_4$ and the solvent removed under reduced pressure. The raw product was purified by vacuum distillation to give a viscous liquid (n_{20}^{D} = 1.4722). Yield: 14.5 g (61 %).

^{1}H-NMR (300 MHz in $CDCl_3$, δ in ppm): δ = 3.11 (s, 6H, C*H*$_3$, 3.27-3.43 (m, 6H, N-C*H*$_2$-C*H*$_2$-O), 5.44 (dd, 1H, C*H*^{E}=C-CO), 6.09 (dd, 1H, C*H*^{Z}=C-CO), 6.46 (dd, 1H, =C*H*-C=O).

^{13}C-NMR (75 MHz in $CDCl_3$, δ in ppm): δ = 46.45 (N-*C*H$_2$), 48.33 (N-*C*H$_2$), 58.16 (O-*C*H$_3$), 58.43 (O-*C*H$_3$), 70.53 (*C*H$_2$-O), 126.93 (*C*H$_2$-CH), 127.71 (*C*H-CO), 166.11 (*C*O).

Elemental analysis, calculated: $C_9H_{17}NO_3$: C 57.7 %, H 9.2 %, N 7.5 %, found: C 56.7 %, H 10.9 %, N 7.4 %

Mass spectrometry: calculated mass M_r: 188.1287 g/mol, found mass: 188.1291 g/mol

FT-IR (selected bands cm^{-1}): 2982, 2929, 2883, 2821, 1647, 1610, 1443, 1363, 1189, 1111, 1012, 978, 960, 795.

Synthesis of *N*-4-(2,5-dioxo-2,5-dihydro-1H-pyrrol-1-yl)-*N*-dodecylbenzamide (DBMI) similar to reported procedures[225,226]

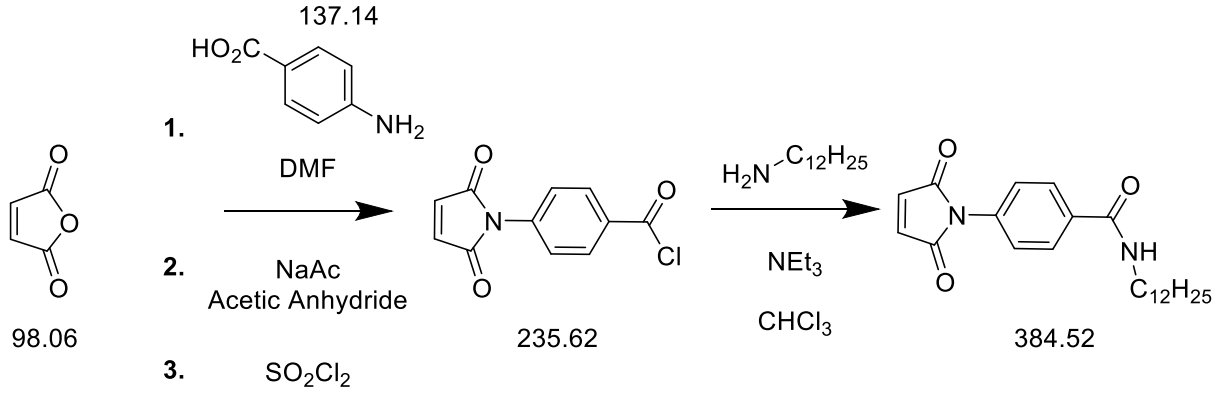

***N*-(4-carboxyphenyl)maleamic Acid (p-CPMA):** A solution of maleic anhydride (6.23 g, 64.49 mmol, 1.5 eq.) in DMF (20 mL) was added to a solution of p-amino-benzoic acid (5.90 g, 42.99 mmol, 1.00 eq.) in DMF (20 mL) within 30 min at room temperature leading to a slight heating of the reaction mixture. After stirring the solution for 4 h at room temperature, it was poured in an excess of water and the preicipitated product was filtered off and washed with water. The brownish product was dried in the vacuum oven (40 °C, 1 mbar). Yield: 7.70 g, 32.7 mmol, 76 %, Lit.: 97 %

^{1}H-NMR (400 MHz in DMSO-d_6, δ in ppm): δ = 6.32 (d, J = 12.0 Hz, 1H, C*H*-CO_2H), 6.48 (d, J = 12.0 Hz, 1H, C*H*-CONH), 7.72 (d, J = 8.6 Hz, 2H, Ar$H^{2,6}$), 7.90 (d, J = 8.8 Hz, 2H, Ar$H^{3,5}$).

***N*-(4-carboxyphenyl)maleimide (p-CPMI):** In the next step, a mixture of p-CPMA (7.70 g, 32.7 mmol) and sodium acetate (0.41 g, 5.00 mmol, 0.12 eq.) in acetic anhydride (18 mL) was heated for 2 h at 55-60 °C. Then, the reaction mixture was poured in water, filtered off, and the raw product was washed with water and recrystallized from MeOH/water (6:1). The product was obtained as beige needles. Yield: 6.03 g, 28.15 mmol, 65 %, Lit.: 85 %

^{1}H-NMR (400 MHz in DMSO-d_6, δ in ppm): δ = 7.21 (d, 1H, C*H*=C*H*), 6.48 (d, 1H, C*H*-CONH), 7.49 (d, J = 8.5 Hz, 2H, Ar$H^{2,6}$), 8.04 (d, J = 8.6 Hz, 2H, Ar$H^{3,5}$).

FTIR (selected bands cm^{-1}): 3103 (COOH), 2956 (CH), 1722 (CO); 1685 (CONCO), 1597 (C=C), 1394 (CH), 719 (cis-CH=CH).

***N*-[4-(chlorocarbonyl)phenyl]maleimide (p-CPMIC):** A mixture of p-CPMI (4.98 g, 23.25 mmol), thionyl chloride (42.2 mL, 69.15 g, 581 mmol, 25 eq.) and 3,5-di-tert-butylcatechol (3.50 mg) was reluxed for 2 h. Then, remaining thionyl chloride was removed under reduced pressure and the residue was recrystallized from benzene (3 times). Unsoluble black precipitate was removed by hot filtration. Yield: 2.72 g, 11.54 mmol, 50 %, Lit.: 73.3 %

FTIR (selected bands cm^{-1}): 1770 (COCI); 1713 (CONCO), 1597 (C=C), 1371 (CH), 719 (cis-CH=CH).

DBMI: Dodecylamine (2.14 g, 11.54 mmol, 1.0 eq.) and trimethylamine (1.60 mL, 1.17 g, 11.54 mmol, 1.0 eq.) were dissolved in $CHCl_3$ (30 mL) and cooled to 0 °C. A solution of p-CPMI (2.72 g, 11.54 mmol) in $CHCl_3$ (40 mL) was added dropwise within 60 min. Then, the reaction mixture was stirred for 4 h at room temperature. Afterwards, the reaction mixture was washed with 0.1 M HCl (30 mL) and water (30 mL) and the combined organic phases were dried over $MgSO_4$. The solvent was removed under reduced pressure and the raw product was further purified by

recrystallization from hexane/ethyl acetate (ca. 1:2) to obtain the product as a colourless solid. Yield: 1.85 g, 4.81 mmol, 42 %, Lit.: 49 %

^{1}H-NMR (400 MHz in $CDCl_3$, δ in ppm): δ = 0.88 (t, *J* = 6.8 Hz, 3H, -C*H*$_3$), 1.26-1.39 (m, 18H, (C*H*$_2$)$_9$-CH$_3$), 1.62 (tt, *J* = 7.3 Hz, *J* = 7.2 Hz, 2H, N-CH$_2$-C*H*$_2$), 3.46 (dt, *J* = 7.1 Hz, *J* = 6.5 Hz, 2H, N-C*H*$_2$), 6.07 (br. t, 1H, N*H*), 6.88 (s, 2H, C*H*=C*H*), 7.48 (d, *J* = 8.6 Hz, 2H, Ar*H*^{3,5}), 7.86 (d, *J* = 8.6 Hz, 2H, Ar*H*^{2,6}).

10.4 Syntheses of Chain Transfer Agents

Synthesis of 3-(trimethylsilyl)propane-1-thiol similar to a reported procedure[253]

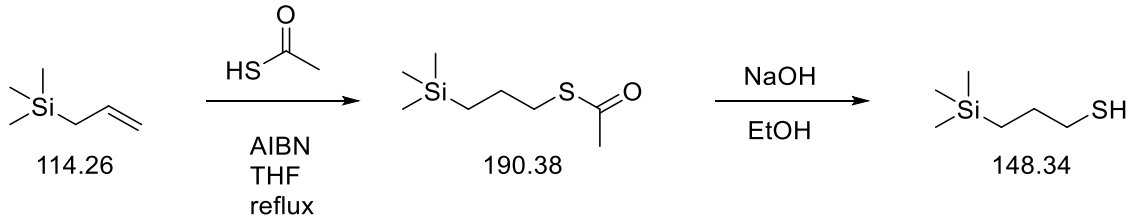

Step1: Allyltrimethylsilane (33.5 mL, 24.1 g, 0.211 mol) was dissolved in THF (120 mL). Thioacetic acid (29.0 mL, 26.9 g, 0.353 mol, 1.67 eq.) and AIBN (0.2729 g, 1.662 mmol, 0.01 eq.) were added and the solution was refluxed under inert gas for 23 h until it was cooled down to room temeperature. Then, 10 wt% NaOH (100 mL) was added at 0 °C while stirring. The organic solvent was removed under reduced pressure and the residue was extracted with ethyl acetate (100 mL). The organic phase was washed with 10 wt% NaOH (3 × 100 mL, 3 × 50 mL) and distilled water (100 mL). The combined aqueous phases were extracted with ethyl acetate (100 mL). The combined organic phases were washed with distilled water (100 mL) and brine (100 mL), and dried over $MgSO_4$. Afterwards, the solvent was removed under reduced pressure to give a colorless liquid. Yield: 38.66 g, 0.2031 mol, 94 %

^{1}H-NMR (300 MHz in $CDCl_3$, δ in ppm): δ = -0.02 (s, 9H, Si-(C*H*$_3$)$_3$), 0.56 (m$_c$, *J* = 7.7 Hz, *J* = 17.1 Hz, 2H, Si-C*H*$_2$), 1.61 - 1.50 (m, 2H, C-C*H*$_2$-C), 2.32 (s, 3H, CO-C*H*$_3$), 2.87 (t, 1.34 (t, *J* = 7.3 Hz, 2H, C*H*$_2$-S).

Step 2: The thiol (41.3 g, 0.217 mol) was dissolved in ethanol and the solution was cooled to 0 °C. Then, 25 wt% NaOH solution (1.5 eq.) was added and the reaction mixture was stirred over night. Thin Layer Chromatography (TLC) control showed completely consumed educt. The reaction mixture was neutralized with conc. HCl and then extracted with DCM (100 mL, 40 mL). The combined organic phases were washed with distilled water (3 × 100 mL), 10 wt% NaOH

(3 × 50 mL), distilled water (100 mL) and brine (100 mL) and dried over $MgSO_4$. Subsequently, the solvent was removed under reduced pressure and the residue was distilled in vacuum to give the product as a colorless liquid. Yield: 12.41 g, 83.66 mmol, 66 %

^{1}H-NMR (300 MHz in $CDCl_3$, δ in ppm): δ = -0.01 (s, 9H, Si-$(CH_3)_3$), 0.58 (m_c, 2H, Si-C*H*$_2$), 1.34 (t, *J* = 7.8 Hz,1H, S-*H*), -), 1.65 - 1.55 (m, 2H, C-C*H*$_2$-C, 2.52 (dt, *J* = 7.4 Hz, *J* = 7.5 Hz, 2H, C*H*$_2$-S).

Synthesis of *S*-benzyl-*S''*-(3-(trimethylsilyl)propyl)carbonotrithioat similar to reported procedures[164,181]

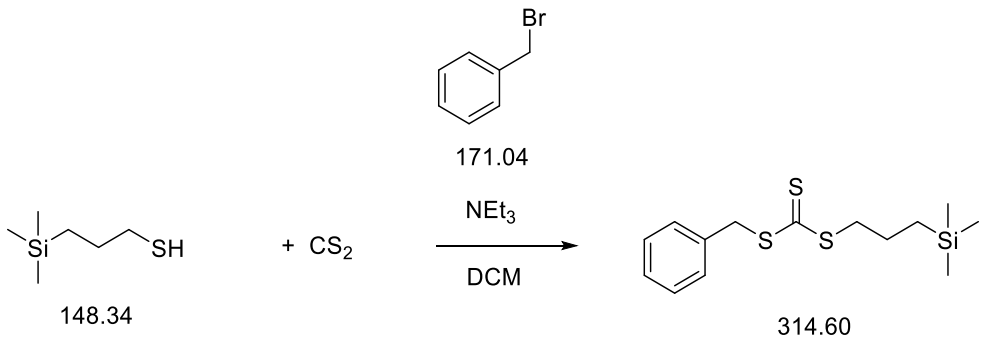

3-(Trimethylsilyl)propane-1-thiol (3.9 mL, 3.3 g, 22.2 mmol) and CS_2 (1.35 ml, 1.70 g, 22.1 mmol, 1.00 eq.) were dissolved in dry DCM (5 mL) and stirred at 0 °C. Triethylamine (3.1 mL, 2.3 g, 22.1 mmol, 1.00 eq.) was added dropwise turning the solution orange. After stirring for 30 min a solution of benzylbromide (2.6 mL, 3.8 g, 22.1 mmol, 1.00 eq.) in dry DCM (3 mL) was added slowly. The solution was stirred overnight. Then, the reaction mixture was diluted with DCM (40 mL) and washed with 1 M HCl (3 × 50 mL). The aqueous layer was reextracted with DCM (20 mL) and the combined organic layers were washed with brine (50 mL) and dried over $MgSO_4$. Subsequently, the crude product was purified by column chromatography (Petrol ether). Yield: 2.46 g, 7.82 mmol, 35 %

^{1}H-NMR (300 MHz in $CDCl_3$, δ in ppm): δ = -0.01 (s, 9H, Si-$(CH_3)_3$), 0.62 (m_c, 2H, Si-C*H*$_2$), 1.70 (m_c, 2H, C-C*H*$_2$-C), 2.38 (t, *J* = 7.4 Hz, 2H, CH_2-C*H*$_2$-S), 4.61 (s, 2H, Ar-C*H*$_2$), 7.33-7.27 (m, 5H, Ar*H*).

Synthesis of 4-chloromethyl-*N*-dodecylbenzamide

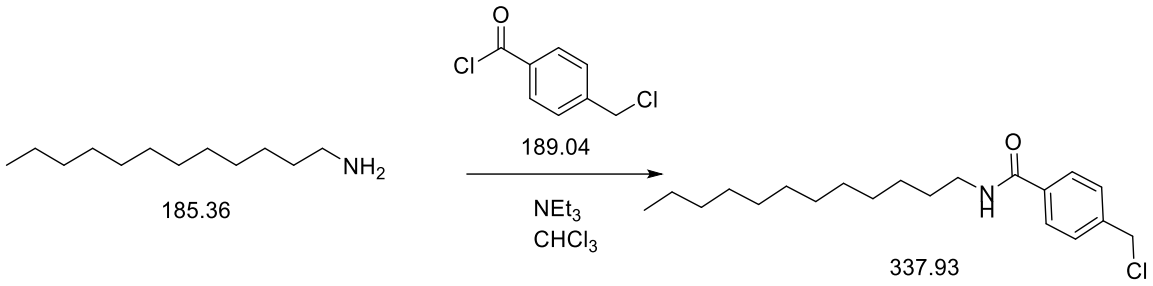

4-Chloromethylbenzoyl chloride (5.86 g, 31.0 mmol, 1.1 eq.) was dissolved in a mixture of DCM (20 mL) and benzene (10 mL) and cooled down to 0 °C. Triethylamine (7.75 mL, 5.66 g, 5.59 mmol, 1.98 eq.) was added to the suspension to produce a yellow reaction mixture. Subsequently, a solution of dodecylamine (5.24 g, 28.3 g) in benzene (20 mL) was added slowly over 1 h. The mixture was stirred overnight at room temperature. Then, the mixture was filtered and washed with benzene (90 mL). The solution was washed with 1 M HCl (3 × 50 mL). The aqueous phase was reextracted with DCM (3 × 50 mL) and the combined organic phases were washed with distilled water (50 mL) and brine (50 mL) and then dried over $MgSO_4$. Subsequently, the solvent was removed under reduced pressure and the residue was recrystallized three times from ethyl acetate. The crude product was purified by column chromatography (Petrol ether/ethyl acetate, increasing polarity from 6:1 to 1:1). Then, the product was recrystallized from petrol ether/ethyl acetate 5:1 (v/v) to give colorless needle shaped crystals. Yield: 2.16 g, 6.39 mmol, 23 %

^{1}H-NMR (300 MHz in $CDCl_3$, δ in ppm): δ = 0.88 (t, *J* = 6.7 Hz, 3H, C*H*$_3$), 1.26-1.33 (m, 18H, CH_3-(C*H*$_2$)$_9$), 1.61 (tt, *J* = 7.3 Hz, 2H, N-CH_2-C*H*$_2$), 3.44 (dt, *J* = 6.5 Hz, *J* = 7.1 Hz, 2H, N-C*H*$_2$), 4.60 (s, 2H, C-C*H*$_2$-S), 6.14 (br. t, 1H, N-*H*), 7.44 (d, *J* = 8.3 Hz, 2H, Ar*H*^{2,6}), 7.75 (d, *J* = 8.3 Hz, 2H, Ar*H*^{3,5}).

R_f = 0.2 (petrol ether:ethyl acetate 5:1)

Synthesis of 4-chloromethyl-*N*,*N*-didodecylbenzamide

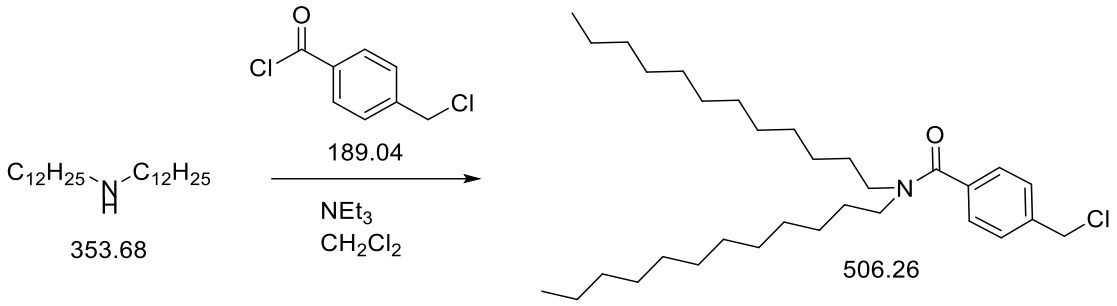

4-Chloromethylbenzoyl chloride (1.66 g, 8.78 mmol, 1.05 eq.) and triethylamine (2.30 mL, 1.68 g, 16.6 mmol, 1.99 eq.) was dissolved in DCM (5 mL) and cooled down to 0 °C when the solution became yellow. Subsequently, a solution of didodecylamine (2.95 g, 8.34 mmol) in DCM (20 mL) was added slowly over 30 min. The mixture was stirred overnight at room temperature. Then, DCM (10 mL) was added to the reaction mixture. The solution was washed with 1 M HCl (3 × 20 mL), saturated $NaHCO_3$ solution, distilled water (3 × 25 mL) and brine (25 mL). The aqueous phases were always reextracted with DCM (25 mL) and the combined organic phases were dried over $MgSO_4$. Subsequently, the solvent was removed under reduced pressure and the residue was recrystallized from MeOH and dried in vacuo to obtain a slightly yellow solid. Yield: 0.90 g, 1.77 mmol, 21 %

^{1}H-NMR (300 MHz in $CDCl_3$, δ in ppm): δ = 0.88 (t, *J* = 6.6 Hz, 6H, C*H*$_3$), 1.26-1.33 (m, 36H, (C*H*$_2$)$_9$-CH$_3$), 1.49 (br. tt, 2H, N-CH$_2$-C*H*$_2$), 1.63 (br. tt, 2H, N-CH$_2$-C*H*$_2$), 3.17 (br. t, 2H, N-C*H*$_2$), 3.46 (br. t, 2H, N-C*H*$_2$), 4.59 (s, 2H, C-C*H*$_2$-S), 7.34 (d, *J* = 8.2 Hz, 2H, Ar*H*^{2,6}), 7.41 (d, *J* = 8.1 Hz, 2H, Ar*H*^{3,5}).

Synthesis of 4-(Dodecylcarbamoyl)benzyl-3-(trimethylsilyl)propyl)carbonotrithioat C12-CTA

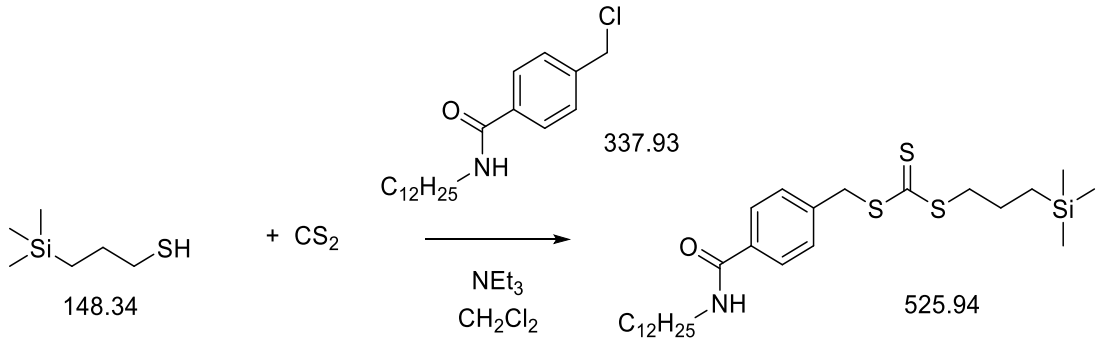

3-(Trimethylsilyl)propane-1-thiol (8.22 g, 0.0554 mol) and CS_2 (3.35 ml, 4.22 g, 55.4 mmol. 1.00 eq.) were dissolved in dry DCM (20 mL) and stirred at room temperature. Triethylamine (7.90 mL, 5.77 g, 57.1 mmol, 1.03 eq.) was added dropwise. A water bath was placed beneath the flask to keep the reaction at room temperature. The so-formed orange solution was stirred for 30 min. Then, the water bath was removed and 4-Chloromethyl-*N*-dodecylbenzamide (17.79 g, 52.64 mmol, 0.95 eq.) was slowly added. The reaction was stirred overnight, then diluted with DCM (40 mL) and washed with distilled water (3 x 100 mL). The aqueous phase was reextracted with DCM (20 mL) and the combined organic layers were washed with brine and dried over $MgSO_4$. The organic solvent was removed under reduced pressure and the raw product was purified twice by column chromatography on silica gel using petrol ether/ethyl acetate (first with gradient: 10:1 (v/v) increasing to 10:4 (v/v); second with a fixed ratio of 20:1 (v/v)). Yield: 9.67 g, 18.4 mmol, 39 %

^{1}H-NMR (300 MHz in $CDCl_3$, δ in ppm): δ = -0.01 (s, 9H, Si-$(CH_3)_3$), 0.61 (m_c, *J* = 17.1 Hz, *J* = 3.8 Hz, 2H, Si-CH_2), 0.88 (t, *J* = 6.6 Hz, 3H, C*H*$_3$), 1.25-1.32 (m, 18H, CH_3-(C*H*$_2$)$_9$), 1.57-1.70 (m, 4H, N-CH_2-C*H*$_2$ & S-CH_2-C*H*$_2$), 3.35-3.46 (m, 4H, N-C*H*$_2$ & S-C*H*$_2$-CH_2), 4.63 (s, 2H, C-*H*$_2$-S), 6.12 (br. t, *J* = 5.0 Hz, 1H, N-*H*), 7.39 (d, *J* = 8.2 Hz, 2H, Ar*H*^{2,6}), 7.70 (d, *J* = 8.2 Hz, 2H, Ar*H*^{3,5}).

^{13}C-NMR (75 MHz in $CDCl_3$, δ in ppm): δ = -1.63 (Si-*C*H_3), 14.21 (*C*H_3-CH_2), 16.69 (Si-*C*H_2), 22.81 (CH_3-*C*H_2), 23.15 (Si-CH_2-*C*H_2), 27.15 (N-$(CH_2)_2$-*C*H_2), 29.47-29.84 (N-$(CH_2)_2$-CH_2-(*C*H_2)$_6$), 32.05 (CH_3-CH_2-*C*H_2), 40.29 (S-*C*H_2-CH_2), 40.68 (N-*C*H_2), 40.81 (Ar-*C*H_2), 127.33 (Ar*C*^{3,5}), 129.51 (Ar*C*^{2,6}), 134.44 (Ar*C*^{4}), 139.09 (Ar*C*^{1}), 167.10 (*C*O), 223.39 (*C*S).

Elemental analysis ($C_{27}H_{47}NOS_3Si$): calculated C 61.7%, H 9.0%, N 2.7%, S 18.3%, found: C 61.5%, H 9.0%, N 2.6%, S 17.6

Electron ionization mass spectrometry: calculated Mr: 526.2662 g/mol, found: m/z: 526.2663 g/mol

FTIR (selected bands cm^{-1}): 2953, 2920, 2850, 1632, 1533, 1504, 1468, 410, 1300, 1248, 1061, 860, 831, 808, 719, 688.

Synthesis of 4-(Didodecylcarbamoyl)benzyl-3-(trimethylsilyl)propyl)carbonotrithioat 2C12-CTA

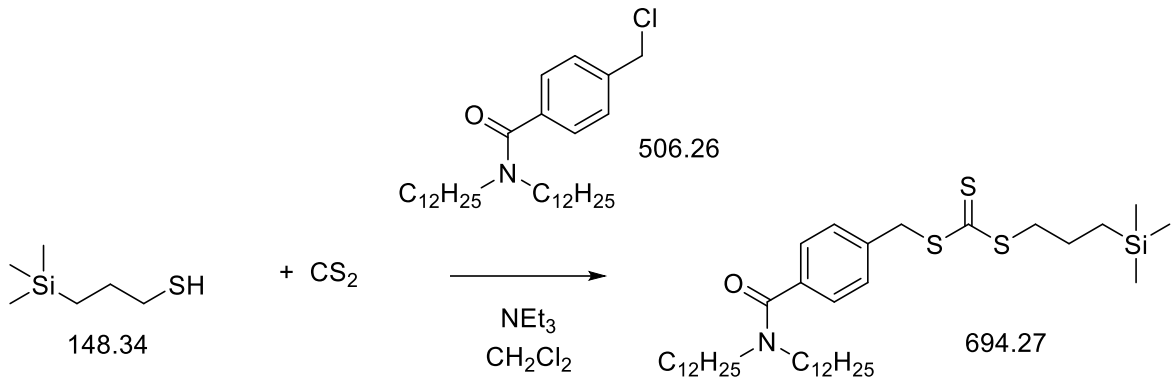

3-(Trimethylsilyl)propane-1-thiol (603.8 mg , 4.07 mmol) and CS_2 (0.25 ml, 310 mg, 4.07 mmol, 1.00 eq.) were dissolved in dry DCM (20 mL) and stirred at room temperature. Triethylamine (0.58 mL, 424.2 mg, 4.19 mmol, 1.03 eq.) was added dropwise. A water bath was placed beneath the flask to keep the reaction at room temperature. The so-formed orange solution was stirred for 30 min. Then, the water bath was removed and 4-Chloromethyl-*N*,*N*-didodecylbenzamide (2.06 g, 4.07 mmol, 1.00 eq.) was slowly added. The reaction was stirred overnight, then diluted with DCM (10 mL) and washed with distilled water (3 x 20 mL). The aqueous phase was reextracted with DCM (10 mL) and the combined organic layers were washed with brine and dried over $MgSO_4$. The organic solvent was removed under reduced pressure and the raw product was purified twice by column chromatography on silica gel first using petrol ether/ethyl acetate (5:1 (v/v); second using Petrolether:DCM 5:1 (v/v)). Furthermore, the product was purified by recrystallization in MeOH at -37 °C. Yield: 1.67 g, 2.41 mmol, 59 %,

R_f: 0.5 (petrol ether:ethyl acetate 5:1)

^{1}H-NMR (300 MHz in $CDCl_3$, δ in ppm): δ = -0.01 (s, 9H, Si-$(CH_3)_3$), 0.62 (m_c, , *J* = 17.1 Hz, *J* = 3.8 Hz, 2H, Si-CH_2), 0.88 (t, *J* = 6.6 Hz, 6H, N(-$(CH_2)_{11}$-C*H*$_3)_2$), 1.12-1.33 (m, 36H, N(-$(CH_2)_2$-$(CH_2)_9$-$CH_3)_2$), 1.47 (br. m, 2H, N-CH_2-C*H*$_2$), 1.62-1.76 (m, 4H, N-CH_2-C*H*$_2$ & S-CH_2-C*H*$_2$), 3.16 (br. t, 2H, N-C*H*$_2$), 3.38 (t, *J* = 7.4 Hz, 2H, S-C*H*$_2$-CH_2), 3.45 (br. t, 2H, N-C*H*$_2$), 4.62 (s, 2H, C-C*H*$_2$-S), 7.29 (d, *J* = 8.2 Hz, 2H, Ar*H*^{2,6}), 7.35 (d, *J* = 8.1 Hz, 2H, Ar*H*^{3,5}).

^{13}C-NMR (75 MHz in $CDCl_3$, δ in ppm): δ = -1.66 (Si-*C*H_3), 14.21 (*C*H_3-CH_2), 16.65 (Si-*C*H_2), 22.79 (CH_3-*C*H_2), 23.13 (Si-CH_2-*C*H_2), 29.45-29.74 (CH_3-CH_2-(*C*H_2)$_9$), (*C*H_2), 32.03 (S-*C*H_2-CH_2), 40.56 (N-*C*H_2), 41.04 (Ar-*C*H_2), 127.01 (Ar*C*^{3,5}), 129.32 (Ar*C*^{2,6}), 136.36 (Ar*C*^{4}), 136.94 (Ar*C*^{1}), 171.22 (*C*O), 223.51 (*C*S).

Elemental analysis, calculated: C39H71NOS3Si: C 67.5%, H 10.3 %, N 2.0 %, S 13.9 % found: C 68.4 %, H 10.6 %, N 2.0 %, S 13.3 % (IAP)

Electron ionization mass spectrometry: calculated Mr: 693.45 g/mol, found: m/z: 694.4535 g/mol

FTIR (selected bands cm^{-1}): 2922, 2852, 1633, 1462, 1421, 1373, 1296, 1248, 1190, 1155, 1109, 1063, 1003, 949, 858, 853, 810, 762, 723, 692.

Synthesis of 3,5-bis(chloromethyl)benzoyl chloride adapted from a reported procedure[254]

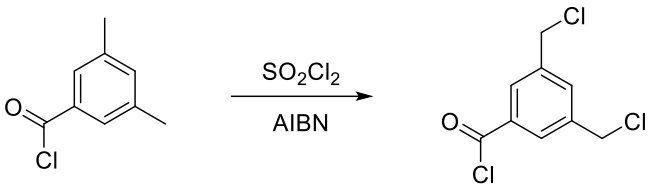

3,5-Dimethylbenzoyl chloride (22.0 mL, 25.1 g, 0.149 mol), Sulfuryl chloride (24.0 mL, 40.1 g, 0.297 mol, 1.98 eq.) and AIBN (101.2 mg, 0.6163 mmol, 4.14 * 10^{-3} eq.) were added in a 100 mL Schlenk flask and heated to 90 °C. After 1 h, additional AIBN (102.3 mg, 0.6230 mmol, 4.18 * 10^{-3} eq.) was added and the reaction was continued for further 3 h. Then, unreacted sulfuryl chloride was removed by bubbling with argon. The residue was purified by fractionated distillation in vacuo (with a 20 cm Vigreux column and column head) to obtain educt, 3-(Chloromethyl)-5-methylbenzoyl chloride which can react again with sulfuryl chloride (1 eq.) and raw product. The raw product was further purified by recrystallization from hexane at -20 °C to remove di- and trichlorinated byproducts. Yield: 3.83 g, 0.0161 mmol, 11 %; Lit.: 40 %

^{1}H-NMR (300 MHz in $CDCl_3$, δ in ppm): δ = 4.64 (s, 4H, CH_2), 7.76 (br. t, 1H, ArH^4), 8.09 (d, J = 1.5 Hz, 2H, Ar$H^{3,5}$).

Synthesis of 3,5-bis(chloromethyl)-*N*-dodecylbenzamide

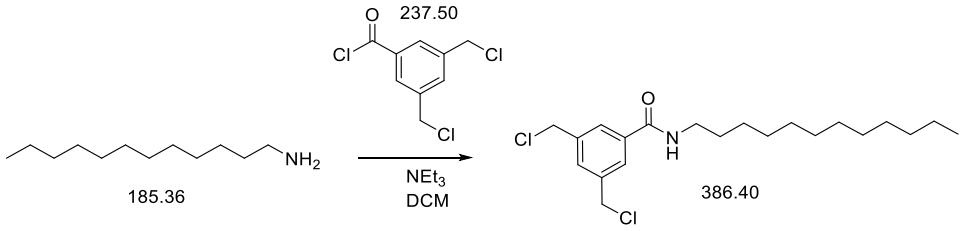

3,5-Bis(chloromethyl)benzoyl chloride (2.47 g, 10.4 mmol) and Triethylamine (2.65 mL 1.93 g, 19.1 mmol. 1.84 eq.) were dissolved in DCM (5 mL) and the solution was cooled down to 0 °C. Then, the solution was stirred for 20 min. Subsequently, dodecylamine (1.82 g, 9.82 mmol, 0.95 eq.) was added slowly over 30 min. Further DCM (5 mL) was added. The reaction was stirred overnight at room temperature. Then, the reaction was diluted with DCM (25 mL) and the organic phase was washed with 1 M HCl-solution (3 x 20 mL), saturated $NaHCO_3$ solution (20 mL),

distilled water (2 x 25 mL), 10 wt% NaOH and brine (30 mL). The aqueous phases were always reextracted with DCM (20 mL). The combined organic phases were dried over $MgSO_4$ and the solvent was removed under reduced pressure. The residue was dissolved in petrol ether/ethyl acetate 1:1 and passed over a short column. The solvent was removed under reduced pressure and the product was purified by recrystallization from petrol ether/ethyl acetate 5:1 v:v to give white powder. Yield: 2.28 g, 5.90 mmol, 57 %

^{1}H-NMR (300 MHz in $CDCl_3$, δ in ppm): δ = 0.88 (t, *J* = 6.5 Hz, 6H, C*H*$_3$), 1.26-1.35 (m, 18H, CH_3-(C*H*$_2$)$_9$), 1.63 (tt, *J* = 7.2 Hz, 2H, N-CH_2-C*H*$_2$), 3.45 (dt, *J* = 7.0 Hz, *J* = 6.6 Hz, 2H, N-C*H*$_2$), 4.62 (s, 4H, Aryl(-C*H*$_2$-Cl)$_2$), 6.09 (br. t, 1H, N-*H*), 7.55 (s, 1H, Ar*H*^{4}), 7.72 (d, *J* = 1.4 Hz, 2H, Ar*H*^{3,5}).

Synthesis of (5-(dodecylcarbamoyl)-1,3-phenylene)bis(methylene) bis(3-(trimethylsilyl)-propyl)bis(carbonotrithioate) Y-CTA

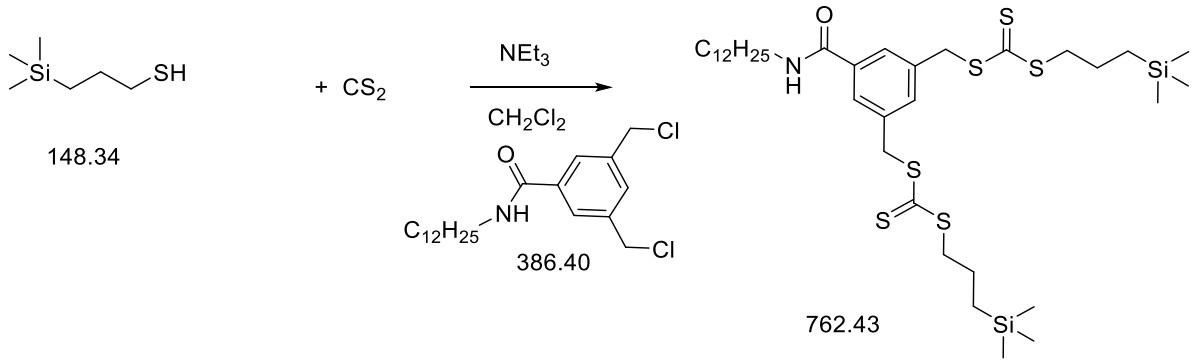

3-(Trimethylsilyl)propane-1-thiol (0.61 mL, 0.52 g , 3.49 mmol) and CS_2 (0.21 ml, 0.26 g, 3.,48 mmol, 1.00 eq.) were dissolved in dry DCM (20 mL) and stirred at room temperature. Triethylamine (0.50 mL, 0.37 g, 3.61 mmol 1.03 eq.) was added dropwise. The so-formed yellow solution was stirred for further 30 min. Then, 3,5-bis(chloromethyl)-*N*-dodecylbenzamid (0.67 g, 1.73 mmol, 0.50 eq.) was slowly added. The reaction was stirred overnight, then diluted with DCM (40 mL) and washed with distilled water (3 x 80 mL). The aqueous phase was reextracted with DCM (20 mL) and the combined organic layers were washed with brine and dried over $MgSO_4$. The organic solvent was removed under reduced pressure and the raw product was purified by column chromatography on silica gel using petrol ether/ethyl acetate (10:1 (v/v), R_f= 0.11). The obtained monosubstituted byproduct was reacted again with 1 eq. of reagents. The product was further purified by recrystallization from MeOH. Yield: 0.33 g, 0.43 mmol, 12 %

^{1}H-NMR (300 MHz in $CDCl_3$, δ in ppm): δ = -0.01 (s, 18H, -(Si-(CH_3)$_3$)$_2$), 0.62 (m_c, *J* = 3.8 Hz, *J* = 17.8 Hz 4H, -(Si-CH_2)$_2$), 0.88 (t, *J* = 6.8 Hz, 3H, CH_3), 1.26-1.34 (m, 18H, CH_3-(CH_2)$_9$), 1.61-1.75 (m, 6H, N-CH_2-CH_2 & S-CH_2-CH_2), 3.36-3.46 (m, 6H, N-CH_2 & S-CH_2-CH_2), 4.61 (s, 4H, C-CH_2-S), 6.01 (br. t, *J* = 6.8 Hz, 1H, N-*H*), 7.44 (br. t, 1H, ArH^4), 7.61 (d, *J* = 1.3 Hz, 2H, Ar$H^{2,6}$).

^{13}C-NMR (75 MHz in $CDCl_3$, δ in ppm): δ = -1.62 (Si-*C*H_3), 14.23 (*C*H_3-CH_2), 16.64 (Si-*C*H_2), 22.80 (CH_3-*C*H_2), 23.08 (Si-CH_2-*C*H_2), 27.12 (N-(CH_2)$_2$-*C*H_2), 29.45-29.77 ((*C*H_2)$_6$), 32.05 (CH_3-CH_2-*C*H_2), 40.36 (S-*C*H_2-CH_2), 40.68 (N-*C*H_2), 40.68 (Ar-*C*H_2), 127.17 (Ar*C*^{4,6}), 132.95 (Ar*C*^{2}), 135.97 (Ar*C*^{5}), 136.76 (Ar*C*^{1,3}), 166.76 (*C*O), 223.24 (*C*S).

Elemental analysis ($C_{35}H_{63}NOS_6Si$): calculated C 55.1%, H 8.3 %, N 1.8 %, S 25.2 % found: C 56.0 %, H 11.1 %, N 1.8 %, S 23.1 %

Electron ionization mass spectrometry: calculated Mr: 761.28 g/mol, found: m/z: 694.4535 g/mol

FTIR (selected bands cm^{-1}): 3300, 3074, 2951, 2922, 2852, 2677, 1734, 1637, 1597, 1543, 1450, 1416, 1373, 1331, 1306, 1248, 1161, 1101, 1063, 1001, 970, 949, 904, 858, 831, 810, 764, 715, 690.

Synthesis of *N*-methyldodecylamine adapted to a reported procedure[255]

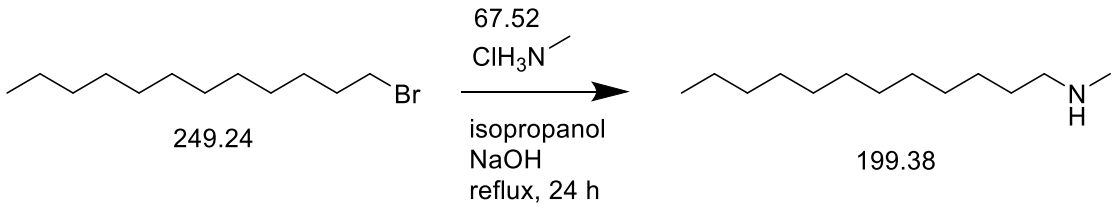

1-Bromododecane (48.25 mL, 50.18 g, 201.3 mmol) in *i*-PrOH (50 mL) was added to a solution of methylamine hydrochloride (150.06 g, 2.22 mol, 11.0 eq.) and NaOH (44.48 g, 1.11 mol, 5.5 eq.) in i-PrOH (250 mL). The mixture was refluxed for 24 h. Then, the solvent was removed under reduced pressure and $NaOH_{(aq)}$ (5 M, 600 mL) was added. The product containing phase was separated and the aqueous phase was extracted with DCM (6 x 100 mL). The combined organic layers were dried over $MgSO_4$. The residue was distilled ($bp_{0.43mbar}$ 74 °C) and the crude product was further purified by recrystallization from n-heptane to obtain the product as a colorless oil. Yield: 22.96 g, 115.16 mmol, 57 % (Lit.: 38 %)

^{1}H-NMR (300 MHz in $CDCl_3$, δ in ppm): δ = 0.88 (t, *J* = 7.0 Hz, 3H, C*H*$_3$), 1.26 – 1.30 (m, 18H, CH_3-(C*H*$_2$)$_9$), 1.50 (tt, *J* = 7.0 Hz, 2H, N-CH_2-C*H*$_2$), 2.43 (s, 3H, N-CH_3), 2.56 (t, *J* = 7.3 Hz, 2H, N-C*H*$_2$).

Synthesis of 4-chloromethyl-*N*-dodecyl-*N*-methylbenzamide

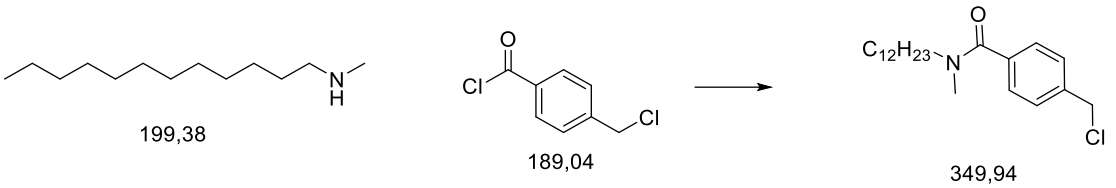

Triethylamine (3.40 mL 2.48 g, 24.5 mmol, 1.5 eq.) and N-methyldodecylamin (3.28 g, 16.5 mmol) were dissolved in DCM (15 mL) and cooled to 0 °C. A solution of 4-chloromethylbenzoyl chloride (3.12 g, 16.5 mmol, 1.00 eq.) in DCM (15 mL) was added dropwise within 30 min. The reaction was stirred overnight. Triethylammoniumhydrochloride was filtered off and washed with DCM (20 mL). The organic layer was washed with 1 M HCl (50 mL). The aqueous layer was reextracted with DCM (20 mL). The combined organic layers were adsorbed on silica and the raw product was purified by a short column chromatography in DCM. After drying in the vacuum oven (40 °C, 1 mbar), the product was obtained as colorless crystals. Yield: 2.76 g, 7.87 mmol, 48 %

^{1}H-NMR (300 MHz in $CDCl_3$, δ in ppm): δ = 0.88 (t, *J* = 6.9 Hz, 3H, C*H*$_3$), 1.14-1.26 (m, 18H, CH_3-(C*H*$_2$)$_9$), 1.53-1.64 (br. tt, 2H, N-CH_2-C*H*$_2$), 2.93-3.06 (br. s, 3H, N-C*H*$_3$), 3.21-3.52 (br. t, 2H, N-C*H*$_2$), 4.59 (s, 2H, C-C*H*$_2$-S), 7.41 (m, 4H, Ar*H*).

Synthesis of 4-(dodecyl(methyl)amino)-*N*-2-hydroxyethyl-1,8-naphthalimide similar to a reported procedure[213]

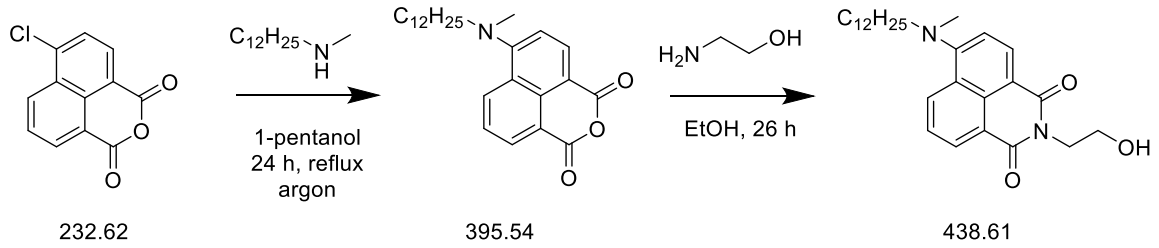

Step 1: 4-Chloro-1,8-naphthalic anhydride (10.00 g, 42.99 mmol) and *N*-methyldodecylamine (17.14 g, 85.98 mmol, 2.00 eq.) were weighed in a Schlenk flask. Pentanol (100 mL) was added and the mixture was refluxed for 24 h with stirring under argon. Then, the solution was left to cool

to room temperature for 24 h. The so-formed crystals were filtered off, washed with EtOH, and recrystallized from EtOH twice. The contaminated fractions were further purified by column chromatography on silica gel using petrol ether/ethyl acetate (5:1 (v/v), R_f= 0.16). The product was recrystallized by petrol ether/ethyl acetate (5:1 (v/v)). Yield: 4.76 g, 12.03 mmol, 28 %

^{1}H-NMR (400 MHz in $CDCl_3$, δ in ppm): δ = 0.87 (t, *J* = 6.9 Hz, 3H, CH_2-C*H*$_3$), 1.24-1.29 (m, 18H, (C*H*$_2$)$_9$-CH_3), 1.76 (br. tt, *J* = 7.3 Hz, 2H, N-CH_2-C*H*$_2$), 3.11 (s, 3H, N-C*H*$_3$), 3.39 (br. t, *J* = 7.6 Hz, 2H, N-C*H*$_2$), 7.14 (d, *J* = 8.4 Hz, 1H, Ar^3), 7.67 (dd, *J* = 7.3 Hz, 1H, Ar^6), 8.45 (dd, *J* = 1.1 Hz, *J* = 8.2 Hz, 1H, Ar*H*^{2}), 8.47 (d, *J* = 8.2 Hz, 1H, Ar*H*^{7}), 8.57 (dd, *J* = 1.1 Hz, *J* = 7.4 Hz, 1H, Ar*H*^{5}).

Step 2: A mixture of 4-(dodecyl(methyl)amino)-1,8-naphthalic anhydride (1.59 g, 4.02 mmol) and ethanolamine (0.84 mL, 0.86 g, 14.03 mmol, 1.3 eq) in EtOH (100 mL) was refluxed for 26 h. Then, the mixture was left to cool to room temperature leading to crystal formation. The so-formed crystals were filtered off, and the filtrate was concentrated to for further recrystallization. The product was obtained as a yellow solid. Yield: 1.45 g, 3.31 mmol, 82 %.

^{1}H-NMR (400 MHz in $CDCl_3$, δ in ppm): δ = 0.87 (t, *J* = 6.9 Hz, 3H, CH_2-C*H*$_3$), 1.24-1.29 (m, 18H, (C*H*$_2$)$_9$-CH_3), 1.74 (br. tt, *J* = 7.0 Hz, 2H, N-CH_2-C*H*$_2$), 3.07 (s, 3H, N-C*H*$_3$), 3.33 (br. t, *J* = 7.6 Hz, 2H, N-C*H*$_2$), 3.97 (t, *J* = 5.1 Hz, 2H, -N-C*H*$_2$-), 4.46 (t, *J* = 5.2 Hz, 2H, O-C*H*$_2$-), 7.15 (d, *J* = 8.4 Hz, 1H, Ar^3), 7.66 (dd, *J* = 7.3 Hz, *J* = 8.4 Hz, 1H, Ar^6), 8.42 (dd, *J* = 1.1 Hz, *J* = 8.5 Hz, 1H, Ar*H*^{2}), 8.48 (d, *J* = 8.2 Hz, 1H, Ar*H*^{7}), 8.58 (dd, *J* = 1.1 Hz, *J* = 7.3 Hz, 1H, Ar*H*^{5}).

Synthesis of (4-(dodecyl(methyl)amino)-1,3-dioxo-1H-benzo[de]isoquinolin-2(3H)-yl)ethyl 2-bromopropanoate

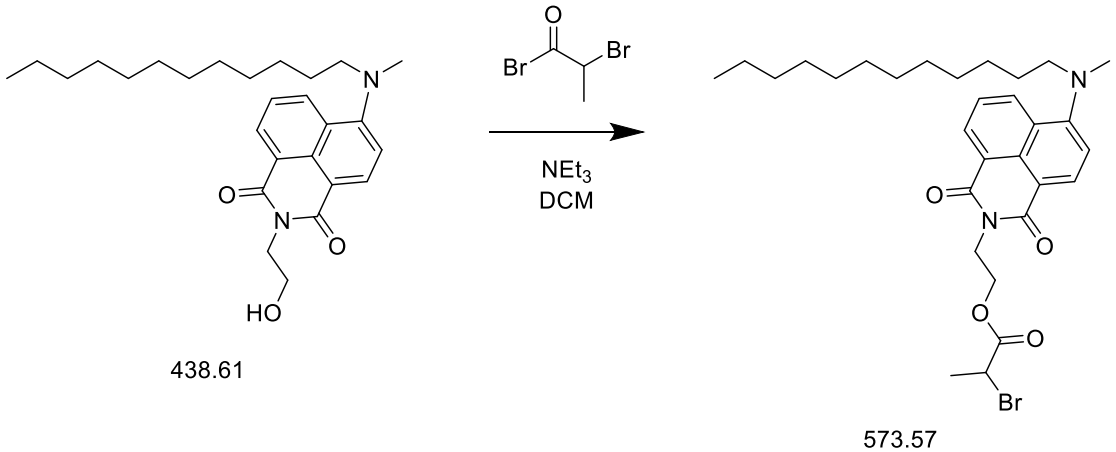

A solution of 4-(dodecyl(methyl)amino)-N-2-hydroxyethyl-1,8-naphthalimide (1.45 g, 3.31 mmol) und triethylamine (0.52 mL, 0.38 g, 3.77 mmol 1.14 eq.) in DCM (40 mL) was cooled to 0 °C. Then, 2-bromopropionyl bromide (0.40 mL, 0.82 g, 3.82 mmol, 1.15 eq.) was added and the reaction was monitored by TLC. After 1 day, more triethylamine (0.52 mL, 0.38 g, 3.77 mmol 1.14 eq.) as well as 2-bromopropionyl bromide (0.40 mL, 0.82 g, 3.82 mmol, 1.15 eq.) was added at 0 °C. After 1.5 h the reaction was complete and DCM (35 mL) was added. Then, the organic phase was washed with water (100 mL), 1 M HCl (2 × 50 mL), saturated $NaHCO_3$-solution (50 mL) and brine (50 mL). The combined organic phases were dried over $MgSO_4$ and the solvent was removed under reduced pressure. The residue was purified by column chromatography using petrol ether/ethyl acetate 10:1 (v/v) increasing to 5:1 (v/v). The obtained product had still small impurities but was further used as received. Yield: 1.50 g, ca. 2.62 mmol, 79 %

^{1}H-NMR (400 MHz in $CDCl_3$, δ in ppm): δ = 0.87 (t, J = 6.9 Hz, 3H, CH_2-CH_3), 1.24-1.29 (m, 18H, (CH_2)$_9$-CH_3), 1.74 (br. tt, J = 7.0 Hz, 2H, N-CH_2-CH_2), 1.80 (d, J = 7.0 Hz, 3H, CH-CH_3), 3.06 (s, 3H, N-CH_3), 3.32 (br. t, 2H, N-CH_2), 4.33 (q, J = 6.9 Hz, 1H, CH-CH_3) 4.45-4.60 (m, 4H, -N-CH_2-CH_2-O), 7.15 (d, J = 8.3 Hz, 1H, Ar^3), 7.66 (dd, J = 8.4 Hz, J = 7.3 Hz, 1H, Ar^6), 8.42 (dd, J = 8.5 Hz, J = 1.1 Hz, 1H, ArH^2), 8.47 (d, J = 8.2 Hz, 1H, ArH^7), 8.57 (dd, J = 7.3 Hz, J = 1.1 Hz, 1H, Ar^5).

Synthesis of 7-(3-mercaptopropoxy)-4-methylcoumarin similar to a reported procedure [256]

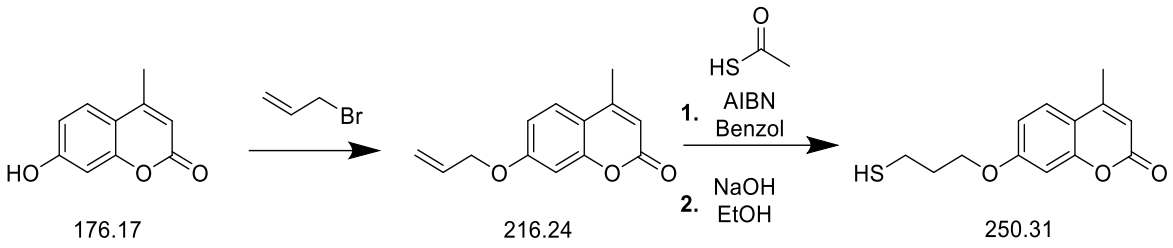

Step 1: 7-Hydroxy-4-methylcoumarin (12.04 g, 68.34 mmol) and allylbromide (8.90 mL, 12.46 g, 102.99 mmol, 1.5 eq.) were dissolved in DMF (100 mL). K_2CO_3 (9.44 g, 68.31 mmol, 1.00 eq.) and KI (0.38 g, 2.29 mmol, 0.03 eq.) were added. The solution was heated to 100 °C stirred for 24 h under argon atmosphere. Then, water (300 mL) was added and the precipitated raw product was filtered off. The raw product was recrystallized from EtOH (200 mL) six times to remove all impurities. Yield: 11.19 g, 51.75 mmol, 76 %

^{1}H-NMR (400 MHz in $CDCl_3$, δ in ppm): δ = 2.17 (d, J = 1.0 Hz, 3H, CH_3), 4.38 (dt, 2H, *J* = 1.4 Hz, *J* = 5.3 Hz, O-CH_2), 5.12 (dd, *J* = 1.2 Hz, *J* = 10.5 Hz, 1H, CH_2^{cis}-CH), 5.22 (dd, *J* = 1.4 Hz,

J = 17.3 Hz, 1H, C*H*$_2^{trans}$-CH), 5.81 (m, 1H, CH_2-C*H*), 5.91 (br. q, *J* = 1.0 Hz, 1H, Ar^3), 6.60 (d, *J* = 2.5 Hz, 1H, Ar^8), 6.66 (dd, *J* = 2.5 Hz, *J* = 8.8 Hz, 1H, Ar^6), 7.27 (d, *J* = 8.8 Hz, 1H, Ar^5).

Step 2: 7-Allyloxy-4-methylcoumarin (2.00 g, 9.25 mmol) and thioacetic acid (1.30 mL, 1.41 g, 18.50 mmol, 2.0 eq.) were dissolved in benzene (100 mL). After addition of AIBN (0.76 g 4.62 mmol, 0.5 eq.) the solution was refluxed for 24 h. Then, the solution was cooled to room temperature and 10 wt% NaOH-solution (70 mL) was added under stirring for 10 min. The organic layer was separated and washed with more 10 wt% NaOH-solution (2 x 70 mL), water and brine (70 mL). The organic layer was then dried over $MgSO_4$. The solvent was evaporated and the residue was recrystallized from EtOH four times. Yield: 2.02 g, 75 %

^{1}H-NMR (400 MHz in $CDCl_3$, δ in ppm): δ = 2.11 (tt, J = 6.6 Hz, 2H, CH_2-C*H*$_2$-CH_2), 2.35 (s, 3H, C*H*$_3$-CO), 2.40 (d, J = 1.1 Hz, 3H, Ar-C*H*$_3$), 3.07 (t, J = 7.1 Hz, 2H, S-C*H*$_2$), 4.07 (t, J = 6.1 Hz, 3H, O-C*H*$_2$), 6.14 (d, J = 1.1 Hz, 1H, Ar^3), 6.80 (d, J = 2.5 Hz, 1H, 1H, Ar^8), 6.85 (dd, J = 8.8 Hz, J = 2.5 Hz, 1H, Ar^6), 7.49 (d, J = 8.8 Hz, 1H, Ar*H*^{5}).

Step 3: The thioacetate (0.63 g, 2.15 mmol) was given to EtOH (15 mL) cooled to 0 °C. NaOH (0.50 g, 12.5 mmol, 5.8 eq.) was added and the mixture was stirred. Within 1-2 h the reaction became clear. After the solution was stirred over night under argon atmosphere, it was acidified with conc. $HCl_{(aq)}$ to precipitate the product. The so obtained raw product was filtrated and washed with water. Then, it was dissolved in DCM (40 mL) and the organic phase was washed with brine (20 & 50 mL). The organic phase was dried over $MgSO_4$ and the organic solvent was removed by reduced pressure. The product was obtained as slightly yellow solid. Yield: 0.52 g, 2.08 mmol, 97 %

^{1}H-NMR (400 MHz in $CDCl_3$, δ in ppm): δ = 1.40 (t, J = 8.1 Hz, 1H, S*H*), 2.12 (tt, J = 6.5 Hz, J = 6.4 Hz, 2H, CH_2-C*H*$_2$-CH_2), 2.40 (d, J = 1.1 Hz, 3H, -C*H*$_3$), 2.75 (dt, J = 7.0 Hz, J = 7.5 Hz, 2H, S-C*H*$_2$), 4.15, (t, J = 5.9 Hz, 2H, O-C*H*$_2$), 6.14 (d, J = 1.0 Hz, 1H, C*H*) 6.83 (d, J = 2.4 Hz, 1H, Ar*H*^{8}), 6.86 (dd, J = 8.8 Hz, J = 2.5 Hz, J = 2.5 Hz, 1H, ArH^6), 7.50 (d, J = 8.7 Hz, 1H, ArH^5).

Synthesis of 4-(dodecyl(methyl)amino)-1,3-dioxo-1H-benzo[de]isoquinolin-2(3H)-yl)ethyl 2-methyl-3-((((3-((4-methyl-2-oxo-2H-chromen-7-yl)oxy)propyl)thio)carbonothioyl)thio)-propanoate FRET-CTA similar to a reported procedure[205]

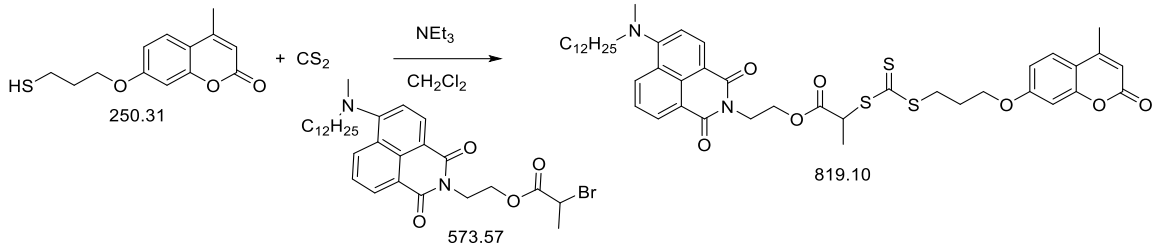

7-(3-Mercaptopropoxy)-4-methylcoumarin (0.39 g, 1.55 mmol) was dissolved in DCM (7 mL). Triethylamine (0.32 mL, 0.23 g, 2.28 mmol, 1.1 eq.) was slowly added. After 30 min of stirring, CS_2 (0.11 ml, 0.14 g, 1.82 mmol, 1.2 eq.) was added and the solution was stirred for 1 h. Afterwards, a solution of naphthalimide derivative (0.89 g, 1.55 mmol, 1.0 eq.) in DCM (7 mL) was slowly added and the solution was stirred over night at room temperature. The product was purified by column chromatography using petrolether/ethyl acetate 5:1 (v/v) increasing to 1:1 (v/v). The product was obtained as a orange oil. Yield: 0.24 g, 0.29 mmol, 19 %

^{1}H-NMR (400 MHz in $CDCl_3$, δ in ppm): δ = 0.87 (t, J = 6.9 Hz, 3H, CH_2-C*H*$_3$), 1.24-1.29 (m, 18H, (C*H*$_2$)$_9$-CH_3), 1.57 (d, J = 7.4 Hz,1H, CH-C*H*$_3$) 1.73 (br. tt, 2H, N-CH_2-C*H*$_2$), 2.16 (tt, J = 6.5 Hz, 2H, S-CH_2-C*H*$_2$), 2.39 (d, J = 1.1 Hz, 3H, C-C*H*$_3$), 3.07 (s, 3H, N-C*H*$_3$), 3.33 (br. t, J = 7.4 Hz, 2H, N-C*H*$_2$), 3.46 (t, J = 7.1 Hz, 2H, S-C*H*$_2$), 4.05 (t, J = 6.0 Hz, 2H, ArylO-C*H*$_2$), 4.32-4.56 (m, 4H, CO_2-(C*H*$_2$)$_2$), 4.79 (q, J = 7.4 Hz, 1H, C*H*-CH_3), 6.13 (d, J = 1.1 Hz, 1H, CouAr*H*^{3}), 6.78 (d, J = 2.5 Hz, 1H, CouAr*H*^{6}), 6.84 (dd, J = 8.8 Hz, J = 2.5 Hz, 1H, CouAr*H*^{8}), 7.18 (d, J = 8.3 Hz, 1H, *NaphArH*^{3}), 7.49 (d, J = 8.8 Hz, 1H, CouAr*H*^{5}), 7.67 (dd, J = 7.9 Hz, J = 7.9 Hz, 1H, *NaphArH*^{6}), 8.46-8.49 (m, 2H, NaphAr*H*$^{2\&7}$), 8.57 (dd, J = 7.2 Hz, J = 1.0 Hz, 1H, NaphAr*H*^{5}).

^{13}C-NMR (75 MHz in $CDCl_3$, δ in ppm): δ = 14.22 (*C*H_3-CH_2), 16.89 (*C*H_3-CH), 18.77 (*C*H_3-C), 22.77 (CH_3-*C*H_2), 27.11 (N-(CH_2)$_2$-*C*H_2), 27.53 (N-CH_2-*C*H_2-CH_2), 27.82 (S-CH_2-*C*H_2), 29.43-29.71 (N-(CH_2)$_3$-(*C*H_2)$_6$), 32.00 (CH_3-CH_2-*C*H_2), 33.34 (S-*C*H_2-CH_2), 38.65 (CONCO-*C*H_2), 41.77 (N-*C*H_0), 48.26 (CH_3-*C*H), 57.34 (N-*C*H_2-(CH_2)$_2$), 63.29 (COO-*C*H_2), 66.73 (C-O-*C*H_2), 101.64 (CouAr*C*^{8}), 112.21 (CouAr*C*^{3}), 112.57 (CouAr*C*^{6}), 113.88 (CouAr*C*^{4a}), 114.73 (NaphAr*C*$^{1+3}$), 122.98 (NaphAr*C*^{8}), 125.16 (NaphAr*C*^{6}), 125.70 (CouAr*C*^{5}), 126.02 (NaphAr*C*^{4a}), 130.51 (NaphAr*C*^{8a}), 131.29 (NaphAr*C*^{7}), 131.39 (NaphAr*C*^{5}), 132.82 (NaphAr*C*^{2}), 152.60 (CouAr*C*^{4}), 155.35 (CouAr*C*^{8}), 161.36 (CouAr*C*^{7}), 161.78 (CouAr*C*^{2}), 164.10 (*C*ON), 164.73 (NaphAr*C*^{4}), 170.97 (*C*OO), 221.48 (*C*S).

Elemental analysis ($C_{44}H_{54}N_2O_7S_3$) calculated: C 64.52 %, H 6.65%, N 3.42 %, S 11.74% found: C 64.19 %, H 6.74 %, N 3.35 %, S 10.80 %

ESI: calculated mass M: 842.09 g/mol, found: $[M+Na]^+$: 841.64 g/mol

FTIR (selected bands cm^{-1}): 2924, 2852, 1730, 1693, 1653, 1612, 1585, 1514, 1466, 1452, 1387, 1369, 1354, 1292, 1281, 1263, 1240, 1201, 1147, 1068, 1024, 1016, 872, 849, 833, 816, 781, 760, 735, 706.

UV-vis absorbance, determination of ε: in DCM (λ_{max}=424 nm, ε = 8500 $L \cdot mol^{-1} \cdot cm^{-1}$), in THF ($\lambda_{max}$=424 nm, ε = 10700 $L \cdot mol^{-1} \cdot cm^{-1}$)

Synthesis of 2-(bromomethyl)-2-methylpropane-1,3-diol adapted from a reported procedure[257]

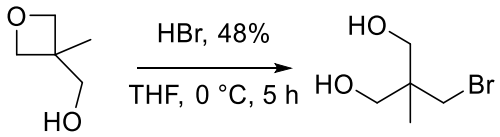

102.13 183.05

3-Methyl-3-oxetanemethanol (101.21 g, 991.00 mmol) was dissolved in THF (750 mL) and stirred at 0 °C. HBr (48 %, 327 mL, 487 g acid, 6.40 mol, 6.5 eq.) was added dropwise within 5 h, while the temperature was kept below 10 °C. Afterwards, the reaction was stirred overnight at room temperature. Then, distilled water (400 mL) was added and the aqueous phase was extracted with diethylether (6 x 350 mL). The combined organic phases were dried over $MgSO_4$ and concentrated. Pentane (ca. 5 mL) was added to precipitate the raw product. The raw product was further purified by recrystallization from DCM and was then dried at 5 mbar. The product was obtained as a colorless solid and was stored at around 5 °C. Yield: 71.93 g, 39.30 mol, 40 %, Lit.: 96 %

^{1}H-NMR (400 MHz in $CDCl_3$, δ in ppm): δ = 0.93 (s, 3H, C*H*$_3$), 3.56 (s, 2H, C*H*$_2$-Br), 3.68 (s, 4H, C*H*$_2$-OH).

Synthesis of 2-(mercaptomethyl)-2-methylpropane-1,3-diol adapted to a reported procedure[257]

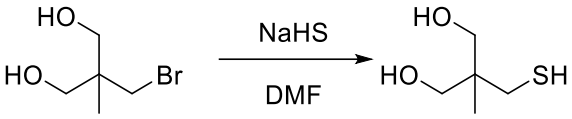

183.05 136.21

2-(Bromomethyl)-2-methylpropane-1,3-diol (30.00 g, 116.4 mmol) was added with stirring to a solution of NaHS (27.56 g, 491.7 mol, 3 eq.) in DMF (350 mL) and stirred for 20 h at 75 °C. Solvent was removed under reduced pressure, and the residue was dissolved in water (350 mL). The aqueous phase was extracted with ethyl acetate (4 x 150 mL) and the combined organic phases were dried over $MgSO_4$. The solvent was removed under reduced pressure and the residue was distilled (1 mbar, 200 °C). The product was dried under high vacuum at 45 °C to remove residual DMF. The product was then obtained as a colorless solid. Yield: 3.35, 24.6 mmol, 20 % (Lit. 52 %)

^{1}H-NMR (400 MHz in $CDCl_3$, δ in ppm): δ = 0.85 (s, 3H, C*H*$_3$), 1.31 (t, *J* = 8.8 Hz, 1H, S*H*), 2.69 (d, *J* = 8.8 Hz, 2H, C*H*$_2$-S), 3.65 (dd, *J* = 13.6 Hz, *J* = 10.6 Hz, 4H, C*H*$_2$-OH).

Synthesis of 2-(((2-(2-(2-mercaptoethoxy)ethoxy)ethyl)thio)methyl)-2-methylpropane-1,3-diol similar to a reported procedure[258]

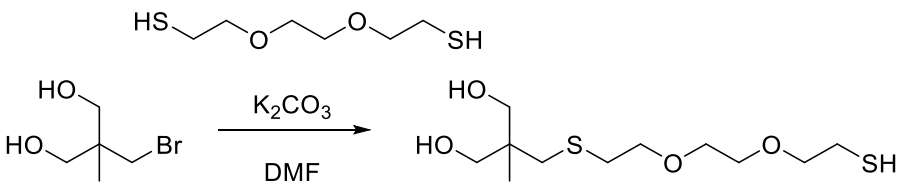

183.05 284.43

2-(Bromomethyl)-2-methylpropane-1,3-diol (24.00 g, 0.131 mol), K_2CO_3 (27.81 g, 0.20 mol, 1.5 eq.) and 2,2′-(ethylenedioxy)diethanethiol (21.5 mL, 24.1 g, 0.132 mol, 1.01 eq.) were placed in a 500 mL flask and DMF (150 mL) was added. The mixture was stirred for 24 h at room temperature under argon atmosphere. Formed salt was filtered off, and the solvent was removed under reduced pressure. Ethyl acetate was added to remove further unsoluble salt again by filtration. The solvent was removed under reduced pressure and the residue was purified by column

chromatophry using a gradient of petrol ether:ethyl acate starting with 10:1 (v/v), over 5:1 (v/v) to 1:1(v/v). The last composition was ethyl acetate:MeOH 9:1 to obtain the product, which was then dried in the high vacuum for 2 nights at 40 °C to remove residual DMF. Yield: 12.06 g, 0.042 mol, 32 %

^{1}H-NMR (400 MHz in $CDCl_3$, δ in ppm): δ = 0.84 (s, 3H, C*H*$_3$), 1.62 (t, *J* = 8.2 Hz, 1H, S*H*), 2.71 (dt, *J* = 6.6 Hz, *J* = 7.1 Hz 2H, C*H*$_2$-S), 2.77 (t, *J* = 6.2 Hz, 2H, 2H, C-CH$_2$-S-*C*H$_2$), 2.81 (s, 2H, C-*C*H$_2$), 3.58-3.73 (m, 12H, (C*H*$_2$-O-*C*H$_2$)$_2$ & *C*H$_2$-OH).

Synthesis of 2-(((((4-((2-chloropropanoyl)(dodecyl)carbamoyl)benzyl)thio)-carbonothioyl)thio)methyl)-2-methylpropane-1,3-diyl bis(2-chloropropanoate) A-CTA1c

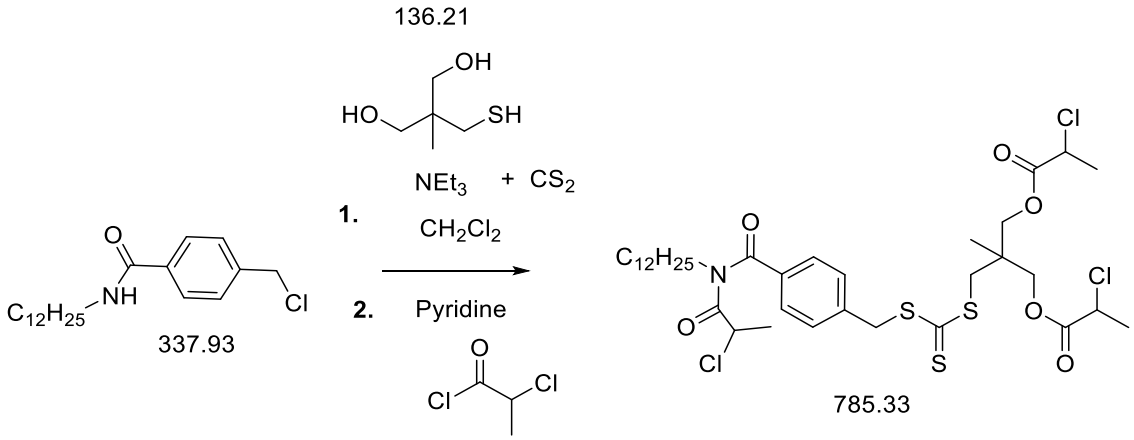

The mercaptodiol (0.85 g, 6.21 mmol) was dissolved in acetonitrile (10 mL) at room temperature. Then, the solution was cooled to 0 °C and triethylamine (1.1 mL, 0.80 g, 7.93 mmol 1.3 eq.) was added. CS_2 (0.75 ml, 0.95 g, 12.42 mmol, 2.00 eq.) was added slowly turning the solution yellow. After 30 min of stirring, a solution of 4-(chloromethyl)-*N*-dodecylbenzamide (2.10 g, 6.21 mmol) in DCM (35 mL) was added within 30 min. The solution was then stirred overnight at room temperature. Afterwards, triethylammonium hydrochlorid was precipitated in acetone and the solution was filtered. The solvent was removed under reduced pressure. DCM (15 mL) was added as well as pyridine (1.60 mL, 1.57 g, 19.8 mmol 3.2 eq.). The reaction mixture was cooled to 0 °C and 2-chloropropionyl chloride (1.85 mL, 2.42 g, 19.1 mmol, 3.1 eq.) in DCM (10 mL) was added within 45 min. Then, the solution was stirred overnight. The reaction was monitored via TLC. More pyridine (3.2 mL) was added at 0 °C and a solution of 2-chloropropionyl chloride (3.70 mL) in DCM (10 mL) was added dropwise. The reaction mixture was stirred for 5 h, afterwards more pyridine (3.2 mL) was added at 0 °C and a solution of 2-chloropropionyl chloride (3.70 mL) in

DCM (10 mL) was added dropwise. After 2 h, the reaction was kept in the fridge, where pyridinium chloride was formed. The mixture was filtrated and the crystals washed with DCM (30 mL). Organic layer was washed with 1 M HCl (3 x 100 mL) and distilled water (100 mL). Organic layer was then dried over $MgSO_4$ and the solvent was removed under reduct pressure. Raw product was purified by two consecutive column chromatographies using petrol ether:ethyl acate 5:1 (v/v). Yield: 1.46 g, 30 %

^{1}H-NMR (400 MHz in $CDCl_3$, δ in ppm): δ = 0.88 (t, *J* = 6.8 Hz, 3H, CH_2-C*H*$_3$), 1.11 (s, 3H, C*H*$_3$-C) 1.20-1.29 (m, 18H, CH_3-(C*H*$_2$)$_9$), 1.61 (m, 2H, N-CH_2-C*H*$_2$), 1.66 (d, *J* = 6.6 Hz, 3H, C*H*$_3$-imide), 1.70 (d, *J* = 6.9 Hz, 6H, C*H*$_3$-ester), 3.56-3.87 (m, 4H, N-C*H*$_2$ & C-C*H*$_2$-S), 4.06-4.16 (m, 4H, C*H*$_2$-O), 4.41 (q, *J* = 6.9 Hz, 2H, COO-C*H*), 4.67 (s, 2H, Ar-C*H*$_2$), 4.90 (q, *J* = 6.6 Hz, 2H, CON-C*H*), 7.44 (d, *J* = 8.1 Hz, 2H, Ar*H*^{2,6}), 7.75 (d, *J* = 8.2 Hz, 2H, Ar*H*^{3,5}).

Elemental analysis (C35H52Cl3NO6S3) calculated: C 53.53 %, H 6.67%, N 1.78 %, S 12.25 % found: C 52.89 %, H 6.59 %, N 1.77 %, S 12.02 %

ESI: calculated M: 842.09 g/mol, found: $[M+CH_3OH+H]^+$: 727.91 g/mol

FTIR (selected bands cm^{-1}): 2925, 2854,l 1747, 1689, 1608, 1446, 1377, 1265, 1242, 1173, 1069, 1007, 798.

Synthesis of 2-(1-(4-(dodecyl(methyl)carbamoyl)phenyl)-3-thioxo-7,10-dioxa-2,4,13-trithiatetradecan-14-yl)-2-methylpropane-1,3-diyl bis(2-chloropropanoate) A-CTA2b

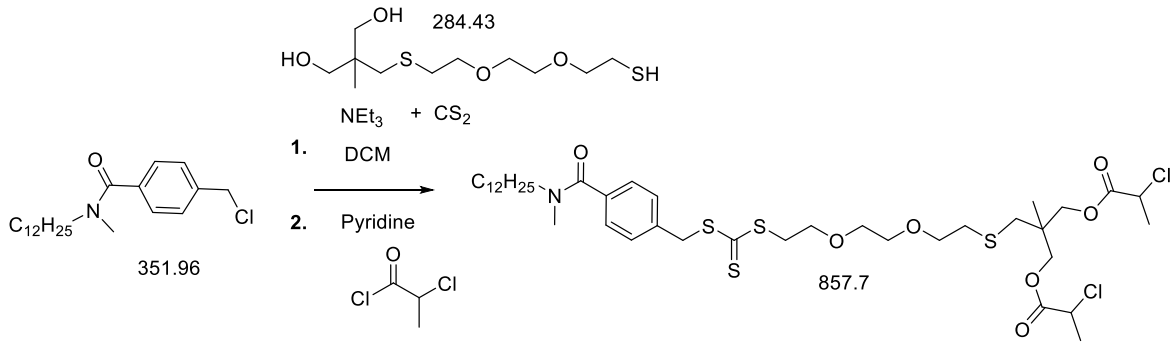

The mercaptodiol (1.77 g, 6.21 mmol) was dissolved in DCM (10 mL) at room temperature. Then, the solution was cooled to 0 °C and triethylamine (1.05 mL, 0.77 g, 7.57 mmol, 1.2 eq.) was added. CS_2 (0.75 ml, 0.95 g, 12.42 mmol, 2.00 eq.) was added slowly turning the solution yellow. After 30 min of stirring, a solution of 4-(chloromethyl)-N-dodecyl-N-methylbenzamide (2.19 g,

6.21 mmol) in DCM (15 mL) was added within 30 min. The solution was then stirred overnight at room temperature. Afterwards, triethylammoniumhydrochloride was precipitated in acetone and the solution was filtrated. The solvent was removed under reduced pressure. Then, the next step was continued with half of the obtained raw product. The raw product was dissolved in DCM (25 mL) and pyridine (0.80 mL, 0.79 g, 9.93 mmol 3.2 eq.). The reaction was cooled to 0 °C and 2-chloropropionyl chloride (0.85 mL, 1.11 g, 8.77 mmol, 2.8 eq.) in DCM (10 mL) was added within 20 min. The reaction was monitored via TLC. More pyridine (0.80 mL) was added after 3 h at 0 °C and a solution of 2-chloropropionyl chloride (0.85 mL, 1.11 g, 8.77 mmol, 2.8 eq.) in DCM (10 mL) was added dropwise within 20 min. Then, the reaction was stirred at room temperature overnight. The organic layer was washed with water (2 x 60 mL), 1 M HCl (60 mL), water (60 mL) and brine (100 mL). Aqueous layers were reextracted with DCM (10 mL). Combined organic layers were dried over $MgSO_4$. Raw product was purified by two consecutive column chromatographies using petrol ether:ethyl acate 1:1 (v/v). Yield: 1.08 g, 41 %

^{1}H-NMR (400 MHz in $CDCl_3$, δ in ppm): δ = 0.88 (t, *J* = 6.9 Hz, 3H, CH_2-C*H*$_3$), 1.07 (s, 3H, C*H*$_3$-C) 1.23-1.31 (m, 18H, CH_3-(C*H*$_2$)$_9$), 1.52 (br. m, 2H, N-CH_2-C*H*$_2$), 1.68 (d, *J* = 7.0 Hz, 3H, C*H*$_3$-ester), 2.69 (d, *J* = 1.5 Hz, 2H, S-C*H*$_2$-O), 2.72 (t, *J* = 6.6 Hz, 2H, C*H*$_2$-S-CH_2-O), 2.93 & 3.04 (br. m, 3H, N-C*H*$_3$), 3.20 & 3.50 (br. m, 2H, N-C*H*$_2$), 3.59-3.65 (m, 8H, CH_2-C*H*$_2$-O-(C*H*$_2$)$_2$-OC*H*$_2$), 3.74 (t, *J* = 6.2 Hz, 2H, CS_3-C*H*$_2$), 4.06-4.18 (m, 4H, COO-C*H*$_2$), 4.41 (q, *J* = 6.9 Hz, 2H, COO-C*H*), 4.62 (s, 2H, Ar-C*H*$_2$), 7.32-7.37 (m, 4H, Ar*H*).

^{13}C-NMR (75 MHz in $CDCl_3$, δ in ppm): δ = 14.25 (CH_2-*C*H_3), 19.00 (*C*H_3-C), 21.18 (CH_3-*C*), 21.54 (*C*H_3-CH), 22.82 (*C*H_2-CH_3), 29.48 (N-CH_2-*C*H_2), 29.70-29.76 ((C*H*$_2$)$_8$), 32.04 (*C*H_3-N), 33.69 (OCH_2-*C*H_2-S), 36.59 (*C*H_3-N), 38.15 (C-*C*H_2-S), 39.63 (N-*C*H_2), 41.15 (Ar-*C*H_2), 52.49 (*C*H-CH_3), 68.21 (COO-*C*H_2), 68.68 (CS_3-*C*H_2-CH_2), 70.44-70.60 (CH_2-*C*H_2-O-(*C*H_2)$_2$-O), 71.12 (O-(CH_2)$_2$-O*C*H_2), 127.34 (A*r*^{4}), 129.39 (A*r*^{2,3,5,6}), 136.36 (A*r*^{1}), 170.97 (*C*O), 169.72 (*C*S).

Elemental analysis (C39H63Cl2NO7S4) calculated: C 54.65 %, H 7.41 %, N 1.63 %, S 14.96 % found: C 54.20 %, H 7.41 %, N 1.61 %, S 14.82 %

ESI: calculated M: 857.70 g/mol, found: $[M+Na]^+$ = 880.33, $[M+K]^+$ = 896.32

10.5 SYNTHESES OF POLYMERS

Typical polymerization for homo- and block copolymers with BPT, BTPT, C12, 2C12-CTA, and FRET-CTA

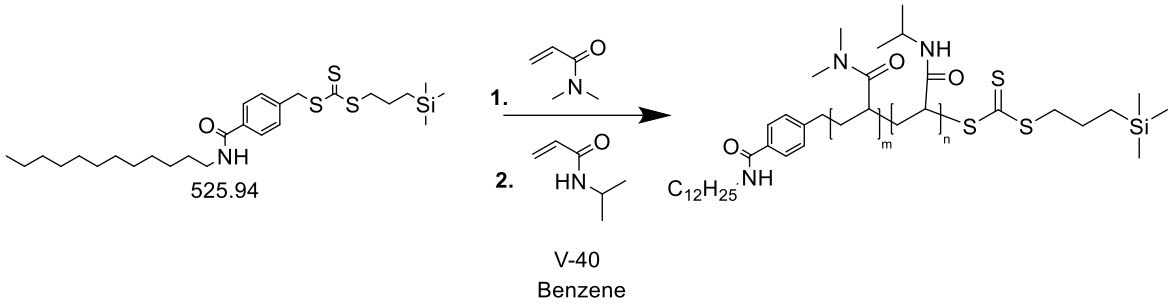

The first block was synthesized as follows: DMAm (17.5 mL, 16.9 g, 0.170 mol, 202 eq.), V-40 (20.6 mg, 0.0843 mmol, 0.1 eq.) and C12-CTA (442.6 mg, 0.8415 mmol, 1 eq.) were dissolved in benzene (76 mL). The solution was purged with argon for 45 min and immersed into a preheated oil bath with a temperature of 90 °C. After stirring for 3 h, the reaction was stopped by opening the flask to the air and cooling the flask with liquid nitrogen or dry ice/*i*-propanol. The polymer was isolated by two subsequent precipitations into diethylether. The polymer was dried in vacuum oven, dissolved in distilled water and lyophilized. Yield: 10.98 g, 63 %

In case of PNiPAm homopolymers, the polymer was usually isolated by twofold precipitations in pentane:diethylether mixtures of 5:1 v/v. In case of PNPAm homopolymer, the polymer was isolated by twofold precipitations in pentane:diethylether mixtures of 3:1 v/v.

Second block: MacroCTA PDMAm (1.03 g, 0.050 mmol) and NiPAm (226.9 mg, 2.01 mmol, 40 eq.) were dissolved in benzene (5.1 mL). A stock solution of V-40 in benzene (2 mg/mL) was prepared and 0.61 mL of this solution (equivalent to 0.0050 mmol, 0.1 eq.) was added. The solution was purged with argon for 40 min and immersed into a preheated oil bath with a temperature of 90 °C. After stirring for 4 h, the reaction was stopped by opening the flask to the air and cooling the flask with liquid nitrogen or dry ice/*i*-propanol. Yield: 1.03 g, 82 %

Z-group removal of L1a-3b

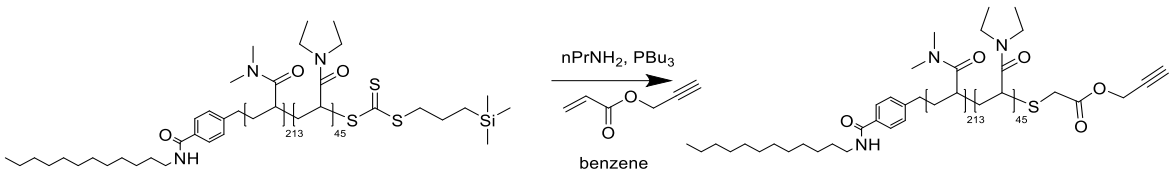

$C_{12}DMAm_{168}DEAm_{27}$ (0.40 g, 0.015 mmol) was dissolved in benzene (5.33 mL). *N*-propylamine (12 µL, 8.6 mg, 0.15 mmol, 9.9 eq) and tributylphosphine (0.36 mL, 0.30 mg, 0.0015 mmol, 0.1 eq.) were added. The reaction was stirred for 1 h at room temperature under argon atmosphere. Then, propargyl acrylate (0.02 mL, 16 mg, 0.15 mmol, 10 eq.) was added and the reaction was stirred overnight. The polymer was isolated by two subsequent precipitations into diethyl ether and dialysis for 3 days. Then, the polymer was lyophilized. Yield: 0.24 g, 60 %

Typical Polymerization procedure for DMAm with Y-CTA

The first block was synthesized as follows: DMAm (16.2 mL, 15.6 g, 0.157 mol, 403 eq.), V-40 (stock solution 2 mg/mL: 4.8 mL, 9.6 mg, 0.039 mmol, 0.1 eq.) and Y-CTA (0.30 g, 0.39 mmol) were dissolved in benzene (66 mL). The solution was purged with argon for 30 min and immersed into a preheated oil bath with a temperature of 90 °C. After stirring for 3.5 h, the reaction was stopped by opening the flask to the air and cooling the flask with liquid nitrogen or dry ice/*i*-propanol. The polymer was isolated by two subsequent precipitations into diethylether. The polymer was dried in vacuum oven, dissolved in distilled water and lyophilized. Yield: 11.93 g, 75 %

Table 10.2: Reaction conditions for the RAFT polymerization of DMAm in benzene at 90 °C using different CTAs and initiator V-40.

Code	CTA	molar ratio DMAm : CTA : V-40	m_{DMAm} g	m_{CTA} g	m_{V-40} mg	[monomer+CTA] wt%	t h
L1a	C12-CTA	202 : 1 : 0.1	16.9	0.443	20.6	22	3
L1b	C12-CTA	202 : 1 : 0.1	16.9[a)]	0.443	20.6	22	3
TH1a	2C12-CTA	200 : 1 : 0.1	11.6	0.406	14.4	20	3
TH1b	2C12-CTA	203 : 1 : 0.1	12.7	0.44	15.8	33	2.5
YS1	Y-CTA	403 : 1 : 0.1	15.6	0.30	9.6	22	3.5

[a)] Instead of distillation, DMAm was passed through a short silica column prior to use.

Table 10.3: Reaction conditions for the RAFT polymerization of block copolymers in benzene at 90 °C using different macroCTAs and initiator V-40.

Code	macroCTA	monomer	molar ratio monomer : macroCTA : V-40	$m_{monomer}$ g	$m_{macroCTA}$ g	m_{V-40} mg	[monomer + macroCTA] wt%	t h
L1a-2a	L1a	NiPAm	20 : 1 : 0.1	0.27	2.47	2.94	22	5
L1a-2b	L1a	NiPAm	40 : 1 : 0.1	0.23	1.03	1.22	22	4
L1b-2c	L1b	NiPAm	65 : 1 : 0.1	0.42	0.90	1.39	50	5
L1a-3a	L1a	DEAm	20 : 1 : 0.1	0.30	2.47	2.94	22	4
L1a-3b	L1a	DEAm	40 : 1 : 0.1	0.23	1.42	1.69	22	4
L1b-3c	L1b	DEAm	65 : 1 : 0.1	0.47	0.90	1.39	50	3.5
L1a-4a	L1a	NAP	20 : 1 : 0.1	0.30	2.47	2.94	22	5
L1a-4b	L1a	NAP	40 : 1 : 0.1	0.35	1.40	1.67	22	4
L1b-5a	L1b	NPAm	43 : 1 : 0.1	0.28	0.90	1.38	33	4
TH1a-2	H1a	NiPAm	40 : 1 : 0.1	0.72	3.18	3.90	22	3
TH1a-3	H1a	DEAm	40 : 1 : 0.1	0.34	1.34	1.64	22	3
TH1a-5	H1a	NPAm	45 : 1 : 0.1	0.61	2.39	2.92	33	5.5
YS1-2	YS1	NiPAm	90 : 1 : 0.2	0.20	0.73	0.98	33	2.5
YS1-3	YS1	DEAm	90 : 1 : 0.2	0.23	0.73	0.98	33	3
YS1-5	YS1	NPAm	49 : 1 : 0.2	0.22	0.73	0.98	33	2.5

Table 10.4: Reaction conditions of homo- and block copolymerization of FRET-polymers in benzene at 90 °C.

Code	CTA	monomer	molar ratio DMAm : CTA : V-40	$m_{monomer}$ g	m_{CTA} mg	m_{V-40} mg	[monomer+CTA] wt%	t h
F1a	FRET-CTA	DMam	205 : 1 : 0.1	2.44	94	3.0	31	10[a)]
F1b	FRET-CTA	DMAm	196 : 1 : 0.1	3.47	150	4.5	50	3
F2	FRET-CTA	NiPAm	205 : 1 : 0.1	2.78	94	2.9	33	15
F1a-2a	F1a	NiPAm	45 : 1 : 0.1	0.12	0.50	0.57	33	20
F1b-2b	F1b	NiPAm	45 : 1 : 0.1	0.47	1500	2.2	50	3

[a)] Long polymerization time due to wrong amount of initiator in the first 5 h.

Table 10.5: Reaction conditions for the RAFT polymerization of bMOEAm in benzene at 90 °C using different CTAs and initiator V-40.

Code	CTA	molar ratio monomer : CTA : V-40	$m_{monomer}$ g	m_{CTA} g	m_{V-40} mg	[monomer + macroCTA] wt%	t h
P6a	BPT	9 : 1 : 0.1	1.00	0.14	14.0	22	17
P6b	BPT	25 : 1 : 0.1	1.00	0.51	5.1	22	5
P6c	BPT	53 : 1 : 0.1	1.03	$25 \cdot 10^{-3}$	2.5	22	17
P6d	BPT	159 : 1 : 0.1	0.98	$8.0 \cdot 10^{-3}$	0.80	22	5
P6e	BPT	269 : 1 : 0.1	1.00	$4.8 \cdot 10^{-3}$	0.49	22	17
P6f	BPT	539 : 1 : 0.1	1.01	$2.4 \cdot 10^{-3}$	0.24	22	2
L6a	C12-CTA	152 : 1 : 0.1	2.70	0.05	1.76	22	72
L1b-6a	L1b	40 : 1 : 0.1	1.20	2.54	3.9	22	17
L1b-6b	L1b	100 : 1 : 0.1	1.02	0.87	1.3	23	17

Pretests of SUMI reactions similar to a reported procedure[221]

MacroCTA (0.22 g, 0.011 mmol), DBMI (96.9 mg, 0.252 mmol, 23 eq.) were dissolved in benzene (0.58 mL). A 2.0 mg/mL stock solution of V-40 was added (0.12 mL, 0.24 mg, 0.00098 mmol, 0.1 eq.). The solution was purged with argon for 15 min and immersed into a preheated oil bath with a temperature of 90 °C. After stirring for 20 h, the reaction was stopped by opening the flask to the air and adding acetone. The polymer was isolated by two subsequent precipitations into diethylether. The polymer was dried in vacuum oven, dissolved in distilled water and lyophilized. Yield: not determined

Table 10.6: Reaction conditions of DMAm homopolymerization and SUMI pre-experiments in benzene at 90 °C.

Code	CTA	monomer	molar ratio monomer : CTA : V-40	$m_{monomer}$ g	m_{CTA} g	m_{V-40} mg	[monomer+CTA] wt%	t h
YN1a	BTPT	DMAm	201 : 1 : 0.1	6.4	0.10	7.77	28	9[a)]
YN1b	BTPT	DMAm	200 : 1 : 0.1	9.64	0.15	11.9	50	3
YN1a-7	YN1a	DBMI	23 : 1 : 0.1	0.10	0.22	0.24	25	20
YN1b-7	YN1b	DBMI	27 : 1 : 0.1	0.38	0.70	0.61[b)]	40[c)]	17

YN1b-7-1a	YN1b	DMAm	200 : 1 : 0.1	0.31	0.31	0.29	50	7.5

[a)] Long polymerization time due to wrong amount of initiator in the first 7 h. [b)] AIBN as initiator, [c)] DMF as solvent

SUMI reaction at high conversions of DMAm polymerization

DMAm (1.50 mL, 1.44 g, 14.6 mmol, 200 eq.) and macroCTA PNPAm **YN5** (0.36 g, 0.07 mmol) were dissolved in benzene (1.190 mL). A 2.0 mg/mL stock solution of V-40 (0.855 mL, 1.71 mg, 0.007 mmol, 0.1 eq.) was added. The solution was purged with argon for 15 min and immersed into a preheated oil bath with a temperature of 90 °C. After 1 h, more benzene (0.60 mL) was added. After 3 h, again more benzene (1.0 mL) was added. After 5 h, when the conversion of DMAm was > 99 % (monitored by ^{1}H-NMR), a preheated solution of DBMI (28.23 mg, 0.07 mmol, 1. eq.) in deoxygenated THF (0.70 mL) was added and the SUMI reaction was continued for 11.5 h at 90 °C. The reaction was stopped by opening the flask to the air and adding acetone. The polymer was isolated by four subsequent precipitations into pentane:diethylether 5:1 v/v. The polymer was dried in vacuum oven, dissolved in distilled water and lyophilized. Yield = 1.02 g, 57 %

The following RAFT polymerization steps were similar as for the typical polymerization for homo- and block copolymers with BPT, BTPT, C12, 2C12 CTA, and FRET-CTA.

Table 10.7: Reaction conditions of RAFT polymerization and SUMI experiment in benzene at 90 °C.

Code	CTA	monomer	molar ratio monomer : CTA : V-40	$m_{monomer}$ g	m_{CTA} g	m_{V-40} mg	[monomer+CTA] wt%	t h
YN2	BTPT	NiPAm	40 : 1 : 0.1	5.0	0.35	27.2	50	3
YN5	BTPT	NPAm	45 : 1 : 0.1	2.49	0.15	12.4	50	2
YN2-1a-7	YN2	DMAm+DBMI	(200+2) : 1 : 0.1	1.44+0.05	0.35	1.2[a)]	50[b)]	18
YN2-1b-7	YN2	DMAm+DBMI	(200+1): 1 : 0.1	1.44+0.03	0.35	1.7	50[b)]	6
YN5-1c-7	YN5	DMAm+DBMI	(200+1): 1 : 0.1	1.44+0.03	0.36	1.7	50	12
YN2-1a-7-1d	YN2-1a-7	DMAm	200 : 1 : 0.1	0.43	0.50	0.54	50	5.5
YN2-1b-7-1e	YN2-1b-7	DMAm	200 : 1 : 0.1	0.56	0.70	0.68	50	5
YN5-1c-7-1f	YN5-1c-7	DMAm	200 : 1 : 0.1	0.54	0.70	0.66	50	3

YN2-1a-7-1d-5a	YN2-1a-7-1d	NPAm	39 : 1 : 0.1	0.033	0.30	0.18	50	4
YN5-1c-7-1f-2a	YN5-1c-7-1f	NiPAm	46 : 1 : 0.1	0.040	0.30	0.18	50	11

[a)] AIBN instead of V-40 was used as initiator, [b)] more benzene (1.0-2.4 mL) was added, when stirring bar stopped moving usually after 3 h

Typical polymerization for block copolymers with Cl-CTA2b

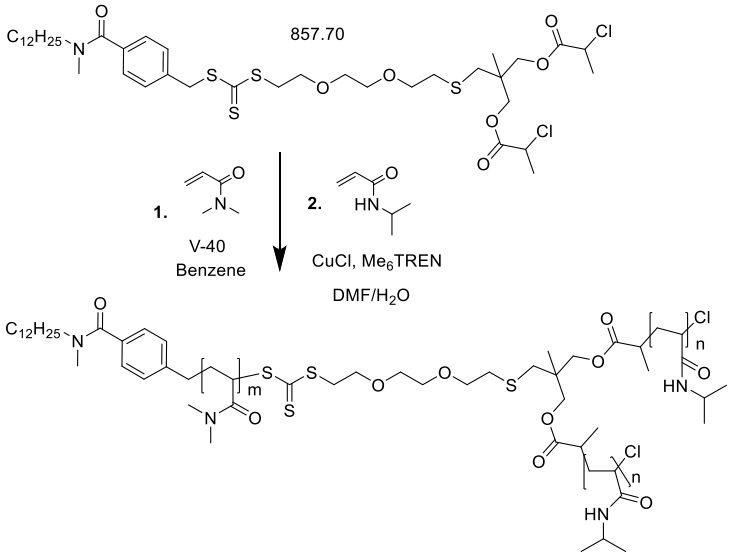

The first block was synthesized as follows: DMAm (2.55 mL, 2.46 g, 24.8 mmol, 200 eq.), 2 mg·mL^{-1} stock solution of V-40 (1.50 mL, 3.01 mg, 0.0123 mmol 0.1 eq.) and **Cl-CTA2b** (106.00 mg, 0.124 mmol) were dissolved in benzene (1.39 mL). The solution was purged with argon for 25 min and immersed into a preheated oil bath with a temperature of 90 °C. After stirring for 3 h, the reaction was stopped by opening the flask to the air and adding acetone. The polymer was isolated by two subsequent precipitations into diethylether. The polymer was dried in vacuum oven, dissolved in distilled water and lyophilized. Yield: 1.25 g, 49 %

Second block is similar to a reported procedure:[250] MacroCTA PDMAm (0.41 g, 0.02 mmol) and NiPAm (0.20 g, 1.8 mmol, 90 eq.) were dissolved in DMF (1.770 mL) and the solution was purged with argon for 10 min. CuCl (7.90 mg, 0.08 mmol, 4.0 eq.) and Me_6TREN (21.4 µL, 18.4 mg, 0.08 mmol, 4.0 eq.) in water were purged with argon for 5 min and then added to the DMF solution

via a deoxygenated syringe. Note, that solid Cu was formed, which remain partly in the syringe. After stirring for 6 h, the reaction was stopped by opening the flask to the air and adding THF. The solution was passed over basic AlO_x and the organic solvent was removed by reduced pressure. Water was added to the residue and the polymer was purified by dialysis. After that, the polymer was lyophilized. Yield: 0.39 g, 64 %

Table 10.8: Reaction conditions for ATRP of different monomers using **TT1** as the initiator, Cu(I)Cl as the catalyst and Me_6TREN as the ligand in DMF/H_2O (2/1, v/v) at 25 °C.

Code	Iniatior	monomer	molar ratio monomer : initiator : Cu(I)Cl : Me_6TREN	$m_{monomer}$ g	$m_{initiator}$ g	m_{CuCl} mg	$m_{Me6TREN}$ mg	t h
TT1-2a	TT1	NiPAm	90 : 1 : 4 : 4	0.20	0.41	7.9	18.4	6
TT1-2b	TT1	NiPAm	90 : 1 : 4 : 4	0.10	0.20	4.3	9.2	4
TT1-2c	TT1	NiPAm	181 : 1 : 4.6 : 4.1	0.20	0.20	4.4	9.2	4
TT1-3a	TT1	DEAm	92 : 1 : 4 : 4	0.11	0.20	4.1	9.2	5
TT1-3b	TT1	DEAm	88 : 1 : 4 : 4	0.11	0.21	4.0	9.2	6
TT1-4a	TT1	NPAm	92 : 1 : 4 : 4	0.10	0.20	4.1	9.2	6.5

Test ATRP with PDMAm as „disturber"

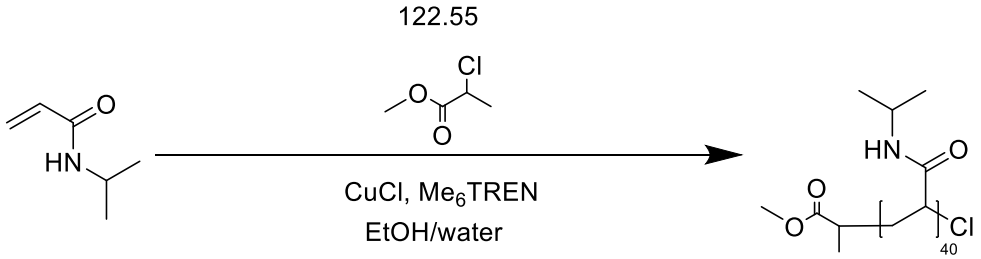

NiPAm (0.41 g, 3.62 mmol, 45 eq.), PDMAm (0.76 g, 0.08 mmol, 0.5 eq.) and methyl 2-chloropropionate (9.1 µL, 9.8 µg, 0.08 µmol) were dissolved in a mixture of EtOH:water (v/v) 3:1 (1.278 mL) and purged with argon for 5 min. CuCl (8.15 mg, 0.08 mmol, 1.0 eq.) was weighed to a mixture of EtOH:water (v/v) 3:1 (0.213 mL) in a separate flask. Me_6TREN (21.4 µL, 18.4 mg, 0.08 mmol, 1.0 eq.) was added to the catalyst and the mixture was purged with argon for

5 min. Then, the monomer/initiator solution was added to the catalyst and the reaction was stirred at room temperature for 1:40 h. Conversion: 48 %. Yield was not determined

Aminolysis of TT1-2c similar to a reported procedure[242]

TT1-2c (0.05 g, 1.8 µmol) was dissolved in a solution of ethylendiamine (0.12 mL, 0.11 g, 1.79 µmol, 1000 eq.) und triethylamine (4.0 µL/4 mL stock solution in THF, 1.00 mL, 0.73 µg, 7.27 µmol, 4 eq.) in THF (7 mL) and stirred for 4 days at room temperature. Solution was then analysed by SEC.

Hydrolysis of TT1-2c similar to a reported procedure[242]

TT1-2c (12.7 mg, 0.46 µmol) was dissolved in water (1.5 mL). A 1 M solution of sodium hydroxide (0.12 mL, 0.11 g, 1.79 µmol, 1000 eq.) was added and the solution was stirred for 4 days. Then, the solution was neutralized with aqueous HCl and lyophilized. The obtained product was directly analysized by SEC.

11 APPENDIX

11.1 FTIR-SPECTRA

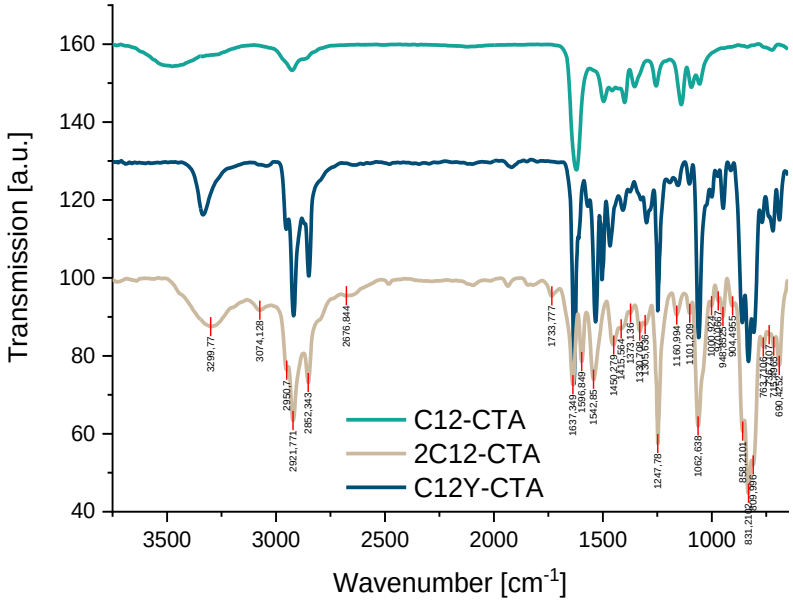

Figure 11.1: FTIR-spectra of **C12-CTA**, **2C12-CTA** and **C12Y-CTA**.

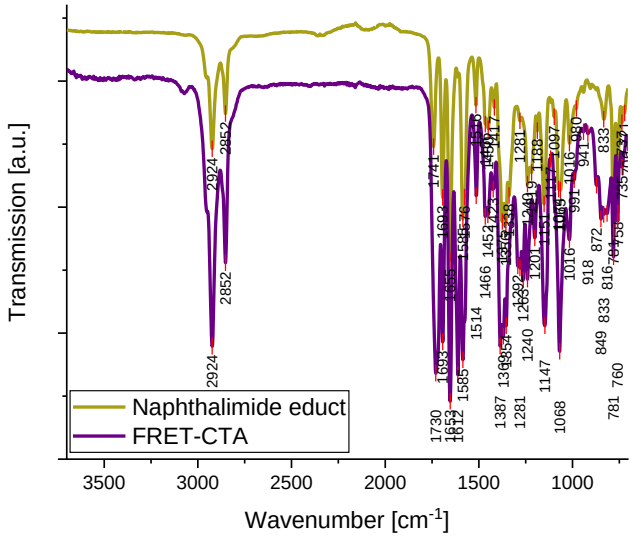

Figure 11.2: FTIR-spectrum of **FRET-CTA** and its naphthalimide educt.

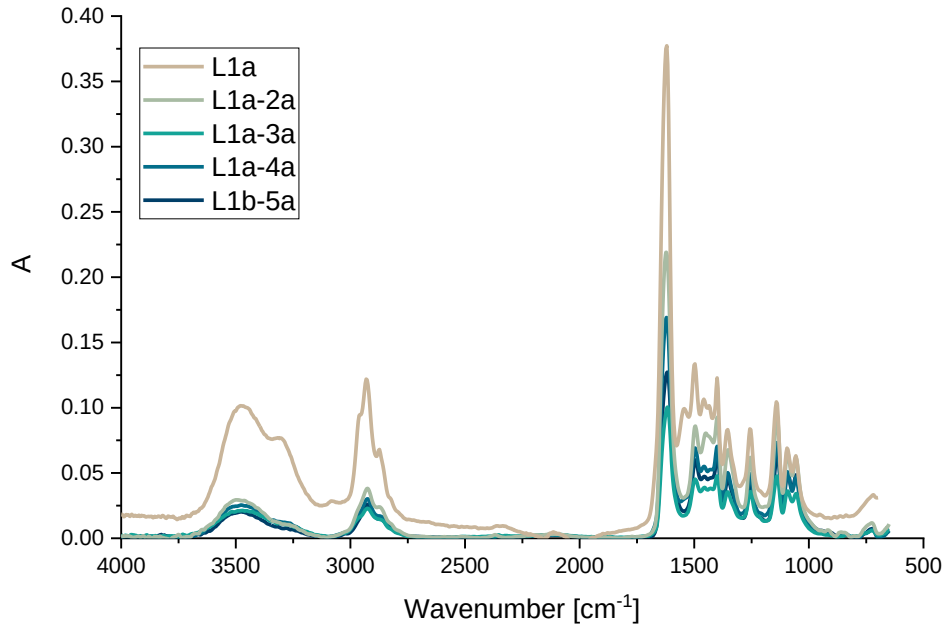

Figure 11.3: FTIR-spectra for homo-and block copolymers **L1a**, **L1a-2a**, **L1a-3a**, **L1a-4a**, and **L1b-5a**.

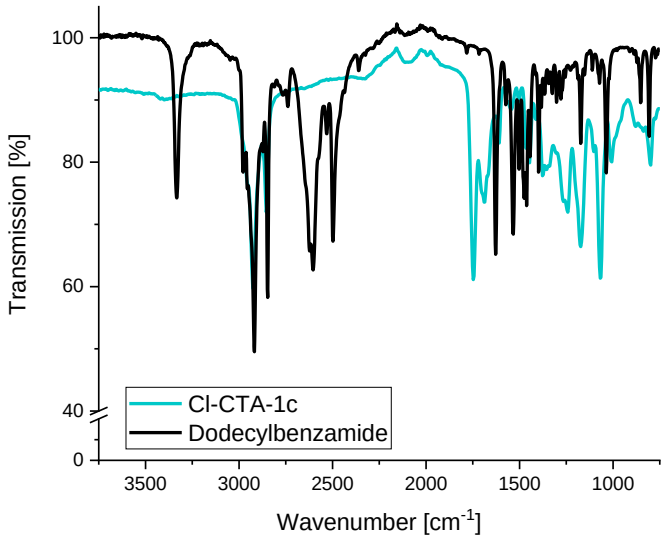

Figure 11.4: FTIR spectra of **Cl-CTA-1c** and its educt ***N*-dodecylbenzamide**.

11.2 DLS MEASUREMENTS

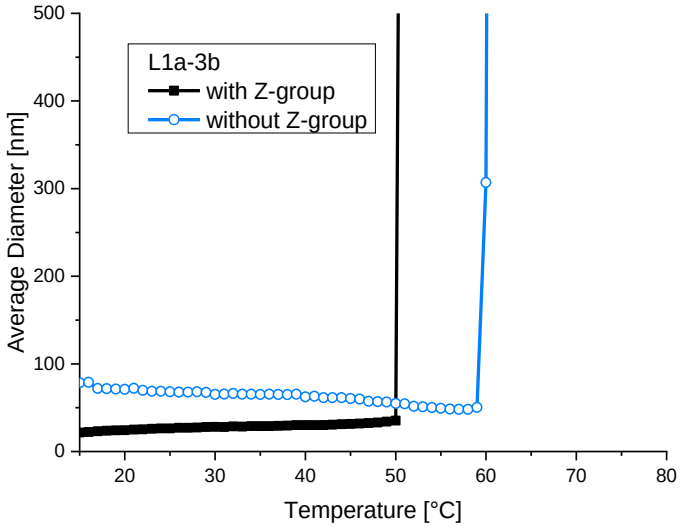

Figure 11.5: DLS measurement of 5 g·L^{-1} aqueous solution of **L1a-3b** with (full black squares) and without (empty blue circles) Z-group.

11.3 Turbidimetry Measurements

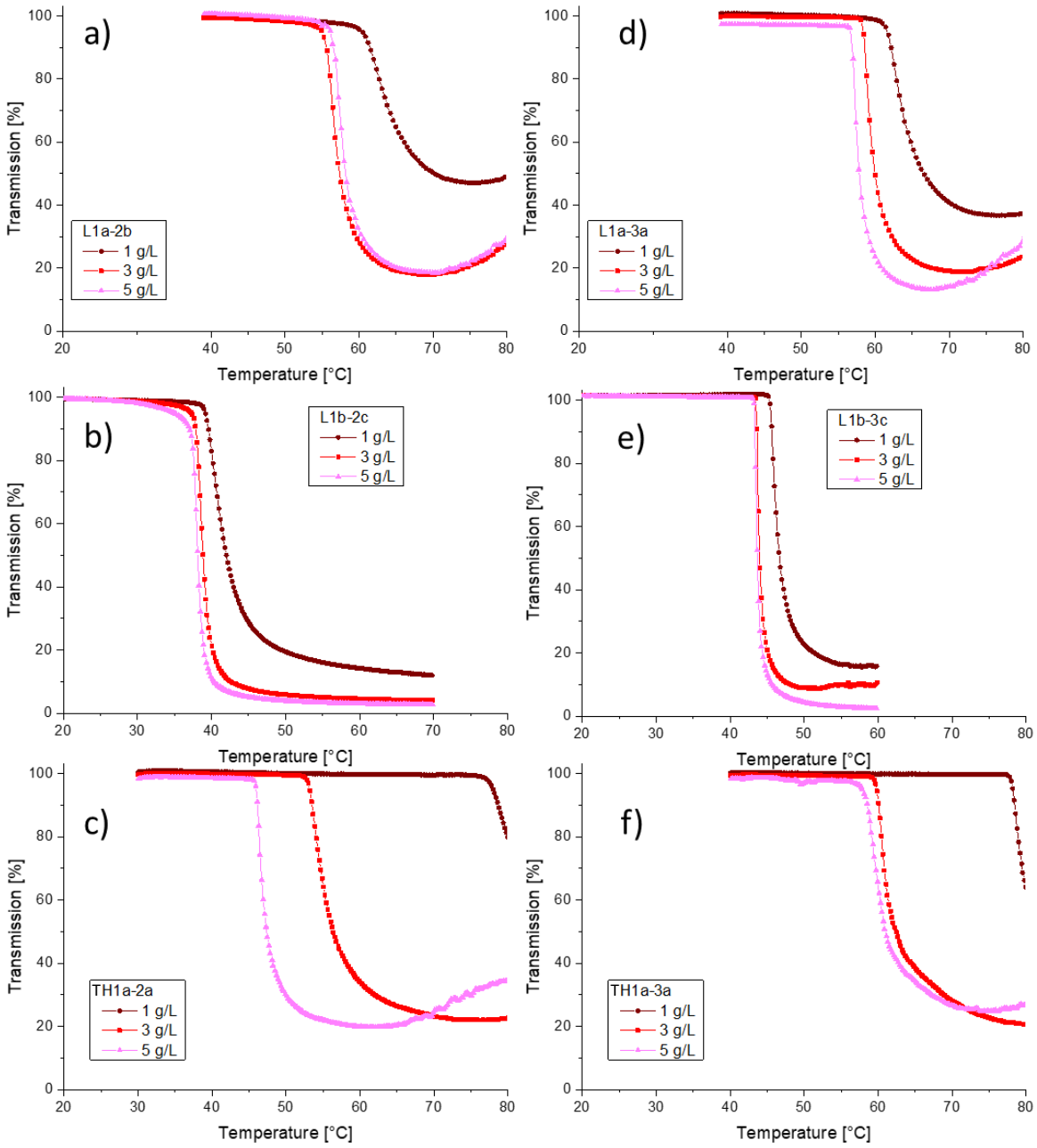

Figure 11.6: Temperature-dependent turbidimetry measurements for different concentrations for linear and twinned hydrophobic PDMAm-b-PNiPAm (left coloumn a-c) and PDMAm-b-PDEAm (right coloumn d-f).

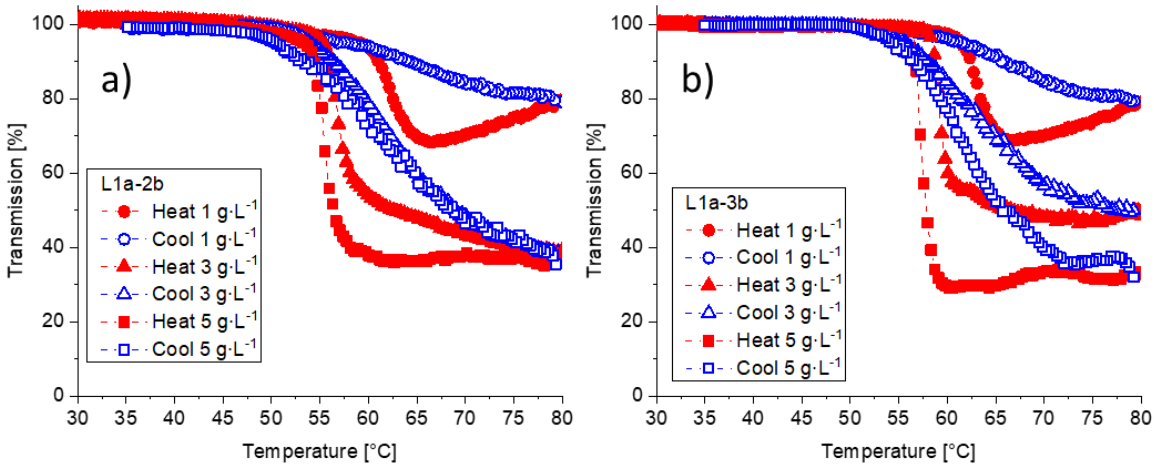

Figure 11.7: Temperature-dependent turbidimetry measurements with stirring for different concentrations for sample (a) **L1a-2b** and (b) **L1a-3b**, heating cycles are shown by full symbols, cooling cycles by open symbols.

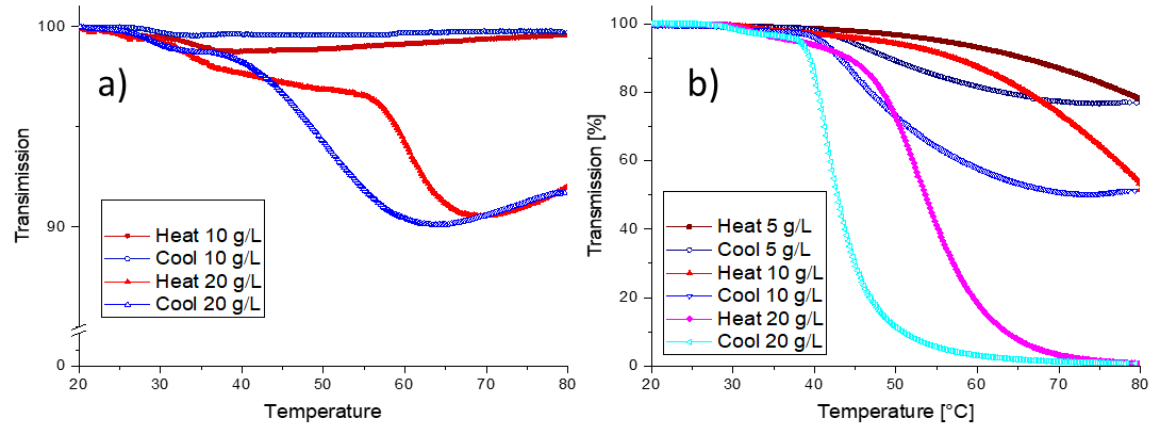

Figure 11.8: Temperature-dependent turbidimetry measurements for different concentrations for linear (a) **L1b-5a** and twinned hydrophobic **TH1a-5** (b) PDMAm-b-PNPAm, heating cycles are shown by full symbols, cooling cycles by open symbols.

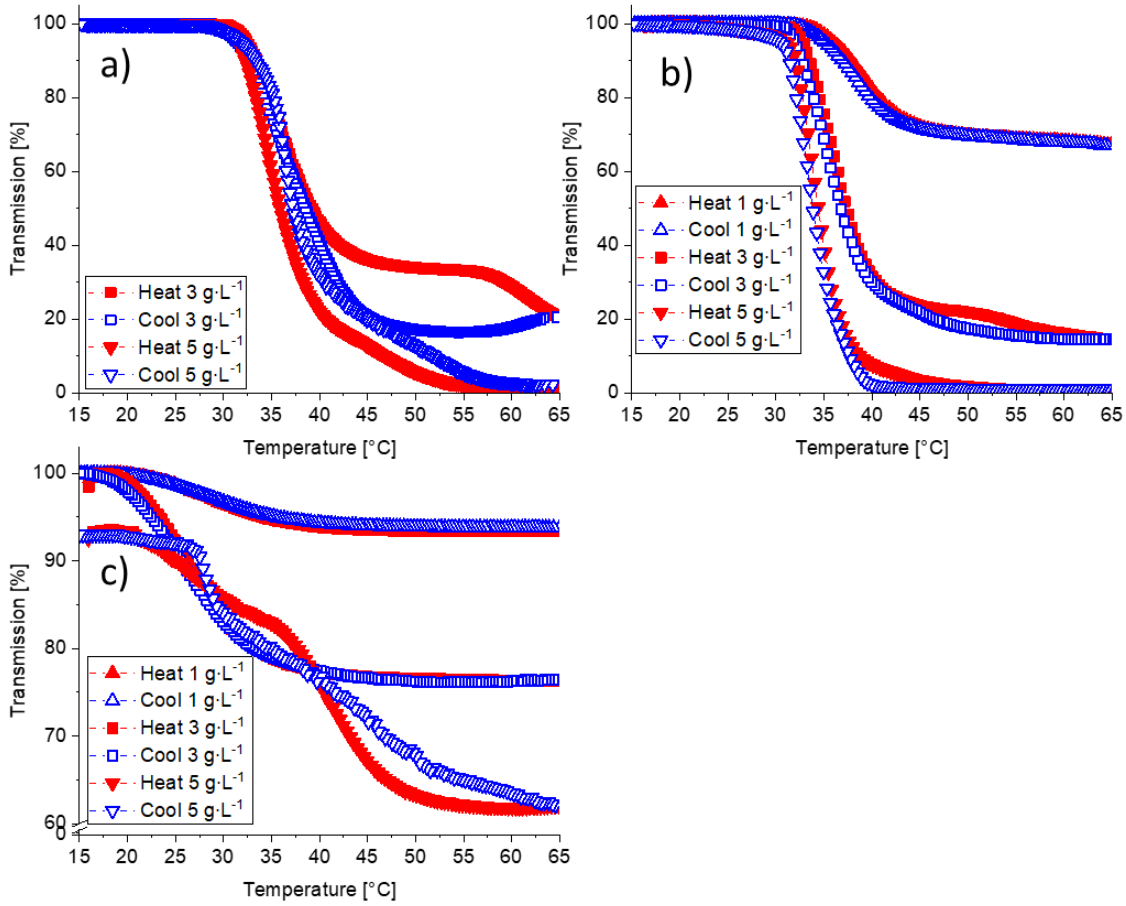

Figure 11.9: Temperature-dependent turbidimetry measurements for different concentrations for block copolymers with twinned thermoresponsive architecture a) **TT1-2a**, b) **TT1-3a** and c) **TT1-5**.

11.4 UV-VIS MEASUREMENTS

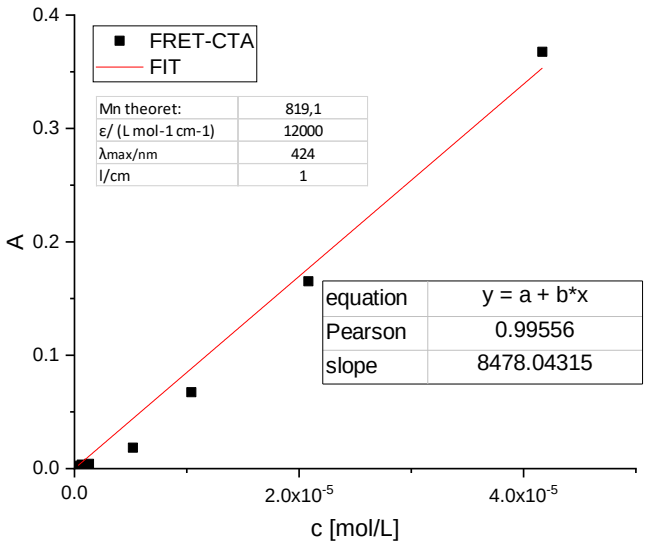

Figure 11.10: UV-vis measurement of FRET-CTA for determination of the extinction coefficient ε in dichloromethane at a maximum wavelength λ_{max} = 424 nm.

11.5 NMR-SPECTRA

Monomers and CTA compounds

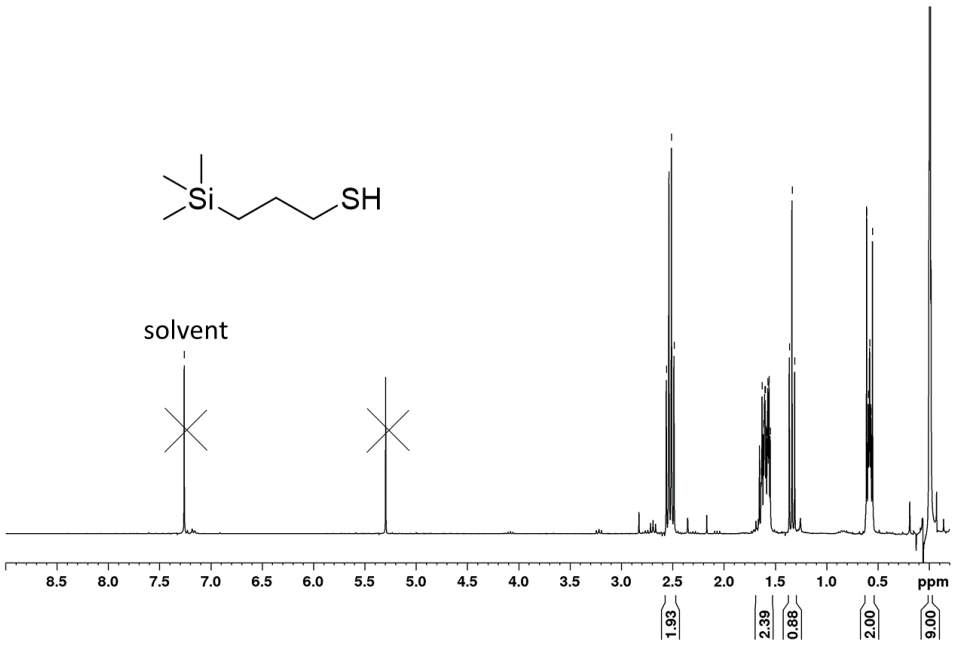

Figure 11.11: ^{1}H NMR spectrum of **3-(trimethylsilyl)propane-1-thiol** in $CDCl_3$.

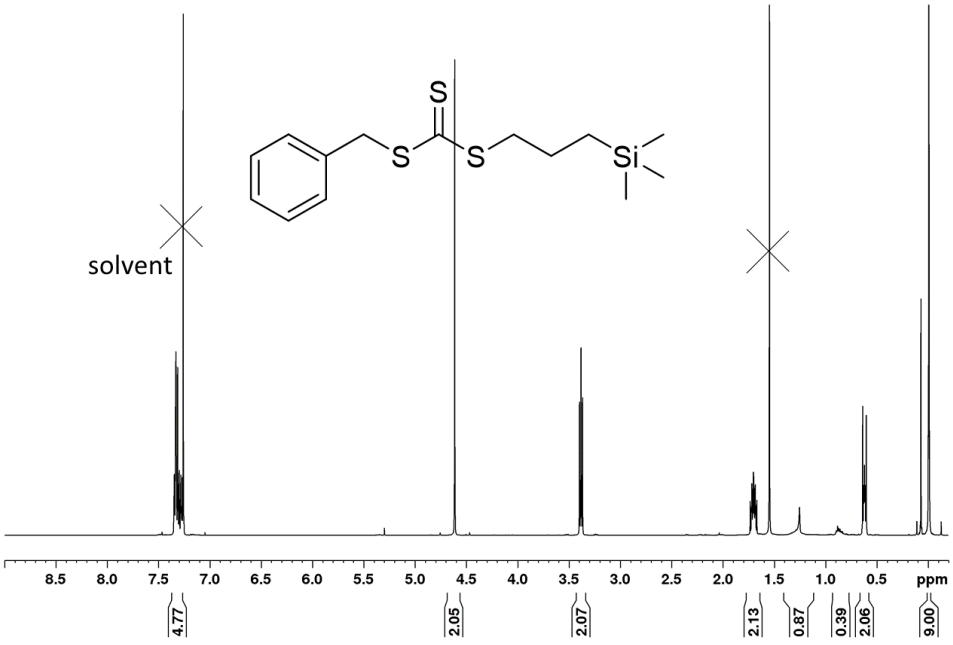

Figure 11.12: ^{1}H NMR spectrum of **BTPT** in $CDCl_3$.

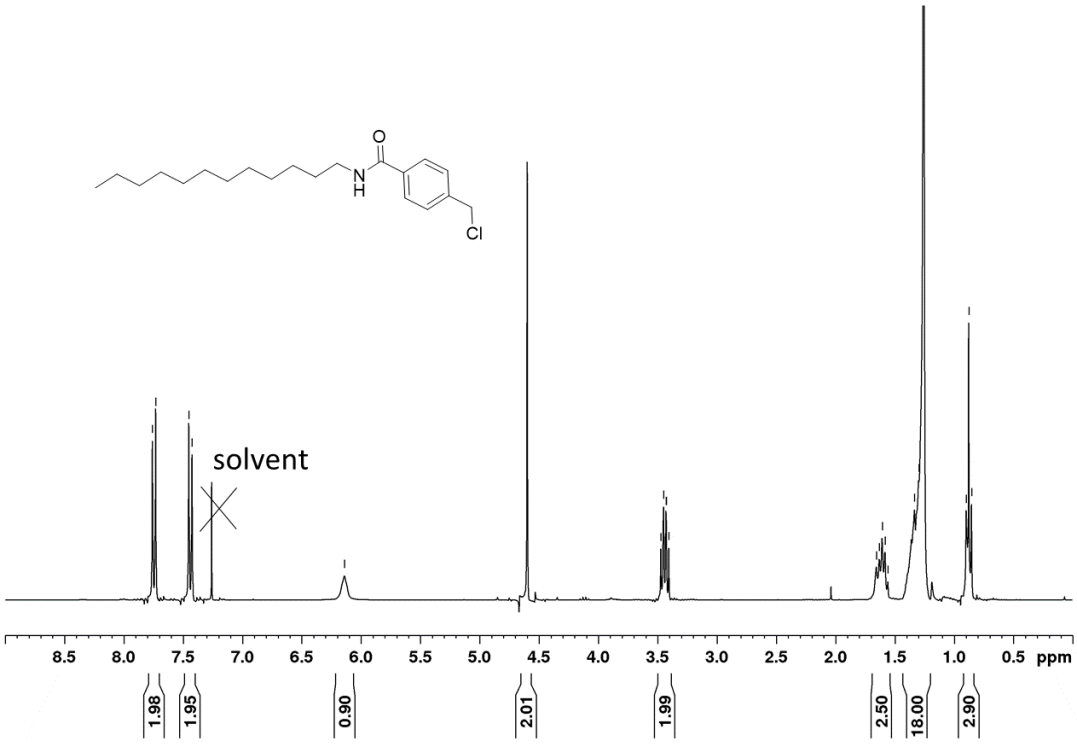

Figure 11.13: ^{1}H NMR spectrum of **4-chloromethyl-*N*-dodecylbenzamide** in $CDCl_3$.

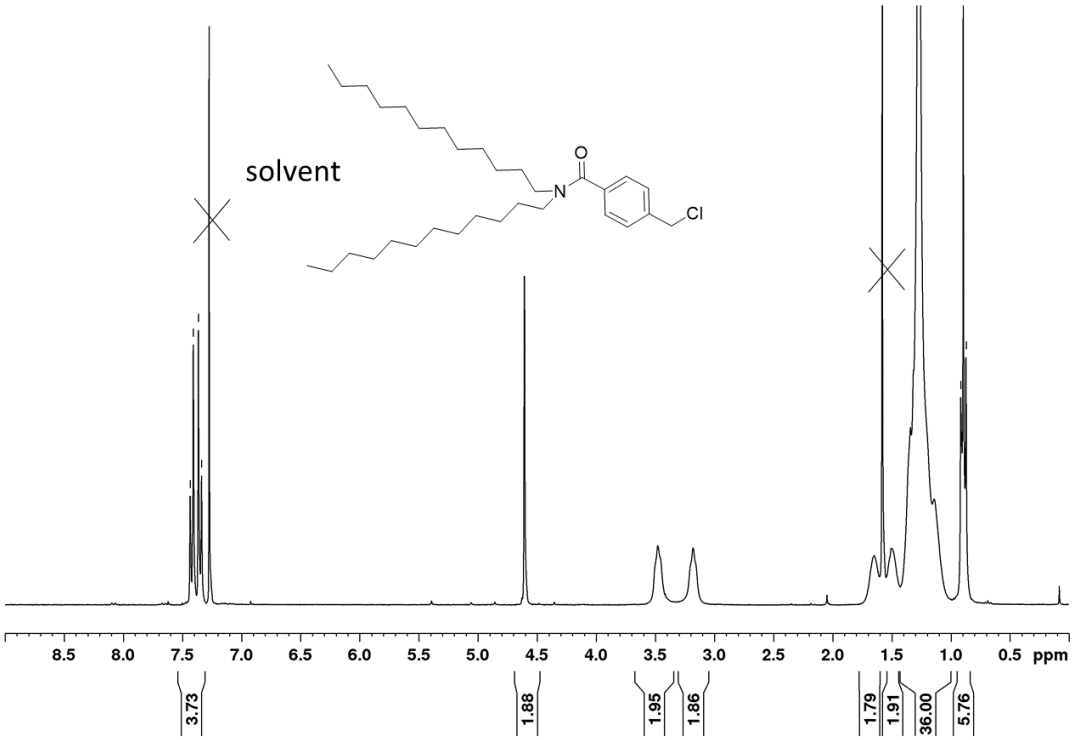

Figure 11.14: ^{1}H NMR spectrum of **4-chloromethyl-*N,N*-didodecylbenzamide** in $CDCl_3$.

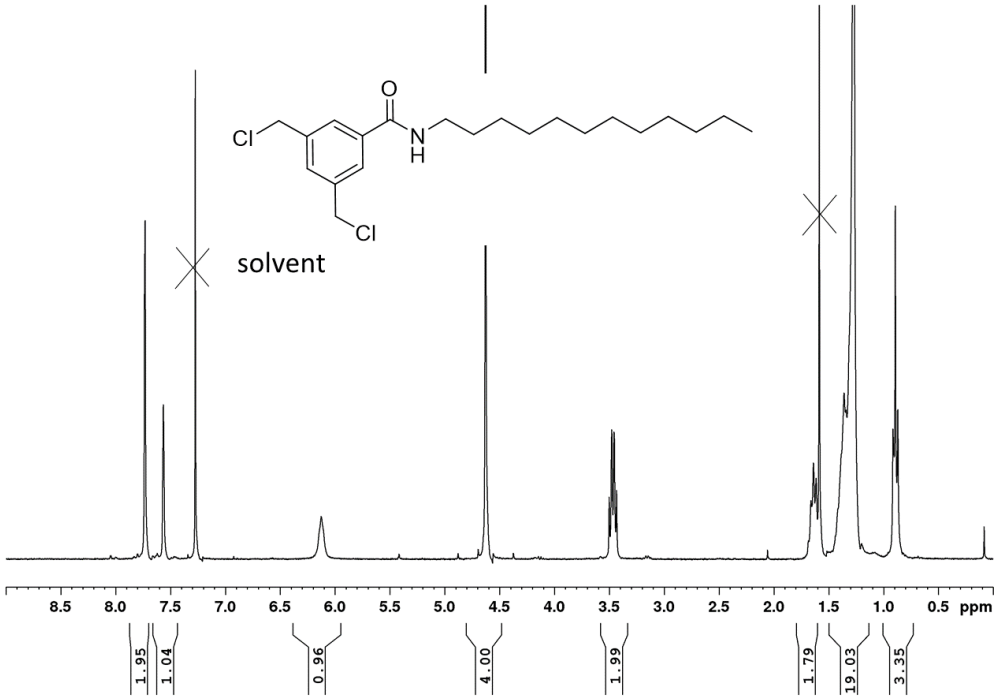

Figure 11.15: ^{1}H NMR spectrum of **3,5-bis(chloromethyl)-*N*-dodecylbenzamide** in $CDCl_3$.

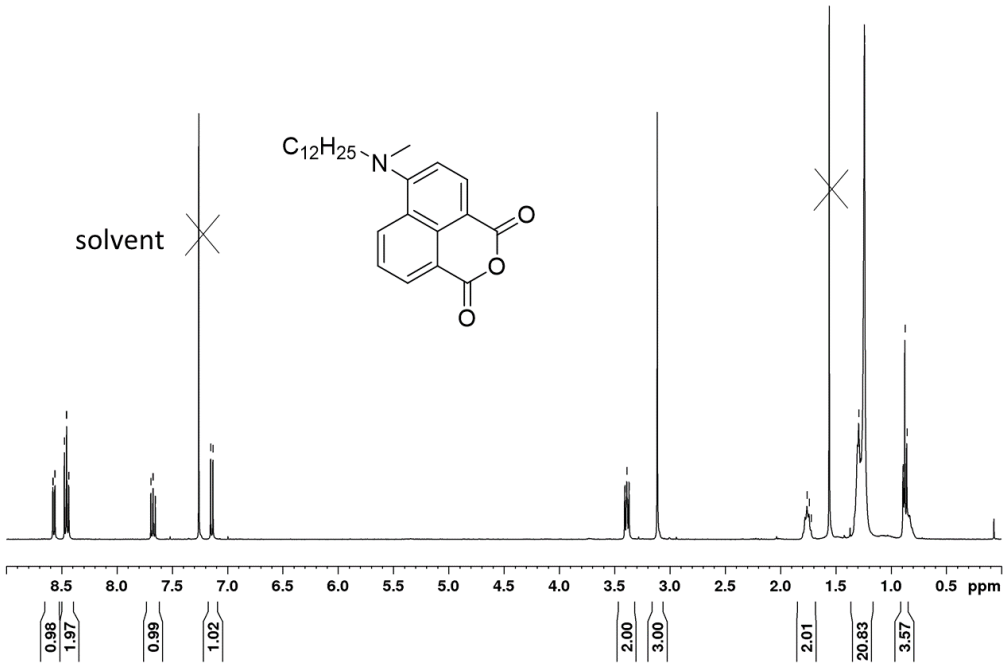

Figure 11.16: ^{1}H NMR spectrum of **4-(dodecyl(methyl)amino)-1,8-naphthalic anhydride** in $CDCl_3$.

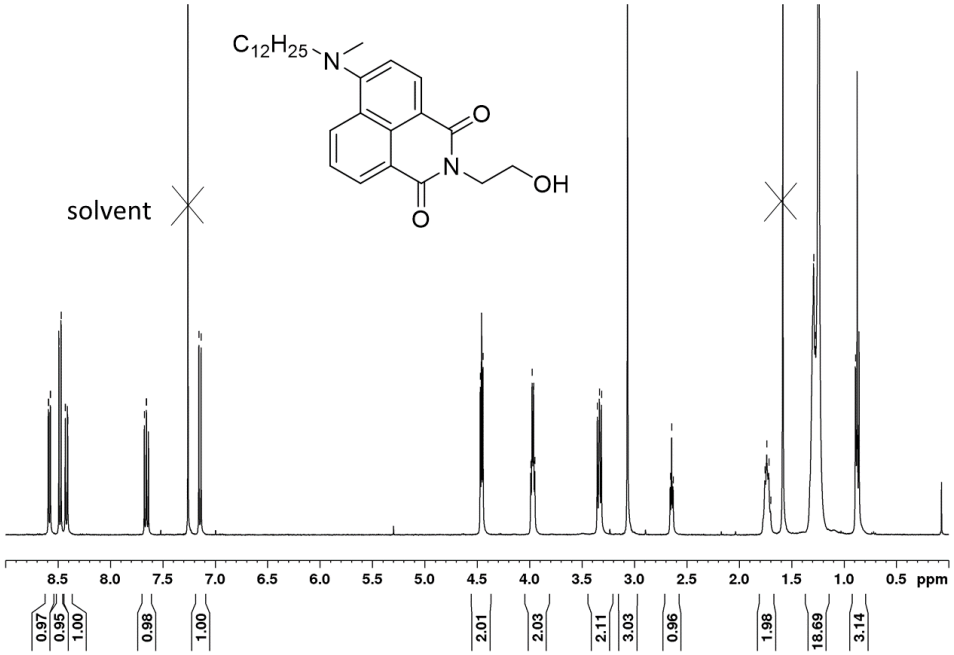

Figure 11.17: ^{1}H NMR spectrum of **4-(dodecyl(methyl)amino)-*N*-2-hydroxyethyl-1,8-naphthalimide** in $CDCl_3$.

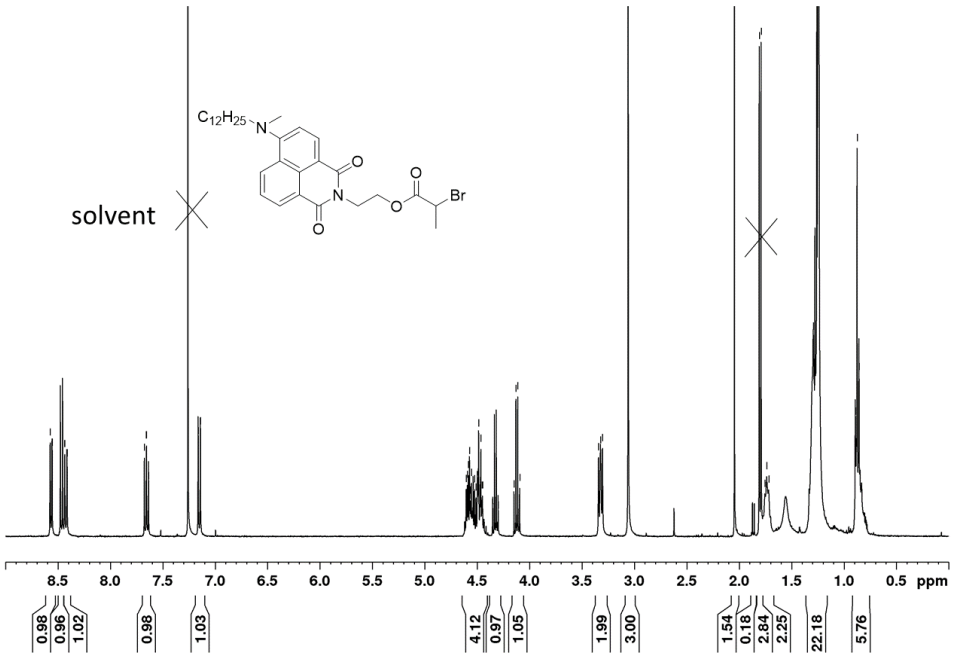

Figure 11.18: ^{1}H NMR spectrum of **(4-(Dodecyl(methyl)amino)-1,3-dioxo-1H-benzo[de]isoquinolin-2(3H)-yl)ethyl 2-bromopropanoate** in $CDCl_3$.

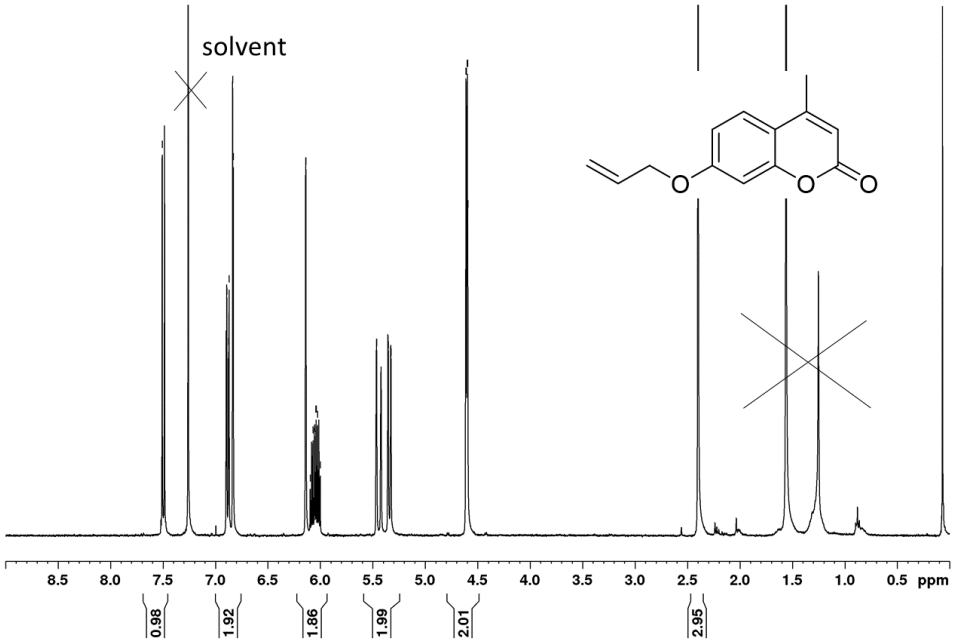

Figure 11.19: ^{1}H NMR spectrum of **7-allyloxy-4-methylcoumarin** in $CDCl_3$.

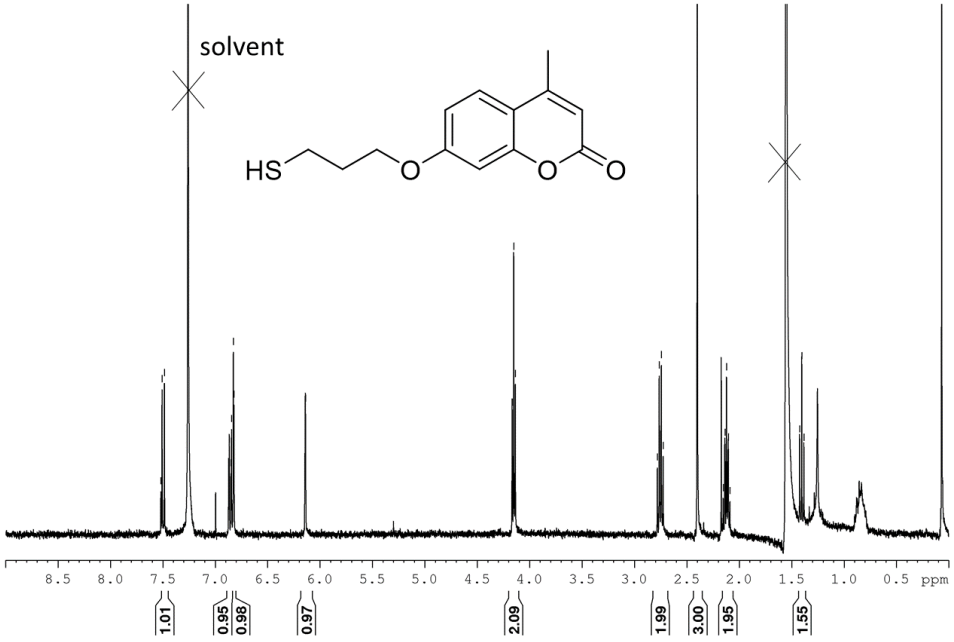

Figure 11.20: ^{1}H NMR spectrum of **7-(3-mercaptopropoxy)-4-methylcoumarin** in $CDCl_3$.

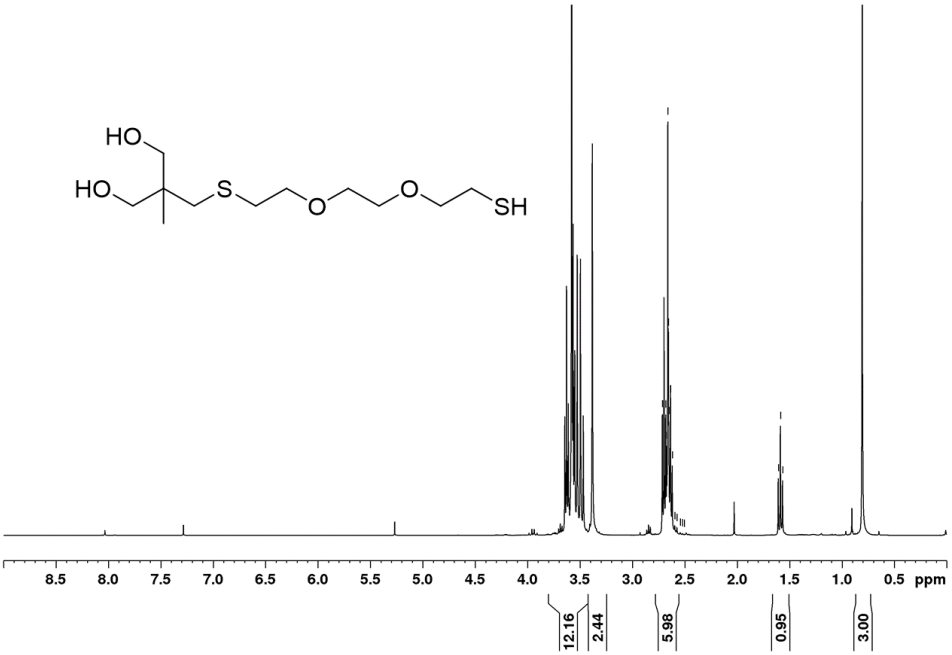

Figure 11.21: ^{1}H NMR spectrum of **2-(((2-(2-(2-mercaptoethoxy)ethoxy)ethyl)thio)methyl)-2-methylpropane-1,3-diol** in $CDCl_3$.

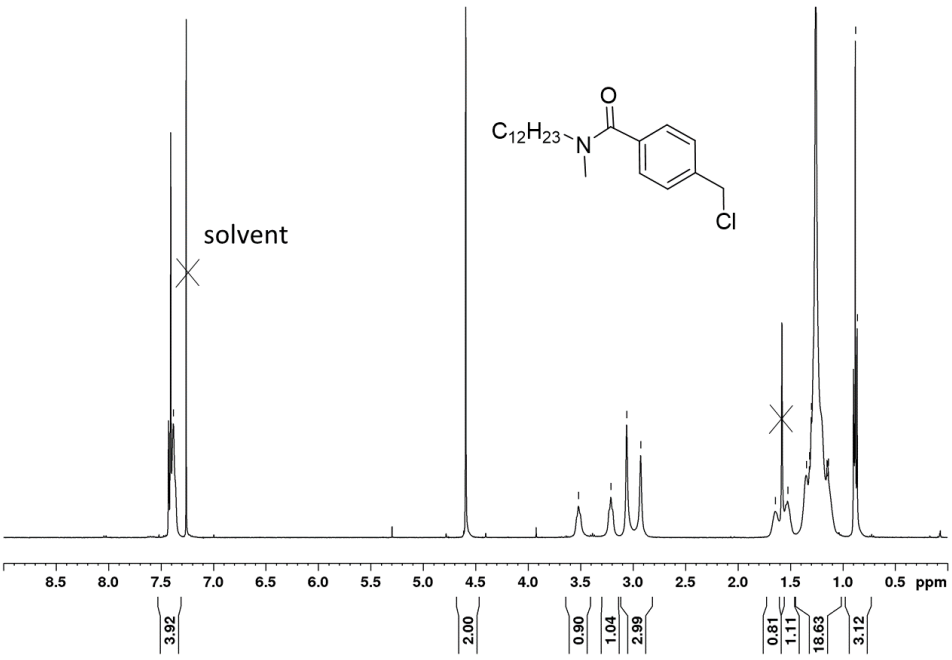

Figure 11.22: : ^{1}H NMR spectrum of **4-chloromethyl-N-dodecyl-N-methylbenzamide** in $CDCl_3$.

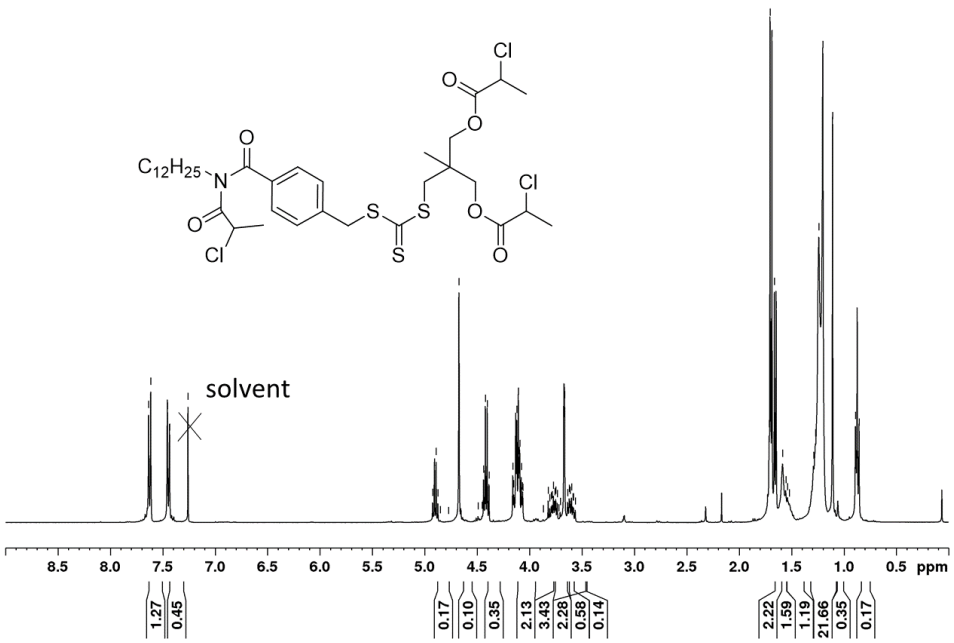

Figure 11.23: ^{1}H NMR spectrum of **A-CTA1c**in $CDCl_3$.

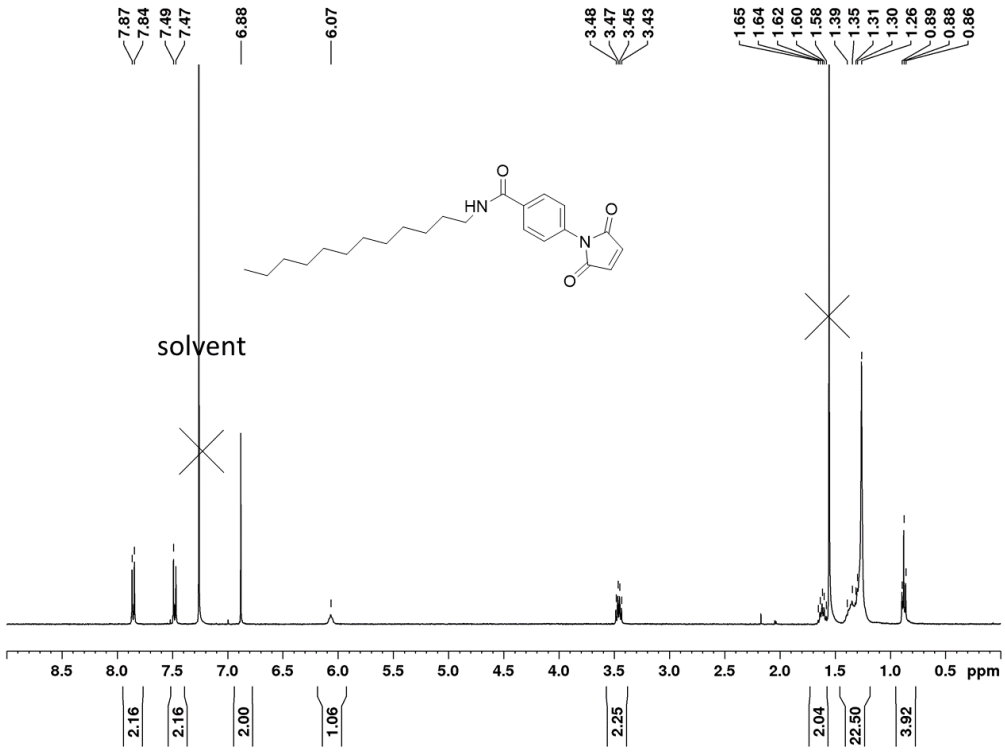

Figure 11.24: ^{1}H NMR spectrum of **DBMI** in $CDCl_3$.

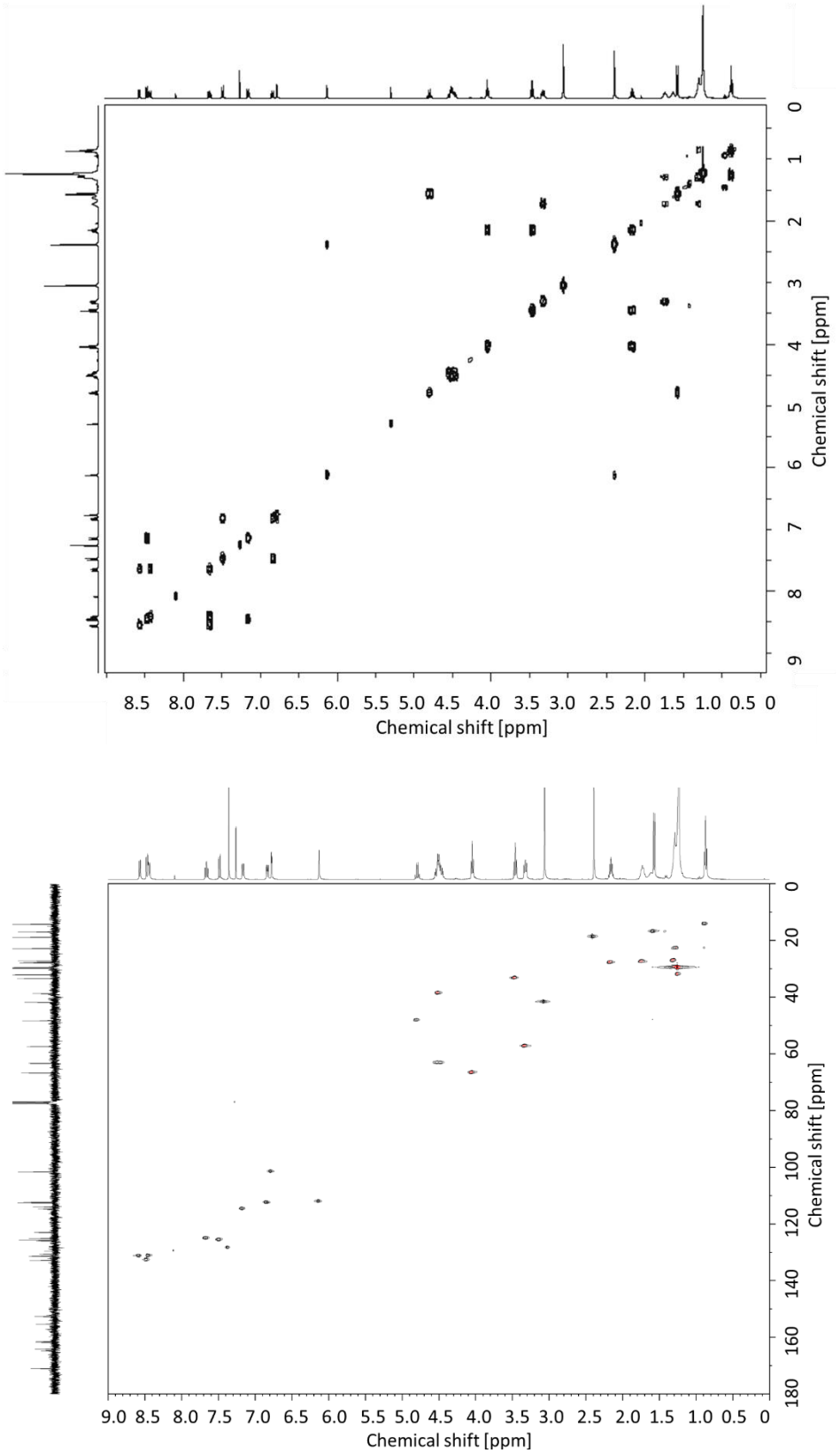

Figure 11.25: ^{1}H-^{1}H-COSY (top) and ^{1}H-^{13}C-HMQC (bottom) NMR spectra of **FRET-CTA** in $CDCl_3$.

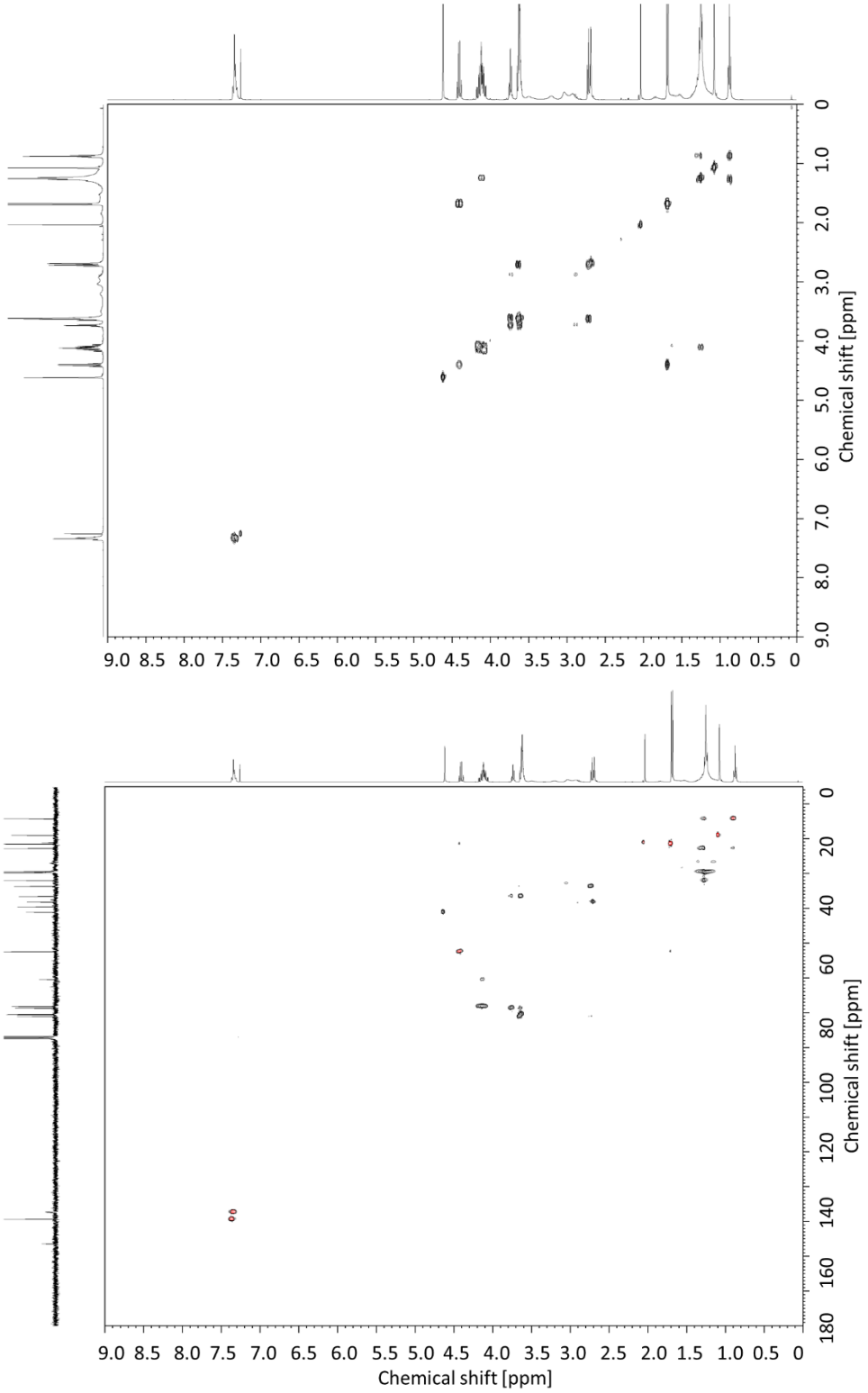

Figure 11.26: ^{1}H-^{1}H-COSY (top) and ^{1}H-^{13}C-HMQC (bottom) NMR spectra of **Cl-CTA2b** in $CDCl_3$.

Polymers

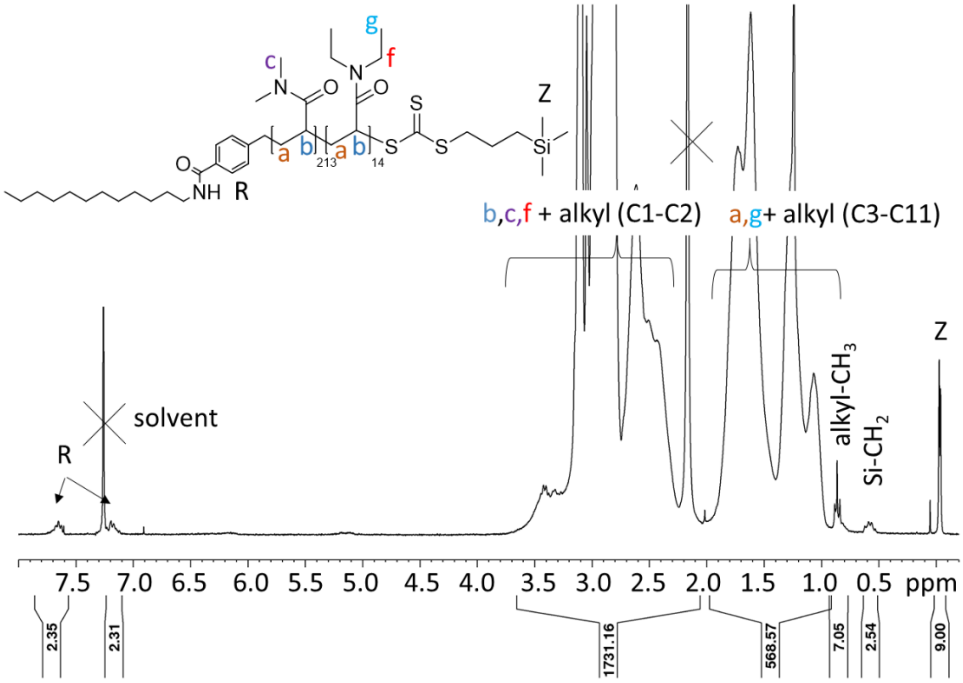

Figure 11.27: ^{1}H-NMR spectrum of **L1a-3a** in $CDCl_3$.

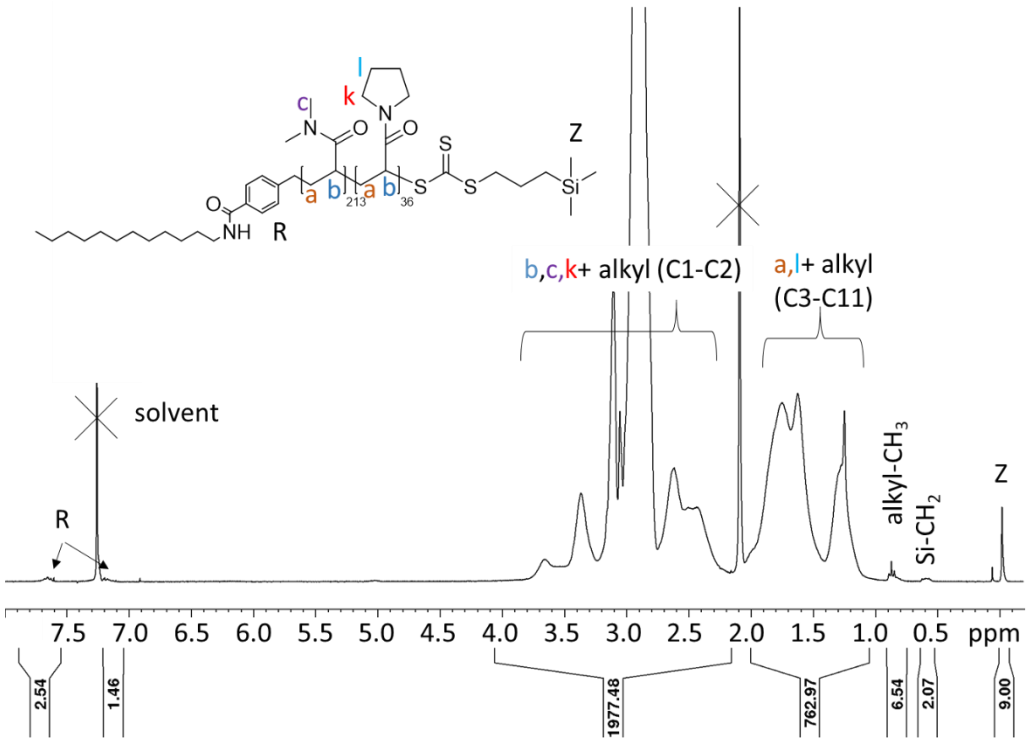

Figure 11.28: ^{1}H-NMR spectrum of **L1a-4b** in $CDCl_3$.

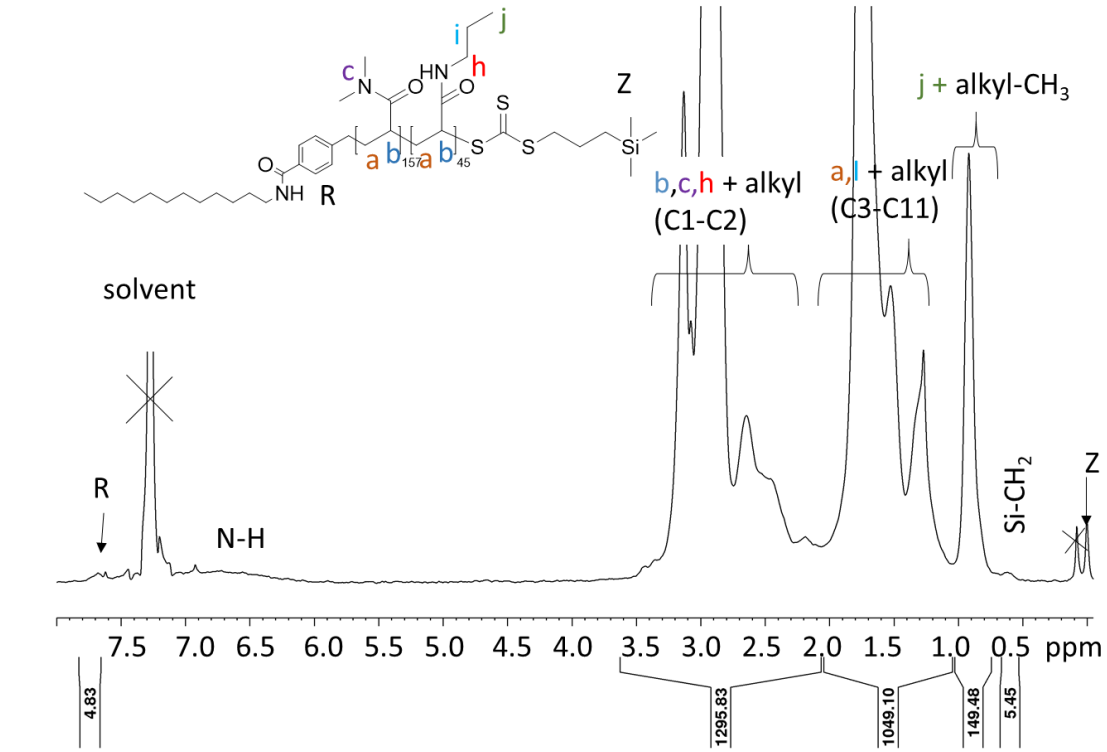

Figure 11.29: ^{1}H-N MR spectrum of **L1a-5a** in $CDCl_3$.

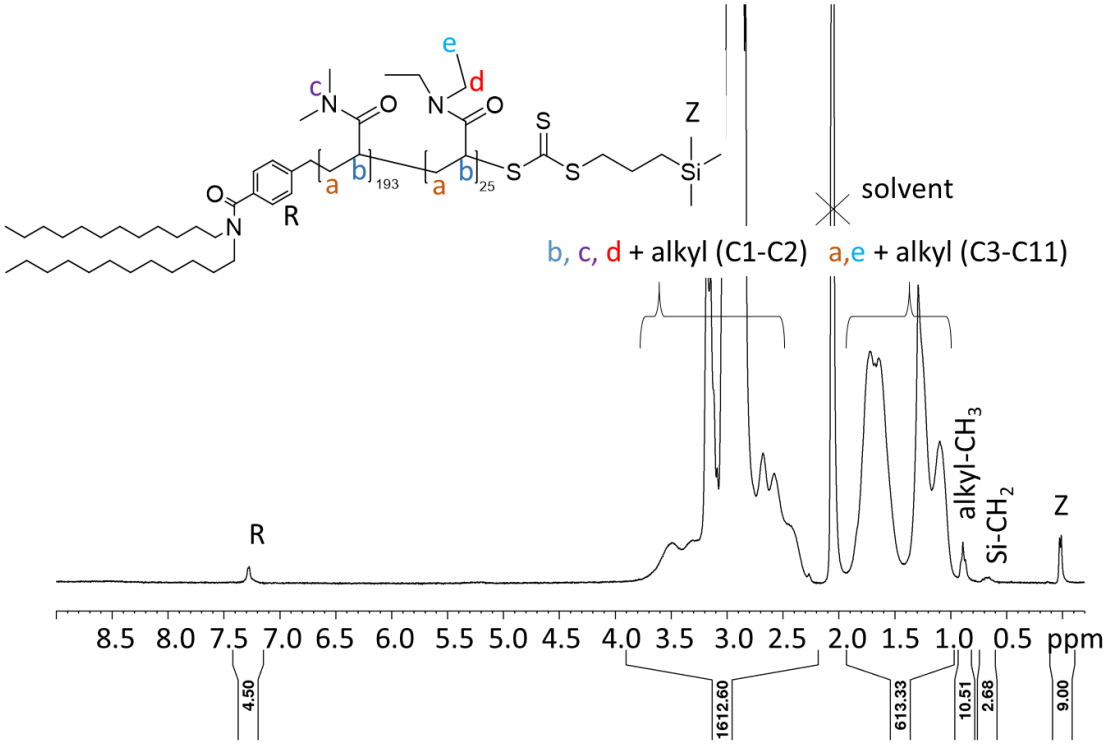

Figure 11.30: ^{1}H-NMR spectrum of **TH1a-3** in D_2O.

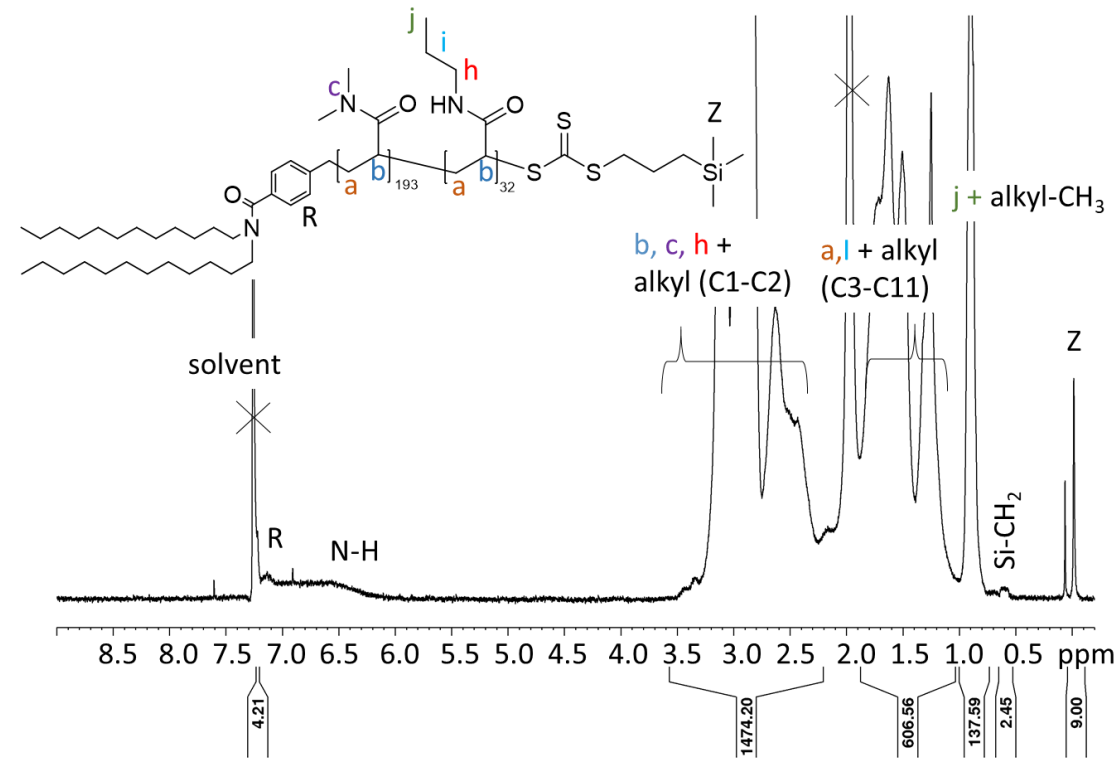

Figure 11.31: ^{1}H-NMR of **TH1a-5** in $CDCl_3$.

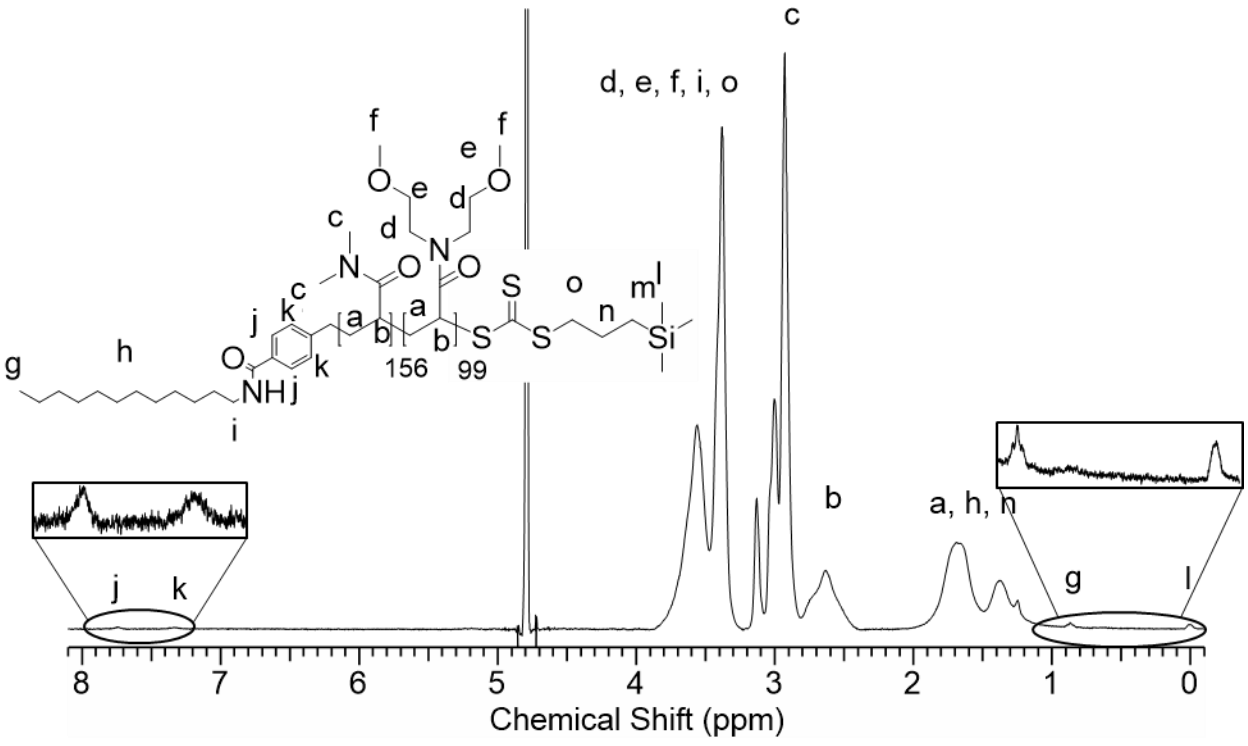

Figure 11.32: ^{1}H-NMR of **L1b-6b** in D_2O

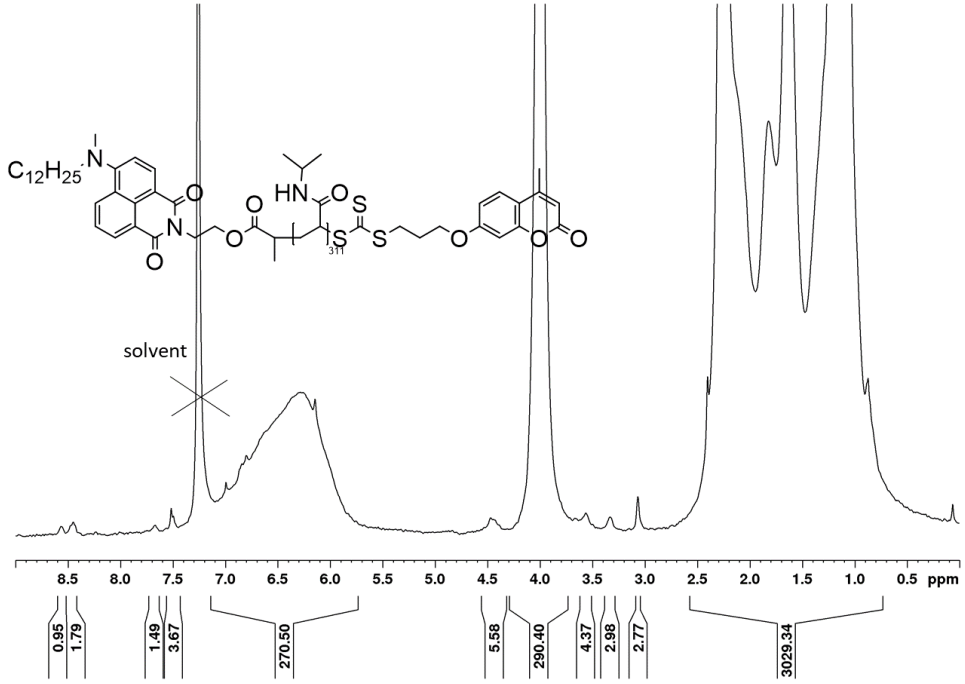

Figure 11.33: ^{1}H NMR spectrum of **F2** in $CDCl_3$.

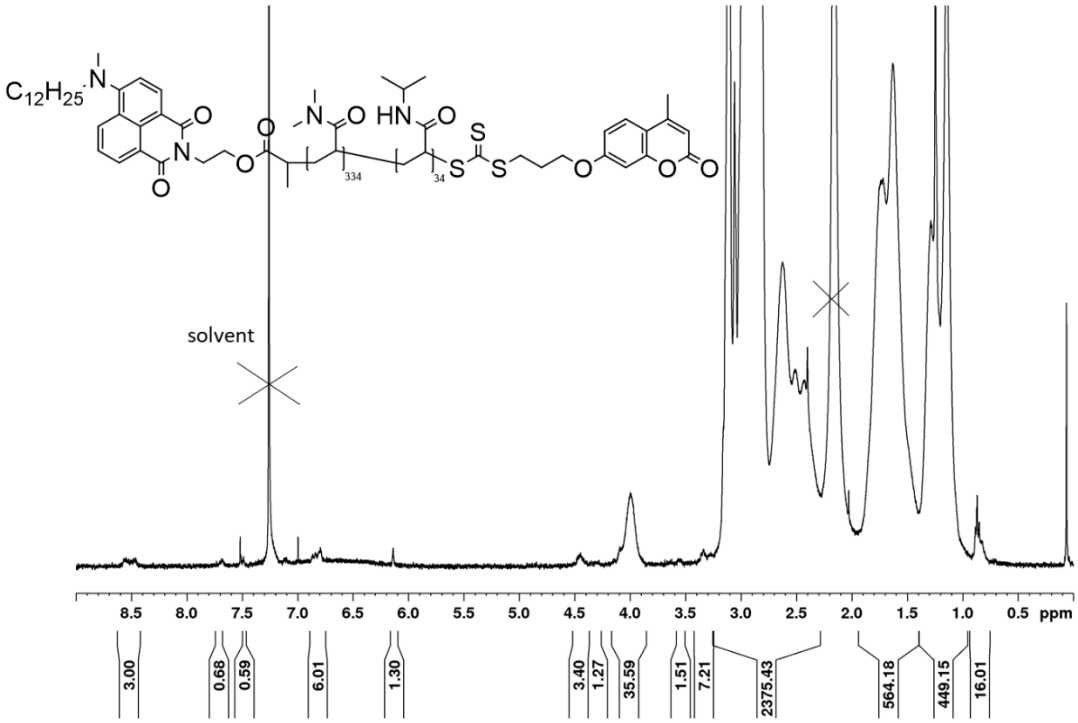

Figure 11.34: ^{1}H NMR spectrum of **F1a-2a** in $CDCl_3$.

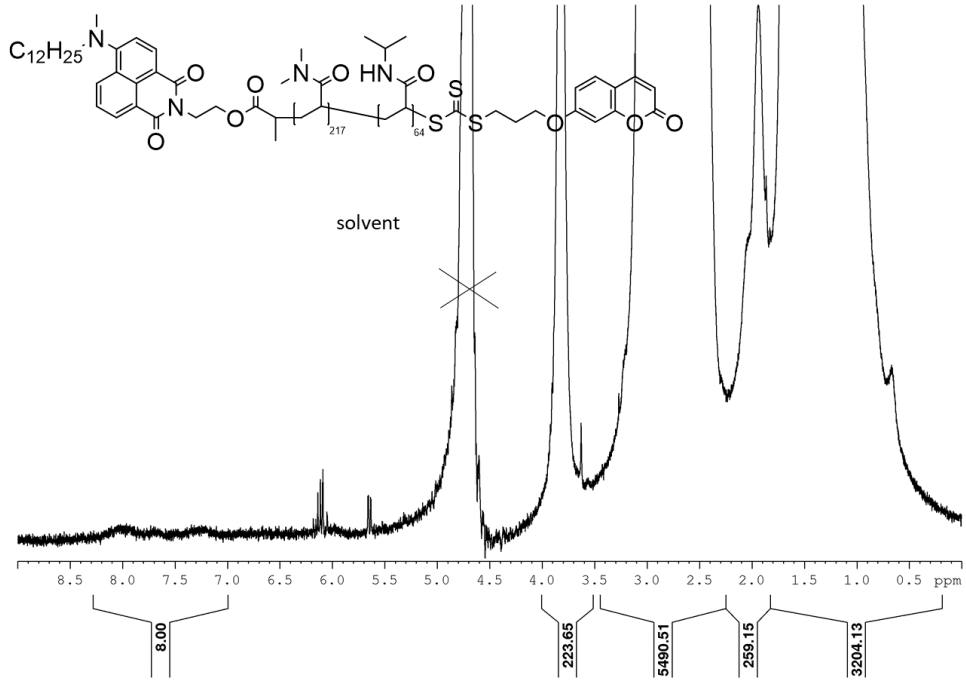

Figure 11.35: ^{1}H NMR spectrum of **F1b-2b** in D_2O.

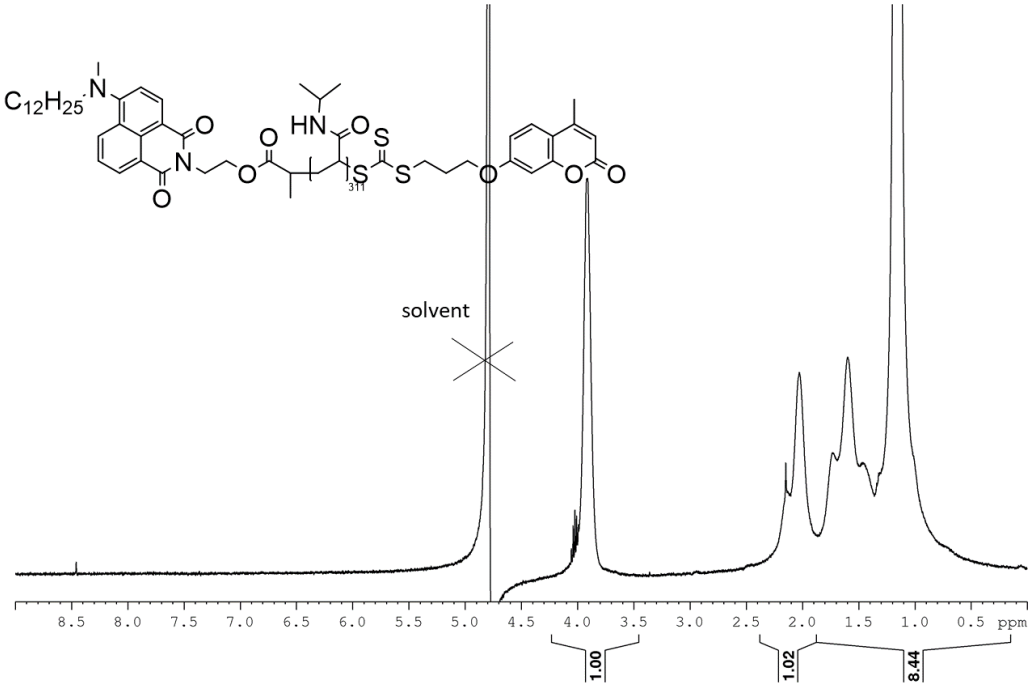

Figure 11.36: ^{1}H NMR spectrum of **F2** in D_2O.

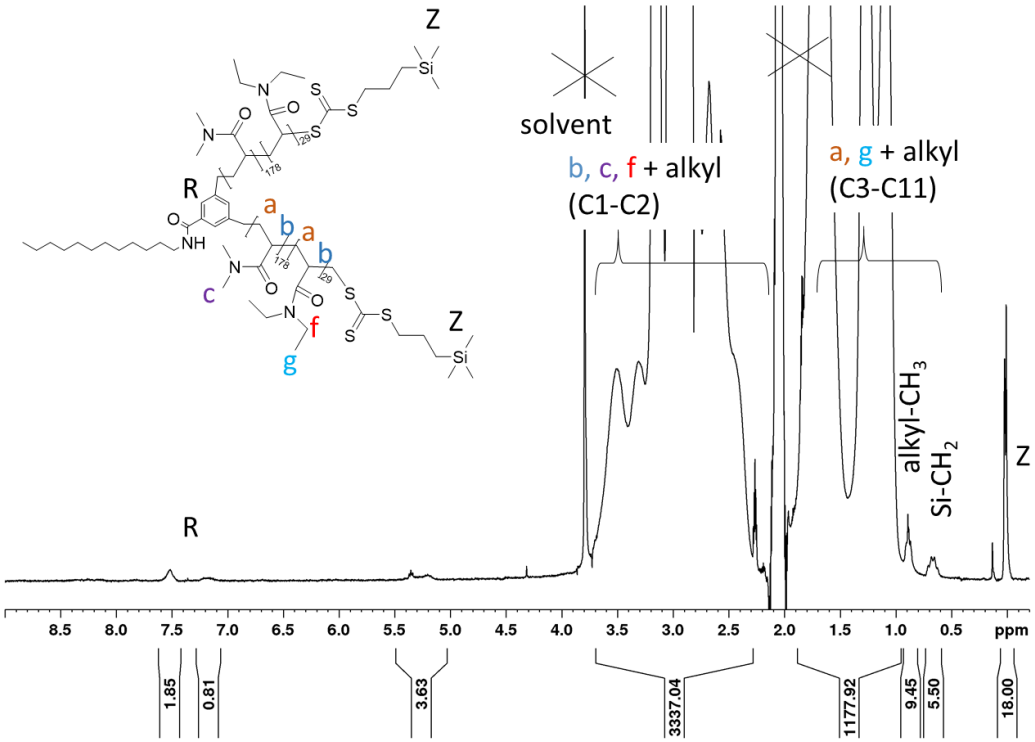

Figure 11.37: ^{1}H NMR spectrum of **YS1-3** in acetone-d_6.

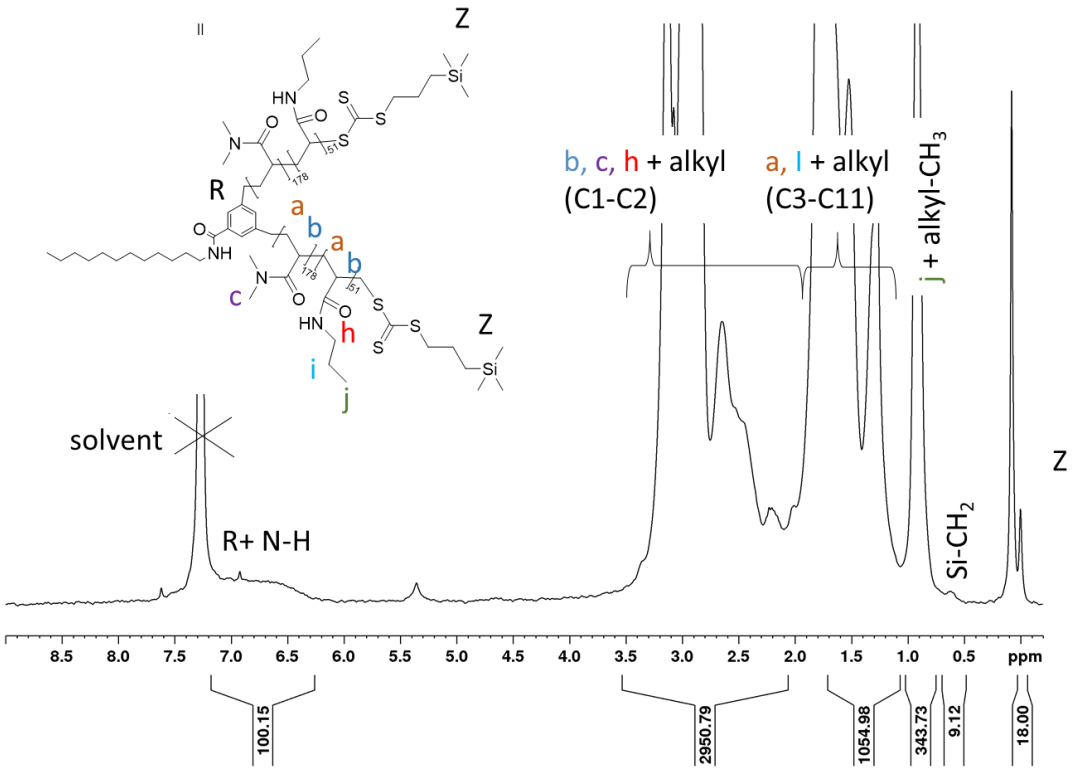

Figure 11.38: ^{1}H NMR spectrum of **YS1-5** in $CDCl_3$.

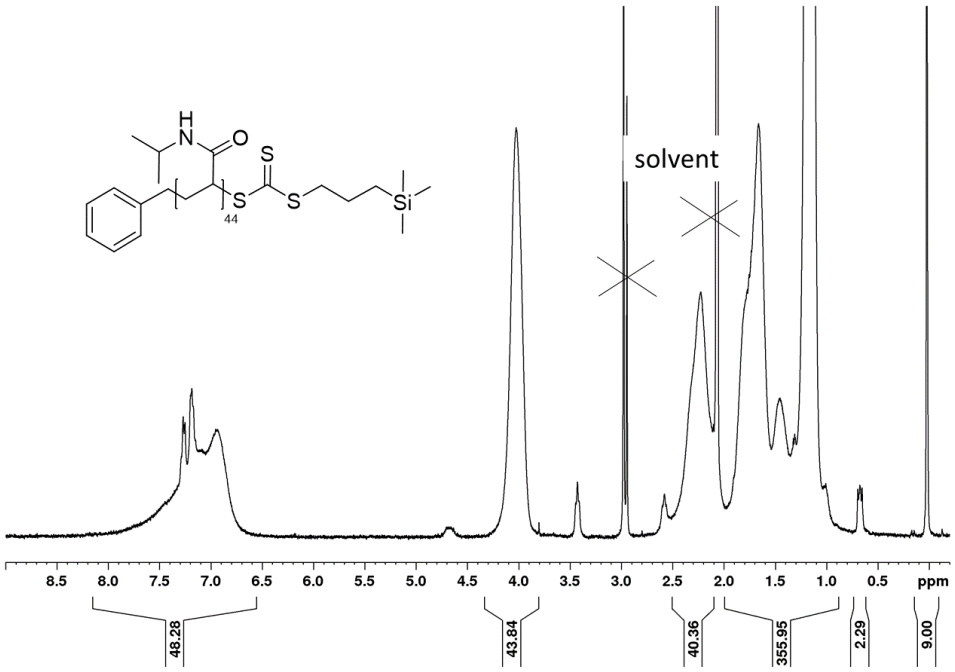

Figure 11.39: ^{1}H-NMR of **YN2** in acetone-d_6.

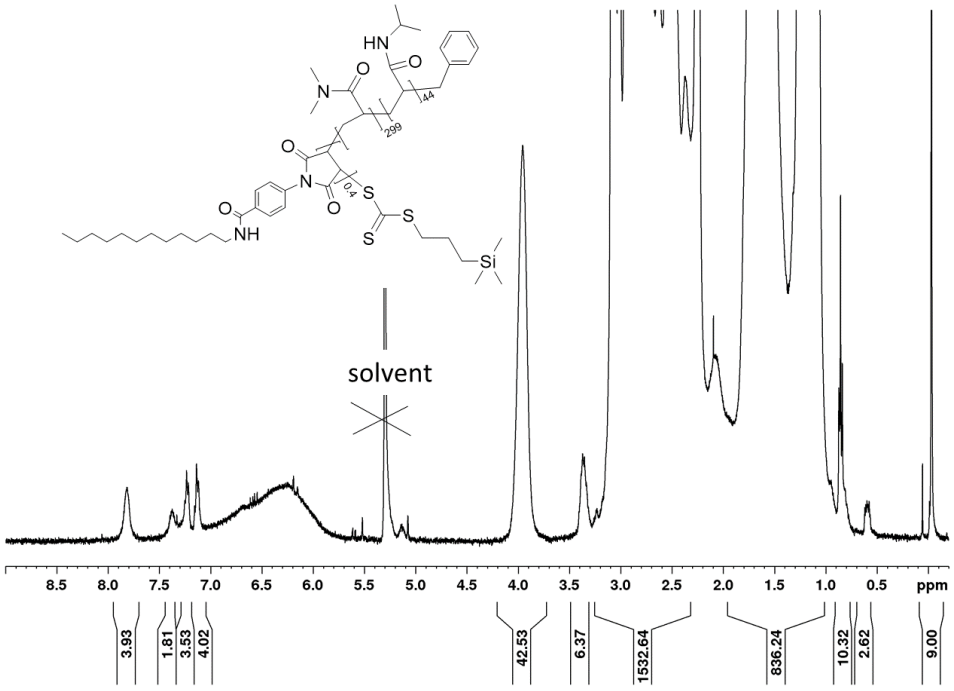

Figure 11.40: ^{1}H-NMR of **YN2-1a-7**in CD_2Cl_2. Note that the polymer was dialysed afterwards due to residual monomer.

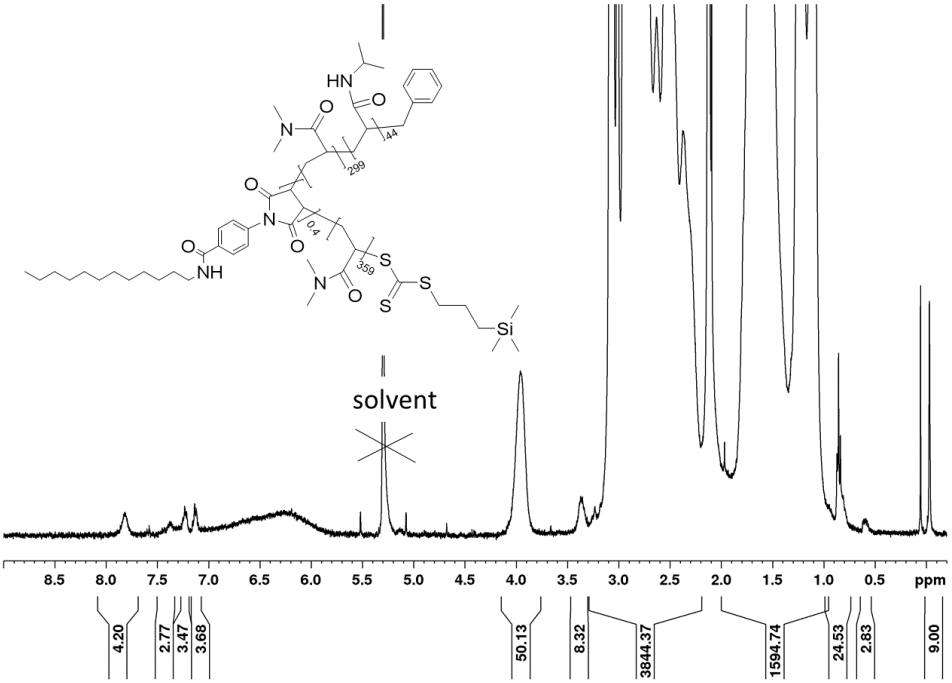

Figure 11.41: ^{1}H-NMR of **YN2-1a-7-1d** in CD_2Cl_2.

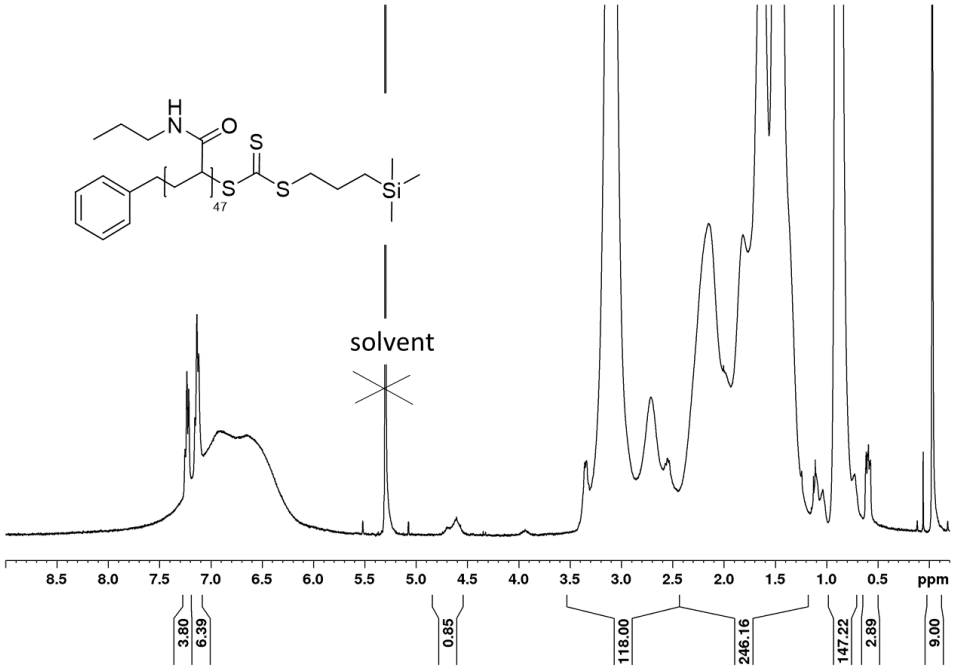

Figure 11.42: ^{1}H-NMR of **YN5** in CD_2Cl_2.

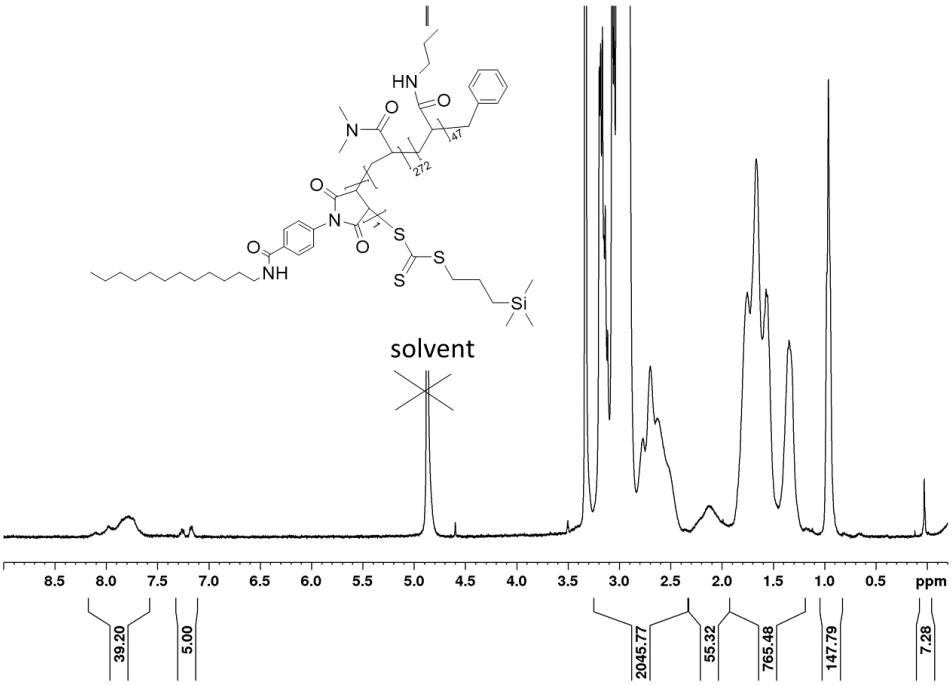

Figure 11.43: ^{1}H-NMR spectrum of **YN5-1c-7** in CD_2Cl_2.

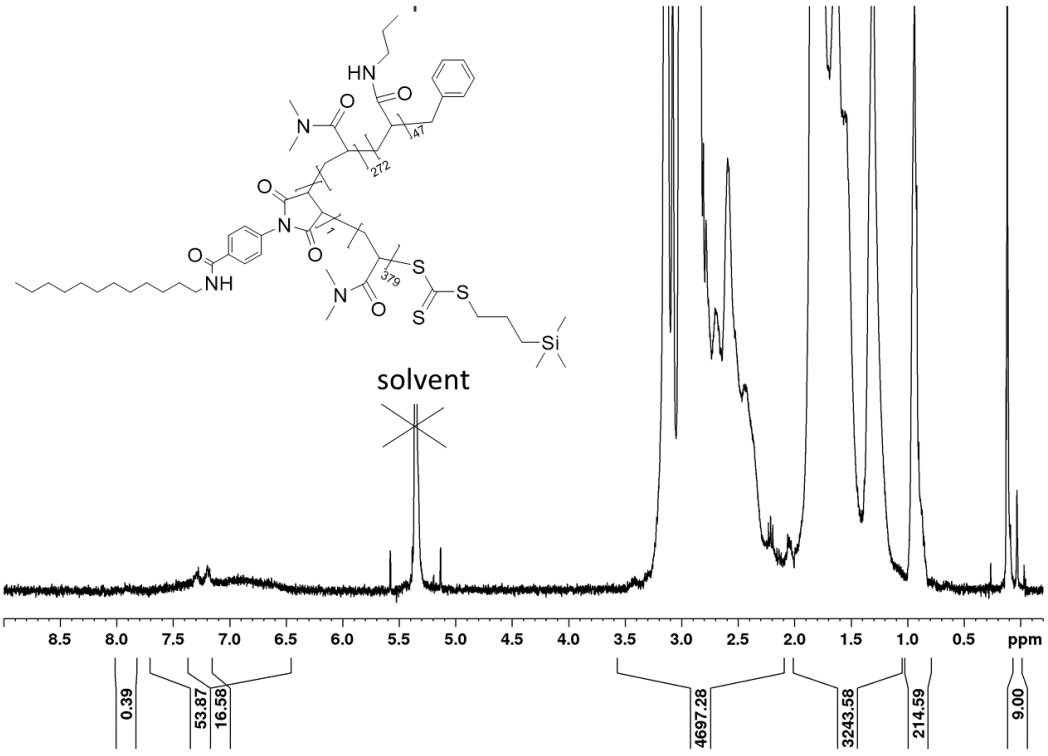

Figure 11.44: ^{1}H-NMR spectrum of **YN5-1c-7-1f** in CD_2Cl_2.

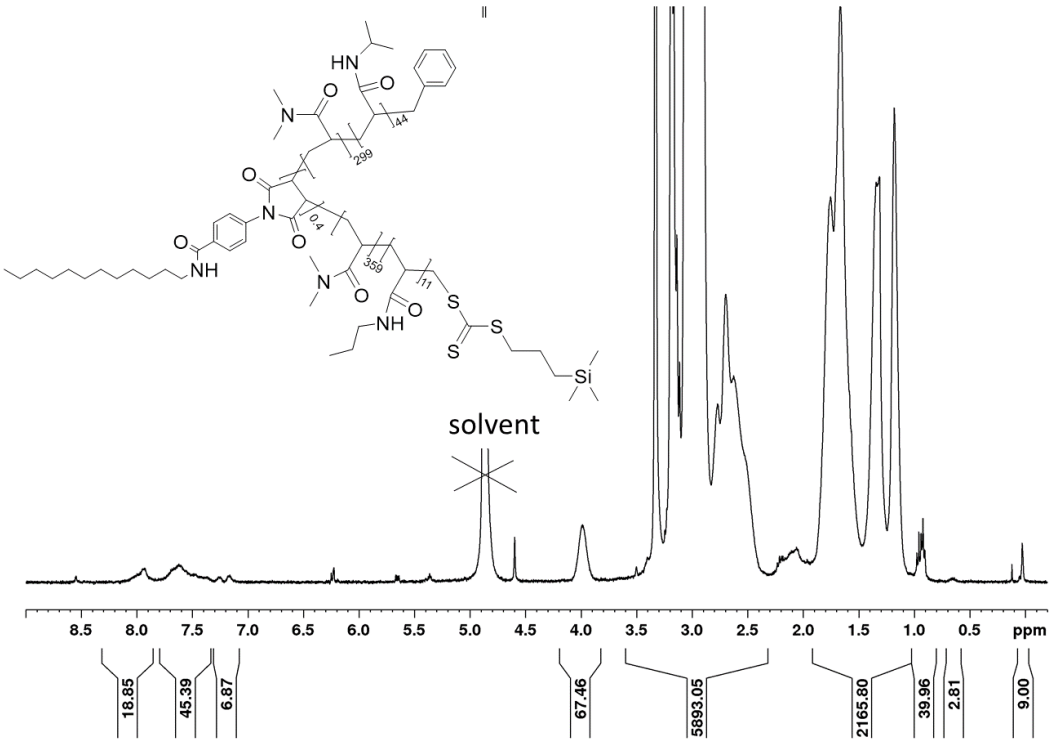

Figure 11.45: ^{1}H-NMR spectrum of **YN2-1a-7-1d-5a** in D_2O.

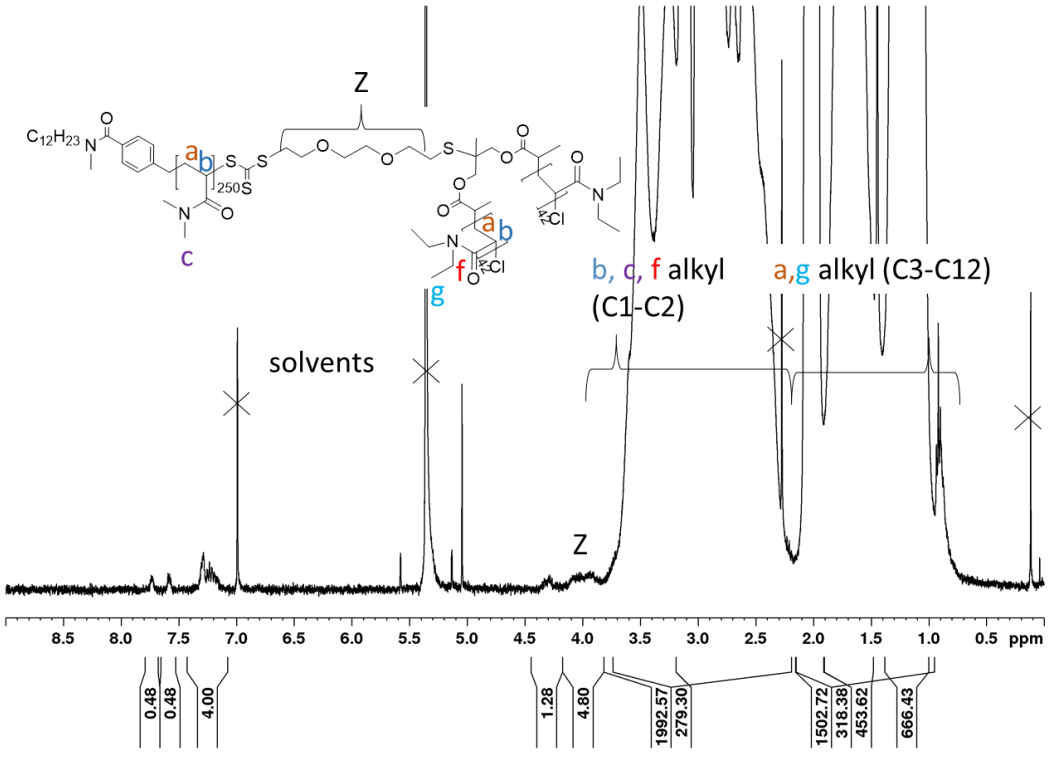

Figure 11.46: ^{1}H NMR spectrum of **TT1-3a** in CD_2Cl_2.

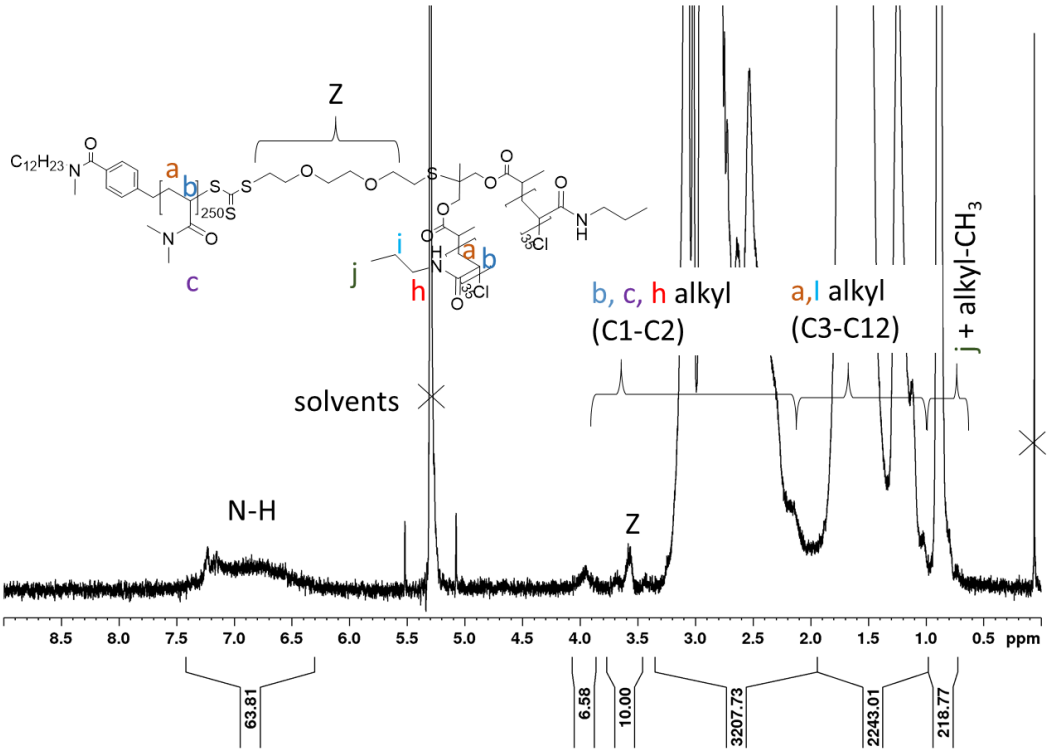

Figure 11.47: ^{1}H NMR spectrum of **TT1-5** in CD_2Cl_2.

11.6 SEC

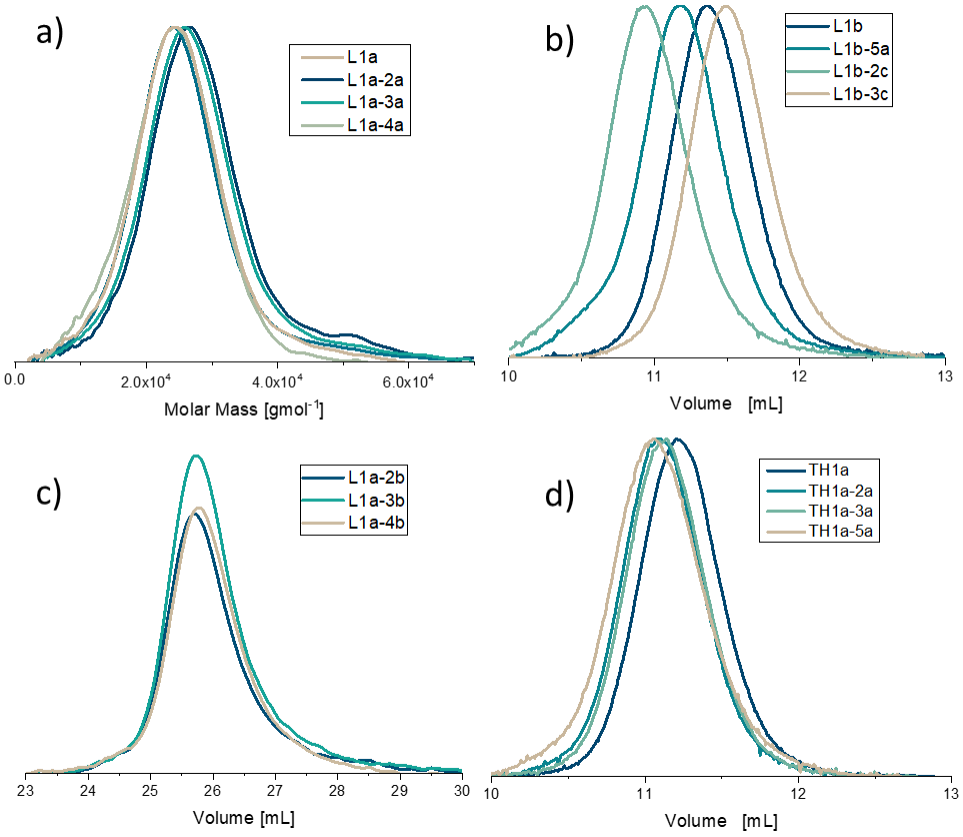

Figure 11.48: SEC molar mass distribution and elugrams of homo and block copolymers with linear (a-c) and twinned hydrophobic (d) architecture.

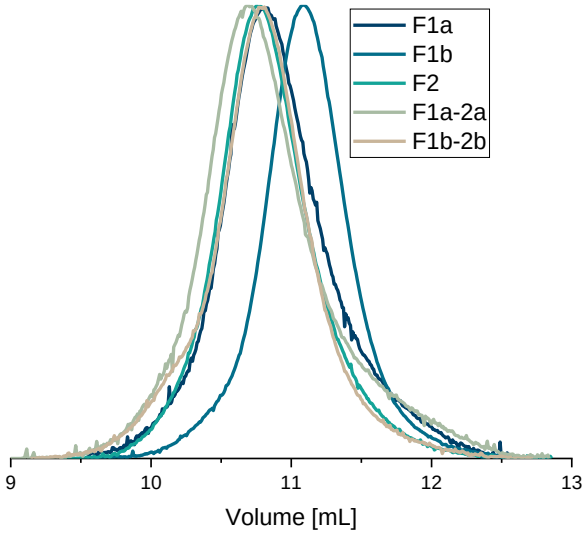

Figure 11.49: SEC elugrams of homo- and block copolymers derived from **FRET-CTA**.

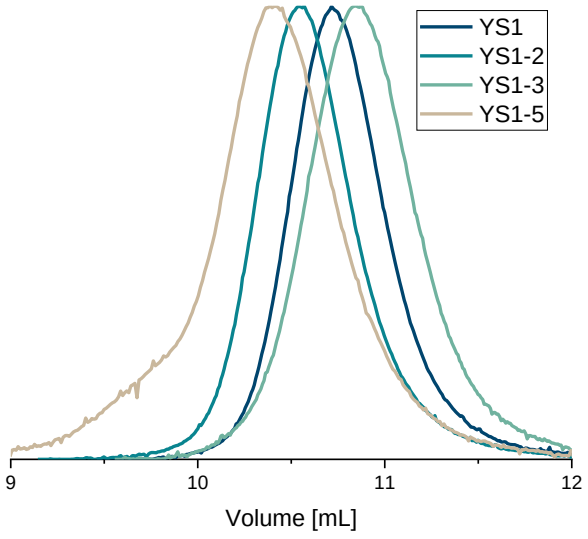

Figure 11.50: SEC elugrams of homo and block copolymers with symmetrical quasi miktoarm architecture **YS**.

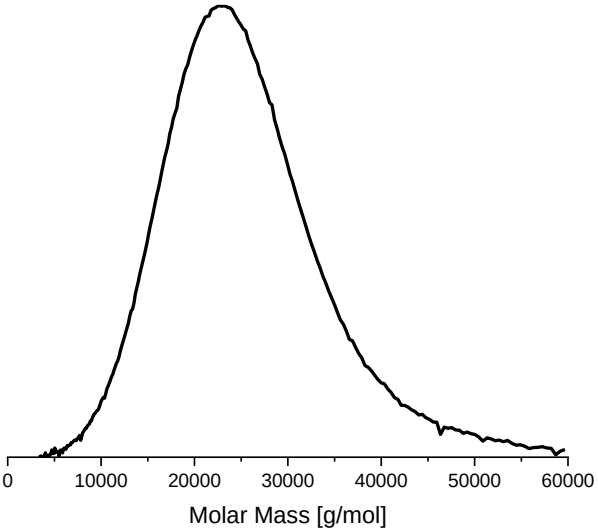

Figure 11.51: SEC molar mass distribution of PDMAm derived from **Cl-CTA1c**.

11.7 DSC & TGA

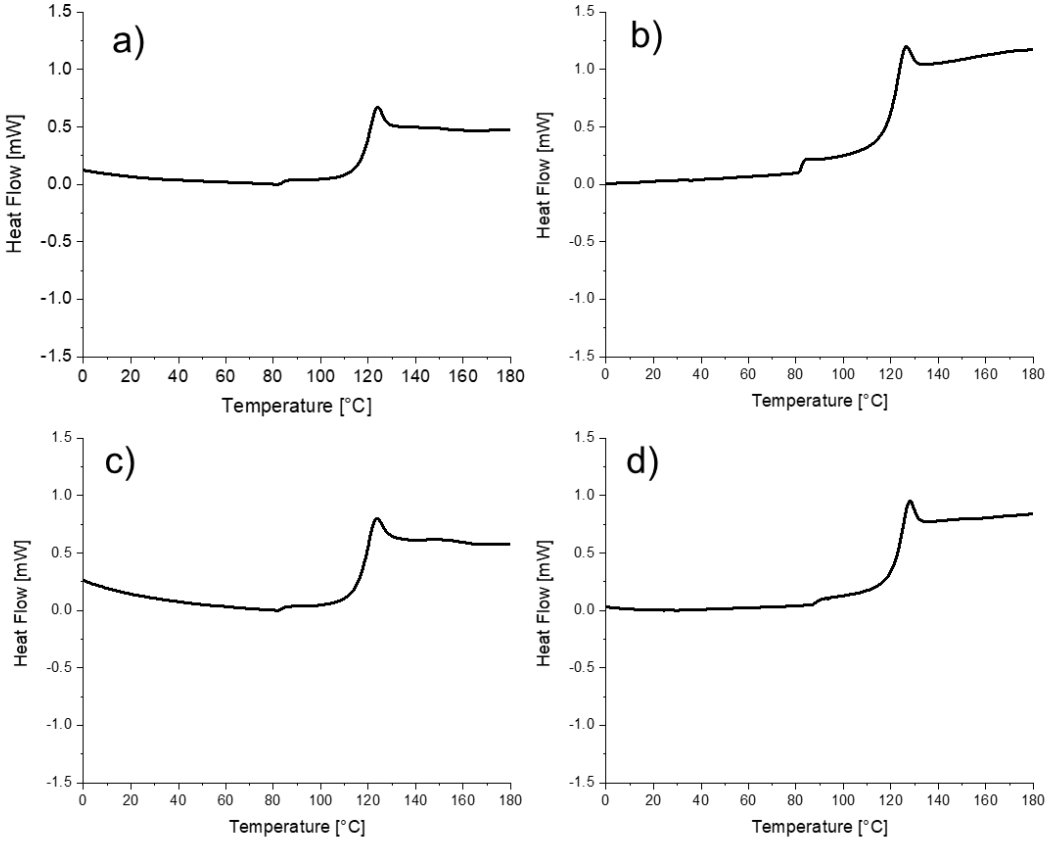

Figure 11.52: DSC of homo- and block copolymers derived from **C12-CTA** a) **L1a**, b**) L1a-2a**, c) **L1a-3a**, and d) **L1a-4a**.

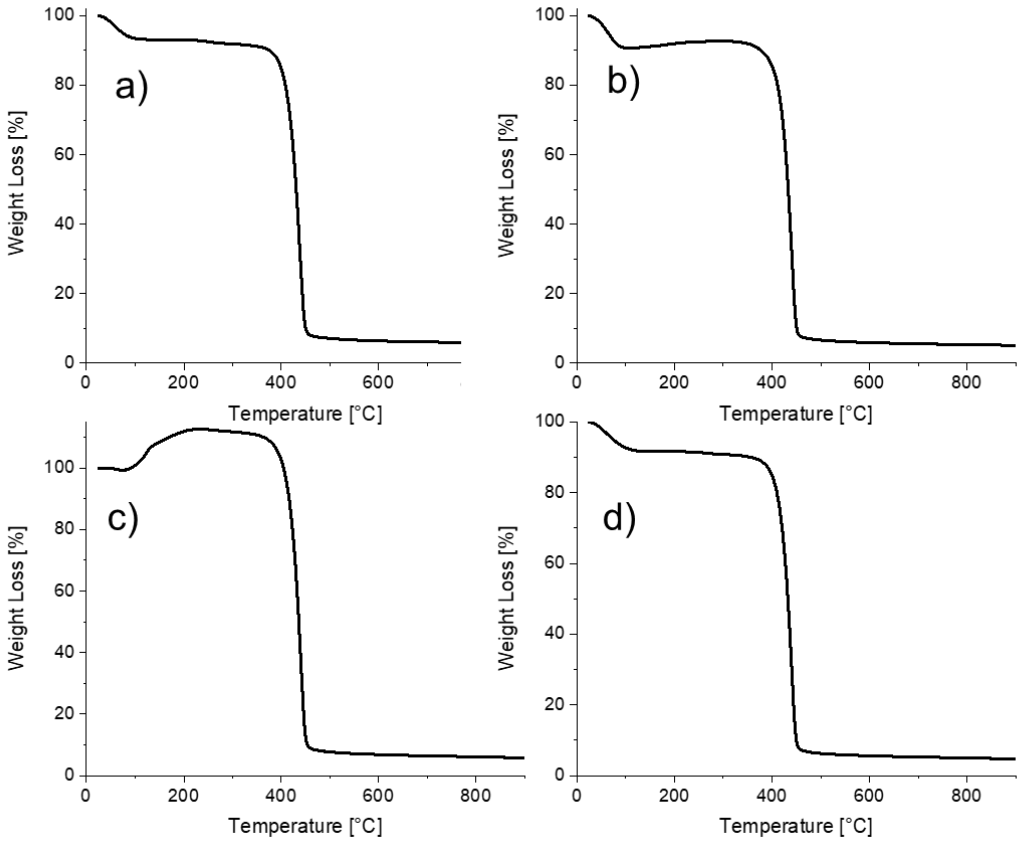

Figure 11.53: TGA of homo- and block copolymers derived from **C12-CTA** a) **L1a**, b**) L1a-2a**, c) **L1a-3a**, and d) **L1a-4a**.

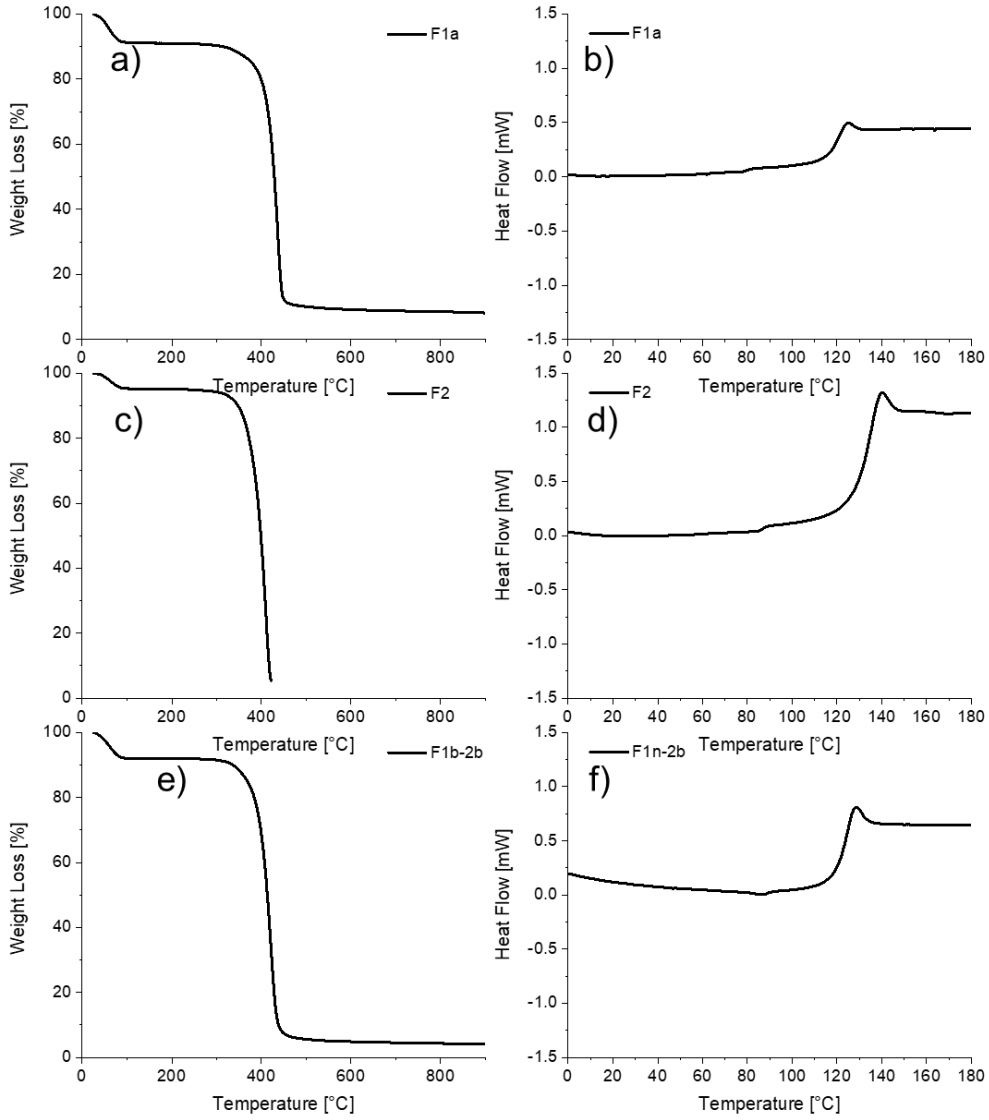

Figure 11.54: TGA (left column) and DSC (right column) of FRET homo- and block copolymers derived from **FRET-CTA**.

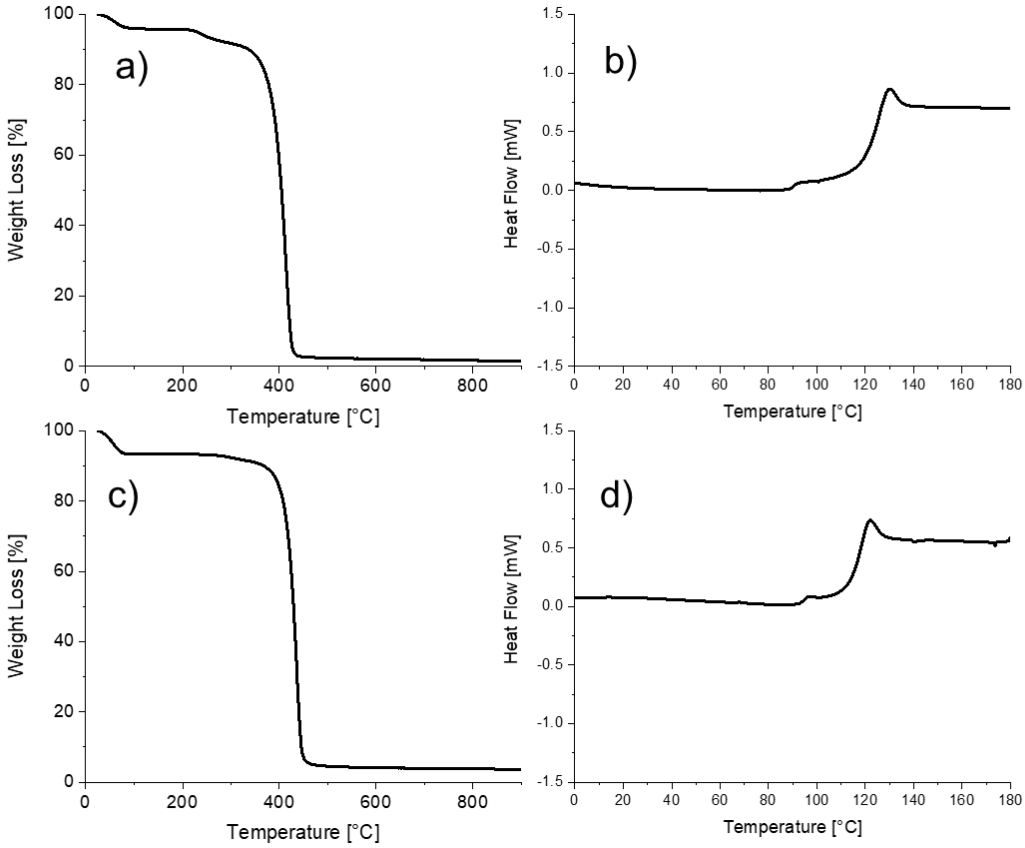

Figure 11.55: TGA (left column) and DSC (right column) of PNiPAm **YN2** (a,b) and PDMAm **TT1** (c,d).

LITERATURE

[1] R. Kröger, H. Menzel, M. L. Hallensleben, *Macromol. Chem. Phys.* **1994**, *195*, 2291.

[2] C. Gota, K. Okabe, T. Funatsu, Y. Harada, S. Uchiyama, *J. Am. Chem. Soc.* **2009**, *131*, 2766.

[3] Y. Noguchi, K. Okeyoshi, R. Yoshida, *Macromol. Rapid Commun.* **2005**, *26*, 1913.

[4] J. Isaksson, C. Tengstedt, M. Fahlman, N. Robinson, M. Berggren, *Adv. Mater.* **2004**, *16*, 316.

[5] A. M. Y Osada, *Nature* **1995**.

[6] E. Wischerhoff, K. Uhlig, A. Lankenau, H. G. Börner, A. Laschewsky, C. Duschl, J.-F. Lutz, *Angew. Chem. Int. Ed.* **2008**, *47*, 5666.

[7] E. Wischerhoff, T. Zacher, A. Laschewsky, E.-D. Rekaï, *Angew. Chem. Int. Ed.* **2000**, *39*, 4602.

[8] A. Miasnikova, Benítez-Montoya, C. Adrián, A. Laschewsky, *Macromol. Chem. Phys.* **2013**, *214*, 1504.

[9] M. A. C. Stuart, W. T. S. Huck, J. Genzer, M. Müller, C. Ober, M. Stamm, G. B. Sukhorukov, I. Szleifer, V. V. Tsukruk, M. Urban et al., *Nat. Mater.* **2010**, *9*, 101.

[10] C. Mangeney, F. Ferrage, I. Aujard, V. Marchi-Artzner, L. Jullien, O. Ouari, E. D. Rékaï, A. Laschewsky, I. Vikholm, J. W. Sadowski, *J. Am. Chem. Soc.* **2002**, *124*, 5811.

[11] M. A. Hempenius, C. Cirmi, F. Lo Savio, J. Song, Vancso, G. Julius, *Macromol. Rapid Commun.* **2010**, *31*, 772.

[12] A. K. Bajpai, S. K. Shukla, S. Bhanu, S. Kankane, *Prog. Polym. Sci.* **2008**, *33*, 1088.

[13] K. Skrabania, J. Kristen, A. Laschewsky, Ö. Akdemir, A. Hoth, J.-F. Lutz, *Langmuir* **2007**, *23*, 84.

[14] D. Roy, W. L. A. Brooks, B. S. Sumerlin, *Chem. Soc. Rev.* **2013**, *42*, 7214.

[15] I. Dimitrov, B. Trzebicka, A. H. E. Müller, A. Dworak, C. B. Tsvetanov, *Prog. Polym. Sci.* **2007**, *32*, 1275.

[16] F. Meeussen, E. Nies, H. Berghmans, S. Verbrugghe, E. Goethals, F. Du Prez, *Polymer* **2000**, *41*, 8597.

[17] K. van Durme, S. Verbrugghe, F. E. Du Prez, B. van Mele, *Macromolecules* **2004**, *37*, 1054.

[18] V. Aseyev, H. Tenhu, F. Winnik, *Adv. Polym. Sci.* **2011**, *242*, 29.

[19] D. G. Lessard, M. Ousalem, X. X. Zhu, *Can. J. Chem.* **2001**, *79*, 1870.

[20] A. Halperin, M. Kröger, F. M. Winnik, *Angew. Chem. Int. Ed.* **2015**, *54*, 15342.

[21] H. Schäfer-Soenen, R. Moerkerke, H. Berghmans, R. Koningsveld, K. Dušek, K. Šolc, *Macromolecules* **1997**, *30*, 410.

[22] S. Grobelny, C. H. Hofmann, M. Erlkamp, F. A. Plamper, W. Richtering, R. Winter, *Soft Matter* **2013**, *9*, 5862.

[23] K. Otake, R. Karaki, T. Ebina, C. Yokoyama, S. Takahashi, *Macromolecules* **1993**, *26*, 2194.

[24] S. Kunugi, K. Takano, N. Tanaka, K. Suwa, M. Akashi, *Macromolecules* **1997**, *30*, 4499.

[25] C. Boutris, E. G. Chatzi, C. Kiparissides, *Polymer* **1997**, *38*, 2567.

[26] M. L. Ohnsorg, J. M. Ting, S. D. Jones, S. Jung, F. S. Bates, T. M. Reineke, *Polym. Chem.* **2019**, *10*, 3469.

[27] S. Furyk, Y. Zhang, D. Ortiz-Acosta, P. S. Cremer, D. E. Bergbreiter, *J. Polym. Sci., Part A: Polym. Chem.* **2006**, *44*, 1492.

[28] Y. Xia, Burke, Nicholas A. D., Stöver, Harald D. H., *Macromolecules* **2006**, *39*, 2275.

[29] Y.B. Zhulina, O. V. Borisov, T. M. Birshtein, *Polym. Sci. (USSR)* **1988**, *30*, 780.

[30] A. Miasnikova, A. Laschewsky, *J. Polym. Sci., Part A: Polym. Chem.* **2012**, *50*, 3313.

[31] A. Hirao, R. Inushima, T. Nakayama, T. Watanabe, H.-S. Yoo, T. Ishizone, K. Sugiyama, T. Kakuchi, S. Carlotti, A. Deffieux, *Eur. Polym. J.* **2011**, *47*, 713.

[32] C. Herfurth, A. Laschewsky, L. Noirez, B. von Lospichl, M. Gradzielski, *Polymer* **2016**, *107*, 422.

[33] L. A. Picos-Corrales, A. Licea-Claverie, J. M. Cornejo-Bravo, S. Schwarz, K.-F. Arndt, *Macromol. Chem. Phys.* **2012**, *213*, 301.

[34] B. Ray, Y. Okamoto, M. Kamigaito, M. Sawamoto, K.-i. Seno, S. Kanaoka, S. Aoshima, *Polym. J.* **2005**, *37*, 234.

[35] T. Tada, T. Hirano, K. Ute, Y. Katsumoto, T.-A. Asoh, T. Shoji, N. Kitamura, Y. Tsuboi, *J. Phys. Chem. B* **2016**, *120*, 7724.

[36] Y. Tsuboi, Y. Yoshida, K. Okada, N. Kitamura, *J. Phys. Chem. B* **2008**, *112*, 2562.

[37] Y. Katsumoto, Y. Etoh, N. Shimoda, *Macromolecules* **2010**, *43*, 3120.

[38] M. Kobayashi, S. Okuyama, T. Ishizone, S. Nakahama, *Macromolecules* **1999**, *32*, 6466.

[39] T. Baltes, F. Garret-Flaudy, R. Freitag, *J. Polym. Sci., Part A: Polym. Chem.* **1999**, *37*, 2977.

[40] T. Mori, T. Hirano, A. Maruyama, Y. Katayama, T. Niidome, Y. Bando, K. Ute, S. Takaku, Y. Maeda, *Langmuir* **2009**, *25*, 48.

[41] T. Hirano, H. Yamamoto, K. Ute, *Polymer* **2011**, *52*, 5277.

[42] T. Hirano, M. Li, K. Maeda, M. Oshimura, K. Ute, *Polymer* **2020**, *198*, 122530.

[43] F. Hofmeister, *Arch. Pharmacol.* **1888**, *1*, 1.

[44] S. Zajforoushan Moghaddam, E. Thormann, *Langmuir* **2017**, *33*, 4806.

[45] Y. Zhang, S. Furyk, D. E. Bergbreiter, P. S. Cremer, *J. Am. Chem. Soc.* **2005**, *127*, 14505.

[46] X. Chen, T. Yang, S. Kataoka, P. S. Cremer, *J. Am. Chem. Soc.* **2007**, *129*, 12272.

[47] M. Heskins, J. E. Guillet, *J. Macromol. Sci. A: Pure Appl. Chem.* **1968**, *2*, 1441.

[48] Z. Tong, F. Zeng, X. Zheng, T. Sato, *Macromolecules* **1999**, *32*, 4488.

[49] Q. Zheng, C.-Y. Pan, *Eur. Polym. J.* **2006**, *42*, 807.

[50] N. A. Platé, T. L. Lebedeva, L. I. Valuev, *Polymer J.* **1999**, *31*, 21.

[51] D. Ito, K. Kubota, *Macromolecules* **1997**, *30*, 7828.

[52] Y. Cao, X. X. Zhu, J. Luo, H. Liu, *Macromolecules* **2007**, *40*, 6481.

[53] J. Pang, H. Yang, J. Ma, R. Cheng, *J. Theor. Comp. Chem.* **2011**, *10*, 359.

[54] L. D. Taylor, L. D. Cerankowski, *J. Polym. Sci., Part A: Polym. Chem.* **1975**, *13*, 2551.

[55] D. G. Lessard, M. Ousalem, X. X. Zhu, A. Eisenberg, P. J. Carreau, *J. Polym. Sci, Part B: Polym. Phys.* **2003**, *41*, 1627.

[56] S. Ito, *Kobunshi Ronbunshu* **1990**, *47*, 467.

[57] T. Hidaka, S. Sugihara, Y. Maeda, *Eur. Polym. J.* **2013**, *49*, 675.

[58] J. M. Song, F. M. Winnik, J. L. Brash, *Macromolecules* **1998**, *31*, 109.

[59] M. Hechenbichler, A. Laschewsky, M. Gradzielski, *Colloid Polym. Sci* **2021**, *299*, 205.

[60] S. Ito, *Kobunshi Ronbunshu* **1989**, *46*, 437.

[61] S. Garnier, A. Laschewsky, *Colloid Polym. Sci.* **2006**, *284*, 1243.

[62] P. Alexandridis, B. Lindman, *Amphiphilic block copolymers*. *Self-assembly and applications*, 1. Aufl., Elsevier, Amsterdam, **2000**.

[63] P. Alexandridis, *Curr. Opin. Coll. Interface Sci.* **1996**, *1*, 490.

[64] P. Raffa, D. A. Z. Wever,, F. Picchioni, A. A. Broekhuis, *Chem. Rev.* **2015**, *115*, 8504.

[65] F. Renou, T. Nicolai, L. Benyahia, E. Nicol, *J. Phys. Chem. B* **2009**, *113*, 3000.

[66] J. Berret, *Curr. Opin. Colloid Interface Sci* **2003**, *8*, 296.

[67] M. Karayianni, S. Pispas in *Procházka (Ed.) 2016 – Fluorescence Studies of Polymer Containing*, S. 27–63.

[68] N. Hadjichristidis, H. Iatrou, M. Pitsikalis, S. Pispas, A. Avgeropoulos, *Prog. Polym. Sci.* **2005**, *30*, 725.

[69] M. L. Adams, A. Lavasanifar, G. S. Kwon, *J. Pharm. Sci.* **2003**, *92*, 1343.

[70] L. Hong, G. Sun, J. Cai, T. Ngai, *Langmuir* **2012**, *28*, 2332.

[71] P. J. G. Stevens, *Pestic. Sci.* **1993**, *38*, 103.

[72] A. Laschewsky, C. Herfurth, A. Miasnikova, F. Stahlhut, J. Weiss, C. Wieland, E. Wischerhoff, M. Gradzielski, P. Malo de Molina, *ACS Symp. Ser.* **2013**, *1148*, 125.

[73] A. J. Convertine, B. S. Lokitz, Y. Vasileva, L. J. Myrick, C. W. Scales, A. B. Lowe, C. L. McCormick, *Macromolecules* **2006**, *39*, 1724.

[74] C. Booth, D. Attwood, *Macromol. Rapid Commun.* **2000**, *21*, 501.

[75] S. Cui, L. Yu, J. Ding, *Macromolecules* **2019**, *52*, 3697.

[76] B. Chu, *Langmuir* **1995**, *11*, 414.

[77] C. Chassenieux, T. Nicolai, L. Benyahia, *Curr. Opin. Coll. Interface Sci.* **2011**, *16*, 18.

[78] I. R. Schmolka, *J. Amer. Oil Chem. Soc.* **1977**, *54*, 110.

[79] V. Castelletto, I. W. Hamley, X.-F. Yuan, A. Kelarakis, C. Booth, *Soft Matter* **2005**, *1*, 138.

[80] A. M. Bivigou-Koumba, E. Görnitz, A. Laschewsky, P. Müller-Buschbaum, C. M. Papadakis, *Colloid Polym. Sci.* **2010**, *288*, 499.

[81] I. W. Wyman, G. Liu, *Polymer* **2013**, *54*, 1950.

[82] J.-F. Lutz, A. Laschewsky, *Macromol. Chem. Phys.* **2005**, *206*, 813.

[83] R. R. Taribagil, Hillmyer, M. A., Lodge, T. P., *Macromolecules* **2009**, *42*, 1796.

[84] S. Strandman, X. X. Zhu, *Prog. Polym. Sci.* **2015**, *42*, 154.

[85] S. Sugihara, S. Kanaoka, S. Aoshima, *J. Polym. Sci., Part A: Polym. Chem.* **2004**, *42*, 2601.

[86] Y.-G. Jia, X. X. Zhu, *Polym. Chem.* **2014**, *5*, 4358.

[87] J. Weiss, A. Laschewsky, *Langmuir* **2011**, *27*, 4465.

[88] S. Slomkowski, J. V. Alemán, R. G. Gilbert, M. Hess, K. Horie, R. G. Jones, P. Kubisa, I. Meisel, W. Mormann, S. Penczek et al., *Pure Appl. Chem.* **2011**, *83*, 2229.

[89] E. Ruckenstein, J. C. Chi, *J. Chem. Soc., Faraday Trans. 2* **1975**, *71*, 1690.

[90] M. Gradzielski, M. Duvail, P. M. de Molina, M. Simon, Y. Talmon, T. Zemb, *Chem. Rev.* **2021**, *121*, 5671.

[91] B. K. Paul, S. P. Moulik, *J. Dispers. Sci. Technol.* **1997**, *18*, 301.

[92] T. P. Hoar, J. H. Schulman, *Nature* **1943**, *152*, 102.

[93] H. Hoffmann, G. Oetter, B. Schwandner, *Progr. Colloid Polym. Sci.*, *73*, 95.

[94] M. Gradzielski, *Langmuir* **1998**, *14*, 6037.

[95] M. Zoumpanioti, H. Stamatis, A. Xenakis, *Biotechnol. Adv.* **2010**, *28*, 395.

[96] M. F. Nazar, S. S. Shah, M. A. Khosa, *Petrol. Sci. Tech.* **2011**, *29*, 1353.

[97] A. Weiss (Hrsg.) *Progr. Colloid and Polymer Sci., Vol. 69*, Steinkopff, Darmstadt, **1984**.

[98] M. Zackrisson, R. Andersson, J. Bergenholtz, *Langmuir* **2004**, *20*, 3080.

[99] Y. Mao, M. E. Cates, H.N.W. Lekkerkerker, *Physica A Stat. Mech. Appl.* **1995**, *222*, 10.

[100] F. Matter, A. L. Luna, M. Niederberger, *Nano Today* **2020**, *30*, 100827.

[101] D. Byelov, H. Frielinghaus, O. Holderer, J. Allgaier, D. Richter, *Langmuir* **2004**, *20*, 10433.

[102] F. E. Antunes, K. Thuresson, B. Lindman, M. G. Miguel, *Colloids Surf. A: Physicochem. Eng. Asp.* **2003**, *215*, 87.

[103] G. Fleischer, F. Stieber, U. Hofmeier, H.-F. Eicke, *Langmuir* **1994**, *10*, 1780.

[104] P. Malo de Molina, C. Herfurth, A. Laschewsky, A. Gradzielski, *Langmuir* **2012**, *28*, 15994.

[105] K. Matyjaszewski, *Macromolecules* **2012**, *45*, 4015.

[106] W. A. Braunecker, K. Matyjaszewski, *Prog. Polym. Sci.* **2007**, *32*, 93.

[107] G. Moad, E. Rizzardo, S. H. Thang, *Chem. Asian J.* **2013**, *8*, 1634.

[108] S. Perrier, *Macromolecules* **2017**, *50*, 7433.

[109] D. J. Keddie, G. Moad, E. Rizzardo, S. H. Thang, *Macromolecules* **2012**, *45*, 5321.

[110] J. Chiefari, Mayadunne, Roshan T. A., C. L. Moad, G. Moad, E. Rizzardo, A. Postma, M. A. Skidmore, S. H. Thang, *Macromolecules* **2003**, *36*, 2273.

[111] G. Gody, T. Maschmeyer, P. B. Zetterlund, S. Perrier, *Macromolecules* **2014**, *47*, 639.

[112] E. Rizzardo, M. Chen, B. Chong, G. Moad, M. Skidmore, S. H. Thang, *Macromol. Symp.* **2007**, *248*, 104.

[113] M. G. Fröhlich, M. M. Nardai, N. Förster, P. Vana, G. Zifferer, *Polymer* **2010**, *51*, 5122.

[114] M. H. Stenzel, L. Zhang, Huck, Wilhelm T. S., *Macromol. Rapid Commun.* **2006**, *27*, 1121.

[115] M. Destarac, *Polym. Rev.* **2011**, *51*, 163.

[116] L. Fetzer, V. Toniazzo, D. Ruch, F. di Lena, *Isr. J. Chem.* **2012**, *52*, 221.

[117] F. di Lena, K. Matyjaszewski, *Progr. Polym. Sci.* **2010**, *35*, 959.

[118] W. Tang, K. Matyjaszewski, *Macromolecules* **2006**, *39*, 4953.

[119] W. Tang, Y. Kwak, W. Braunecker, N. V. Tsarevsky, M. L. Coote, K. Matyjaszewski, *J. Am. Chem. Soc.* **2008**, *130*, 10702.

[120] M. Teodorescu, K. Matyjaszewski, *Macromol. Rapid Commun.* **2000**, *21*, 190.

[121] M. Teodorescu, K. Matyjaszewski, *Macromolecules* **1999**, *33*, 4826.

[122] J. T. Rademacher, M. Baum, M. E. Pallack, W. J. Brittain, William J. Simonsick, Jr., *Macromolecules* **2000**, *33*, 284.

[123] J. Zhang, E. Liarou, J. Town, Y. Li, A. M. Wemyss, D. M. Haddleton, *Polym. Chem.* **2020**, *11*, 5534.

[124] E. A. Appel, J. del Barrio, X. J. Loh, J. Dyson, O. A. Scherman, *J. Polym. Sci. A Polym. Chem.* **2012**, *50*, 181.

[125] F. Alsubaie, A. Anastasaki, P. Wilson, D. M. Haddleton, *Polym. Chem.* **2015**, *6*, 406.

[126] D. A. Z. Wever, P. Raffa, F. Picchioni, A. A. Broekhuis, *Macromolecules* **2012**, *45*, 4040.

[127] G. R. Jones, A. Anastasaki, R. Whitfield, N. Engelis, E. Liarou, D. M. Haddleton, *Angew. Chem. Int. Ed. Engl.* **2018**, *57*, 10468.

[128] G. Lligadas, B. M. Rosen, M. J. Monteiro, V. Percec, *Macromolecules* **2008**, *41*, 8360.

[129] Q. Zhang, P. Wilson, Z. Li, R. McHale, J. Godfrey, A. Anastasaki, C. Waldron, D. M. Haddleton, *J. Am. Chem. Soc.* **2013**, *135*, 7355.

[130] F. Alsubaie, A. Anastasaki, V. Nikolaou, A. Simula, G. Nurumbetov, P. Wilson, K. Kempe, D. M. Haddleton, *Macromolecules* **2015**, *48*, 6421.

[131] N. H. Nguyen, B. M. Rosen, G. Lligadas, V. Percec, *Macromolecules* **2009**, *42*, 2379.

[132] M. C. Haven, G. A. Tetrault, J. R. Schenken, *Laboratory Instrumentation*, 4. Aufl., Wiley, New York, **1995**.

[133] Q. Zhang, C. Weber, U. S. Schubert, R. Hoogenboom, *Mater. Horiz.* **2017**, *4*, 109.

[134] K. van Durme, G. van Assche, B. van Mele, *Macromolecules* **2004**, *37*, 9596.

[135] V. Hildebrand, A. Laschewsky, E. Wischerhoff, *Polym. Chem.* **2016**, *7*, 731.

[136] J. Stetefeld, S. A. McKenna, T. R. Patel, *Biophys Rev* **2016**, *8*, 409.

[137] A. Einstein, *Ann. Phys.* **1905**, *322*, 132.

[138] R. Pecora (Hrsg.) *Dynamic Light Scattering. Applications of Photon Correlation Spectroscopy*, Springer US, Boston, MA, **1985**.

[139] K. S. Schmitz, *An introduction to dynamic light scattering by macromolecules*, Academic Press, Boston, **1990**.

[140] J. Weiss, C. Böttcher, A. Laschewsky, *Soft Matter* **2011**, *7*, 483.

[141] T. Förster, *Ann. Phys.* **1948**, *437*, 55.

[142] P. Rajdev, S. Ghosh, *J. Phys. Chem. B* **2019**, *123*, 327.

[143] H. Sahoo, *J. Photochem. Photobiol. C: Photochem. Rev.* **2011**, *12*, 20.

[144] T. Rager, W. H. Meyer, G. Wegner, M. A. Winnik, *Macromolecules* **1997**, *30*, 4911.

[145] A. Laukkanen, F. M. Winnik, H. Tenhu, *Macromolecules* **2005**, *38*, 2439.

[146] C. Pietsch, A. Vollrath, R. Hoogenboom, U. S. Schubert, *Sensors* **2010**, *10*, 7979.

[147] S. Piçarra, P. T. Gomes, Martinho, J. M. G., *Macromolecules* **2000**, *33*, 3947.

[148] C. Pietsch, R. Hoogenboom, U. S. Schubert, *Polym. Chem.* **2010**, *1*, 1005.

[149] P. J. Roth, M. Haase, T. Basché, P. Theato, R. Zentel, *Macromolecules* **2010**, *43*, 895.

[150] F. M. Winnik, *Macromolecules* **1990**, *23*, 1647.

[151] Y. Sha, Y. Xu, D. Qi, Y. Wan, L. Li, H. Li, X. Wang, G. Xue, D. Zhou, *Macromolecules* **2016**, *49*, 8274.

[152] Y. Sha, Q. Zhu, Y. Wan, L. Li, X. Wang, G. Xue, D. Zhou, *J. Polym. Sci., Part A: Polym. Chem.* **2016**, *54*, 2413.

[153] R. Merckx, T. Swift, R. Rees, J. F. R. van Guyse, E. Schoolaert, K. de Clerck, H. Ottevaere, H. Thienpont, V. V. Jerca, R. Hoogenboom, *J. Mater. Chem. C* **2020**, *8*, 14125.

[154] S. A. Ruetten, J. K. Thomas, *J. Phys. Chem. B* **1999**, *103*, 1278.

[155] C. D. Geddes, *Meas. Sci. Technol.* **2001**, *12*, R53-R88.

[156] E. Miller, D. Jóźwik-Styczyńska, *Colloid Polym Sci* **2007**, *285*, 1561.

[157] G. Saito, D. Velluto, M. Resmini, *R. Soc. Open Sci.* **2018**, *5*, 172137.

[158] X. He, Q. Li, P. Shi, Y. Cui, S. Li, W. Zhang, *Polym. Chem.* **2014**, *5*, 7090.

[159] X. Zhou, F. Su, H. Lu, P. Senechal-Willis, Y. Tian, R. H. Johnson, D. R. Meldrum, *Biomaterials* **2012**, *33*, 171.

[160] Q. Zhai, S. Yang, Y. Fang, H. Zhang, G. Feng, *RSC Adv.* **2015**, *5*, 94216.

[161] F. Laflèche, D. Durand, T. Nicolai, *Macromolecules* **2003**, *36*, 1331.

[162] Y. Zhu, H. Yu, Y. Wang, J. Cui, W. Kong, W. Jiang, *Soft Matter* **2012**, *8*, 4695.

[163] C. Li, N. J. Buurma, I. Haq, C. Turner, S. P. Armes, A. L. Lewis, *Langmuir* **2005**, *21*, 11026.

[164] Bivigou-Koumba, A. M., J. Kristen, A. Laschewsky, P. Müller-Buschbaum, Papadakis, C. M., *Macromol. Chem. Phys.* **2009**, *210*, 565.

[165] M. Mertoglu, A. Laschewsky, K. Skrabania, C. Wieland, *Macromolecules* **2005**, *38*, 3601.

[166] J.-F. Baussard, J.-L. Habib-Jiwan, A. Laschewsky, M. Mertoglu, J. Storsberg, *Polymer* **2004**, *45*, 3615.

[167] J. R. Reeve, R. K. Thomas, J. Penfold, *Langmuir* **2021**, *37*, 9269.

[168] M. Päch, D. Zehm, M. Lange, I. Dambowsky, J. Weiss, A. Laschewsky, *J. Am. Chem. Soc.* **2010**, *132*, 8757.

[169] J. Weiss, A. Li, E. Wischerhoff, A. Laschewsky, *Polym. Chem.* **2012**, *3*, 352.

[170] K. Skrabania, A. Miasnikova, A. M. Bivigou-Koumba, D. Zehm, A. Laschewsky, *Polym. Chem.* **2011**, *2*, 2074.

[171] G. Moad, E. Rizzardo, S. H. Thang, *Acc. Chem. Res.* **2008**, *41*, 1133.

[172] H. Y. Liu, X. X. Zhu, *Polymer* **1999**, *40*, 6985.

[173] F. Fischer, D. Zufferey, R. Tahoces, *Polym. Int.* **2011**, *60*, 1259.

[174] C. Herfurth, P. Malo de Molina, C. Wieland, S. H. Rogers, M. Gradzielski, A. Laschewsky, *Polym. Chem.* **2012**, *3*, 1606.

[175] H. Inomata, S. Goto, S. Saito, *Macromolecules* **1990**, *23*, 4887.

[176] K. Ito, S. Kawaguchi, *Adv. Polym. Sci.* **1999**, *142*, 129.

[177] P. Kujawa, F. Segui, S. Shaban, C. Diab, Y. Okada, F. Tanaka, F. M. Winnik, *Macromolecules* **2006**, *39*, 341.

[178] H. Cheng, L. Shen, C. Wu, *Macromolecules* **2006**, *39*, 2325.

[179] P. Kujawa, V. Aseyev, H. Tenhu, F. M. Winnik, *Macromolecules* **2006**, *39*, 7686.

[180] V. Aseyev, S. Hietala, A. Laukkanen, M. Nuopponen, O. Confortini, Du Prez, Filip E., H. Tenhu, *Polymer* **2005**, *46*, 7118.

[181] S. Schweizerhof, D. E. Demco, A. Mourran, H. Keul, R. Fechete, M. Möller, *Macromol. Chem. Phys.* **2017**, *218*, 1600495.

[182] Y. Zhao, S. Perrier, *Macromolecules* **2007**, *40*, 9116.

[183] A. A. S. El-Ejmi, M. B. Huglin, *Polym. Int.* **1996**, *39*, 113.

[184] J. T. Lai, D. Filla, R. Shea, *Macromolecules* **2002**, *35*, 6754.

[185] G. Moad, Chong, Y. K., A. Postma, E. Rizzardo, S. H. Thang, *Polymer* **2005**, *46*, 8458.

[186] A. Laschewsky, G. Pound, K. Skrabania, H.-J. Holdt, J. Teller, *Colloid Polym. Sci.* **2007**, *285*, 947.

[187] P. Köberle, A. Laschewsky, van den Boogaard, D., *Polymer* **1992**, *33*, 4029.

[188] S. Bennour, F. Louzri, *Adv. Chem.* **2014**, [147398] 1-10.

[189] K. Zhou, Y. Lu, J. Li, L. Shen, G. Zhang, Z. Xie, C. Wu, *Macromolecules* **2008**, *41*, 8927.

[190] Y. Lu, K. Zhou, Y. Ding, G. Zhang, C. Wu, *Phys. Chem. Chem. Phys.* **2010**, *12*, 3188.

[191] M. Pühse, M. Keerl, C. Scherzinger, W. Richtering, R. Winter, *Polymer* **2010**, *51*, 3653.

[192] A. Meier-Koll, V. Pipich, P. Busch, C. M. Papadakis, P. Müller-Buschbaum, *Langmuir* **2012**, *28*, 8791.

[193] M. Philipp, K. Kyriakos, L. Silvi, W. Lohstroh, W. Petry, J. K. Krüger, C. M. Papadakis, P. Müller-Buschbaum, *J. Phys. Chem. B* **2014**, *118*, 4253.

[194] M. H. Futscher, M. Philipp, P. Müller-Buschbaum, A. Schulte, *Sci. Rep.* **2017**, *7*, [17012] 1-10.

[195] J.-F. Lutz, Ö. Akdemir, A. Hoth, *J. Am. Chem. Soc.* **2006**, *128*, 13046.

[196] E. E. Dormidontova, *Macromolecules* **2002**, *35*, 987.

[197] Y. Xia, X. Yin, Burke, Nicholas A. D., Stöver, Harald D. H., *Macromolecules* **2005**, *38*, 5937.

[198] T. Munk, S. Baldursdottir, S. Hietala, T. Rades, M. Nuopponen, K. Kalliomäki, H. Tenhu, J. Rantanen, C. J. Strachan, *Polymer* **2013**, *54*, 6947.

[199] C. S. Biswas, B. Hazer, *Colloid Polym. Sci.* **2015**, *293*, 143.

[200] H. Du, R. Wickramasinghe, X. Qian, *J. Phys. Chem. B* **2010**, *114*, 16594.

[201] Y. Maeda, T. Nakamura, I. Ikeda, *Macromolecules* **2001**, *34*, 1391.

[202] E. E. Bruce, P. T. Bui, B. A. Rogers, P. S. Cremer, N. F. A. van der Vegt, *J. Am. Chem. Soc.* **2019**, *141*, 6609.

[203] S. Reinelt, D. Steinke, H. Ritter, *Beilstein J. Org. Chem.* **2014**, *10*, 680.

[204] V. Hildebrand, A. Laschewsky, D. Zehm, *J. Biomater. Sci., Polym. Ed.* **2014**, *25*, 1602.

[205] S. Kessel, C. N. Urbani, M. J. Monteiro, *Angew. Chem. Int. Ed.* **2011**, *50*, 8082.

[206] C. J. Ferguson, R. J. Hughes, Pham, Binh T. T., B. S. Hawkett, R. G. Gilbert, A. K. Serelis, C. H. Such, *Macromolecules* **2002**, *35*, 9243.

[207] C. N. Urbani, M. J. Monteiro, *Macromolecules* **2009**, *42*, 3884.

[208] C.-H. Ko, C. Henschel, G. P. Meledam, M. A. Schroer, P. Müller-Buschbaum, A. Laschewsky, C. M. Papadakis, *Macromolecules* **2021**, *54*, 384.

[209] A. Malfait, F. Coumes, D. Fournier, G. Cooke, P. Woisel, *Eur. Polym. J.* **2015**, *69*, 552.

[210] H. Ren, X.-P. Qiu, Y. Shi, P. Yang, F. M. Winnik, *Polym. Chem.* **2019**, *10*, 5080.

[211] X. Lang, A. D. Patrick, B. Hammouda, Hore, Michael J. A., *Polymer* **2018**, *145*, 137.

[212] J. Maillard, K. Klehs, C. Rumble, E. Vauthey, M. Heilemann, A. Fürstenberg, *Chem. Sci.* **2020**, *12*, 1352.

[213] S. Inal, J. D. Kölsch, L. Chiappisi, D. Janietz, M. Gradzielski, A. Laschewsky, D. Neher, *J. Mater. Chem. C* **2013**, *1*, 6603.

[214] V. Hildebrand, A. Laschewsky, M. Päch, P. Müller-Buschbaum, C. M. Papadakis, *Polym. Chem.* **2017**, *8*, 310.

[215] G. Moad, C. Guerrero-Sanchez, J. J. Haven, D. J. Keddie, A. Postma, E. Rizzardo, S. H. Thang, *ACS Symp. Ser.*, *1170*, 133.

[216] J. Xu, *Macromolecules* **2019**, *52*, 9068.

[217] R. Liu, L. Zhang, Z. Huang, J. Xu, *Polym. Chem.* **2020**, *11*, 4557.

[218] N. Badi, J.-F. Lutz, *Chem. Soc. Rev.* **2009**, *38*, 3383.

[219] J.-F. Lutz, T. Y. Meyer, M. Ouchi, M. Sawamoto, *ACS Symp. Ser.* **2014**, *1170*.

[220] S. Houshyar, D. J. Keddie, G. Moad, R. J. Mulder, S. Saubern, J. Tsanaktsidis, *Polym. Chem.* **2012**, *3*, 1879.

[221] S. M. Henry, A. J. Convertine, Benoit, Danielle S. W., A. S. Hoffman, P. S. Stayton, *Bioconj. Chem.* **2009**, *20*, 1122.

[222] N. Isahak, G. Gody, L. R. Malins, N. J. Mitchell, R. J. Payne, S. Perrier, *Chem. Commun.* **2016**, *52*, 12952.

[223] P. Delduc, C. Tailhan, S. Z. Zard, *J. Chem. Soc., Chem. Commun.* **1988**, 308.

[224] C. Zhou, S. Qian, A. Zhang, L. Xu, J. Zhu, Z. Cheng, E.-T. Kang, F. Yao, G. D. Fu, *RSC Adv.* **2014**, *4*, 8144.

[225] A. Yıldırım, Y. Kaya, *J. Phys. Org. Chem.* **2017**, *30*, e3629.

[226] T. Oishi, T. Fukuda, H. Uchiyama, F. Kondou, H. Ohe, H. Tsutsumi, *Polymer* **1997**, *38*, 3109.

[227] P. B. Zetterlund, G. Gody, S. Perrier, *Macromol. Theory Simul.* **2014**, *23*, 331.

[228] N. A. Hadjiantoniou, T. Krasia-Christoforou, E. Loizou, L. Porcar, C. S. Patrickios, *Macromolecules* **2010**, *43*, 2713.

[229] N. Aljuaid, M. Tully, J. Seitsonen, J. Ruokolainen, I. W. Hamley, *Chem. Commun.* **2021**, *57*, 8360.

[230] D. Xie, X. Ye, Y. Ding, G. Zhang, N. Zhao, K. Wu, Y. Cao, X. X. Zhu, *Macromolecules* **2009**, *42*, 2715.

[231] H. C. Kolb, Finn, M. G., Sharpless, K. Barry, *Angew. Chem. Int. Ed.* **2001**, *40*, 2004.

[232] D. Quémener, T. P. Davis, C. Barner-Kowollik, M. H. Stenzel, *Chem. Comm.* **2006**, 5051.

[233] X. Liu, X. Feng, J. Chen, Y. Cao, *J. Macromol. Sci. A* **2013**, *50*, 65.

[234] Andreas Hess, *Dissertation*, Universität Potsdam, Potsdam (Germany), **2021**.

[235] G. Delaittre, J. Rieger, B. Charleux, *Macromolecules* **2011**, *44*, 462.

[236] A. Fischer, A. Brembilla, P. Lochon, *Eur. Polym. J.* **2001**, *37*, 33.

[237] B. Grassl, G. Clisson, A. Khoukh, L. Billon, *Eur. Polym. J.* **2008**, *44*, 50.

[238] X. Savelyeva, L. Li, M. Marić, *J. Polym. Sci. Part A: Polym. Chem.* **2015**, *53*, 59.

[239] T. Schulte, K. O. Siegenthaler, H. Luftmann, M. Letzel, A. Studer, *Macromolecules* **2005**, *38*, 6833.

[240] Y. Kwak, R. Nicolaÿ, K. Matyjaszewski, *Aust. J. Chem.* **2009**, *62*, 1384.

[241] R. Nicolaÿ, Y. Kwak, K. Matyjaszewski, *Chem. Commun.* **2008**, 5336.

[242] R. N. Y. Kwak, K. Matyjaszewski, *Macromolecules* **2008**, *41*, 4585.

[243] T. Otsu, *J. Polym. Sci., Part A: Polym. Chem.* **2000**, *38*, 2121.

[244] Y. Qiu, W. Zhang, Y. Yan, J. Zhu, Z. Zhang, X. Zhu, *J. Polym. Sci. Part A: Polym. Chem.* **2010**, *48*, 5180.

[245] D. Zehm, A. Laschewsky, H. Liang, J. P. Rabe, *Macromolecules* **2011**, *44*, 9635.

[246] B. M. Rosen, G. Lligadas, C. Hahn, V. Percec, *J. Polym. Sci. A Polym. Chem.* **2009**, *47*, 3931.

[247] A. Giovannini, D. Savoia, A. Umani-Ronchi, *J. Org. Chem.* **1989**, *54*, 228.

[248] M. B. Andrus, W. Li, R. F. Keyes, *Tetrahedron Lett.* **1998**, *39*, 5465.

[249] M. Yao, X. Chen, Y. Lu, Z. Guan, Z. Luo, Y. Zhang, *J. Chem. Res.* **2021**, *45*, 141.

[250] B.-Y. Zhang, W.-D. He, W.-T. Li, L.-Y. Li, K.-R. Zhang, H. Zhang, *Polymer* **2010**, *51*, 3039.

[251] Z. Xu, X. Hu, X. Li, C. Yi, *J. Polym. Sci. Part A: Polym. Chem.* **2008**, *46*, 481.

[252] S. Eggers, T. Eckert, V. Abetz, *J. Polym. Sci., Part A: Polym. Chem.* **2018**, *56*, 399.

[253] M. Roth, A. Oesterreicher, F. H. Mostegel, A. Moser, G. Pinter, M. Edler, R. Piock, T. Griesser, *J. Polym. Sci. Part A: Polym. Chem.* **2016**, *54*, 418.

[254] H. Brunner, S. Altmann, *Chem. Ber.* **1994**, *127*, 2285.

[255] L. Wattebled, A. Laschewsky, *Colloid Polym. Sci.* **2007**, *285*, 1387.

[256] F. Jia, Y. Wang, H. Wang, Q. Jin, T. Cai, Y. Chen, J. Ji, *Polym. Chem.* **2015**, *6*, 2069.

[257] W. Chen, Y. Zou, J. Jia, F. Meng, R. Cheng, C. Deng, J. Feijen, Z. Zhong, *Macromolecules* **2013**, *46*, 699.

[258] J. M. Khurana, P. K. Sahoo, *Synth. Commun.* **1992**, *22*, 1691.

[259] K. Philipps, T. Junkers, J. J. Michels, *Polym. Chem.*, **2021**, *12*, 2522.